Stellingen

1. Het feit dat de toename van de dichtheid van bundels van actine filamenten vlak onder de celtop van wikke wortelharen na toediening van bacteriële signaalmoleculen binnen drie minuten aantoonbaar is, duidt erop dat hiervoor geen transcriptie nodig is.

    De Ruijter *et al.* (1999) *Rhizobium* Nod factors induce an increase in sub-apical fine bundles of actin filaments in *Vicia sativa* root hairs within minutes. *Mol. Plant-Microbe Interact.* 12: 829-832 (dit proefschrift).

2. Omdat cytoplasmastroming plaatsvindt langs bundels van actine filamenten en cytoplasmadraden verdwijnen bij afbraak van actine filamenten (Valster *et al.*, 1997) is de door Cárdenas *et al.* (1998) beschreven fragmentatie van actine filamenten in wortelharen na toediening van lipochito-oligosaccharides zonder verstoring van cytoplasmastroming, niet mogelijk.

    Cárdenas *et al.* (1998) Rearrangement of actin microfilaments in plant root hairs responding to *Rhizobium etli* nodulation signals. *Plant Physiol.* 116: 871-877.

    De Ruijter *et al.* (1999) *Rhizobium* Nod factors induce an increase in sub-apical fine bundles of actin filaments in *Vicia sativa* root hairs within minutes. *Mol. Plant-Microbe Interact.* 12: 829-832 (dit proefschrift).

    Valster *et al.* (1997) Probing the plant actin cytoskeleton during cytokinesis and interphase by profilin microinjection. *Plant Cell* 9: 1815-1824.

3. De veronderstelling dat de kanteling van de spoelfiguur tijdens de deling van platte cortexcellen van de wortel van *Vicia faba* invloed heeft op de ligging van het delingsvlak (Oud and Nanninga, 1992), is onjuist (De Ruijter et al., 1997).

    Oud and Nanninga (1992) Cell shape, chromosome orientation and the position of the plane of division in *Vicia faba* root cortex cells *J. Cell Sc.* 103: 847-855.

    De Ruijter *et al.* (1997) Spatial limitations induce spindle tilting and result in oblique phragmoplasts in *Vicia faba* L. root tip cells, but do not result in oblique cell walls. *Acta Bot. Neerl.* 46: 279-290 (dit proefschrift).

4. Om te bewijzen dat de groei in wortelharen van een infectiedraad voor symbiotische bacteriën vergelijkbaar is met inwaartse celtopgroei, moeten celbiologische kenmerken van celtopgroei aangetoond kunnen worden aan de buitenzijde van de top van een inwaarts groeiende infectiedraad.

5. Kennis en kunde gaan hoofd in hand.

6. Het gras in het tuintje van de buurman lijkt groener, omdat bij kleinere observatiehoek en grotere afstand kleur domineert boven detail.

7. Gezien de hoge snelheid en het geringe remvermogen bij gebruik van inline skates en skeelers is het dragen van een flexibel exoskelet in plaats van sportkleding aan te raden.

8. Het feit dat juiste consumentenvoorlichting essentieel is voor het verkrijgen van acceptatie van genetisch gemodificeerd voedsel wijst erop dat het spreekwoord: "Wat de boer niet kent dat eet hij niet", nog altijd actueel is.
    Beachy (1999) Facing fear of biotechnology. Editorial in *Science* 285: 335.

9. Wanneer de kosten voor herstel van milieuschade bij energieopwekking zouden worden verrekend in de energieprijs, is de toekomst voor natuurstroom nog zonniger dan zij al is.

10. Bij werkoverleg in een grotere groep neemt de ruis toe en het signaal af.

11. De beschaving van een maatschappij is af te lezen aan de wijze waarop zij omgaat met de zwakkeren en kanslozen in de samenleving.

12. De levende aarde, waarin alle ecosystemen elkaar onderling beïnvloeden (het Gaia concept), kan gezien worden als één grote "symbiose".
    Margulis (1998) in Symbiotic Planet : A New Look at Evolution.

Stellingen behorende bij het proefschrift getiteld Aspects of plant cell growth and the actin cytoskeleton: lessons from root hairs.

Wageningen, 4 oktober 1999.   Norbert de Ruijter.

Aspects of
plant cell growth
and the
actin cytoskeleton
lessons from root hairs

Norbert C.A. de Ruijter

Promotor: dr. M.T.M. Willemse
           hoogleraar in de plantkunde
           Laboratorium voor Plantencytologie en -morfologie

Co-promotoren: dr. A.M.C. Emons
                universitair hoofddocent
                Laboratorium voor Plantencytologie en -morfologie

                dr. J.H.N. Schel
                universitair hoofddocent
                Laboratorium voor Plantencytologie en -morfologie

Aspects of plant cell growth and the actin cytoskeleton

lessons from root hairs

Norbert C.A. de Ruijter

Contents

Outline

The main topic this thesis addresses is the role of the actin cytoskeleton in the growth process of plant cells. Plant growth implies a combination of cell division and cell expansion. The cytoskeleton, which exists of microtubules and actin filaments, plays a major role in both processes. Before cell growth takes place, a new cell is formed by cell division. The orientation of the division plane most often predicts the orientation of cell expansion, and a correct positioning of the division plane is therefore important for plant morphogenesis. During most stages of cell division microtubules and actin filaments have a similar configuration.

In Chapter 1 the cytoskeleton of microtubules has been visualized during all stages of cell division for long and short root tip cells of broad bean (*Vicia faba* L.). In all cells the preprophase band of microtubules was positioned in the midplane of the cell, and perpendicular to the long axis of the root. It was observed that the spindle axis in short cells increasingly tilted, from meta- to anaphase, giving rise to oblique cell plates. It appears that this is caused by spatial constraints. During late-telophase, cell plates first rotated towards the transversal plane before they fused with the parental wall at the site of the earlier preprophase band. When cell division is completed, cells grow.

Plant cell growth is the insertion of Golgi vesicles into the plasma membrane and the delivery of their content into the existing wall. If this wall is flexible and under turgor pressure, the membrane becomes larger and the wall expands. The basic principles of plant cell growth can best be studied in cells where this growth process takes place abundantly, that is in the tip of tip-growing cells of higher plants, such as root hairs and pollen tubes.

In Chapter 2, characteristics for cell tip growth are being reported, studied by comparison of developmental stages of root hairs of vetch (*Vicia sativa L.*), from their emergence to their maturity. It is further shown that lipochito-oligosaccharides (LCOs), well-characterized molecules that are excreted by bacteria, reinitiate cell tip growth in hairs that are terminating growth. Tip growth and the site of growth reinitiation correlates with the presence of a steep cytoplasmic calcium gradient at the plasma membrane. Furthermore, it was found that a spectrin-like protein is a good marker for tip growth, and co-localizes with the vesicle rich region, which is known to be present at the tip.

Immunolocalization of this spectrin-like protein in plants was extended to a variety of growing cells and shows, in Chapter 3, that this protein is especially present in young growing cells. Molecular weight and iso-electric point determination, by means of immunoblotting identified the plant spectrin-like protein. The anti-spectrin antibody also labels nuclei, which is further investigated in Chapter 4.

To analyze the presence and localization of nuclear spectrin-like proteins, various plant tissues and isolated pea nuclei were labeled. The data presented in Chapter 4, show that the spectrin-like proteins are distributed in a speckled pattern and occasionally in tracks. The extraction procedures used indicate that the spectrin-like protein is part of the nuclear matrix in which it may be a stabilizing factor.

Chapter 5 the actin cytoskeleton of vetch root hairs at their initiation and during their development is described. Actin filament bundles are the dynamic backbone of the cytoplasmic strands. Growing hairs show dense sub-apical fine bundles of actin filaments (FB-actin) and the very tip is devoid of actin filament bundles, whereas full-grown hairs have actin bundles looping through the tip. Similar actin configurations were obtained when root hairs were freeze substituted and immunolabeled with anti-actin, or chemically fixed by an improved method and stained with fluorescent phalloidin. Since LCOs had been shown to reinitiate root hair growth (Chapter 2), this signal molecule was used to study the actin cytoskeleton during growth reinitiation. Manipulation of the actin cytoskeleton with the actin filament capping drug cytochalasin D inhibited polar growth. However, root hair initiation and swelling after LCO application were not affected. We concluded that elongating FB-actin is another characteristic for tip growth.

Indeed, LCOs altered the configuration of the actin cytoskeleton, which was studied in Chapter 6. The density of sub-apical actin filament bundles increased within 3-15 minutes after the application of LCOs. By a quantitative approach we were able to define the minimal FB-actin density and minimal length, of the area with the FB-actin, needed for growth. Only in hairs in which FB-actin exceeded these values, tip growth was sustained or resumed. The rapid response of actin filaments indicates a role for the actin cytoskeleton in signal transduction cascades.

Such a dynamic actin cytoskeleton must be regulated. Part of this regulation is done by actin binding proteins. Therefore, our limited knowledge of actin binding proteins in plant cells is reviewed in Chapter 7 of this thesis.

Chapter 8 summarizes the characteristics for growth in tip-growing cells and extrapolates them to cells that expand isodiametrically or predominantly along one length axis. We conclude that tip growing cells, like root hairs, shed light on basic principles of plant growth, and provide a system to monitor the effect of signal molecules on cell growth.

- Chapter 1 -

Spatial limitations induce spindle tilting and result in oblique phragmoplasts in *Vicia faba* L. root tip cells, but do not result in oblique cell walls

N.C.A. de Ruijter[1,*], J. Pietrusiewicz[1,3], M.B. Montijn[2],
J.H.N. Schel[1] and A.A.M. van Lammeren[1]

[1]*Department of Plant Cytology and Morphology, Wageningen Agricultural University,
Arboretumlaan 4, 6703 BD Wageningen, The Netherlands*
[2]*Institute for Molecular Cell Biology, Biocentre Amsterdam, University of Amsterdam,
Kruislaan 316, 1098 SM Amsterdam, The Netherland*
[3]*Department of Plant Anatomy and Cytology, University Maria Curie-Sklodowska,
Akademicka 19, Lublin, Poland*

Short title: Spindle orientation and phragmoplast tilting in *Vicia*

SUMMARY

Chromosome and phragmoplast positioning proceed differently during mitosis and cytokinesis in short and long root tip cells of *Vicia faba* L. and has been studied previously (Oud & Nanninga 1992, 1994). No correlations, however, were made with the microtubular cytoskeleton. Here this correlation is investigated using longitudinal sections of hydroxy-urea synchronized root tip cells. Microtubules were labeled with anti α-tubulin, chromosomes were stained with propidium iodide, and both were visualized using confocal scanning laser microscopy. Preprophase bands of microtubules were always positioned in the midplane of both short and long cells, and they were perpendicular to the length axis of the files of cells in the root. Also spindle formation started in a similar way in short and long cells, but from meta- to anaphase, the spindle axis in short cells increasingly tilted, due to spatial constraints. While chromosomes separated, the spindle axis acquired a position inclining to a diagonal of the cell, thus giving rise to the earlier observed oblique chromosome positions in anaphase plates. In short cells oblique phragmoplasts/cell plates expanded in oblique division planes. However, after karyokinesis, oblique cell plates rotated towards the transversal plane and the final site of wall connection was not eccentric, but at the site of the earlier preprophase band. We conclude that the suggestion, that in *Vicia faba* L. oblique walls are due to oblique anaphase plates (Oud and Nanninga 1992), has to be corrected. Even when chromosomal alignment is offset and oblique cell plates are formed in cramped cells, still transverse preprophase bands predict transverse division planes.

Keywords: cell plate orientation, cytoskeleton, microtubules, cell division, oblique spindles, phragmoplast, *Vicia faba* L.

Abbreviations:
FITC: fluorescein isothiocyanate
HU: hydroxy-urea
MSB: microtubule stabilizing buffer
Mt: microtubule
PI: propidium iodide
PPB: preprophase band
CSLM: confocal scanning laser microscopy

INTRODUCTION

The positional control of the plane of cell division is one of the key factors in plant morphogenesis (Barlow & Carr 1984, Lintilhac 1984, Lloyd 1991). To exert this control, various physical factors such as pressure, size and shape of the mother cell and thermodynamical considerations of minimal surface area have been suggested (e.g. Thompson 1945). Later, it was understood that cells also play a more active role in achieving a specific cell plate orientation. In this respect, the role of the preprophase band (PPB) was investigated. At early stages of symmetrical cell division the PPB, a central ring of microtubules (Mts) in the cortical cytoplasm of the cell, is formed (Picket-Heaps & Northcote 1966, Gunning & Sammut 1990), replacing the interphase cytoskeletal array of Mts. In general the PPB, which is visible from G_2-phase to early prophase, marks the site at which the phragmoplast/cell plate complex meets the parental wall during cytokinesis (Gunning 1982, Gunning & Wick 1985, Palevitz 1986, Flanders *et al.* 1990, Mineyuki & Gunning 1990, Wick 1991a). In this manner PPBs determine the position of the new cell walls.

In various cells, the mitotic apparatus is often tilted or distorted (Wick 1991a, Oud & Nanninga 1992, Palevitz 1993). In guard mother cells of onion cotyledons most spindles are oblique (Palevitz & Hepler 1974, Palevitz 1986, Mineyuki *et al.* 1988) and similar tilting of spindles is described for guard mother cells of other species (Cho & Wick 1989, Cleary & Hardham, 1989). Fusiform cambial initials (Bailey 1920) and rib meristem cells (Wada 1965) are other examples of aberrant spindle positions. Usually, however, the phragmoplast-cell plate position is corrected, and transversal division in the midplane (i.e. at the site of the original PPB) takes place. Nevertheless few exceptions exist, where the influence of the PPB is not absolute. For *Triticum* leaf epidermal cells Galatis *et al.* (1984a) described a positional inconsistency between PPB Mts and the final cell plate position during triangular subsidiary cell and atypical hair cell formation. Here strong morphogenetic factors overrule the influence of the PPB in determining the position of the cell wall. Absence of PPBs as in some *Arabidopsis* mutants, results in absence of cell files in roots (Traas *et al.* 1995).

Root cortex cells of *Vicia faba* show many oblique divisions. For these cells Oud & Nanninga (1992, 1994) described a progressive increase in the tilting of the spindle axis by measuring the obliqueness of chromosome orientations and daughter nuclei from prophase to telophase. They concluded that in small cells a tilted spindle axis causes an oblique cell wall. They did not, however, correlate these data with data on cytoskeletal changes. We have reinvestigated the phenomenon of tilted spindle axes in *Vicia faba* in relation to cell size, using a combined approach of both chromosomal and cytoskeletal visualization. Special attention was paid to the location of the PPB and the microtubular arrays during spindle tilting in relation to the cell length. Although oblique spindles and cell plates were often observed in dividing *short*

cells, *Vicia* roots are characterized by regular files of cells with transversal cell walls. We therefore further questioned how cytokinesis proceeded in cells with oblique spindles and focussed on the site of cell plate fusion.

We show that preprophase bands in short cells do not anticipate to oncoming spatial limitations of the spindle and are always perpendicular to the cell file axis and in the midplane of the cell. From our observations we must conclude that the previous suggestion, that oblique cell walls in *Vicia faba* result from oblique phragmoplasts (Oud & Nanninga, 1992), must be reconsidered. Obviously spindle tilting affects phragmoplast orientation to a great extent, but essentially does not affect the orientation of the final cell wall.

MATERIALS AND METHODS

Plant material and conditioning of the cell cycle

Commercially obtained seeds of the broad bean (*Vicia faba* L.) were imbibed in tap water for 1 day and germinated on wet filter paper within 2 days at 23°C in a humid atmosphere. Seedlings were cultured on aerated 0.5 × Hoagland solution (Gamborg & Wetter 1975) for 1-3 days. When the primary roots were 2-4 cm long, they were incubated in aerated 0.5 × Hoagland medium, containing 2.5 mM hydroxy-urea (HU), a drug which blocks the cell cycle at the transition of G_1 to S-phase (Dolezel *et al*. 1992). After 12-14 h the roots were washed for a few minutes in a flow of tap water to remove HU, and the plantlets were cultured further on HU-free medium at 23°C. Using this treatment, the mitotic index increased from 15% cells in mitosis (without HU) to maximally 90% of cells in mitosis (with HU). At 12, 14, 16 and 18 h after the release of the block, some root tips were squashed and stained with acetocarmin to determine the percentage of cells in mitosis and the phase of mitosis. When many mitotic stages were observed, similar root tips were processed for immunolabeling.

HU-treated roots, subcultured for 12 h after HU removal, did not exhibit cell divisions, indicating both the blocking efficiency of HU and also the necessity of a chase longer than 12 h for the transition from G_1-S phase to mitosis. When root tips were sampled at 14 or 16 h after the removal of the drug many metaphase configurations were found and, when sampled at 18 h after HU treatment, telophase and early interphase configurations were most common. Under optimal growth conditions a mitotic index of 90% was achieved after HU treatment. The absence of aeration, and growth temperatures below 18°C during the pulse and chase of HU, lowered the mitotic index to less than 10%. Microtubular configurations did not differ in HU treated cells, when compared to non-treated cells. Also cell shapes and cell dimensions were comparable, and HU treated plantlets developed normal roots and phenotypes.

Fixation and embedding

Roots tips (0.5 cm) were harvested for immunolabeling at 14 h and 16 h after the release of HU and immediately fixed for 1 h at room temperature in 4% (w/v) paraformaldehyde and 0.01% (v/v) glutaraldehyde in microtubule stabilizing buffer (MSB: 100 mM PIPES, pH 6.9, 5 mM EGTA, 5 mM MgSO$_4$) containing 0.1% (v/v) purified Triton X-100 (Surfact-Amps X-100, Pierce). Thick primary roots were incised longitudinally to improve the penetration of the fixative into the stele and cortex. Root tips were embedded in polyethylene glycol (PEG) according to Van Lammeren (1988), but 100% PEG 1500 was used instead of a 3:2 mixture of PEG 1500 : PEG 4000, this to enable sections of 10 to 30 μm thickness. For cryosectioning, root tips were infused stepwise with 10% (30 min), 15% (30 min) and 20% (overnight) sucrose (w/w) in 50 mM phosphate buffer, pH 7.2, quickly frozen in liquid nitrogen and mounted in Tissue-Tek (Agar Scientific Ltd., Essex, GB). For optimal root tissue morphology and to study the site of cell plate connection, root tips were fixed in 3% paraformaldehyde with 2% glutaraldehyde in MSB. They were dehydrated, infused, and polymerized in Technovit 7100 according to the manufacturer's procedure. Sections of 2 μm were stained with 1% toluidine blue in water.

Sectioning and immunolabeling

Longitudinal sections (15-20 μm thickness) were made of PEG embedded root tips using a Microm HM 340 rotary microtome. Frozen longitudinal sections (20 μm thickness) were prepared using a Microm HM500 OM cryomicrotome at -18°C. Sections were affixed to slides that had been coated with 2% (v/v) organosilane. Cell walls were digested with 1% (w/v) hemicellulase (Sigma H2125) for 10 min, and subsequently extracted in a mixture of 1% (v/v) purified Triton X-100 (Surfact-Amps X-100, Pierce), 2 mM EGTA, 0.2 mM phenylmethylsulfonyl fluoride (PMSF) in MSB for 10 min. The sections were blocked with 1% (w/v) bovine serum albumin (BSA, Fraction V, Serva, Heidelberg, FRG) for 10 min, followed by an incubation with 0.1% (w/v) acetylated BSA (BSA-c, Aurion, Wageningen, NL) for another 10 min. Indirect immunolabeling of Mts was done using a monoclonal mouse-IgG anti-α-tubulin (clone DM1a, Sigma) and goat anti-mouse-IgG-Bodipy[TM]-FL (Molecular Probes, Oregon) or GaM-FITC (Sigma). Each antibody was diluted 1/300 in PBS containing 0.1% (w/v) BSA-c, and incubations were performed at room temperature for 2 h. After the first antibody incubation, extensive washings were done with 0.1% BSA-c in PBS (six times 5 min) and after the secondary antibody, washings were done in PBS (six times 5 min). DNA was counter-stained by incubating the slides for 7 min in freshly prepared 0.3 μg/ml propidium iodide (PI) in 0.05 M phosphate buffer, pH 7.8. To reduce fading of both fluorochromes, sections were mounted in Citifluor in glycerol (Citifluor Ltd., London) and slides were stored in the dark at 4°C.

7

Microscopy and image analysis

Fluorescent Mts and chromosomes or nuclei were visualized with a Nikon Microphot epifluorescence microscope at various mitotic stages and at the end of cytokinesis. The fluorochromes FITC and Bodipy-FL 503/512 were visualized using excitation filter 450-490 nm, dichroic mirror DM 510, and barrier filter BP 520-560 nm. Propidium iodide images were obtained with excitation filter 510-560, dichroic mirror DM 580, and barrier filter 590 nm. Further analysis was done with a Bio-Rad MRC 600 Confocal Scanning Laser Microscope (Bio-Rad, Hertfordshire, UK) equipped with an argon-krypton laser on a Nikon Labophot inverted microscope. Cytoskeletons and chromosomes were recorded by dual channel imaging and Kalman filtering.

Confocal BioRad PIC files (378*512, 8 bits) were converted to TIFF format using Confocal Assistant software (BioRad). Light micrographs imaged with a Panasonic wv-E550 3-CCD camera were digitized in TIFF format using a 756*536 (24 bits) Prysm framegrabber (Synoptics Ltd., Cambridge, UK). Files were contrast enhanced in Adobe Photoshop and printed using a Kodak XLS 8600 dye sublimation printer.

Statistics

In five separate experiments roots were harvested at high mitotic index and for each mitotic stage 10 primary roots were sectioned. Over 30.000 cells were labeled for Mts. More than 6000 cells were properly longitudinally sectioned and labeled well. For each mitotic stage more than 300 cells were studied with the CSLM and a selection of 20-40 *short* and *long* cells were recorded.

RESULTS

The results described here are based on the simultaneous staining of chromosomes with propidium iodide (PI) and immunolabeling of microtubules (Mts). Irrespective of cell length, interphase cells in the root meristem showed transverse cortical Mts. At preprophase, these cortical Mts gradually disappeared alongside the upper and lower parts of the longitudinal walls, and a preprophase band (PPB) appeared. Two rings of PPB Mts were sometimes seen temporarily (arrowheads in Fig. 1e). PPBs progressively narrowed and were always positioned in the midplane of the cell, almost transverse to the length axis of the root (Figs. 1a,e). The increase of the mitotic index with hydroxy- urea allowed observing Mt configurations during mitosis in many cells. From each mitotic phase at least 300 cells were observed after labeling. Special attention was given to the position of the PPB in *short* cells. Of all PPBs observed 95% deviated less than 10° from the midplane. The position of PPBs could deviate up to 15° from

the midplane, corresponding with a distance of 2-3 μm from the mid-transversal plane. These slight aberrations occurred in less than 5% of all cells observed and correlated with avoidance of four-way junctions (Flanders *et al.* 1990).

General phenomena observed during anaphase were the increase of the pole-to-pole distance, the persistence of the pole-to-pole Mts, the shortening of the centromere Mts, and the simultaneous separation and movement of the chromatids to the spindle poles. Most anaphase spindles in *long* cells remained parallel to the length axis of the cell file (Fig. 1c). *Short* cells mostly exhibited oblique anaphase spindles, varying up to a fully diagonal position (Fig. 1h). Occasionally, oblique spindles twisted or bended, to gain length. In *long* cells spindle tilting was observed incidentally, but only when the presence of large vacuoles at both sides of the spindle restricted the cytoplasmic space (not shown).

General phenomena observed during anaphase were the increase of the pole-to-pole distance, the persistence of the pole-to-pole Mts, the shortening of the centromere Mts, and the simultaneous separation and movement of the chromatids to the spindle poles. Most anaphase spindles in *long* cells remained parallel to the length axis of the cell file (Fig. 1c). *Short* cells mostly exhibited oblique anaphase spindles, varying up to a fully diagonal position (Fig. 1h). Occasionally, oblique spindles twisted or bended, to gain length. In *long* cells spindle tilting was observed incidentally, but only when the presence of large vacuoles at both sides of the spindle restricted the cytoplasmic space (not shown).

During PPB formation, chromatin condensed and individual chromosomes could be discerned (Figs. 1a',e'). When the length or the width of a cell was a limiting factor, nuclei were not spherical but oval shaped (e.g. Fig. 1e'). Many Mts were formed at the surface of the nuclei, especially at the poles, and some of them ran towards the PPB (pole-to-PPB Mts, Figs. 1a,f, arrows). At prometaphase, PPBs and pole-to-PPB Mts had disappeared, but arrays of Mts emanating from the poles of the nucleus now ran towards the opposite pole and a dense network of fine Mts encaging the condensing chromosomes was formed (Fig. 1b). When the pole-to-PPB Mts had disappeared, the spindle axis was slightly tilted in those cells where the spindle poles were in the vicinity of the transversal walls (not shown). At metaphase these cells exhibited oblique spindles (Fig. 1g). The shorter the cell, the more the spindle axis tilted. Simultaneously, the metaphase plane with chromosome centromeres tilted and remained perpendicularly to the spindle axis (Fig. 1g'). Chromosome arms were never inside the oval shaped spindle, leaving a free central area. Instead chromosomes extended from and bent around the spindle in *short and flat* cells (Fig. 1g'). However, they ran parallel to the length axis of the cell in *long and slender* cells (not shown).

9
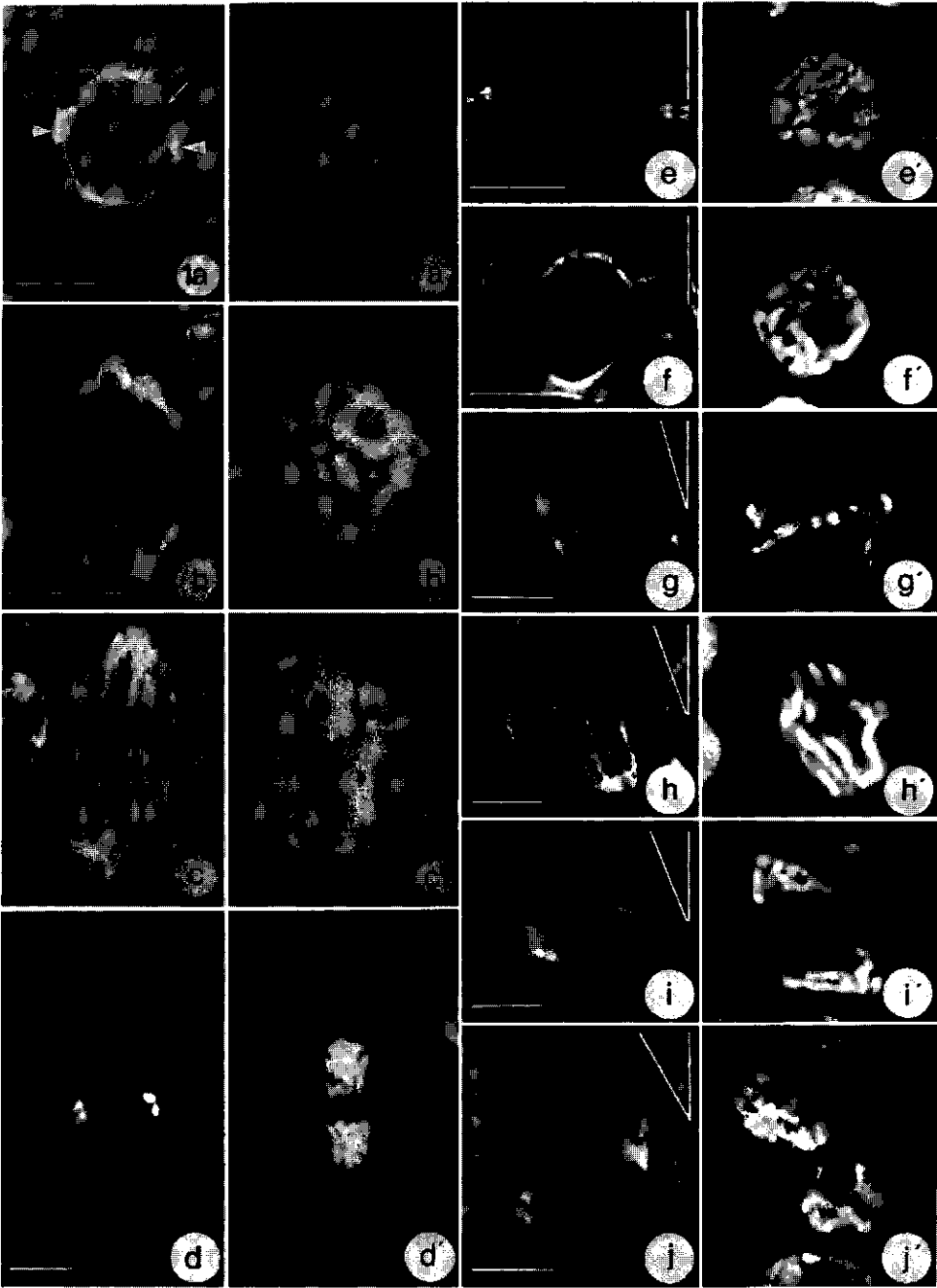
Figure 1 Dual channel confocal images of fluorescent microtubules (Mts) (a-j) and DNA (1a'-j') at successive stages of mitosis in root tip cells of *Vicia faba*.

At telophase, separated chromatids condensed, and a phragmoplast was formed. A cylinder of dense Mts appeared, which expanded laterally in the midplane, meanwhile depositing a cell plate perpendicular to the former spindle axis. Thus in *long* cells, the growing cell plate was mostly transversal and centrally positioned (Fig. 1d). Cytokinesis completed by fusion of the cell plate with the parental wall, forming two daughter cells stacked in the file. In *short* cells with oblique spindles, the phragmoplast developed also in the plane perpendicular to the spindle axis (Fig. 1i), giving rise to an oblique cell plate. When an oblique cell plate approached the lateral parental wall, phragmoplast-Mts aligned parallel to that cell wall, and cell plate edges buckled towards it (Fig. 1j), causing the cell plate to become sigmoidal. To follow the curvature and positioning of such cell plates during cytokinesis we not only used labeled sections, but also toluidine blue stained Technovit sections (Fig. 2). An oblique cell plate (Fig. 2a, upper cell) became more curved at its edges (Fig. 2b, upper cell) or developed a sigmoidal shape (Fig. 2c) as it expanded. Such sigmoidal cell plates, however, did not fuse eccentrically with the lateral wall.

Figure 1 (left) Microtubules (Mts) (a-j) and DNA (1a'-j') at successive stages of mitosis in root tip cells of *Vicia faba*; aa'-dd' long cells; ee'-jj' short cells. Pictures are mounted in the same orientation as cells were positioned in the cell files. Bars represent 10 µm, for all panels.

(a) Preprophase in long cell with PPB Mts (arrowheads) and Mt formation at the nuclear poles. Arrow points to pole-to-PPB Mts. Chromosomes condense (a').

(b) Late prophase with Mts extending from the poles and surrounding the condensed chromosomes (b').

(c) Anaphase with pole-to-pole Mts and dense Mts from centromeres to pole. While centromeres are near a pole, chromosome arms still reach to the middle plane (c').

(d) Late telophase showing phragmoplast, perpendicular to the length axis of the cell. Note that the daughter nuclei are positioned in line with the long axis of the cell (d').

(e) Prophase in short cell showing spindle Mts radiating from the poles, some connecting with the PPB (arrow). Arrow-heads point to the two rings of the PPB. The poles are in line with the cell file. Condensed chromosomes position at the nuclear periphery (e').

(f) Prophase in short cell showing Mts radiating from two poles on the nucleus. Pole-to-PPB Mts are indicated by an arrow.

(g) Metaphase with centromere Mts and pole-to-pole Mts. Note the slightly oblique position of the spindle and chromosomes (g'). Centromeres are in the middle plane and chromosome arms extent from here and surround the spindle.

(h) Anaphase with tilted spindle in diagonal position and tilted chromosomes (h'). The pole at the lower right hand side is in focus, whereas the pole at the upper left hand side is not, due to tilting.

(i) Early telophase showing an oblique phragmoplast/cell plate and daughter chromosomes in diagonal, opposite corners of the cell (i'). Arrows indicate the position of the cell plate.

(j) Late telophase with an oblique phragmoplast/cell plate marked by phragmoplast Mts at its periphery. Newly formed daughter nuclei are still in oblique position (j').
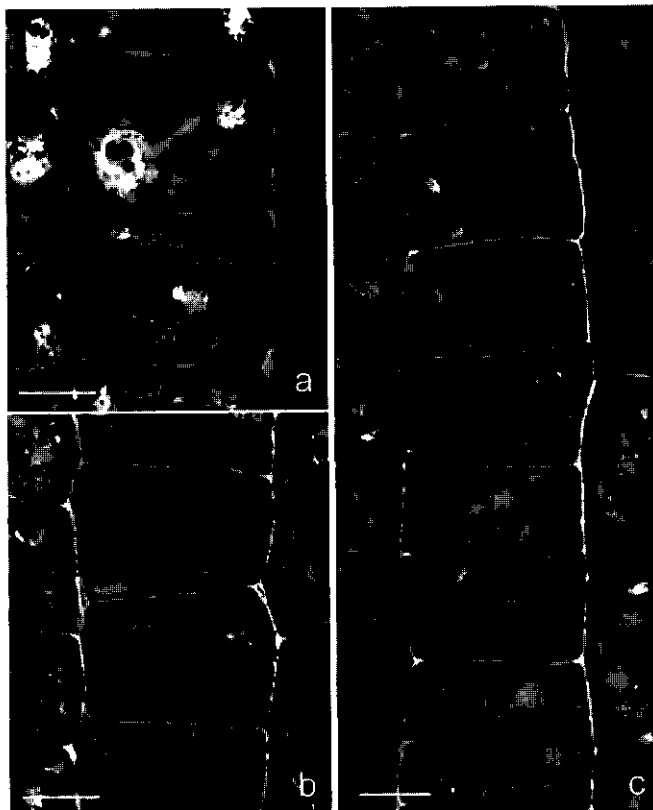
Figure 2 Selection of light micrographs of longitudinal sections of Technovit embedded root tips of *Vicia faba*, showing short cells stained with toluidine blue. Bars represent 10 μm.

(a) Cell file showing a cell at telophase with an oblique cell plate bordered by vacuoles. Below, a pair of daughter cells separated by a cell plate in transversal position.

(b) Two pairs of cells just after division. The upper pair shows a bent cell plate not yet attached to the parental wall. The lower pair exhibits the final stage of cytokinesis with a straight transversal cell plate.

(c) File of cells with (in the middle of the image) a cell during cytokinesis showing a curved cell plate extending towards the lateral walls. The pair of cells (in lower part of the image) exhibits a slightly tilted and curved cell wall

In longitudinal Technovit sections 60 *short* cells were examined at late telophase, all exhibiting oblique cell plates with curved edges. Instead, prior to wall fusion, the flexible cell plate oriented from oblique towards the midplane of the cell (Fig. 2a, lower cell), stretched and fused perpendicularly with the lateral wall (Fig. 2b, lower cell), even in *short* cells of only 15 μm heights.

Figure 3 shows a schematic summary of the Mt arrays during mitosis in *long* and *short* cells of the root cortex. The correction of a tilted phragmoplast towards the midplane, as in *short* cells prior to cytokinesis, is represented in the Figures 3g'-i'.
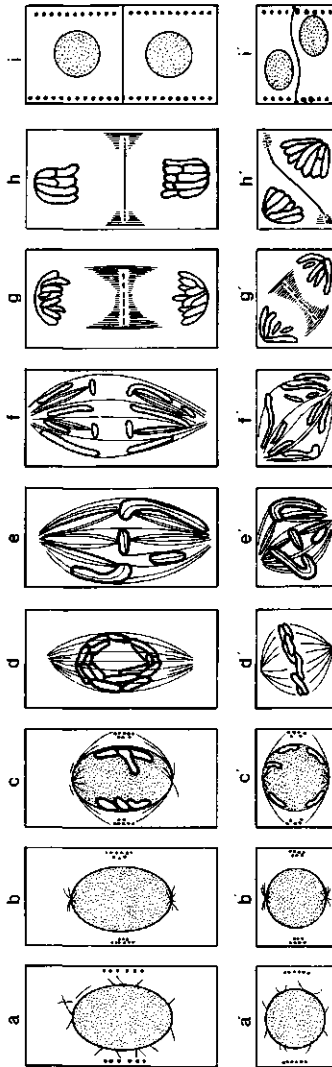
Figure 3. Schematic representation of Mts and chromosome positions in long (a-i) and short (a'-i') cells during mitosis (a,a') Early prophase with PPB formation and Mts radiating from nucleus. (b,b') Mid prophase with established PP and Mts radiating from nuclear poles, which are in line with the cell file. (c,c') Late prophase with pole-to PPB Mts (d,d') Prometaphase, pole-to-PPB Mts disappeared, pole-to-pole and pole-to-centromere Mts were formed, and spindl tilted in short cell and chromosomes were at the periphery of the nucleus (d'). (e,e') Metaphase with centromeres i equatorial plane and chromosome arms extending towards the poles (e) or lateral sides (e'). (f,f') Early anaphase wit centromeres close to the equatorial plane and chromosome arms pushed towards the poles (f) or spindles in diagona position (f). (g,g') Early telophase with phragmoplast extension and cell plate formation in the former equatorial plan (g), and in diagonal position (g'). (h,h') Late telophase with a transversal cell plate (h) or a sigmoidal cell plate (h'). (i,i' Completed cytokinesis with a transversal cell wall both in long (i) and in short cells (i'). In short cells after division slight curvature of the young cell wall can sometimes still be seen.

DISCUSSION

Increasing tilting of the plane of chromosomes coincided with an increasing spindle tilting in successive stages of mitosis. We questioned if the *short* cells anticipated to oncoming spacial limitations, by forming oblique or curved PPBs. However, PPBs were positioned close to the transversal midplane both in *long* and in *short* cells and consequently, spindle initiation always started perpendicular to the PPB. During prophase, Mts radiated from the surface of the nucleus into the cytoplasm, mainly from the nuclear poles. Pole-to-PPB Mts are expected to function in positioning the nucleus in the plane marked by the PPB, and in fixing the spindle pole positions (Mineyuki *et al.*1991). Indeed, as long as this anchorage existed, spindle poles remained in position. At prometaphase the PPB and the pole-to-PPB Mts disappeared, and the spindle was formed. As soon as the spindle elongated and its poles pushed against the transversal walls, spatial limitations occurred, spindle poles glided towards diagonal cell corners, and chromosome tilting occurred. Therefore, we conclude that chromosome tilting is caused by spindle tilting, which on its turn is caused by spatial limitations. Similarly Mineyuki *et al.* (1988) suggested spatial limitation of the spindle, to explain tilting in dividing guard mother cells of *Allium*. The morphological plasticity of the mitotic apparatus is evident (Palevitz 1993).

Wada (1965) has described an increasing chromosome tilting in *Triticum* when the chromosome number enlarged from diploid to hexaploid varieties. In general, in species with relatively large chromosomes, such as in *Allium cepa*, *Crepis capillaris* and *Vicia faba* tilting of the plane of chromosomes is frequently observed (Oud & Nanninga 1994). These data indicate that both the number and the size of chromosomes can contribute to lack of space and increase of steric hindrance. Large *Vicia faba* chromatids extended from the spindle (Fig. 1g'), as was also observed in *Allium* by Palevitz (1988) and in the alga *Oedogonium* by Schibler & Pickett-Heaps (1987). The position of the chromatid arms in *Vicia* was laterally extended in wide cells and longitudinal in long-and-slender cells, demonstrating a direct influence of space limitation on chromosome positioning (see also Oud *et al.* 1995). The Mts connected to chromosomal arms might influence their movement during mitosis as observed by McIntosh & Pfarr (1991) in animal cells.

Tilting of the equatorial plane is correlated with cell size and increases from metaphase to telophase. In 85% of all telophases, equatorial planes deviated more than 5° from the midplane and in 70% equatorial planes deviated over 20° from the midplane (Oud & Nanninga, 1992). Although we observed such oblique phragmoplasts in more than 300 cells, we never saw the fusion of cell plates with parental walls in oblique position. Even in very *short* cells (length < 20μm), the edge of the cell plate fused with the parental wall in the middle of the cell (Fig. 2b). Cell plate fusion was preceded by cell plate bending. The stretching of the sigmoidal cell plates, prior to fusion, is reminiscent to the flattening and stiffening observed in cell plates of dividing

Tradescantia stamen hair cells (Cleary *et al.* 1992). Apparently, there is an interaction of the growing cell plate edge with the zone of the prior PPB (Galatis *et al.* 1984b). The correction of oblique cell plates towards the transversal plane explains the ordered pattern of cells in a file, present in the root cortex of *Vicia faba*. Oud & Nanninga (1992) observed oblique walls and hypothesized that they were the outcome of oblique divisions. When we sectioned longitudinally through the middle of files with many *short* cells, all pairs of daughter cells were separated by transversal walls varying less than 10° from the perpendicular plane; oblique walls were occasionally observed in sections. Since files are roofing over each other in the root cortex, the percentage of oblique walls quickly rose when the root bent or when sections were not parallel to the longitudinal axis of the root. We therefore hereby adjust the model for oblique cell division that was hypothesized by Oud & Nanninga (1992).

Since we have found both PPBs and newly formed walls in transversal position, likely the position of the PPB has determined the division plane. This concept is generally accepted (Wick 1991a,b). We did not study the actin cytoskeleton, but it is known that microfilaments play a role in cell division (Kakimoto & Shibaoka 1987, Lloyd & Traas 1988, Cleary *et al.* 1992, Liu & Palevitz 1992, Mineyuki & Palevitz 1990, Staehelin & Hepler 1996). The role of actin and its associated proteins in the controlled positioning and fusion of the cell plate remains to be elucidated.

ACKNOWLEDGEMENTS

REFERENCES

Bailey, I.W. (1920): The cambium and its derivative tissues. III reconnaissance of cytological phenomena in the cambium. *Am. J. Bot.* 7: 417-434.

Barlow, P.W. & Carr, D.J. (eds.) (1984): *Positional controls in plant development.* Cambridge Univ Press, Cambridge, UK.

Cho, S.O. & Wick, S.M. (1989): Microtubule organization   during stomatal differentiation in grasses. *J. Cell Sc.* 92: 581-594.

Cleary, A.L., Gunning, B.E.S., Wasteneys, G.O. & Hepler, P.K. (1992): Microtubule and F-actin dynamics at the division site in living *Tradescantia* stamen hair cells. *J. Cell Sc.* 103: 977-988.

Cleary, A.L. & Hardham, A.R. (1989): Microtubule organization during development of stomatal complexes of *Lolium rigidum*. *Protoplasma* 149: 67-81.

Dolezel J., Cíhalíková, J. & Lucretti, S. (1992): A high-yield procedure for isolation of metaphase chromosomes from root tips of *Vicia faba* L. *Planta* 188: 93-98.

Flanders, D.J., Rawlins, D.J., Shaw, P.J. & Lloyd, C.W. (1990): Nucleus-associated microtubules help determine the division plane in higher plant epidermal cells: Avoidance of four-way junctions and the role of cell geometry. *J. Cell Biol.* 110: 1111-1122.

Galatis, B., Apostolakis, P. & Katsaros, C. (1984a): Positional inconsistency between preprophase microtubule band and final cell plate during triangular subsidiary cell and atypical hair cell formation in two *Triticum* species. *Can. J. Bot.* 62: 343-359.

Galatis, B., Apostolakis, P. & Katsaros, C. (1984b): Experimental studies on the function of the cortical cytoplasmic zone of the preprophase microtubule band *Protoplasma* 122: 11-26.

Gamborg, O.L., Wetter, L.R, (eds.) (1975): *Plant tissue culture methods*. NRC Saskatoon.

Gunning, B.E.S. (1982): The cytokinetic apparatus: its development and spatial regulation. In: Lloyd C.W. (ed) *The Cytoskeleton in plant growth and development*. Acad. Press, London, 229-292.

Gunning, B.E.S. & Sammut, M. (1990): Rearrangements of microtubules involved in establishing cell division planes start immediately after DNA synthesis and are completed just before mitosis. *Plant Cell* 2: 1273-1282.

Gunning, B.E.S. & Wick S.M. (1985): Preprophase bands, phragmoplasts and spatial control of cytokinesis. *J. Cell Sc. Suppl.* 2: 157-179.

Kakimoto, I. & Shibaoka, H. (1987): Actin filaments and microtubules in the preprophase band and phragmoplast of tobacco cells. *Protoplasma* 140: 151-156.

Lintilhac, P.M. (1984): Positional controls in meristem development. In: Barlow P.W. & Carr D.J. (eds.) *Positional control in plant development*. Cambridge Univ. Press, Cambridge, UK, 83-105.

Liu, B. & Palevitz, B.A. (1992): Organization of cortical microfilaments in dividing root cells. *Cell. Motil. and the Cytoskel.* 23: 252-264.

Lloyd, C.W. (1991): *The cytoskeletal basis of plant growth and form*. Acad. Press, London, UK.

Lloyd, C.W. & Traas, J.A. (1988): The role of F-actin in determining the division plane of carrot suspension cells. Drug studies. *Development* 102: 211-221.

McIntosh, J.R. & Pfarr, C.M. (1991): Mitotic motors. *J. Cell Biol.* 115: 577-585.

Mineyuki, Y. & Gunning, B.E.S. (1990): A role for preprophase bands of microtubules in maturation of new walls, and a general proposal on the function of preprophase band sites in cell division in higher plants. *J. Cell Sc.* 97: 527-537.

Mineyuki, Y. & Palevitz, B.A. (1990): Relationship between preprophase band organization, F-actin and the division site in *Allium*. *J. Cell Sc.* 97: 283-295.

Mineyuki, Y., Marc, J. & Palevitz, B.A. (1988): Formation of the oblique spindle in dividing guard mother cells of *Allium*. *Protoplasma* 147: 200-203.

Mineyuki, Y., Marc, J. & Palevitz, B.A. (1991): Relationship between the preprophase band, nucleus, and spindle in dividing *Allium* cotyledon cells. *J. Plant Phys.* 138: 640-649.

Oud, J.L. & Nanninga, N. (1992): Cell shape, chromosome orientation, and the position of the plane of division in *Vicia faba* root cortex cells. *J. Cell Sc.* 103: 847-855.

Oud, J.L., & Nanninga, N. (1994): The relation between cell size, chromosome length and the orientation of chromosomes in dividing root cortex cells. *Plant and Soil* 167: 23-29.

Oud, J.L., Nickless, E.M. & Rowland, R.E. (1995): Steric hindrance and its effects on chromosome movement in *Vicia faba* somatic cells. *Protoplasma* 188: 192-201.

Palevitz, B.A. (1986): Division plane determination in guard mother cells of *Allium*: video time-lapse analysis of nuclear movements and phragmoplast rotation in the cortex. *Dev. Biol.* 117: 644-654.

Palevitz, B.A. (1993): Morphological plasticity of the mitotic apparatus in plants and its developmental consequences. *The Plant Cell* 5: 1001-1009.

Palevitz, B.A. & Hepler P.K. (1974): The control of the plane of division during stomatal differentiation in *Allium* I Spindle reorientation. *Chromosoma* 46: 297-326.

Pickett-Heaps, J.D. & Northcote, D.H. (1966): Organization of microtubules and endoplasmatic reticulum during mitosis and cytokinesis in wheat meristems. *J. Cell Sc.* 1: 109-120.

Schibler, M.J. & Pickett-Heaps, J.D. (1987): The kinetochore fiber structure in the acentric spindles of the green alga *Oedogonium*. *Protoplasma* 137: 29-44.

Staehelin, L.A. & Hepler, P.K. (1996): Cytokinesis in higher plants. *Cell*, 84: 821-824.

Thompson, D.W. (1945): *On growth and form*. Macmillan, New York.

Traas, J., Bellini, C., Nacry, P., Kronenberger, J., Bouchez, D. & Caboche, M. (1995): Normal differentiation patterns in plants lacking microtubular preprophase bands. *Nature* 375: 676-677.

Van Lammeren, A.A.M. (1988): Structure and function of the microtubular cytoskeleton during endosperm development in wheat: an immunofluorescence study. *Protoplasma* 146: 18-27.

Wada, B. (1965): Analysis of mitosis. *Cytologia* 30 [Suppl]: 93-94.

Wick, S.M. (1991a): Spatial aspects of cytokinesis in plant cells. *Curr. Opin. Cell Biol.* 3: 253-260.

Wick, S.M. (1991b): The preprophase band. In: Lloyd C.W. (ed.) *The cytoskeletal basis of plant growth and form*. Acad. Press, London: 231-244.

- Chapter 2 -

Lipochito-oligosaccharides re-initiate root hair tip growth in *Vicia sativa* with high calcium and spectrin-like antigen at the tip

Norbert C.A. de Ruijter[a], Martin B. Rook[b],
Ton Bisseling[c] and Anne Mie C. Emons[a,*]

[a]*Laboratory of Plant Cytology and Morphology, Wageningen Agricultural University
Arboretumlaan 4, 6703 BD Wageningen, The Netherlands,*
[b]*Department of Medical Physiology and Sports Medicine, University of Utrecht,
Universiteitsweg 100, 3584 CG Utrecht, The Netherlands,*
[c]*Laboratory of Molecular Biology, Wageningen Agricultural University,
Dreijenlaan 3, 6703 HA Wageningen, The Netherlands*

Short title: Lipochito-oligosaccharides re-initiate root hair growth

SUMMARY

Lipochito-oligosaccharides, Nod factors secreted by *Rhizobium* bacteria, are signal molecules that induce deformation of root hairs of their host plant. A bioassay was used for deformation and the cytological changes induced by specific lipochito-oligosaccharides in root hairs of *Vicia sativa* L. (vetch), grown between glass slides, were examined. In the assay, root hairs of a particular developmental stage, those that are terminating growth, are susceptible to deformation. These hairs obtained characteristics of tip growing cells again: *(i)* a polar cytoplasmic organization and reverse fountain streaming, *(ii)* an accumulation of a spectrin-like antigen at the tip, and *(iii)* a tip-focused calcium gradient. Calcium gradients were visualized in Indo-1 loaded root hairs with UV confocal microscopy and ratio imaging. The results show that hairs respond to the bacterial signal by recovering cytoplasmic polarity and exocytosis.

Keywords: calcium, exocytosis, lipochito-oligosaccharide, *Rhizobium* Nodulation factor, root hair tip growth, spectrin.

INTRODUCTION

The rhizobial signal molecules that induce the early steps of legume nodule development are specific lipochito-oligosaccharides called nodulation (Nod) factors (Dénarié and Cullimore, 1993; Spaink and Lugtenberg, 1994). These compounds induce several responses in the epidermis and the cortex of the root (Dénarié and Cullimore, 1993; Fisher and Long, 1992; Long, 1996). Root hair deformation is the most prominent response of root epidermal cells. Root hairs are protrusions of epidermal cells. Their deformation is preceded by depolarization of the plasma membrane (Ehrhardt *et al.*, 1992; Felle *et al.*, 1995; Kurkdjian, 1995) and calcium spiking (Ehrhardt *et al.*, 1996). Deformation is accompanied by the expression of several plant genes such as *ENOD5, ENOD12* (Horvath *et al.*, 1993; Journet *et al.*, 1994), and *Mtrip1* (Cook *et al.*, 1995).

We study Nod factor induced root hair deformation in seedlings that were grown between a slide and a coverslip: a so-called Fåhraeus slide. This allowed continuous microscopic observation of deformation (Heidstra *et al.*, 1994). In this assay, deformation of *Vicia sativa* L. (vetch) root hairs is only induced in the hairs that almost stopped growing (Heidstra *et al.*, 1994). Root hair deformation starts with a swelling of the apex of those hairs. Two hours after Nod factor addition a new tip has emerged from the swelling in 80-90% of these hairs.

Antiserum against chicken or human erythrocyte spectrin recognizes an antigen that is enriched in the growing hyphal tip of the oomycete *Saprolegnia ferax* (Kaminskyj and Heath, 1995). The same antibody recognizes an epitope in tips of growing pollen tubes of tobacco (Derksen *et al.*, 1995). Because we were looking for indicators of tip growth, we tested whether this antigen, which we have observed previously in several young, growing plant tissues (De Ruijter and Emons, 1993), is present in vetch root hairs and correlates with tip growth.

The morphological changes that occur during root hair deformation are similar to those that take place when lily pollen tubes recover from treatment with the calcium chelator BAPTA (Pierson *et al.*, 1994). Microinjection of BAPTA in a growing pollen tube eliminated the cytoplasmic calcium ion concentration ($[Ca^{2+}]_c$) gradient, and resulted in a cessation of tip growth and swelling of the tip. About 30 min after microinjection of BAPTA, the $[Ca^{2+}]_c$ gradient re-established and tip growth resumed. This experiment shows that there is a strict correlation between tip growth and the presence of a tip-focused $[Ca^{2+}]_c$ gradient in tips of growing pollen tubes. Since a tip-focused $[Ca^{2+}]_c$ gradient has also been described for tip growing rhizoids of *Fucus* (Brownlee and Pulsford, 1988; Brownlee and Wood, 1986), fungal hyphae (Garrill *et al.*, 1993; Jackson and Heath, 1993), and *Arabidopsis* root hairs (Gilroy and Wymer, 1995), this correlation appears to be a general characteristic of tip growing cells.

If Nod factors re-initiate tip growth in susceptible hairs, they should cause an increase in the $[Ca^{2+}]_c$ at the site of deformation. However, when Ehrhardt *et al.* (1996) imaged $[Ca^{2+}]_c$ in alfalfa or vetch root hairs after application of host-specific Nod factors, they did not find a tip-focused $[Ca^{2+}]_c$ gradient. These experiments have elegantly shown that Nod factors cause calcium spiking with a mean period of 60 sec, starting approximately 9 min after adding the appropriate Nod factors. The oscillations in $[Ca^{2+}]_c$ typically continued for 20-60 min. These authors used electro-osmotic injection to load the dyes Calcium Green or Fura-2. A reason why a tip-focused $[Ca^{2+}]_c$ gradient did not occur could be a disturbance of cyto-architecture by the injection procedure by which growth stops, which we commonly see, when root hairs of vetch are impaled (personal communication D. Miller). Therefore, we used acid or ester loading of the ratiometric calcium dye Indo-1 (Grynkiewicz *et al.*, 1985). This has the additional advantage that high numbers of root hairs of different developmental stages at the same root can be analyzed. Using this non-invasive approach, we were able to visualize the $[Ca^{2+}]_c$ in all hairs, without affecting growth.

Here we test the hypothesis that root hair deformation induced by lipochito-oligosaccharides, is a re-initiation of tip growth. To do this, a number of cell biological parameters of tip growth were analyzed. We show that the root hairs that are terminating growth first respond by undirected growth, a swelling of the tip. Then, cell polarity is established again and a new tip emerges from the swelling. A spectrin-like antigen accumulates at the site of growth, and the $[Ca^{2+}]_c$ becomes 6 to 10 times higher in the swelling and in the new tip than before application of the signal molecules.

RESULTS

Cyto-architecture of root hairs correlates with susceptibility to deformation by lipochito-oligosaccharides

Considering the developmental stage of root hairs, which correlates with their position on the root, we distinguish three root hair zones (Figure 1a): growing (I), terminating growth (II), and full-grown (III). We compared their cyto-architecture by using differential interference contrast (DIC) microscopy. The growing root hairs of zone I have, just as other tip growing cells, a polar organized cytoplasm (Figure 1b). Transmission electron microscopy has shown that the cytoplasm in these tips contains almost exclusively Golgi vesicles (review Schnepf, 1986). In growing vetch hairs this area is 1-3 µm long (Sherrier and VandenBosch, 1994). In the light microscope a smooth area, the so-called clear zone (cz in Figure 1b) is visible in the tip, but is difficult to distinguish from the subapical area. The subapical area can be up to 40 µm long. It has a dense cytoplasm with organelles such as ER, Golgi bodies, mitochondria, plastids, and small vacuoles, but no large vacuoles. The cytoplasm at the hair tip does not
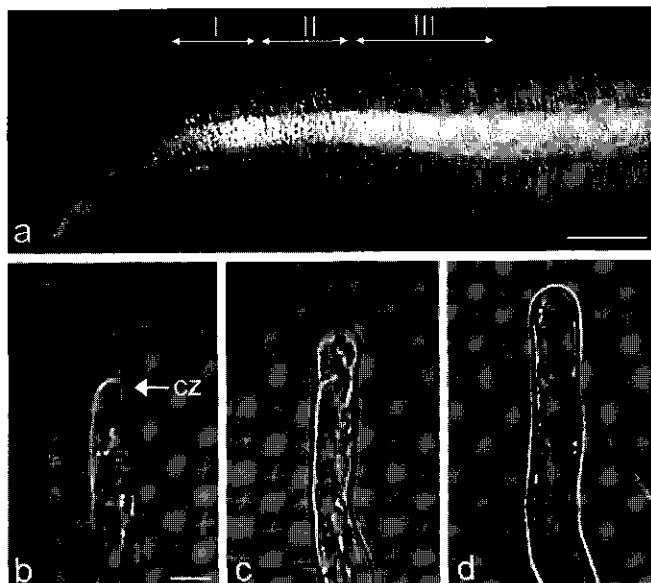
Figure 1. Zones of root hairs on a vetch root can be discriminated by their relative position on the root and by root hair cyto-architecture.

(a) Overview of root hairs on a vetch primary root. The arrows (↔) show the root hair zones I, II and III, from tip to base. Bar equals 1.5 mm.

(b) DIC image of zone I hair with a clear zone at the tip (cz, see arrow), and an area with dense cytoplasm behind the tip. Bar equals 15 μm. (for b, c and d).

(c) DIC image of zone II hair showing vacuoles close to the tip and a short area of dense subapical cytoplasm.

(d) DIC image of zone III hair showing a large central vacuole reaching into the tip.

participate in the flow of cytoplasmic streaming and the direction of streaming reverses before this flow reaches the vesicle-rich area. Although in *Vicia* root hairs, the backward flow is not necessarily in the middle of the cell and may even be located cortically, we call this streaming reverse fountain (see also Shimmen *et al.*, 1995).

In the assay, *Vicia* root hairs of zone II are defined as the hairs that deform by lipochito-oligosaccharides. In these cells large organelles, including vacuoles, are present up to the tip (Figure 1c). The area of dense subapical cytoplasm is less then 10 μm. Cytoplasmic streaming is still reverse fountain, displaying the cytoplasmic polarity of these hairs. These are the hairs that almost stop growing.

The hairs of zone III are full-grown, and characterized by the presence of a large vacuole, which occupies most of the hair and is surrounded by a thin layer of cortical cytoplasm (Figure

1d). These hairs have the rotation type of cytoplasmic streaming, demonstrating the lack of cytoplasmic polarity. The presence of the clear zone and the reverse-fountain type of cytoplasmic streaming are manifestations of cytoplasmic polarity, a prerequisite for tip growth. They are important traits that provide simple criteria to identify the three categories of hairs.

Spectrin-like epitopes occur in growing root hair tips

To check whether the spectrin-like antigen occurs in vetch root hairs and to determine its location, we used antibodies against spectrin from several sources. Anti-chicken erythrocyte spectrin (S1390, Sigma) and anti-human erythrocyte spectrin (S1515, Sigma) antibodies gave the same results. All hairs with clear zones, 80-90% of zone I hairs, of all 35 roots examined, showed distinct labeling in the cytoplasm of the apex (Figure 2a,b). Optical sections, made with the confocal laser-scanning microscope, show a speckled pattern in the clear zone (Figure 3). The 10-20% of hairs of zone I that, by whatever reason, did not have the above described cyto-architecture, lacked the spectrin-like epitope. Immunodepletion

Figure 2. Cytoplasmic polarity and spectrin-like epitopes in vetch root hairs of zone I and II.

(a) and (c) DIC images of a zone I root hair, with a clear zone at the tip.

(b) Fluorescence image of (a) showing abundance of spectrin-like antigen in the tip.

(d) Fluorescence image of (c) showing poor labeling of spectrin-like antigen in the tip after labeling with immunodepleted anti-spectrin.
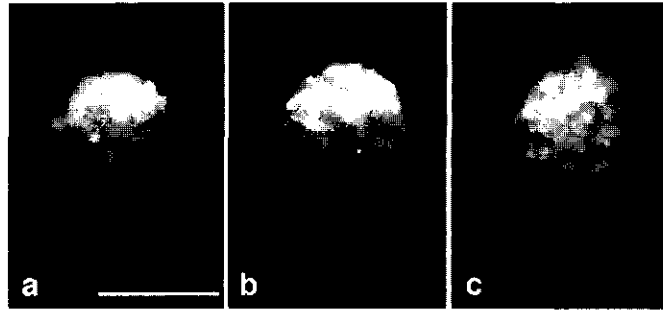
(e) DIC image of a zone II root hair, with large organelles close to the tip.

(f) Fluorescence image of (e) showing little spectrin-like antigen. Bars equal 15 μm.

Figure 3. Optical sections (a - c), 5 µm steps, obtained with the confocal laser scanning microscope through the tip of a growing *Vicia sativa* root hair, labelled with anti-spectrin, showing a speckled pattern in the clear zone. Bar equals 15 µm.

of antibody with pure spectrin before labeling, lowered the signal drastically (Figure 2c,d). All zone II hairs had very low or no labeling (Figure 2e,f). The full-grown hairs of zone III never showed any labeling with anti-spectrin antibody (data not shown). The occurrence of this antigen at the tip of root hairs in fact correlates with tip growth.

Lipochito-oligosaccharides re-initiate tip growth, with spectrin-like epitope at the tip, in root hairs that are terminating growth

The studies described above show that, in our assay, *Vicia* hairs displaying tip growth (zone I) can be distinguished from hairs that have the potential to deform (zone II) by the organization of their cytoplasm and the occurrence of the spectrin-like antigen at their tips. We used these criteria, to test whether lipochito-oligosaccharides re-initiate tip growth in zone II hairs.

Zone II root hairs were examined after replacing the plant growth medium (PGM) with PGM containing 10^{-10} M *Rhizobium leguminosarum* bv *viciae* Nod factor NodRlv-IV (Ac, C18:4). Figure 4 (a-d) shows root hair deformations followed over time. At the periphery of the swelling, cytoplasm accumulated locally, building up a small clear zone (Figure 4b,c). From the clear zone a new tip emerged (Figure 4c,d). This outgrowth resembled a zone I root hair, since at the apex of the outgrowth a clear zone was present (Figures 4d and 5c), devoid of cytoplasmic streaming, and below this clear zone reverse fountain streaming occurred.

At 1 h 15 min and 2 h after lipochito-oligosaccharides application, roots were fixed and labeled with anti-spectrin antibodies. The accumulation of the spectrin-like protein in zone II root hairs started approximately 1 h after application of the signal molecule and always accompanied the onset of swelling of the tip. At 1 h 15 min the apices of 80-90% of these hairs
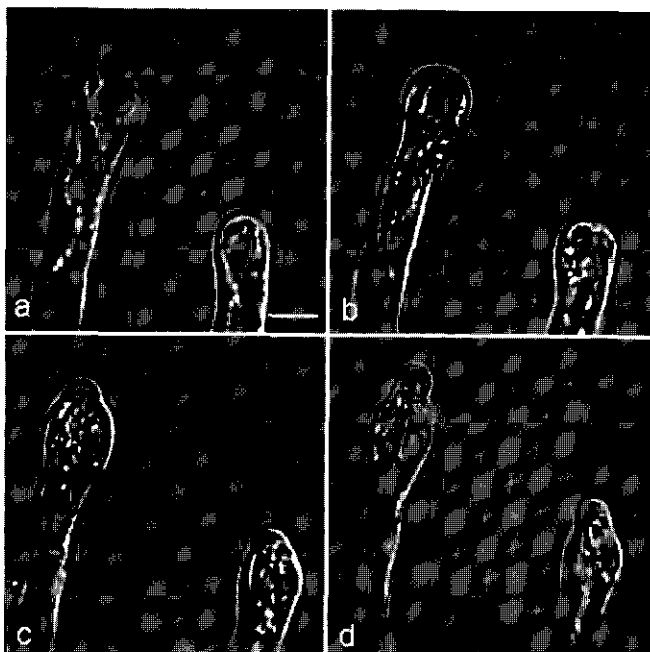
Figure 4.
Time-series showing deformation of zone II hairs after application of
lipochito-oligosaccharides. DIC images of the tips of zone II hairs
(**a**) at 1 h 15 min, (**b**) at 1 h 30 min, (**c**) at 1 h 45 min,
(**d**) at 2 h after application of lipochito-oligosaccharides.
Bar equals 15 µm.

were swollen and the spectrin-like antigen was present at the plasma membrane of the whole
swelling (Figure 5a,b). At 2 h 80-90% of the hairs had the typical deformed appearance, and
the spectrin-like antigen had accumulated at the tip of the outgrowth (Figure 5c,d). Hence,
lipochito-oligosaccharides re-initiate new tip growth in hairs that have reached the
developmental stage in which tip growth stops. None of the responses to lipochito-
oligosaccharides -swelling, building up of a clear zone, reverse fountain streaming, and
accumulation of spectrin-like antigens-, occurred in zone III hairs (data not shown).

Root hair growth is accompanied by a $[Ca^{2+}]_c$ gradient at the root hair tip

To visualize $[Ca^{2+}]_c$ in root hairs, roots were loaded with Indo-1 K^+ salt in PGM acidified
with 2 mM dimethyl-glutaric acid (DMGA) to pH 5.0. In this medium, root hairs were able to
grow and to deform by lipochito-oligosaccharides. After loading for 1 h at 20°C in the dark,
40-50% of all root hairs contained detectable amounts of Indo-1 in their cytoplasm, whereas
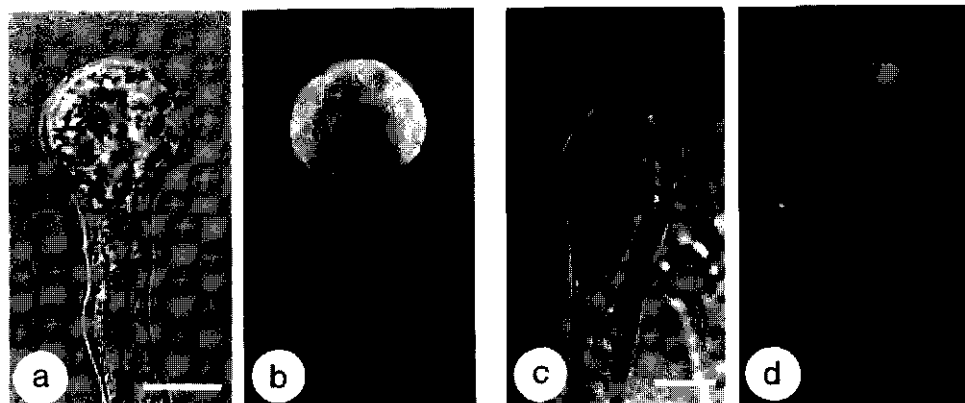
Figure 5. Spectrin-like epitopes accumulate in tips of zone II hairs during deformation after application of lipochito-oligosaccharides. Bars equal 15 μm.

(a) DIC image of a zone II hair after 1 h.

(b) Fluorescence image of (a) showing spectrin-like antigen in the swelling.

(c) DIC image of a zone II hair after 2 h.

(d) Fluorescence image of (c) showing spectrin-like antigen at the tip of the outgrowth.

the dye did not accumulate in the vacuoles. The percentage of the loaded hairs increased with time. After loading, cells were washed and ratio images were made. Settings were chosen such that no autofluorescence was measured and maximal sensitivity achieved. Ratios, obtained when Indo-1 AM ester was loaded into root hairs (not shown), were similar to the ratios obtained when Indo-1 K^+ salt was acid loaded, but dye sequestered into the vacuoles. Ratio-images were made from 100 randomly selected hairs of each zone on 10 roots.

Representative images of the $[Ca^{2+}]_c$ in zone I, II and III root hairs are shown in Figures 6 (a-c) respectively, and Figure 7 shows for each zone percentages of root hair tips, classified for the $[Ca^{2+}]_c$ in the tip. In zone I hairs the $[Ca^{2+}]_c$ was 6 to 10-fold higher at the tip, just below the plasma membrane, than at the base of the hair. The maximal $[Ca^{2+}]$ at the growing tips varied from 1.0 to 2.0 μM (orange-dark red pixels) in 61 % of the hairs to 0.5 to 1.0 μM (yellow-orange pixels) in 34 % of the hairs (Figure 7), whereas the minimal $[Ca^{2+}]_c$, located at the base, was at 0.070 to 0.250 μM (dark blue - dark green pixels) in 80-90% of zone I hairs. The $[Ca^{2+}]_c$ decreased 4 to 10-fold over a distance of 10 μm from the tip. The $[Ca^{2+}]_c$ in the entire zone II hairs was close to that in the base of zone I hairs (Figure 6b), though, occasionally, the $[Ca^{2+}]_c$ at the tip of zone II hairs was up to 3-fold higher than at the base. Zone III hairs never had higher $[Ca^{2+}]_c$ at the tip than in the rest of the hair.

In conclusion, the zone I hairs had a markedly higher $[Ca^{2+}]_c$ at the tip, than zone II and III hairs, showing that root hair growth is indeed correlated with a tip-focused $[Ca^{2+}]_c$.
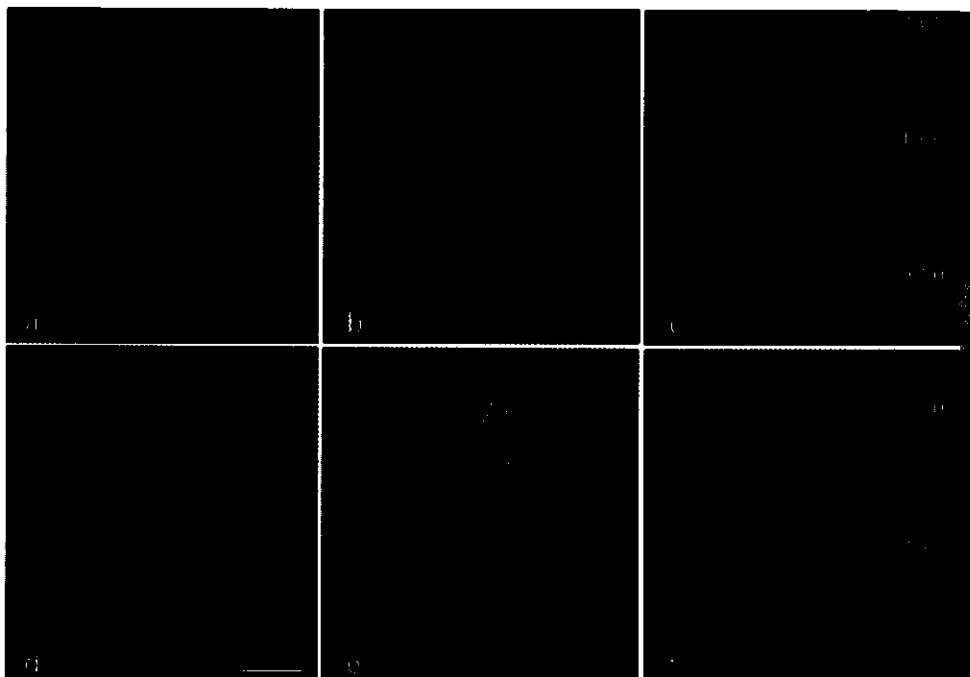
Figure 6. Pseudo-color ratiometric images of median optical sections of $[Ca^{2+}]_c$ in vetch root hairs after acid loading with Indo-1. Ratio values have been calibrated to $[Ca^{2+}]_c$ in µM, as represented by the color bar.

(a) Zone I root hair showing high $[Ca^{2+}]_c$ in red at the growing tip and a steep $[Ca^{2+}]_c$ gradient.

Bar equals 15 µm (for a,b,c).

(b) Zone II hair showing low $[Ca^{2+}]_c$ at the tip and absence of a gradient in the hair. The vacuole is blue.

(c) Zone III hair showing low $[Ca^{2+}]_c$ throughout the cytoplasm.

(d) Zone II hair, 70 min after lipochito-oligosaccharides application, showing high $[Ca^{2+}]_c$ at the plasma membrane of the swelling tip. Note that $[Ca^{2+}]_c$ increased 6-8-fold (compare with (b)).

Bar equals 15 µm (for d,e,f).

(e) Zone II hair, 100 min after lipochito-oligosaccharides induced deformation, just prior to outgrowth of a new tip. Highest $[Ca^{2+}]_c$ is found at the plasma membrane of the swelling in the area of dense cytoplasm.

(f) Zone II hair, 130 min after lipochito-oligosaccharides induced deformation, showing high $[Ca^{2+}]_c$ in the growing tip, emerged from the swelling (compare with (a)).

Root hair deformation by lipochito-oligosaccharides is accompanied by an increase of $[Ca^{2+}]_c$ at the site of growth

If lipochito-oligosaccharides re-initiate growth, their application should cause an increased $[Ca^{2+}]_c$ at the tips of zone II hairs during the deformation process. Therefore, lipochito-oligosaccharides were applied for at least 10 min, after which Indo-1 salt was loaded for 1 h in 2 mM DMGA in PGM at pH 5.0. Changes were recorded in responding hairs at 70, 100 and 130 min after application of the lipochito-oligosaccharides. Roots were washed before scanning, but they were never removed from the slides. Scanning with a UV-beam at 351 nm did not influence growth or response to lipochito-oligosaccharides, but did cause fading of Indo-1 fluorescence within 1-5 min. Therefore, we could image the cells during 1-5 min only. Since the required amount of fluorescence did not recover, Figure 6(d-f) could not be made from one single hair during its deformation, but were made from different hairs at different developmental stages. At 70 and 100 min after application of lipochito-oligosaccharides the $[Ca^{2+}]_c$ was measured in 25 hairs, and after 130 min the $[Ca^{2+}]_c$ was measured in 50 hairs.
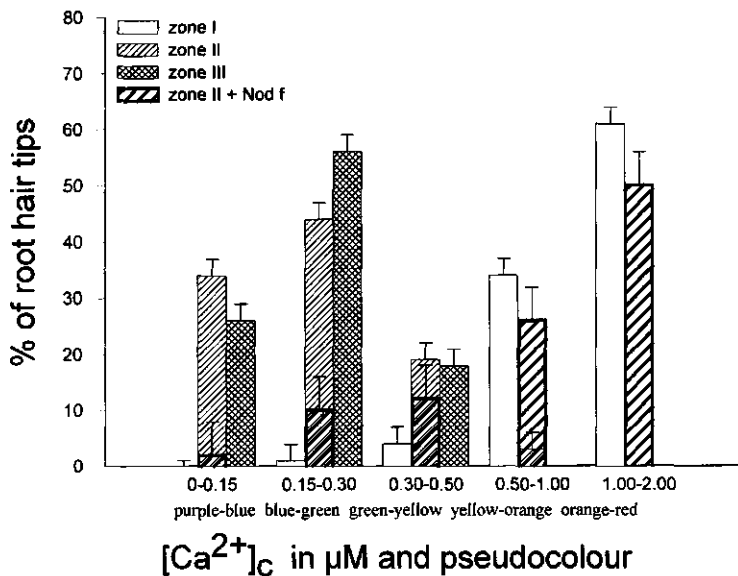
Figure 7. Graph showing the percentage of root hair tips of zone I, II and III, and of zone II at 2 h after Nod factor application (y-axis) with a certain $[Ca^{2+}]_c$ (x-axis). The absolute $[Ca^{2+}]_c$ is expressed in μM and corresponding pseudo-colors similar to the colorbar of Figure 6 (x-axis). The absolute number of root hairs measured in zone I, II and III is 100, and for zone II after deformation is 50.

A representative ratio-image of a zone II hair at 70 min after application of lipochito-oligosaccharides shows elevated $[Ca^{2+}]_c$ in the swelling (Compare Figure 6b with 6d,). Initially, the rise in $[Ca^{2+}]_c$ is along the plasma membrane of the swelling. Often the increase in $[Ca^{2+}]_c$ became more localized on one side of the root hair (Figure 6d). In most hairs the $[Ca^{2+}]_c$ locally increased 6 to 10-fold during the swelling. The $[Ca^{2+}]_c$ at the base of the hair remained low. At 100 min after lipochito-oligosaccharide application, cytoplasm accumulated in an area of the swelling under the plasma membrane. Ratio images through this area showed high $[Ca^{2+}]_c$ (Figure 6e). This cluster of cytoplasm with high $[Ca^{2+}]_c$ was moving and changed its position at the periphery of the swelling for approximately 10 min, before initiating a new tip. At 130 min after application of lipochito-oligosaccharides, a new outgrowth had emerged from the swelling at the site of high $[Ca^{2+}]_c$. At the new tip, a tip-focused $[Ca^{2+}]_c$ gradient was present (Figure 6f), similar to that of zone I hairs (Figure 6a).

Figure 7 gives a quantitative comparison of the maximal $[Ca^{2+}]_c$ in the median optical section of root hairs, with and without application of lipochito-oligosaccharides and shows that Nod factor perception results in a considerable increase of the $[Ca^{2+}]_c$ at the tips of susceptible hairs. An increase of the $[Ca^{2+}]_c$ in tips of zone I hairs was not observed, and zone III hairs never acquired a $[Ca^{2+}]_c$ gradient at their tips after Nod factor application.

DISCUSSION

Here we show for *Vicia sativa* roots growing between glass slides, that deformation of root hairs by lipochito-oligosaccharides is in fact re-initiation of growth in hairs that were terminating growth. The reaction involves *(i)* swelling of the hair tip, a switch from polar to isodiametric growth, and *(ii)* subsequent re-initiation of polar growth from the swelling. That swelling is a growth phenomenon was already indicated by the fact that it requires *de novo* protein synthesis (Vijn *et al.*, 1995). We think that growth re-initiation is the general reaction of legume root hairs to Nod factors, but susceptibility to deformation of zone II hairs may be typical for vetch growing in Fåhraeus slides. In transgenic alfalfa plants carrying fusions between a Nod factor inducible promoter (*ENOD12*) and a reporter gene (*GUS*), Nod factors do elicit transcription of the *ENOD12* gene in root hairs of zone I and even in epidermal cells younger than zone I (Journet *et al.*, 1994). Furthermore, when rhizobia interact with root hairs, most of the deformations and subsequent infections are observed in root hairs of zone I (Kijne, 1992). However, the bacteria may attack the pre-root hair stage, a small bulge on the epidermal cell. In the light microscope, the cyto-architecture of this developmental stage resembles that of zone II; a clear zone is not visible. However, whether a vesicle-rich area is really absent has to be checked by electron microscopy.

The susceptible, zone II, hairs have reverse fountain streaming, showing that they still possess polarity. These hairs are in the developmental program of growth termination. In the root hair deformation assay developed for vetch, their typical cyto-architecture appears to predict their susceptibility for lipochito-oligosaccharides. Moreover, when *Vicia* roots are treated with ethylene inhibitors, the zone I hairs acquire the cyto-architecture as described here for zone II hairs, stop growing, and indeed become susceptible to lipochito-oligosaccharides (Heidstra *et al.*, 1997).

Zone III hairs appear to have lost the ability to respond. Swelling, the first morphological reaction to lipochito-oligosaccharides, is isodiametric growth. This exocytosis process requires the presence or delivery of Golgi vesicles, their incorporation in the plasma membrane, and a flexible cell wall. In our assay, zone III root hairs had no clear zone and no reverse fountain streaming required to build such a zone, and did not reconstitute these after Nod factor application. They also lacked and did not reconstitute, the machinery, of which calcium and spectrin seem to be two of the requirements, to incorporate the vesicles in the plasma membrane. Furthermore, they probably had, as found in other full-grown root hairs (Emons and Wolters-Arts, 1983), a secondary cell wall at the tip, which obstructs expansion, unless it is weakened by enzymes.

In vetch root hairs a spectrin-like antigen is present in the tip of a normally growing root hair, and accumulates in the swelling and tip of the new outgrowth. Spectrin is a large (220-240 kDa) multi-functional protein. It has actin, calmodulin, and PIP_2 binding sites, calcium-binding EF-hand motifs, an *Src* homology 3 (SH3) domain and a pleckstrin motif (Hartwig, 1994; Viel and Branton, 1996). In red blood cells, spectrin is a prominent part of the membrane-associated cytoskeleton (Goodman *et al.*, 1988). The same anti-spectrin antibody that we used also recognizes antigens enriched at the tips of growing hyphae of the oomycete *Saprolegnia ferax* (Kaminskyj and Heath, 1995), and at the tips of growing pollen tubes (Derksen *et al.*, 1995). Spectrin-like proteins also border the plasma membrane of elongating plant cells (De Ruijter and Emons, 1993; Michaud *et al.*, 1991) where exocytosis takes place. Furthermore, they concentrate in purified plasma membrane fractions of young rice root tissue (Faraday and Spanswick, 1993). A pretreatment of the antibody with chicken spectrin reduced the signal in root hair tips, showing that the antibody specifically recognizes a spectrin epitope. This spectrin-like antigen appears to be a good marker for polar growth and is a candidate for a protein involved in exocytosis in plant cells.

We used Indo-1 as Ca^{2+} indicator and found $[Ca^{2+}]_c$ of 160 ± 90 nM at the base, to 1.25 ± 0.75 µM Ca^{2+} in the tips of growing root hairs of vetch (Figure 7). Possibly, the variation of $[Ca^{2+}]_c$ in the tip correlates with the growth speed, but this was not studied. Herrmann and Felle (1995) used Ca^{2+}-selective microelectrodes to measure $[Ca^{2+}]_c$ in root hairs of *Sinapis alba* L., and found $[Ca^{2+}]_c$ of 190 ± 60 nM at the base, to 644 ± 103 nM a few micrometers

31

behind the tip. The concentrations found by direct measurements with a Ca^{2+}-selective microelectrode are believed to be more accurate than those calculated after *in vitro* calibration of a ratiometric calcium dye. Despite the different techniques and root hairs of different origin, the values for $[Ca^{2+}]_c$ are in the same range.

In the vetch root hairs, the high $[Ca^{2+}]_c$ was observed in growing tips (Figure 6a,f), at the swelling edge of a deforming tip (Figure 6d), and in the new outgrowth that emerged from the swelling (Figure 6e). Thus, it appears that the area of highest $[Ca^{2+}]_c$ is strictly correlated with the site of growth. These observations support the hypothesis of calcium-mediated exocytosis (Battey and Blackbourn, 1993; Thiel *et al.*, 1994; Zorec and Tester, 1993).

Ehrhardt *et al.* (1996) have shown that host-specific Nod factors induce calcium oscillations in both alfalfa and vetch root hairs. Our experimental set up did not allow the observation of $[Ca^{2+}]_c$ oscillations for two reasons. First, the earliest calcium images were taken 60 min after lipochito-oligosaccharide application when, in the study of Ehrhardt *et al.* (1996), the frequency and amplitude of spiking were already low. Second, because the fluorescent dye faded within 1-5 min of continuous scanning at 351 nm, images of individual hairs could only be taken during this short period. In this period, calcium spiking with a more than 1-min interval can hardly be detected. On the other hand, Ehrhardt *et al.* (1996) reported that root hairs, that had been injected with indicator dye and in which calcium spiking was observed after application of Nod factors, did not have a calcium gradient at the tip. However, they did not use a confocal microscope. To observe and measure the steep tip-focused calcium gradient in vetch root hairs, we had to use a confocal microscope with a small pinhole that allowed less than 2 μm depth resolution. It is now essential to study whether or not Ca^{2+} spiking and formation of a tip-focused $[Ca^{2+}]_c$ gradient occur in the same hairs and are linked, and to study the cascade, triggered by lipochito-oligosaccharides, that leads to re-initiation of tip growth.

MATERIALS AND METHODS

Plant material

Vicia sativa spp. *nigra* L. (vetch) seeds were surface sterilized in 96% H_2SO_4 for 20 min, extensively washed for 3 h with running water, placed on 1.5% agarose plates, and incubated for at least 3 days at 4°C, followed by 2 days at 20°C in the dark. This procedure synchronized germination.

Root hair deformation assay

Seedlings with approximately 7 mm long roots were transferred to Fåhraeus slides containing plant growth medium (PGM) consisting of 1.36 mM $CaCl_2$, 0.97 mM $MgSO_4$, 1.12 mM, Na_2HPO_4, 1.36 mM KH_2PO_4 and 20 µM Fe citrate, pH 6.5 (modified from Fåhraeus, 1957), and treated as described by Heidstra *et al.* (1994). Each slide contained 5 seedlings. In the assay, PGM was replaced by PGM containing *Rhizobium leguminosarum* bv *viciae* Nod factor (NodRlv-IV (Ac, C18:4)) (Spaink *et al.*, 1991) at 10^{-10} M.

Imaging of root hairs during growth and deformation

Root hairs were examined with DIC microscopy (Nikon Optiphot). Cytoplasmic streaming was recorded with video-microscopy and digital imaging was done with a Panasonic wv-E550 3-CCD camera using a Prysm framegrabber (Synoptics Ltd., Cambridge, UK). Files were contrast enhanced with Adobe Photoshop 3.0 and printed using a Kodak XLS 8600 dye sublimation printer.

Fixation and labeling of spectrin-like antigens

At 0, 70 and 120 min after lipochito-oligosaccharide treatment, root tips were fixed for 1 h at room temperature in freshly prepared 4% paraformaldehyde with 0.1% glutaraldehyde in 50 mM PIPES (pH 6.9) with 5 mM EGTA and 5 mM $MgSO_4.7H_2O$. Cell walls were partially degraded with 0.3% cellulase Onozuka R10 (Serva, Heidelberg, FRG), 0.3% cellulysine (Calbiochem, La Jolla, CA) and 0.3% pectinase (Sigma) in 25 mM 2-N-morpholino-ethane sulfonic acid (MES) (pH 5.8), containing 2 mM phenylmethylsulfonyl-fluoride (PMSF) for 10 min at 30°C. After three washes in MES buffer, cells were extracted with 0.1% Triton X-100 (Surfact-Amps, Pierce, Rockford, IL, USA) and 0.05% Nonidet P-40 (Surfact-Amps, Pierce), containing 2 mM PMSF. Roots were treated with 0.1 M $NH_3(OH)Cl$ in 10 mM PBS, pH 7.2 for 10 min, followed by incubation in freshly prepared 0.05% $NaBH_4$ in PBS for another 10 min and blocked in this buffer with 0.1% (w/v) acetylated BSA (BSA_c) (Aurion, Wageningen, NL) and 0.05% (v/v) Tween-20. The first antibody was directed against chicken erythrocyte α- and β-spectrin (S1390, Sigma) or against human erythrocyte α- and β-spectrin (S1515, Sigma), both raised in rabbit and diluted 1/300 in PBS/BSA_c/Tween-20. The secondary antibody was a goat anti-rabbit IgG, diluted 1/300, conjugated to the fluorochrome Bodipy 503/512 (Molecular Probes Inc., Eugene, OR). Controls were done with pre-immune rabbit serum, or immunodepleted anti-spectrin S1319.

Immunodepletion was done according to Thurston and Henley (1988) by incubating 500 ml prediluted antibody with 10 mg purified human erythrocyte spectrin antigen (Sigma) for 2 h at 4°C. The immunoprecipitate was spun at 12,000 g for 15 min and the supernatant was used for immunolabeling.

Root hairs were examined with a Microphot, a Nikon epifluorescence microscope, equipped with a 100 W Hg lamp and a Nikon 60x PlanApo, NA 1.4 oil objective. For visualization of spectrin-like epitopes, the excitation filter BP 450-490 nm and emission filter BP 520-560 nm were used. For photography exposure times were standardized. Images were recorded on Kodak 400 ASA B/W. Optical sections of 5 μm steps were obtained with a Bio-Rad MRC 600 confocal laser scanning microscope equipped with an Argon-Krypton laser.

Ratiometric measurement of $[Ca^{2+}]_c$

Loading of Indo-1:

Root hairs were loaded at 20°C in the dark, with 20 μM Indo-1 penta-potassium salt (Molecular Probes Inc., Eugene, OR) in PGM, acidified with 2 mM dimethyl-glutaric acid (DMGA) to pH 5.0 (Bush and Jones, 1988). After 1 h acid loading, the Indo-1/DMGA/PGM was removed, and roots were washed in PGM (3 x 0.8 ml for 1 min). Root hair vitality, scored by cytoplasmic streaming and presence of a clear zone in root hairs of zone I, was not affected. To record root hairs during deformation, Indo-1 acid loading started 1 h before ratio imaging, and was preceded by (10, 40 or 70 min of) incubation in 10^{-10} M Nod factor in PGM.

Calibration of $[Ca^{2+}]_c$:

Optics and settings of the system were standardized for proper comparison of the ratio images from different roots and different experiments. The voltages of the photo-multipliers PMT 1 and PMT 2 were set for dark current (black level), maximal gain, laser power and pinhole size. For small pinholes the laser power was set at 60 mW with a voltage ratio of 458/603 for PMT1/PMT2. The minimal value of the ratio (R_{min}) was set at blue-violet color in the cytoplasm at the base of the root hair. The maximal value (R_{max}) was set at a red-purple color in calcium saturated cytoplasm of leaking or damaged root hairs. With these settings, optimal sensitivity was achieved, while control roots were negative, and virtually no autofluorescence was recorded.

To assign pixel color to approximate $[Ca^{2+}]_c$ (see Grynkiewicz *et al.*, 1985), *in vitro* calibration was done with EGTA-containing calcium calibration buffers (Molecular Probes, C3008) and calibration curves were determined with K_d (Indo-1)=250. *In vivo* calibration could not be done since root hairs died and collapsed when combinations of external EGTA at 1-10 mM and the ionophore 4-Bromo A-23187 were applied.

Imaging of $[Ca^{2+}]_c$:

After loading the dye and washing the roots, Fåhraeus slides with intact plants were placed on the stage of a Nikon Diaphot 300 inverted microscope, connected to a Nikon RCM 8000 confocal laser scanning unit, equipped with an Argon UV laser, which excites Indo-1 at 351

nm. Hairs were imaged at video-rate with a Nikon CF Fluor 40x, 1.15 numerical aperture, 0.20-mm working distance, water-immersion objective. Root hair vitality was monitored by cytoplasmic streaming and the presence of cytoplasmic polarity in zone I root hairs.

The wavelength of Indo-1 emission changes from a 405 nm peak at high $[Ca^{2+}]$ to a 485 nm peak at low $[Ca^{2+}]$. High and low Ca^{2+} related emissions were simultaneously recorded with two photo-multiplier detectors and corrected for background and shading. Images were collected in 1 or 2 sec by averaging the ratio of 16 or 32 images, one scan taking 64 msec. With a small pinhole and 2 μm steps in the z-axis, ratio images of sequential optical sections through the root hair were obtained. The ratio images of E(405)/E(485) were displayed in real-time and calculated with Nikon/Osg software; they represent relative $[Ca^{2+}]_c$ in pseudo-colors. Median optical sections through root hair tips were selected and processed with Adobe PhotoShop 3.0. Color prints were made on a Pictrography 3000 (Fujix).

ACKNOWLEDGEMENTS

REFERENCES

Battey, N.H. and Blackbourn, H.D. (1993) The control of exocytosis in plant cells. Tanksley Rev. no. 57. *New Phytologist* 125, 307-308.

Brownlee, C. and Pulsford, A.L. (1988) Visualization of the cytoplasmic Ca^{2+} gradient in *Fucus serratus* rhizoids: correlation with cell ultrastructure and polarity. *J. Cell Sc.* 91, 249-256.

Brownlee, C. and Wood, J.W. (1986) A gradient of cytoplasmic free calcium in growing rhizoid cells of *Fucus serratus*. *Nature* 320, 624-626.

Bush, D.S. and Jones, R.L. (1988) Cytoplasmic calcium and α-amylase secretion from barley aleurone protoplasts. *Eur. J. Cell Biol.* 46, 466-469.

Cook, D., Dreyer, D., Bonnet, D., Howell, M., Nony, E. and VandenBosch, K. (1995) Transient induction of a peroxidase gene in *Medicago truncatula* precedes infection by *Rhizobium meliloti*. *Plant Cell* 7, 43-55.

Dénarié, J. and Cullimore, J. (1993) Lipo-oligosaccharide nodulation factors: A new class of signaling molecules mediating recognition and morphogenesis. *Cell* 74, 951-954.

Derksen, J., Rutten, T., Van Amstel. T., De Win, A., Doris, F. and Steer, M. (1995) Regulation of pollen tube growth. *Acta Bot. Neerl.* 44, 93-119.

De Ruijter, N.C.A. and Emons, A.M.C. (1993) Immunodetection of spectrin antigens in plant cells. *Cell Biol. Int.* 17, 169-182.

Ehrhardt, D.W., Atkinson, E.M. and Long, S.R. (1992) Depolarization of alfalfa root hair membrane potential by *Rhizobium melliloti* Nod factors. *Science* 256, 998-1000.

Ehrhardt, D.W., Wais, R., Long, S.R. (1996) Calcium spiking in plant root hairs responding to *Rhizobium* nodulation signals. *Cell* 85, 673-681.

Emons, A.M.C. and Wolters-Arts, A.M.C. (1983) Cortical microtubules and microfibril deposition in the cell wall of root hairs of *Equisetum hyemale*. *Protoplasma*, 117, 68-81.

Fåhraeus, G. (1957) The infection of clover root hairs by nodule bacteria studied by a simple glass slide technique. *J. Gen. Microbiol.* 16, 374-381.

Faraday, C.D. and Spanswick, R.M. (1993) Evidence for a membrane skeleton in higher plants. *FEBS* 318, 313-316.

Felle, H.H., Kondorosi, E., Kondorosi A. and Schultze, M. (1995) Nod signal-induced plasma membrane potential changes in alfalfa root hairs are differentially sensitive to structural modifications of the lipochitooligosaccharide. *Plant J.* 7, 939-947.

Fisher, R.F. and Long, S.R. (1992) *Rhizobium*-plant signal exchange. *Nature* 357, 655-660.

Garrill, A., Jackson, S.L., Lew, R.R. and Heath, I.B. (1993) Ion channel activity and tip growth: tip-localized stretch-activated channels generate an essential Ca^{2+} gradient in the oomycete *Saprolegnia ferax*. *Eur. J. Cell Biol.* 60, 358-365.

Gilroy, S. and Wymer, C.L. (1995) Cytoplasmic calcium and root hair growth and development in *Arabidopsis thaliana*. *Royal Micr. Soc. Proc.* 30, 13-14.

Goodman, S.R., Krebs, K.E., Whitfield, C.F., Riederer, B.M. and Zagon I.S. (1988) Spectrin and related molecules. *CRC Crit. Rev. Biochem.* 23, 171-234.

Grynkiewicz, G., Poenie, M. and Tsien, R.J. (1985) A new generation of Ca^{2+} indicators with greatly improved fluorescence properties. *J. Biol. Chem.* 260, 3440-4350.

Hartwig, J. (1994) Subfamily 1 :the spectrin family. In *Protein Profile, Actin binding proteins 1: spectrin superfamily* (Sheterline, P., ed.), Vol. 1, issue 7. London: Academic Press, pp. 715-740.

Heidstra, R., Geurts, R., Franssen, H., Spaink, H.P., Van Kammen, A. and Bisseling, T. (1994) Root hair deformation activity of Nod factors and their fate on *Vicia sativa*. *Plant Physiol.* 105, 787.

Heidstra, R., Yang, W.C., Yalcin, Y., Peck, S., Emons, A.M.C., Van Kammen, A. and Bisseling, T. (1997) Ethylene provides positional information on cortical cell division but is not involved in Nod factor-induced tip growth in *Rhizobium* induced nodulation. *Development.* 24, 1781-1787.

Herrmann, A. and Felle, H.H. (1995) Tip growth in root hair cells of *Sinapis alba* L.: significance of internal and external Ca^{2+} and pH. *New Phytol.* 129, 523-533.

Horvath, B., Heidstra, R., Lados, M., Moerman, M., Spaink, H.P., Promé, J.C., Van Kammen, A. and Bisseling, T. (1993) Lipo-oligosaccharides of *Rhizobium* induce infection related early nodulin gene expression in pea root hairs. *Plant J.* 4, 727-733.

Jackson, S.L. and Heath, I.B. (1993) Roles of calcium ions in hyphal tip growth. *Microbiol. Rev.* 57, 367-382.

Journet, E.P., Pichon, M., Dedieu, A., De Billy, F., Truchet, G. and Barker, D.G. (1994) *Rhizobium meliloti* Nod factors elicit cell-specific transcription of the *ENOD12* gene in transgenic alfalfa. *Plant J.* 6, 241-249.

Kaminskyj, S.G.W. and Heath, I.B. (1995) Integrin and spectrin homologues and cytoplasm-wall adhesin in tip growth. *J. Cell Sci.*, 108, 849-856.

Kijne, J. (1992) The Rhizobium infection process. In *Biological Nitrogen Fixation*, (Stacy, G., Burris, R. H. and Evans, H.J. eds.) New York: Chapman and Hall, pp. 349-398.

Kurkdjian, A.C. (1995) Role of the differentiation of root epidermal cells in Nod factor (from *Rhizobium meliloti*)-induced root-hair depolarization of *Medicago sativa*. *Plant Physiol.* 107, 783-790.

Long, S.R. (1996) *Rhizobium* symbiosis: Nod factors in perspective. *Plant Cell* 8, 1885-1898.

Michaud, D., Guillet, G., Rogers, P.A. and Charest, P.M. (1991) Identification of a 220 kDa membrane-associated plant cell protein immunologically related to human ß-spectrin. *FEBS* 294, 1-2, 77-80.

Pierson, E.S., Miller, D.D., Callaham, D.A., Shipley, A.M., Rivers, B.A., Cresti, M. and Hepler, P.K. (1994) Pollen tube growth is coupled to the extracellular calcium ion flux and the intracellular calcium gradient: effect of BAPTA-type buffers and hypertonic media. *Plant Cell* 6, 1815-1828.

Schnepf, E. (1986) Cellular polarity. *Annu. Rev. Plant Physiol.* 37, 23-47.

Sherrier, D.J. and VandenBosch, K.A. (1994) Secretion of cell wall polysaccharides in *Vicia* root hairs. *Plant J.* 5, 185-195.

Shimmen, T., Hamatani, M., Saito, S., Yokota, E., Mimura, T., Fusetani, N. and Karaki, H. (1995) Roles of actin filaments in cytoplasmic streaming and organization of transvacuolar strands in root hair strands of *Hydrocharis*. *Protoplasma* 185 (3-4), 188-193.

Spaink, H.P., Sheely, D.M., Van Brussel, A.A.N., Glushka, J., York, W.S.T., Geiger, O., Kennedy, E.P., Reinhold, V.N. and Lugtenberg, B.J.J. (1991) A novel highly unsaturated fatty acid moiety of lipo-oligosaccharides signals determines host specificity of *Rhizobium*. *Nature* 354, 125-130.

Spaink, H.P. and Lugtenberg, B.J.J. (1994) Role of rhizobial lipo-chitin oligosaccharide molecules in root nodule organogenesis. *Plant Mol. Biol.* 26, 1413-1422.

Thiel, G., Rupnik, M. and Zorec, R. (1994) Raising the cytosolic Ca^{2+} concentration raises the membrane capitance of maize coleoptile protoplasts: Evidence for Ca^{2+} -stimulated exocytosis. *Planta* 195, 305-308.

Thurston, C.F. and Henley, L.F. (1988) Direct immunoprecipitation of protein. In *Methods in molecular biology*, Vol. 3, New protein techniques (Walker, J.M., ed). ISBN 89603-126-8. Clifton, New Jersey, USA: Humana Press, pp. 149-158.

Viel, A. and Branton, D. (1996) Spectrin: on the path from structure to function. *Curr. Opin. Cell Biol.* 8, 49-55.

Vijn, I., Martinez-Abarca, F., Yang, W.C., Das Neves, L., Van Brussel, A., Van Kammen, A. and Bisseling, T. (1995) Early nodulin gene expression during Nod factor induced processes in *Vicia sativa*. *Plant J.* 8, 111-119.

Zorec, R. and Tester, M. (1993) Cytoplasmic calcium stimulates exocytosis in a plant secretory cell. *Biophys. J.* 63, 864-867.

- Chapter 3 -

Immunodetection of spectrin antigens in plant cells

Norbert de Ruijter and Anne Mie Emons

Department of Plant Cytology and Morphology, Wageningen Agricultural University, Arboretumlaan 4, 6703 BD Wageningen, The Netherlands.

Short title: Spectrin antigens in plant cells

SUMMARY

The occurrence of spectrin in plant cells was studied by Western blotting of extracts, and its localization by immunolabeling of cells, using two polyclonal antibodies raised against spectrin from human and chicken erythrocytes. A variety of plant cells was studied. The two antibodies gave the same results on blots as well as on cells. Western blots of extracts showed weak immunolabeling at 220 kD, where spectrin can be expected, but bands at 85 kD stained more heavily. Because the latter bands were also seen on blots with commercial purified spectrin, we conclude that they are breakdown products of spectrin. Native plant extracts on blots from IEF gels showed a band at pI 4.8, where the purified animal spectrin is also found. Immunolocalizations done on whole cells, PEG-, BMM-, or cryo-sections gave similar date. In most cells the labeling was localized predominantly at the plasma membrane, especially of thin-walled cells. Labeling was also seen in the periphery of a particular class of organelles, probably plastids. This labeling was tissue specific in maize somatic embryos. During carrot somatic embryogenesis a cytoplasmic labeling was observed depending on the developmental stage. Many cells with cytoplasmic labeling also had stained nuclei. Labeled nuclei had more condensed chromatin than non-labeled nuclei.

Keywords: actin-associated protein, immunocytochemistry, membrane cytoskeleton, plant cells, spectrin antigens, immuno-blotting.

Abbreviations:
anti-sp C.= anti-human erythrocyte spectrin from Calbiochem
anti-sp S.= anti-chicken erythrocyte spectrin from Sigma
BMM = butyl-methyl methacrylate
DAB   = diaminobenzidine
DIC   = differential interference contrast
FITC = fluoresceine-isothiocyanate
GaR   = goat anti-rabbit
hrp   = horseradish peroxidase
MtSB = microtubule stabilizing buffer
MS   = Murashi & Skoog
PEG   = poly-ethylene glycol
PEM   = pro-embryogenic mass
PM   = plasma membrane

INTRODUCTION

The cortical cytoskeleton in plant cells is thought to function in cell expansion processes, and in elongating cells microtubules might be involved in the deposition of cellulose microfibrils (Emons *et al.*, 1992), but we know even less about the tubulin- and actin-associated cortical network which determines the function of these filamentous proteins.

One of the important structural proteins of this network in animal cells is spectrin. Spectrin and fodrin (non-erythrocyte spectrin) are thought to be ubiquitous in animal cells, since this protein, which is abundantly present in erythrocytes has also been found in numerous non-erythroid tissues (Burridge *et al.*, 1982; Bennett, 1990). Together with actin and a number of membrane-associated proteins, spectrin in animal cells forms the so-called membrane skeleton. This meshwork on the cytoplasmic surface of the plasma membrane (PM) is anchored to integral membrane proteins of the PM and forms a dynamic structure that functions in maintaining shape and mechanical properties of red blood cells (Moon and McMahon, 1990). Spectrin is involved in the regulation of vesicle membrane interactions (Bennett, 1990) and in the Ca^{2+}/calmodulin regulated coupling of plasma membrane proteins to actin (Tanaka *et al.*, 1991), and it mediates signal transduction through interactions with extracellular proteins via integrins (Burridge *et al.*, 1988). Spectrin molecules are not only cross-linked at their ends, but also coupled as heterodimers side to side (Speicher *et al.*, 1992). In plant cells spectrin-like antigens have also been found (Wang and Yan, 1988, 1991) and have been shown to be localized at the plasma membrane in tomato leaf cells (Michaud *et al.*, 1991).

We investigated the occurrence of spectrin in various plant cells and tissues by immuno-blotting and its cellular localization by immunocytochemistry, using two polyclonal antibodies raised against spectrin from human and chicken erythrocytes. Immunodetection in cells was done after various fixation and embedding procedures. The plant materials studied included potato protoplasts, single cells, cell clusters and developmental stages of carrot somatic embryos, maize zygotic embryos, maize callus and root tips of maize and bean.

MATERIALS AND METHODS

Plant tissues

Protoplasts were isolated from leaves of 3-6 weeks old potato plants (*Solanum tuberosum* cv. SVP-11). The protoplasts were prepared as described by Puite and coworkers (1986), and immobilized on glass-slides in a thin layer of 0.8% low melting point agarose in Murashige and Skoog medium (Van der Valk *et al.*, 1988). Suspension cultures of carrot (*Daucus carota* L.) were maintained as described by De Vries and coworkers (1988). At 4 to 5 days after induction of somatic embryogenesis, different size-fractions were obtained by sieving the suspension over

nylon meshes. Single cells (passing 50 μm), pro-embryogenic masses (PEMs) and globular stage somatic embryos (fraction 50-125 μm) and various developmental stages of somatic embryos (125-200 μm; 200-300 μm) were used. Immature zygotic maize (*Zea mays* L.) embryos were excised from kernels at 10 to 12 days after pollination (Van Lammeren, 1986). Embryogenic calli of *Zea mays* L. were obtained as described by Emons and Kieft (1991). Maize seeds were incubated for 3 days at 24°C on moistened paper in the dark. Seedlings of bean with primary roots about 2 cm long were incubated another 3 days in aerated water at 24°C in the dark, until secondary roots were formed.Primary root tips from germinating seeds from maize and secondary root tips from bean (*Vicia faba* L.) were cut off at 2-3 mm.

Antibodies

Two affinity-purified, polyclonal antibodies were used. Primary antibodies were either rabbit anti-human erythrocyte spectrin (Calbiochem, Art.nr. 567622) coded anti-sp.C or rabbit anti-chicken erythrocyte spectrin (Sigma, Art.nr. S-1390) coded anti-sp.S. In controls the primary antibody was omitted or changed for a rabbit poolserum, diluted 1/20. Secondary antibodies were goat-anti-rabbit-IgG-Bodipy 503/512 (Molecular Probes, Eugene, U.S.A.) or goat-anti-rabbit-FITC.

Protein extraction and gel electrophoresis

Embryogenic calli of maize, 5-10 mm root tips of maize and PEMs and globular stage somatic embryos (fractions 50-125 μm) from carrot culture were selected for protein extraction. Samples were ground in liquid nitrogen and thawed in a spectrin extraction buffer (0.3 mM TRIS-HCl, pH 8.0, 0.1 mM EDTA, 1mM dithiothreitol (DTT), 1 mM phenylmethylsulfonyl-fluoride (PMSF), 3% w/v polyvinyl-pyrrolidone (PVP), 2 mg/ml each of leupeptin, pepstatin and antipapain, ratio fresh weight (g) to buffer (ml) was 1:3. After 30 minutes at 4°C the extract was centrifuged at 20,000 x g and a clear supernatant was collected. The proteins were precipitated in cold acetone (-20°C) for 1 hour and pelleted at 20,000 x g. Protein pellets were either dissolved in SDS-buffer or in focussing buffer. SDS-samples were prepared by boiling the acetone pellet for 3 minutes in 2% SDS and 5% ß-mercapto-ethanol in 60 mM TRIS-HCl, pH 6.8 and denatured proteins were separated on SDS-gels. Native protein samples were prepared by dissolving the acetone pellet in focussing buffer of low ionic salt (1 mM TRIS-HCl, pH 7.4, 0.1 mM EDTA, 1 mM DTT). SDS-gels (Phastgel gradient 4-15%) and isoelectric focussing gels (Phastgel IEF pH 4-6.5) were run on the PhastSystem (Pharmacia), an automatic electrophoresis device. Parallel to plant extracts, purified human erythrocyte spectrin (Sigma, Art.no. S3644), was run as a reference.

Western blotting

After electrophoresis, gels were equilibrated in transfer buffer (25 mM TRIS, 192 mM glycine and 5% methanol) for 5 minutes (IEF-gels) or 15 minutes (SDS-gels) and proteins were semidry electroblotted with a PhastTransfer Unit (Pharmacia) (for 8.0 AVh) to PVDF-membranes (0.45 µm Immobilon-Millipore). The Western blots were labeled with an anti-spectrin diluted 1:1500 and horseradish-peroxidase (hrp) secondary antibody, diluted 1:2500 in TBST (10 mM TRIS-HCl, buffered to pH 8.0, 150 mM NaCl Saline, 0.05% Tween-20). Chromogenic development in freshly prepared hrp-substrate (0.05 M TRIS-HCl, pH 7.6, 1.4 mM DAB, 10.3 mM imidazol and 0.03 % H_2O_2) was employed, to visualize antibody-antigen complexes.

Fixation and embedding

All samples were fixed for 1 hour at room temperature in 4% paraformaldehyde (with or without 0.1% glutaraldehyde) in microtubule stabilizing buffer (MtSB: 50 mM PIPES, pH 6.9, 5 mM EGTA, 5 mM $MgSO_4.7H_2O$). After washing 3 times for 10 minutes in this buffer, potato protoplasts were detergent extracted and labeled while immobilized in the agarose matrix. Extraction was done with 0.05% Triton X-100 in MtSB to enhance antibody accessibility. Single cells and small cell clusters of carrot were partially wall digested at 24°C, with 1% cellulase Onozuka R-10 and 0.25% pectinase in digestion buffer (0.1 M MES buffer, pH 6.0, 0.2 M mannitol, 80 mM $CaCl_2$ and 0.005% n-propyl-gallate). Cells were concentrated at 10 x g and washed three times in digestion buffer. Subsequently protein extraction of the cells was done with non-ionic detergents, as described for potato protoplasts and cells were immunolabeled. Other single cells and clusters were prepared for embedding, and were labeled after sectioning. Carrot PEMs and globular stage somatic embryos were sucrose-infused for cryomicrotomy stepwise as described by Sanchez-Pina and coworkers (1989). Samples were mounted on stubs, quickly frozen in liquid propane and stored in liquid nitrogen. Carrot and maize embryos and maize and bean root tips were gradually dehydrated in ethanol and embedded in polyethyleneglycol (PEG) according to Van Lammeren (1986). Maize root tips were dehydrated and embedded in butyl-methyl methacrylate (BMM) (Gubler *et al.*, 1989).

Sectioning and immunolabeling

BMM-sections of 1-3 µm thickness were placed on drops of water to stretch. Wrinkles in the resin were removed by holding a chloroform-saturated cotton swab near the surface of the section. To affix the sections to the slides, either the slides had been coated with 0.1% poly-L-lysine or with silane (2% aminopropyl-triethoxysilane in 100% ethanol). Sections were briefly baked on the slides on a 60 °C stretching plate. The methacrylate resin was removed from the sections by dissolving it in 100% acetone. Slides were washed three times for 10 minutes in

43

acetone with agitation, followed by rehydration in PBS (137 mM NaCl, 2.7 mM KCl, 7 mM Na$_2$.HPO$_4$, 1.5 mM KH$_2$PO$_4$, pH 7.3). PEG sections were stretched in a platinum wire loop with 40% PEG 6000 and also put on poly-L-lysine or silane coated slides. Subsequently, the PEG was removed from the sections by dissolving in PBS. To reduce free aldehydes and quench autofluorescence of the tissue, sections were incubated for 10 min in 0,1 M NH$_3$(OH)-HCl in 0.1 M PBS and proteins were blocked with 1% acetylated BSA (Aurion, Wageningen, The Netherlands) in 0.1 M PBS before immunolabeling. Labelings were done in 0.1% acetylated BSA at various conditions of antibody concentration, temperature and duration of labeling.

Microscopy

After extensive washings, cells were counter-stained with the DNA-specific fluorochrome 4,6-diamidino-2-phenylindole (DAPI) (1 μM.ml^{-1}). Sections were mounted in Citifluor in glycerol (Citifluor Ltd., London) to reduce fading. Image contrast was visualized with Nomarski optics. Immunostaining was visualized with a Nikon Microphot fluorescence microscope equiped with a 100 W Hg lamp. An excitation filter BP 450-490 nm and an emission filter BP 520-560 nm for FITC or Bodipy 503/512 labels were used. DAPI stained images were obtained with excitation filter 360/10 nm and emission filter 400/420 nm. Photographs were recorded on Kodak 400 ASA B/W film.

RESULTS

Protein extraction and immunoblotting

Plant tissue extracts were prepared at alkaline and low salt conditions, optimal for spectrin extraction (Kasturi *et al.*, 1983, Michaud *et al.*, 1991). Plant proteins were concentrated and partially purified with acetone precipitation (-20°C). Proteolytic breakdown could be inhibited with the chelating agent and enzymes described in the methods' section.

All steps were registered on silver stained SDS 4-15% gradient gels, as shown in Figure 1, A2-A4. Human erythrocyte spectrin served as a reference and, as described by Kasturi *et al.* (1983), the α/β-spectrin polypeptides, with molecular weights of 240 and 220 kD respectively, migrated as a tight doublet of bands (Fig. 1, A1). To facilitate the transfer of high molecular weight proteins from the SDS gels to the PVDF membranes, the protein mobility was raised by lowering the methanol concentration from 20% (standard) to 5% (Millipore Bioforum nr 1, 5-6). Figure 1, A'1 shows the α and β spectrin subunits after immunoblotting with anti-human erythrocyte spectrin and chromogenic peroxidase detection of the conjugate. Despite the selected conditions preventing protein degradation, only weak or no bands were seen at 240/220
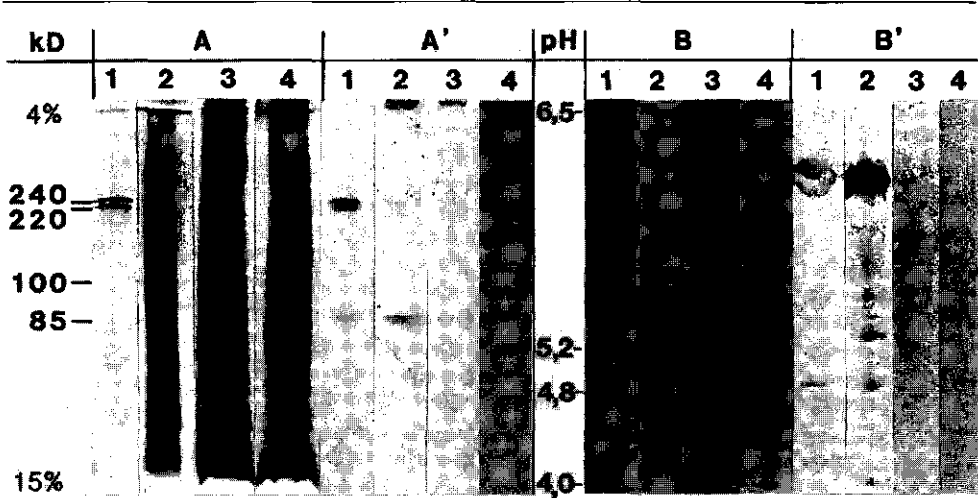
Figure 1. Lanes A and A' show silver staining (A) and Western blotting (A') of protein extracts run on 4-15% SDS-PAGE gels. Lanes B and B' show silver staining (B) and Western blotting (B') of native proteins run on 4-6.5 IEF-gels. Focussing gels were loaded centrally (lanes B), at the cathodal side (lanes B' 1,2) or in between (lanes B' 3,4). Western blots (A' and B') were labeled with anti-spectrin C. 1/1500 and GaR-hrp 1/2500 and bands were visualized with DAB/H_2O_2 at pH 7.6.

Lane 1: Purified human erythrocyte spectrin.

Lane 2: Protein extract of PEM sieve-fraction of carrot culture.

Lane 3: Protein extract of embryogenic callus of maize culture.

Lane 4: Protein extract of 5-10 mm long root tips of maize.

kD in plant extracts (Fig. 1, lanes A2-A4, A'2-A'4). However, in all samples, including the purified human spectrin, a specific immunoreaction could be seen at 85 kD (Fig. 1, A'1-A'4). In maize root tip extract, labelings were found at 100 kD, 85 kD and lower (Fig. 1, A'4). Native proteins were separated and silverstained on focussing gels of pH 4.0-6.5 as shown in Figure 1, B. The immunolabeling on the corresponding Western blot is shown in Figure 1, B'. When using concentrated protein samples (> 1 mg/ml), some precipitation often occurred at the site where the sample was loaded (Fig. 1, lane B2, B'2, B'3). Due to glycerol in the purified spectrin sample some background staining occurred where the sample was loaded, but specific labeling of human spectrin was found at its IEP of 4.8 (Fig. 1, lane B'1). Also in PEMs of carrot (lane B'2), embryogenic callus of maize (lane B'3), root tips of maize (lane B'4) and other plant tissues (not shown) specific labeling was seen on immunoblots from focussing gels. At high protein loading not only at pH 4.8 but also at pH 5.2 a band was seen in the extract of carrot PEMs (Fig. 1, B'2).
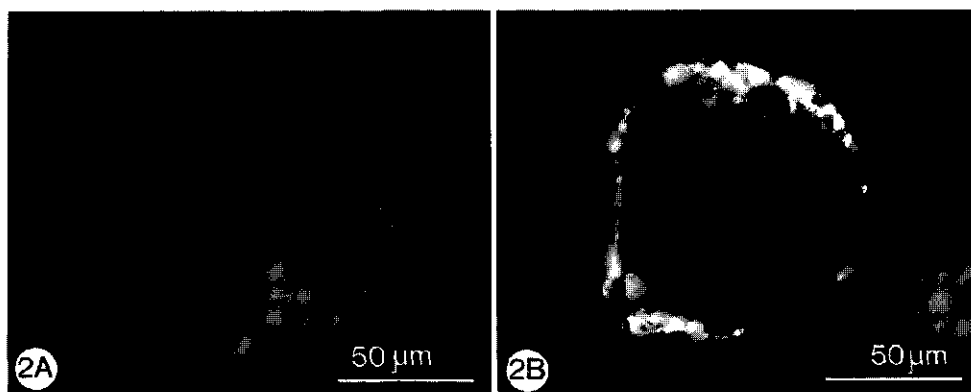
Figure 2A and 2B are images of intact (Fig. 2A) and damaged (Fig. 2B) protoplasts of potato showing labeling with anti-spectrin C. 1/80 predominantly at the plasma membrane (PM).

Immunocytochemistry

Protoplasts from potato leaves showed a clear labeling at the plasma membrane (Figs. 2A, B). Cells with few or no chloroplasts, like the mesophyl cells, were selected for photographs. Anti-spectrin S. (diluted 1/80) and anti-spectrin C. (diluted 1/80) gave similar localization. Strong labeling was found, when the protoplast was slightly damaged (Fig. 2B). Only weak labeling was found, when glutaraldehyde (0.1%) was used or when detergent extraction was omitted. In general, lower signal and higher autofluorescence were seen, when glutaraldehyde was used. All data shown were obtained from specimens fixed with 4% paraformaldehyde only.

Single cells from carrot suspension strongly exhibited a labeling for spectrin, lining the plasma membranes (Fig. 3). Damaged, degenerating and dead cells, as judged from DIC and DAPI-stained images, did not show fluorescence. Also control labelings were negative. Enzymatic wall breakdown for only 10 minutes followed by mild detergent extraction for 5 minutes was sufficient to permit labeling (Fig. 3). Similar images with higher resolution were obtained when cryo-sections of carrot suspension cells (Fig. 4) or PEG-sections (not shown) were labeled.

Fig. 3 (right) shows single elongated cells of carrot suspension, strongly labeled at the PM with anti-spectrin C. 1/100, after partial wall digestion and extraction; dead cells do not label; nuclei show weak autofluorescence

Fig. 4 shows suspension cells of an embryogenic carrot culture after cryo-sectioning and labeling with anti-spectrin C. 1/100; arrow indicates negative cell wall.
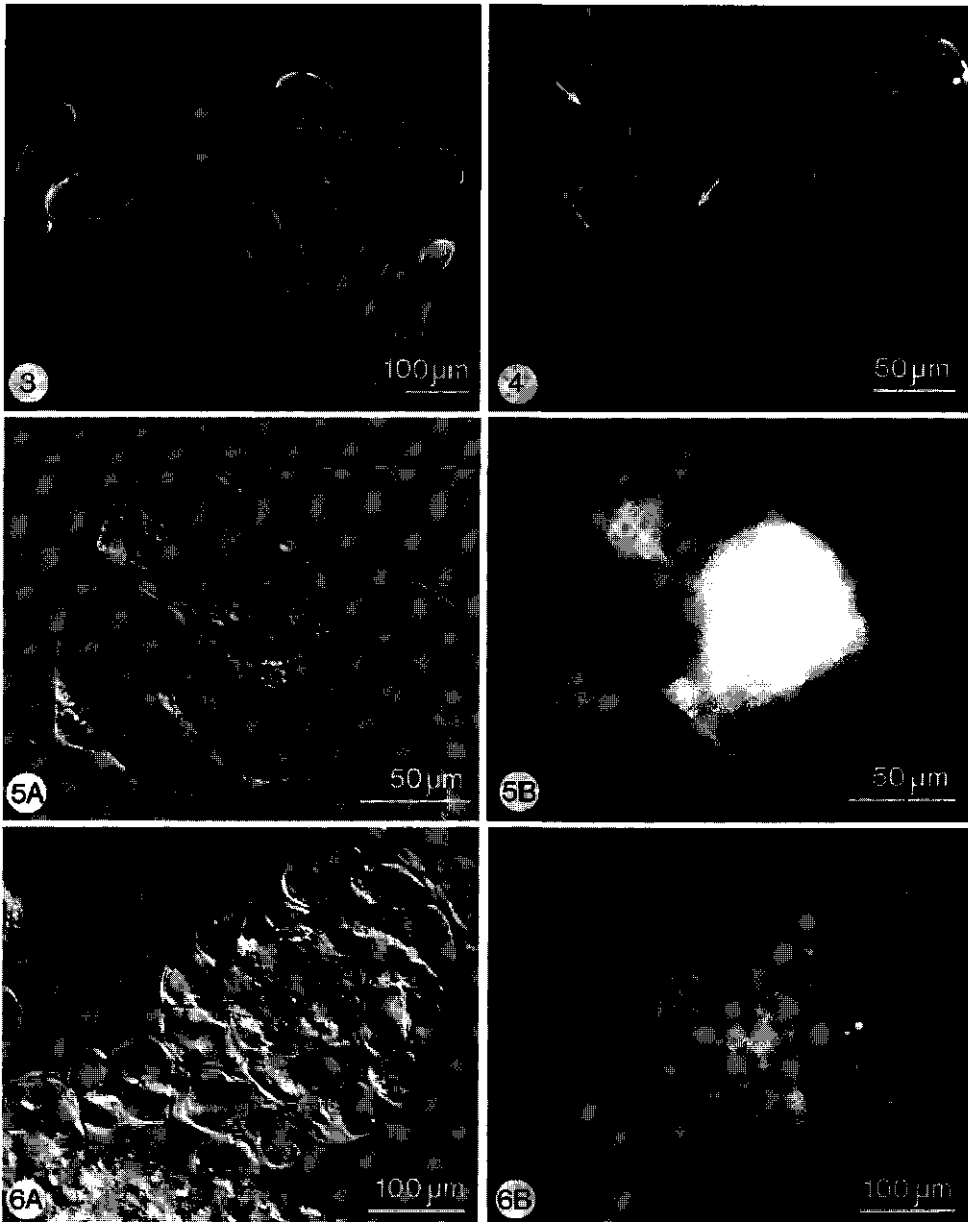
Fig. 5A is a Nomarski image of a small carrot cell cluster after partial wall digestion and extraction.
Fig. 5B is the corresponding fluorescence image after labeling with anti-spectrin C. 1/80, showing bright staining of cytoplasmic dense cell in center; plasma membranes and plastid membranes are labeled.
Fig. 6A is a Nomarski image of pro-embryogenic mass (PEM) of carrot after partial wall digestion and extraction.Fig. 6B is the corresponding fluorescence image, after labeling with anti-spectrin S. 1/160; PMs are labeled and cytoplasm is slightly stained.
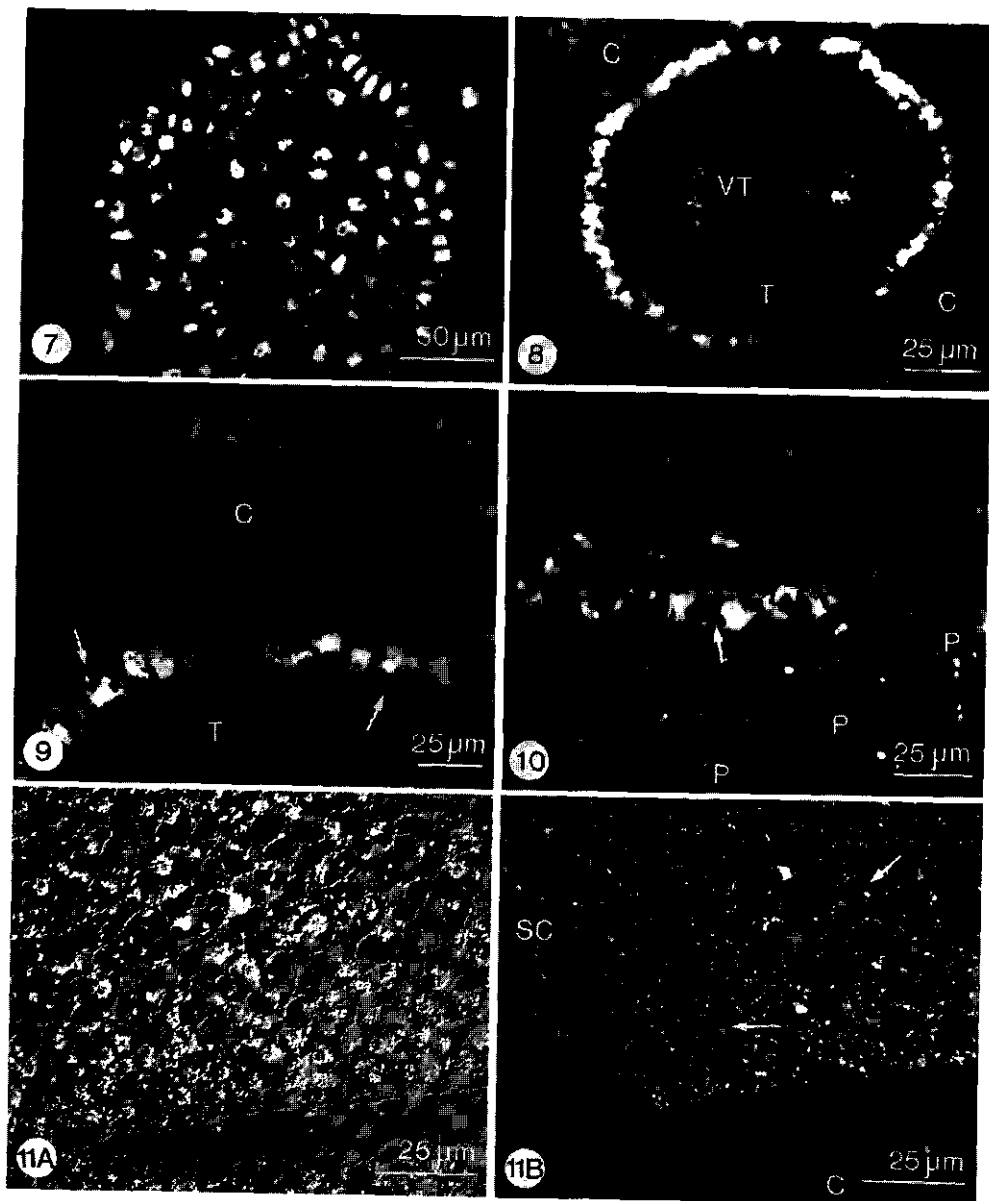
During somatic embryogenesis of carrot, various spectrin distributions were found. In pro-embryogenic masses a plasma membrane labeling was found (Figs. 5B and 6B) as described above for single cells of carrot suspensions (Figs. 3 and 4). Some cells, however, were strongly labeled throughout the cytoplasm (Fig. 5B). In globular stage somatic embryos, plasma membranes and nuclei were labeled (Fig. 7), especially in the protoderm. In general, when

Fig. 7 (left) is an immunofluorescence image of a globular stage somatic embryo of carrot, after cryo-sectioning and labeling with anti-spectrin C. 1/25, showing weak labeling at the PM and strong nuclear labeling; nucleoli are negative.

Fig. 8 is an immuno fluorescence image of a torpedo shaped somatic embryo of carrot embedded in PEG, cross-sectioned, and labeled with anti-spectrin C. at 1/80; epidermal cells show strong labeling at the PM, in the cytoplasm and in nuclei. C indicates a section through callus tissue. The color of the autofluorescence in the vascular tissue (VT) is distinct from FITC-conjugate fluorescence.

Fig. 9 is a detail of figure 8; arrows indicate PM-labeling in the epidermal cells; C is a section through callus tissue.

Fig. 10 show epidermal cells of torpedo shaped somatic embryo of carrot in longitudinal section with labeling in cytoplasmic strands (arrow); subepidermal cell layers show labeled plastids (P).

Fig. 11A shows a Nomarski-image of a PEG-section of the scutellum (SC) and coleoptile (C) of a zygotic maize embryo; epidermal cells contain only small plastids; arrow indicates amyloplasts.

Fig. 11B is the corresponding fluorescence image after labeling with anti-spectrin C. 1/60, showing labeling of many organelles, probably plastids, in the scutellum but almost none in the coleoptile; amyloplasts do not label (arrow).

---

nuclei were labeled, the nucleoli were negative (Figs. 7, 9, 10 and 14). Controls of PEMs and globules of carrot were completely negative (not shown). In torpedo shaped embryos labeling of the epidermal cells was not only seen at the plasma membrane, but the cytoplasm and the nuclei of these cells also labeled (Figs. 8, 9 and 10). Calli, present in the 200 to 300 µm sieve fraction, which do not have a developed epidermis, did not show this type of labeling (C in Figure 8 and 9). Subepidermal layers of the maturing embryos showed no labeling in the cytoplasm or nuclei (Figs. 9 and 10), but only a weak labeling at the plasma membranes. However, in this tissue organelles, probably plastids, labeled (Fig. 10). Controls did not exhibit any labeling. In the epidermis and in vascular tissue (VT) a weak orange-yellowish autofluorescence was observed, but this could easily be discriminated from the bright green-yellowish FITC- or Bodipy-fluorescence.

Another example of tissue-specific spectrin labeling was found in maize zygotic embryos. In all cells of the scutellum (Fig. 11) many small plastids were labeled (Fig. 11B). In the adjacent coleoptile tissue, however, hardly any labeling could be observed. Yet, in Nomarski images (Fig. 11A), the presence of small plastids in cells of the coleoptile, could be seen clearly. The heavily contrasted amyloplasts, seen as bright spots around the nuclei in the Nomarski-image (Fig. 11A), did not label. Smaller plastids, positioned at the boundary of the cells, labeled at their membranes. Organel labeling is not only seen in the scutellum of maize embryos (Fig. 11B), but also in carrot suspension cells (Fig. 5B), carrot somatic embryos (Fig. 10), maize root tip cells (Figs. 13 and 14) and bean root cells (Fig. 15). Higher magnifications showed that this
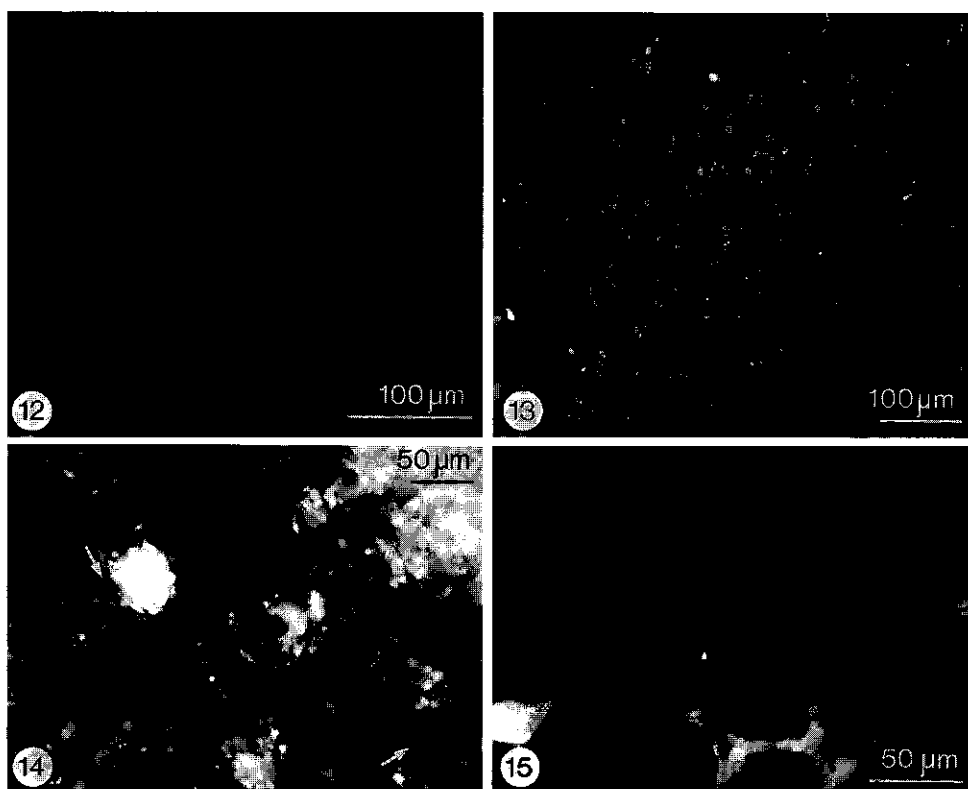
Fig. 12 shows a BMM-section of maize root cells after control labeling with rabbit pool serum (diluted 1/20); the photograph was taken with 4 times prolonged illumination and shows no labeling.

Fig. 13 shows a BMM-section of maize root cells after labeling with anti-spectrin C. 1/100; labeling is seen in the periphery of organelles.

Fig. 14 shows a PEG-section of cells in the root tip of maize, labeled with anti-spectrin C. 1/100; label intensity of nuclei varies; labeling is seen at the PMs and ring-like around many organelles.

Fig. 15 shows a PEG-section of bean root cells, labeled with anti-spectrin S. 1/250; labeling is seen at the PM and weakly in the cytoplasm and on organelles, probably plastids.

labeling is around organelles, because ring-like structures were seen (Fig. 13). In controls never labeled plastids were found (Fig. 12).

Figs. 14 and 15 show the spectrin labeling in maize respectively bean root tissue. In the meristematic zone many nuclei are labeled (Fig. 14). This labeling in the nuclei of mitotically active cells was also seen in developing globular stage somatic embryos of carrot (Fig. 7). Nucleoli were always negative. Controls never showed labeling in the nuclei. Just above the meristematic zone, both in roots of maize and bean, less spectrin labeling was found in the nuclei. Labeling of the PM, however, remained, as is clearly seen in root cells of bean (Fig. 15). In maize root cells labeling at the PM was less bright than in bean.

DISCUSSION

Protein extraction and immunoblotting

Western blots show the presence of spectrin epitopes in native as well as in SDS-treated extracts of several plant tissues. In SDS gels only poor labeling was observed at the expected molecular weights of 240 and 220 kD. However, strong labeling was found at a doublet of bands at 85 kD. Besides the 85 kD bands, also some labeling could be found at 100 and 45 kD. Because the pure spectrin obtained from Sigma also showed these bands on similarly processed blots, we expect that these bands represent breakdown products of spectrin, and that this labeling is a specific immunoreaction. Spectrins are very sensitive to degradation (Burridge *et al.*, 1982; Kastari *et al.*, 1983; Harris *et al.*, 1985; Chailly *et al.*, 1989) and plants are particularly rich in proteases (Jervis and Pierpoint, 1989). Probably, proteases were active in our material, despite the presence of protease inhibitors in the extraction buffer. Nevertheless, some cross-reactivity with other proteins of the spectrin family, which might also be present in plant cells, can not be excluded. Filamin, α-actinin and MAP-2 are rod-shaped actin-binding proteins and it is likely that they have epitopes related to spectrin (Bennett, 1990). Sharing of epitopes of spectrin and α-actinin, a so-called mini-spectrin of 100 kD has been described by Bennett (1990), and of spectrin and MAP-2 by Davis and Bennett (1982). In blots of focussing gels, the expected band at pI 4.8 was seen in all plant extracts, which does not necessarily mean that in the native extract no proteolytic breakdown had occurred, since degraded spectrin polypeptides could have the same iso-electric point as spectrin itself.

Immunocytochemistry

Labeling at the plasma membrane:
Spectrin-like antigens were localized in several plant tissues with different techniques and antibodies. Anti-sp. C. and anti-sp. S. gave similar localizations. Labeling is found predominantly, but not exclusively, at the plasma membrane. Sometimes cytoplasmic strands connecting the cytoplasm around the nucleus to the cortical cytoplasm were also stained (Fig. 10). As discussed above, it cannot be excluded that some cytoplasmic labeling is based on cross-reactivity with other proteins than spectrin. Labeling conditions on Western blots showed specificity and only limited cross-reactivity, but in situ labeling conditions were less restrictive since higher antibody concentrations were used.

Labeling of organelles:
In several tissues, such as root tip cells of maize and the scutellum of maize zygotic embryos, a specific class of organelles, probably plastids, is labeled at their membranes with the anti-spectrin antibodies. This phenomenon has not been reported by Wang and Yan (1991), nor by Michaud and co-workers (1991). The latter authors worked with leaf cells in which the plastids

are chloroplasts and reported that the fluorescence of the plastids was due to autofluorescence. Most of our material did not possess chlorophyl-containing plastids and the controls showed that there was no autofluorescence. Kengen (1992) has recently reported that some vesicular, mitochondrial and plastid membranes in protoplasts of tobacco were positive after anti-spectrin labeling. Also in amoebae (Choi and Jeon, 1989), cells of sea urchin eggs (Bonder *et al.*, 1989, Fishkind *et al.*, 1990) and lymphocytes (Black *et al.*, 1988) spectrin can be found localized on membranes of vesicles and organelles. These authors speculate that the spectrin protein binds to membrane proteins and thus stabilizes the organelles.

Labeling of nuclei:

In mitotically active tissues like PEMs, globular stages somatic embryos and root tips, a number of nuclei were stained. Some cells showed no labeling, while neighbouring cells could have very strongly stained nuclei, but nucleoli were always negative. Except for a faint autofluorescence, nuclei were negative in control labelings. Comparison of labeled nuclei and DAPI stained images show that the intensity of spectrin labeling correlates with the DAPI intensity. Since nuclei are notorious for aspecific labeling, these findings have to be interpreted carefully. However Choi and Jeon (1989) have reported that in *Amoebae proteus* a spectrin-like protein was present on nuclear membranes.

Functions of spectrin in plant cells

At the moment it is too early to assign definitive functions to spectrin-like proteins in plant cells, but the data give some hints. Spectrin-like proteins are especially localized at the plasma membranes of protoplasts, single cells or small cell clusters of suspension cells and calyptra cells. The hypothesized functional explanation for the presence of spectrin in protoplasts seems obvious, since these plant cells without a wall may need a spectrin network to stabilize the plasma membrane. Single cells, small clusters of cells in suspension and calyptra cells share the characteristics of having little or no cell-to-cell contact, and possessing a non-rigid cell wall, subject to deformation. Therefore, these cells might need plasma membrane stabilization too. However, this does not explain the abundance of spectrin at the plasma membrane of for instance *Vicia faba* root cells, just starting to elongate. Spectrin at the plasma membrane might be involved in exocytotic processes. In growing pollen tubes, spectrin was mainly present at the growing tip, where exocytosis takes place (Kengen, 1992). Experiments with chromaffin cells have shown that fodrin participates in the exocytosis process (Perrin *et al.* 1987). More research on subcellular localization, developmental expression, actin-binding properties of plant 'spectrin' and other actin-associated cytoskeletal proteins is imperative.

ACKNOWLEDGEMENTS

REFERENCES

Bennett, V. (1990). Spectrin-based membrane skeleton: A multipotential adaptor between plasma membrane and cytoplasm. Physiol. Rev. **70**, 1029-1065.

Black, J.D., Koury, S.T., Bankert, R.B. and Repasky, E.A. (1988). Heterogeneity in lymphocyte spectrin distribution: ultrastructural identification of a new spectrin-rich cytoplasmic structure. J.Cell Biol. **106**, 97-109.

Bonder, E.M., Fishkind, D.J., Cotran, N.M. and Begg, D.A. (1989). The cortical actin-membrane cytoskeleton of unfertilized sea urchin eggs: Analysis of the spatial organization and relationship of filamentous actin, onfilamentous actin, and egg spectrin. Dev. Biol. **134**, 327-341.

Burridge, K., Fath, K., Kelly, T., Nuckolls, G. and Turner, C. (1988). Focal adhesions: Transmembrane junctions between the extracellular matrix and the cytoskeleton. Ann. Rev. Cell Biol. **4**, 487-527.

Burridge, K., Kelly, T. and Mangeat, P. (1982). Nonerythrocyte spectrins: Actin-membrane attachment proteins occurring in many cell types. J. Cell Biol. **95**, 478-486.

Chailly, B., Frappier, T., Regnouf, F. and Laine, M. (1989). Immunological detection of spectrin during differentiation and in mature ciliated cells from quail oviduct. J. Cell Sci. **93**, 683-690.

Choi, E.Y. and Jeon, K.W. (1989). A spectrin-like protein present on membranes of *Amoeba proteus* as studied with monoclonal antibodies. Exp. Cell Res. **185**, 154-165.

Davis, J. and Bennett, V. (1982). Microtubule-associated protein 2, a microtubule-associated protein from brain, is immunologically related to the α-subunit of erythrocyte spectrin. J. Biol. Chem. **257**: 5816-20.

De Vries, S.C., Booij, H., Meijerink, P., Huisman, G., Wilde H.D., Thomas, T.L. and Van Kammen, A. (1988). Acquisition of embryogenic potential in carrot cell-suspension cultures. Planta **176**: 196-204.

Emons, A.M.C., Derksen, J. and Sassen, M.M.A. (1992). Do microtubules orient plant cell wall microfibrils? Physiol. Plant. **84**, 486-493.

Emons, A.M.C. and Kieft, H. (1991). Histological comparison of single somatic embryos of maize from suspension cilture with somatic embryos attached to callus cells. Plant Cell Rep. **19**, 485-488.

Fishkind, D.J., Bonder, E.M. and Begg, D.A. (1990). Subcellular localization of sea urchin egg spectrin: evidence for assembly of the membrane-skeleton on unique classes of vesicles in eggs and embryos. Dev. Biol. **142**, 439-452.

Gubler, F. (1989). Immunofluorescence localisation of microtubules in plant root tips embedded in butyl-methyl methacrylate. Cell Biol. Int. Rep. **13**, nr. 1, 137-145.

Harris, A.S., Green, L.A.D., Ainger, K.J. and Morrow, J.S. (1985). Mechanism of cytoskeletal regulation (I): functional differences correlate with antigenic dissimilarity in human brain and erythrocyte spectrin. Biochim. biophys. Acta **830**, 147-158.

Jervis, L. and Pierpoint, W.S. (1989). Purification technologies for plant proteins. J. of Biotechn., **11**, 161-198.

Kasturi, K., Fleming, J. and Harrison, P. (1983). A monoclonal antibody against erythrocyte spectrin reacts with both α- and ß-subunits and detects spectrin-like molecules in non-erythroid cells. Exp. Cell Res. **144**, 241-247.

Kengen, H.M.P. (1992). Cytoskeletal linkages. PhD thesis Catholic University Nijmegen, Nijmegen Quickprint, ISBN 90-9005401-4

Michaud, D., Guillet, G., Rogers, P.A. and Charest, P.H. (1991). Identification of a 200 kD membrane-associated plant cell protein immunologically related to human ß-spectrin. FEBS **294**, 77-80.

Moon, R.T. and McMahon, A.P. (1990). Generation of diversity in non-erythroid spectrins. J. of Biol. Chem. **265**, 4427-4433.

Perrin, D., Keith Langley, O. and Aunis, D. (1987). Anti-α-fodrin inhibits secretion from permeabilized chromaffin cells. Nature **326**, 498-501.

Puite, K.J., Roest, S. and Pijnacker, L.P. (1986). Somatic hybrid potato plants after electrofusion of diploid *Solanum tuberosum* and *Solanum phureja*. Pl. Cell Rep. **5**, 262-265.

Sanchez-Pina, M.A., Kieft, H. and Schel, J.H.N. (1989). Immunocytochemical detection of non-histone nuclear antigens in cryosections of developing somatic embryos from *Daucus carota* L. J. of Cell Sci. **93**, 615-622.

Speicher, D.W., Weglarz, L. and DeSilva, T.M. (1992). Properties of human red cell spectrin heterodimer (side-to-side) assembly and identification of an essential nucleation site. J. of Biol. Chem. **267**, 14775-14782.

Tanaka, T., Kadowaki, K., Lazarides, E. and Sobue, K. (1991). Ca^{2+}-dependent regulation of the spectrin/actin interaction by calmodulin and protein 4.1. J. of Biol. Chem. **266**, 1134-1140.

Van der Valk, H.C.P.M., Blaas, J., Eck, J.W. van and Verhoeven, H.A. (1988). Vital DNA staining of agarose-embedded protoplasts and cell suspensions of *Nicotiana plumbaginifolia*. Plant Cell Rep. 7: 489-492.

Van Lammeren, A.A.M. (1986). Developmental morphology and cytology of the young maize embryo (*Zea mays* L.). Acta Bot. Neerl. **35 (3)**. 169-188.

Wang, Y. and Yan, L. (1988). The membrane proteins of leaf cell membrane of *Vicia faba*. Chin. Sc. Bull. **33**, 231-235.

Wang, Y. and Yan, L. (1991). Immunochemical identification of spectrins on the plasma membrane of leaf cells of *Vicia faba*. Chin. Sc. Bull. **36**, 862-866.

- Chapter 4 -

Spectrin-like proteins in plant nuclei

Norbert C.A. de Ruijter[1,*], Tijs Ketelaar[1], Sonal S.D. Blumenthal[2],
Anne Mie C. Emons[1] and Jan H.N. Schel[1]

[1] *Laboratory of Plant Cytology and Morphology, Wageningen University,*
Arboretumlaan 4, 6703 BD Wageningen, The Netherlands
[2]*University of Texas, Dept. of Botany, Austin, Texas, 78713 USA.*

SUMMARY

We analyzed the presence and localization of spectrin-like proteins in nuclei of various plant tissues using several anti-erythrocyte spectrin antibodies on isolated pea nuclei and nuclei in cells. Western blots of extracted purified pea nuclei show a cross-reactive pair of bands at 240-220 kDa, typical for human erythrocyte spectrin, and a prominent 60 kDa band. Immunolocalization by means of confocal laser scanning microscopy reveals spectrin-like proteins in distinct spots equally distributed in the nucleoplasm and over the nuclear periphery, independent of the origin of the anti-spectrin antibodies used. In some nuclei also tracks of spectrin-like proteins are observed. No signal is present in nucleoli. The amount and intensity of signal increases when nuclei were extracted, successively, with detergents, DNAse I and RNAse A, and high salt, indicating that the spectrin-like protein is associated with the nuclear matrix. The labeling is similar in nuclei of various plant tissues. These data are the first that show the presence and localization of spectrin-like epitopes in plant nuclei, where they may stabilize specific interchromatine domains.

Keywords: confocal laser scanning microscopy, immunolocalization, nucleus, nuclear matrix, spectrin, *Pisum sativum*

INTRODUCTION

Nuclei contain a highly organized nuclear skeleton with associated proteins, the nuclear matrix (NM). This scaffold consists of a protein mesh that underlies the nuclear membrane, and extends throughout the interior of nuclei (reviews: Spector, 1993; Van Driel *et al.*, 1995; review plant nuclear matrix: Moreno Díaz de la Espina, 1995). The nuclear matrix is thought to provide nuclear structure, mediate DNA replication and transcription, bind proteins of the splicing machinery, fold chromatin, spatially arrange nuclear pore complexes, and anchor nuclear envelope proteins (Moir *et al.*, 1995; Stuurman *et al.*, 1998). Many of these functions reside in lamins, which are the best-characterized proteins of the nuclear matrix (Hozák *et al.*, 1995). Also higher plants contain nuclear lamin-like proteins, as was shown in nuclear matrix fractions from onion cells by cross-reactivity with polyclonal and monoclonal antibodies against different lamins from vertebrates (Mínguez and Moreno Díaz de la Espina, 1993). Nuclear lamins show transient patterns of distribution (Moir *et al.*, 1995), indicating, contrary to previous views, that the nuclear matrix itself is not a static structure. In analogy with the cytoskeleton, the nuclear skeleton not only functions as a rigid framework, but is also very dynamic and able to respond to signals (Lamond and Earnshaw, 1998).

Considerable evidence has accumulated that actin is a constituent of the nucleoskeleton of interphase cells (for a review, see De Boni, 1994). Sauman and Berry (1994) showed that nuclear filamentous actin (F-actin) is directly associated with *Drosophila* polytene chromosomes, and is able to link RNA polymerase II to DNA. Wan and Xing (1998) immunolocalized actin in nuclei of meristematic cells of onion (*Allium cepa*), after DNAse I and 2 M NaCl treatment. The presence of actin after these treatments indicates that actin is part of a nuclear matrix. Actin in the cytoplasm is regulated by actin binding proteins (ABPs; review on ABPs in animals: Carlier, 1998; Puius *et al.*, 1998; in plants: De Ruijter and Emons, 1999). It is likely, therefore, that nuclear actin is modulated by nuclear actin binding proteins. Indeed, when actin binding proteins were injected into amphibian oocytes, strong inhibition of transcriptional activity of protein-coding genes was observed, nuclear actin filaments altered (Scheer *et al.*, 1984), and chromosome morphology changed (Ankenbauer *et al.*, 1989). In *Xenopus laevis* oocytes the nuclear distribution of actin and myosin altered during oocyte maturation (Ryabova *et al.*, 1994). In plant nuclei, myosin (De Boni, 1994), and actin depolymerizing factor (Jiang *et al.*, 1997) have so far been found. It is not known whether these nuclear ABPs serve similar functions as in the cytoplasm.

This paper deals with the presence of another class of ABPs in plant nuclei, the spectrin-like proteins. Spectrin is a member of the family of actin cross-linking proteins. It is a large (240-220 kDa) and multi-functional polypeptide, which not only has binding sites for actin,

but also for calcium, calmodulin, and PIP$_2$. Each molecule is made of two distinct α- and β-subunits. Spectrin molecules are cross-linked by filamentous actin oligomers and other proteins, and are often associated with membrane proteins. Spectrin was first identified in red blood cells (Marchesi and Steer, 1968), and most knowledge on the organization and function of spectrin comes from membrane skeletons of avian and mammalian erythrocytes. In these cells it was shown that spectrin, with its many binding sites, forms an extensive sub-membranous network that provides both structural integrity and dynamic flexibility (Bennett, 1990; Bennett and Gilligan, 1993). Recently it was shown that spectrins also play a role in membrane protein sorting and Golgi dynamics (Beck and Nelson, 1996; Lippincott-Schwartz, 1998).

Several spectrin isoforms and genes have been identified in a wide variety of tissues and cells other than erythrocytes, ranging from primitive amoebae to man (Dubreuil, 1991; Hartwig, 1994). Spectrin-like proteins have also been found in leaf extracts in higher plants (Michaud *et al.*, 1991; Sikorski *et al.*, 1993). Further, Faraday and Spanswick (1993) detected a 230 kDa protein with anti-spectrin in purified plasma membrane fractions from rice (*Oryza sativa*) roots, while also at the periphery of growing cells of carrot (*Daucus carota* L.) (De Ruijter and Emons, 1993), and in the tips of growing root hairs of vetch (*Vicia sativa* L.), spectrin-like epitopes were abundant (De Ruijter *et al.*, 1998). Plant spectrin-like proteins also appear on the endo-membranes of onion epidermal cells, as was shown by Reuzeau *et al.* (1997), by injected fluorescent antibodies against animal spectrin.

When we previously reported the presence of spectrin-like antigens in plant tissues (De Ruijter and Emons, 1993), we observed some labeling in nuclei of meristematic cells of somatic embryos of carrot. Also in tomato root meristem cells, immunolocalization showed spectrin-like epitopes in nuclei, but this was not studied in detail (A. Geitmann, pers.comm.). Nuclear spectrin-like proteins were also observed in other eukaryotic cells. In nuclear extracts of amphibian oocytes a 230 kDa protein was recognized as a spectrin, which was localized in the nucleoplasm and at the periphery of nucleoli (Ryabova *et al.*, 1994; Carotenuto *et al.*, 1997). With affinity purified anti-α-spectrin Bachs *et al.* (1990) detected a 240 kDa nuclear α-spectrin in rat liver cells that was localized in the nuclear matrix and accumulated at the nuclear envelope. Also in nuclear matrix samples of rat brain cells, α-spectrin is enriched (Vendrell *et al.*, 1991).

The aim of the present study was to determine whether indeed spectrin-like proteins are present in plant nuclei and to localize them. We first optimized the conditions for antibodies to access the epitopes. Among others, Hozák *et al.* (1995) showed that it is important to extract nuclei to increase the accessibility for antibodies to localize structural nuclear proteins. When nuclei are extensively extracted with detergents, DNAse and RNAse treatment followed by high or low ionic extraction protocols an accessible nuclear matrix

remains. Various protocols have been developed for the isolation of nuclear matrices from different systems (De Jong *et al.*, 1990; Stuurman *et al.*, 1992). The protein composition of the final remaining matrix greatly depends upon the procedures used.

We used a well-established isolation and extraction procedure for nuclei from etiolated pea plumules. The isolation procedure yields intact nuclei of at least 85% purity, and little or no plasma membrane contamination (Datta *et al.*, 1985). The extraction procedure yields nuclear matrices (NM) which are essentially free of DNA, RNA and most ionically bound proteins, and these matrices are highly enriched in lamin-like proteins (Li and Roux, 1992; Blumenthal, 1997), which characterize NM fractions in animal nuclei (Stuurman *et al.*, 1998). By use of this method, several pea nuclear proteins were isolated and localized before e.g. casein kinase II protein kinase (Li and Roux, 1992), annexin (Clark *et al.*, 1998), and a nucleolin-like protein (Tong *et al.*, 1997). With Western blots of extracts of isolated pea nuclei we show that spectrin-like proteins are part of the nuclear skeleton. This is supported by persistent labeling of isolated extracted nuclei. We used confocal laser scanning microscopy on various fluorescent-labeled plant tissues and on isolated pea nuclei to localize the spectrin-like proteins in more detail.

MATERIALS AND METHODS

Plant material

Seeds of *Pisum sativum* cv. finale were germinated and grown for 7 days on soil covered with 1 cm silver sand in the dark at $23 \pm 2°C$. After 6-8 days, etiolated plumules (including the shoot apical meristem with developing leaves and hypocotyl from the hook region) were harvested for nuclear isolation or fixed and embedded for sectioning.

Processing of plant tissue

Plumules of etiolated pea seedlings were fixed at room temperature for 5 h in 3% paraformaldehyde and 0.1% glutaraldehyde in 50 mM phosphate buffer pH 7.2, with 0.01% Triton X-100. After fixation the material was rinsed in this buffer, dehydrated in an ethanol series, embedded in LR White hard grade (London Resin Company Ltd., Hampshire, UK), with 0.5% benzoin-methylether as a hardener, and polymerized under UV at -20°C. Semithin sections of 2-4 μm were cut on a LKB 8800 Ultratome III (Leica Microsystems BV) with glass knives, and transferred to slides. Roots of *Vicia faba* and *Vicia sativa* seedlings, grown on moist paper, were fixed with 4% paraformaldehyde and 0.1% glutaraldehyde in 100 mM PIPES, pH 6.9 with 5 mM EGTA and 5 mM $MgSO_4$. Root tips were infused in 1.5 M sucrose in 50 mM phosphate buffer, pH 7.2 and frozen to stubs. Longitudinal sections (15-20 μm thickness) were

cut with a Microm HM 500 OM rotary cryo-microtome at -18°C. Cryo-sections, sticking to glass slides pre-coated with 2% 3-aminopropyl-triethoxy silane (Sigma A3648), were treated with 1% hemicellulase (Sigma H2125) in 0.1 M 2-N-morpholino-ethanesulfonic acid (MES buffer) at pH 6.1 for 10 min at room temperature, and washed in the same buffer. Prior to immunolabeling, some samples were treated with 0.5-1% Triton X-100 in PBS for 5 min and 250 µg/ml DNAse I for 10 min.

Nuclear isolation and staining

Nuclei were isolated from a minimal of 10 g fresh weight plumules of 7 days old etiolated pea seedlings according to Datta *et al.* (1985), with some modifications. For the preparation of nuclear extracts, at least 50 g fresh weight was used. Care was taken to collect only the extreme tip, since vascular tissue of the hypocotyl usually lowered the yield of intact nuclei. Plumules were collected under green safe light and kept on ice. All other steps were done at 4°C. Homogenization of plumules was done in isolation buffer with mortar and pestle (as recommended by Willmitzer and Wagner, 1981), instead of the use of a Polytron homogenizer (Datta *et al.*, 1985). Typically, for 10 g of pea plumules, 50 ml of isolation buffer (10 mM N-[2-hydroxyethyl]-piperazine-N'-[2-ethanesulfonic acid] (HEPES), pH 7.0 supplemented with 5 mM $MgCl_2$, 1.0 M sucrose, and 10 mM phenylmethylsulfonylfluoride (PMSF)) was used. If not mentioned, chemicals were purchased from Sigma-Aldrich Inc. (St. Louis, Missouri, USA) and were the highest grade available. The homogenate was filtered through 3 layers of Miracloth (Calbiochem, 475855), followed by nylon filters (Merrem & La Porte, Zaltbommel, NL) of 88 µm and 30 µm mesh, and centrifuged at 1900 x *g* (4000 rpm, Sorvall SM-24) for 10 min. The pellet yielded from 10 g fresh plumules was resuspended in 4-6 ml isolation buffer, and then fractionated at 7800 x *g* for 30 min over a discontinuous gradient of 25% - 50% Percoll in isolation buffer. The pellets contained mostly starch grains and cell debris. Purified nuclei were collected from the interface of the two layers, and washed in isolation buffer to remove residual Percoll. For increased purity of nuclei the gradient was run twice. Washed nuclei were pelleted at 1900 x *g* for 10 min, and resuspended in isolation buffer. To keep nuclear membranes intact, no detergents were used. Yield was scored by counting the number of isolated nuclei in a Bürker-cytometer. Nuclei were stained with a freshly diluted staining solution of 0.4% methylgreen and 0.1% pyronine Y in isolation buffer.

Isolation of nuclear matrices

For preparation of nuclear matrices (NMs), 3-5 x 10^8 purified nuclei were suspended in buffer A (10 mM Tris-HCl, pH 7.5, 0.2 mM $MgCl_2$, and 1 M sucrose) and incubated twice in 250 µg/ml DNAse I and 250 µg/ml RNAse A for 1 h each at 10°C. After digestion, the

nuclei were three times extracted with 1.6 M NaCl (with and without β-mercaptoethanol) for 10 min each at 0°C (Li and Roux, 1992). The nuclease digestion and salt extraction steps were carried out in a protease inhibitor cocktail (0.5% aprotinin, 1 mM n-α-p-tosyl-L-arginine methyl ester (TAME), and 1 mM phenylmethylsulfonyl fluoride (PMSF)). After digestion, the nuclei were centrifuged at relative centrifugal force of 1500 x *g* for 10 min. After salt extraction, centrifuge steps were done at 2500 x *g* for 15 min.

Antibodies

Anti-spectrin S1390 (Sigma) is a rabbit polyclonal antibody raised against purified chicken α and β erythrocyte spectrin. Anti-spectrin S1515 and anti-spectrin C567622 (Calbiochem) are rabbit polyclonal antibodies raised against purified human erythrocyte α- and β-spectrin. Anti-spectrin C567622 was diluted 1:200, and anti-spectrins S1390 and S1515 were diluted 1:300 to 1:600 for immunolocalization. Controls were done by omitting the first antibody or replacing it for pooled normal rabbit serum (NRS, diluted 1:50) or pooled normal mouse serum (NMS, diluted 1:100). Secondary antibodies were goat anti-rabbit (GaR)-Bodipy 503-512 (Molecular Probes), GaR-fluorescein-isothiocyanate (FITC), or goat anti-mouse (GaM)-FITC, diluted 1:300. To check the permeability of nucleoli for antibodies we used a monoclonal anti-fibrillarin antibody diluted 1:200. This mouse IgG_{2a} monoclonal antibody clone 72-B9 recognizes a highly conserved 34 kDa fibrillarin, associated with U3 RNP particles (Reimer *et al.*, 1987).

Electrophoresis and immunoblotting of nuclear extracts

Purified nuclei as well as NMs were extracted in 2% boiling SDS sample buffer with 10 mM dithiothreitol (SDS/DTT) for 3 min or in a spectrin extraction buffer of 0.1 mM EDTA, 1 mM PMSF in 0.3 mM phosphate, pH 8.5 (Michaud *et al.*, 1991), followed by boiling in 2% SDS with 10 mM DTT. Protein concentration was determined with the bicinchoninic acid (BCA) Protein Assay (Pierce, 23225), and 20 μg protein was loaded per lane and separated on a 4-15% gradient SDS-PAGE (according to Laemmli, 1970). Molecular weight markers (Promega) indicated protein size, and purified human erythrocyte spectrin (S3644) served as a reference. Proteins were semidry transferred to nitrocellulose membrane with a maximal current of 1.0 mA/cm^2 at 15°C for 75 min. To check the transfer, blots were stained with 0.2% Ponceau-S in 1% acetic acid and destained in ddH$_2$0. The total protein profile was visualized on the blot with silver staining (Kovarík *et al.*, 1987). For storage at 4°C, membranes were washed in 0.02% NaN$_3$ in H$_2$0 and air-dried. For immunolabeling, strips of nitrocellulose were blocked with 1% BSA (fraction V) in 10 mM TRIS-HCl, pH 7.5, and incubated for 2 h with anti-spectrin antibodies diluted 1:1000, or with pooled normal rabbit serum (NRS) diluted 1:250. The secondary antibody goat anti-rabbit, conjugated to alkaline

phosphatase (GaR-AP, BioRad 172-1016), was used at 1:3000. Blots were developed for 5-15 min at room temperature with a chromogenic reaction in freshly prepared 370 μM nitroblue tetrazolium with 460 μM toluidin 5-bromo-4-chloro-3-indolyl- phosphate in 0.1 M NaHCO$_3$, pH 8.7, supplemented with 1 mM MgCl$_2$.

Fixation and extraction of isolated nuclei

Purified isolated nuclei were resuspended in isolation buffer and freshly prepared concentrated fixative was added in drops under agitation to prevent clumping of nuclei during the fixation. Nuclei were fixed for 20 min at room temperature at a final concentration of 2% paraformaldehyde and 0.05% glutaraldehyde in 10 mM HEPES pH 7.3, with 5 mM MgCl$_2$, 10 mM β-mercapto-ethanol and 0.5 M sucrose. Prior to collecting nuclei at 1100 g (3000 rpm, Sorvall SM-24 for 5 min), the fixing solution was diluted 10 fold with PBS (137 mM NaCl, 2.7 mM KCl, 1.5 mM KH$_2$PO$_4$, 8.1 mM Na$_2$HPO$_4$ .2H$_2$O; pH 7.4) to prevent clumping of nuclei in the pellets. Pellets of fixed nuclei were gently resuspended in PBS. Dense drops of fixed nuclei were put on glass slides that had been pre-coated with 2% 3-aminopropyl-triethoxy silane (Sigma A3648). Nuclei were allowed to sink and stick for at least 20 min at room temperature. To obtain nuclear matrices, some nuclei were first extracted with 0.5% Triton X-100, digested with 250 μg/ml DNAse I and 250 μg RNAse A for 10 min at room temperature, and then extracted with 1.6 M NaCl for another 10 min. Detergent, nuclease and salt extractions were done in 10 mM Tris-HCl, pH 7.5 supplemented with 0.2 mM MgCl$_2$. Nuclei remained attached to the slides during extractions and immunolabeling.

Immunolabeling on tissue sections and isolated nuclei

The labeling procedure was similar for nuclei in cells and for isolated nuclei. Slides with sections or nuclei were incubated in the reducing buffer, 0.1 M NH$_3$ClOH in PBS, for 10 min, washed in PBS for 5 min and blocked with 1% BSA (fraction V) in PBS for 15 min, followed by treatment with 0.1-1% acetylated BSA in PBS (BSA-c, Aurion, Wageningen, NL) for 15 min. Next, nuclei were incubated with primary antibodies diluted in 0.1% BSA-c and 0.05% Triton X-100 in PBS for 1 h 30 min at 37°C. After 5 washes (3 min each) in the same buffer, the nuclei were incubated with secondary antibodies for 1 h 30 min at 37°C. DNA was stained with 0.1 μg/ml propidium-iodide in PBS for 5 min. After labeling, the nuclei were mounted in glycerol Citifluor AF2 (Citifluor Ltd, London) anti-fading agent.

Microscopy and image processing

Isolated nuclei were imaged on a Nikon Optiphot with a 40x Plan DIC/0.7 NA or 100x Plan DIC/1.25 NA oil objective, and they were recorded with a Panasonic wv-E550 3-CCD

camera equipped with a Prysm frame-grabber with AcQuis 2.0 software (Synoptics Ltd., Cambridge, UK). Fluorescently labeled nuclei were visualized on a conventional epifluorescence microscope (Nikon Microphot) equipped with 100 W Hg lamp and DIC optics. Optical sections through double labeled nuclei were imaged on a MRC-600 Bio-Rad Confocal Laser Scanning Microscope with an argon-krypton ion laser attached to a Nikon Diaphot 300 inverted microscope equipped with a 60x FL/1.4 NA oil immersion objective. The images were collected in dual channel mode with FITC image in K2 (DM 488 BA 522 DF 35) and PI image in K1 (DM 560 BA 585 long pass). The filters K1/K2 selectively discriminate green/red fluorescence. The pinholes were moderately closed at 4-6 range and images were collected in Kalman filter mode (4-6x). Confocal images in BioRad PIC format were converted to TIF format with Confocal Assistant 2.04, contrast enhanced in Adobe PhotoShop 4.0 (Adobe Systems Inc., CA, USA), and printed with a Kodak XLS 8600 dye sublimation printer.

RESULTS

Immunolocalization of spectrin-like epitopes in nuclei in tissue

Root cortex cells of *Vicia faba* L. (broad bean) and *Vicia sativa* L. (vetch) were labeled with anti-spectrin antibodies against animal spectrin. All growing and full-grown cortex cells showed a dotted labeling of spectrin-like epitopes in the nucleoplasm (Fig. 1a, 1b), and often an almost continuous staining at the nuclear periphery (Fig. 1a). This speckled pattern, present throughout the nucleoplasm, increased when thick cryo-sections (15 μm) were extracted with 1% Triton X-100 for 5 min (Fig. 1b). A strong speckled nuclear staining was also observed when anti-spectrin antibodies were applied on LR White resin sections of etiolated pea plumules treated with 0.5% Triton X-100 for 5 min, followed by 250 μg/ml DNAse I for 10 min (Fig. 1c1, 1c2). A labeling with anti-spectrin antibodies was never observed in nucleoli (Fig. 1b, 1c2). Similar labelings were obtained with anti-human erythrocyte spectrin (C567622 and S1515) and anti-chicken erythrocyte spectrin (S1390). The amount of labeling in nuclei in tissues was not consistent; it depended on the fixation and extraction procedure. For instance, when *Vicia faba* roots were fixed with 2% instead of 0.1% glutaraldehyde no labeling was observed in 15 μm cryo-sections after an incubation with 1% Triton X-100 for 10 min (not shown). We needed an optimal accessibility to epitopes for the antibodies, to study the presence and localization of nuclear spectrin-like epitopes in more detail. Therefore, we used isolated nuclei.
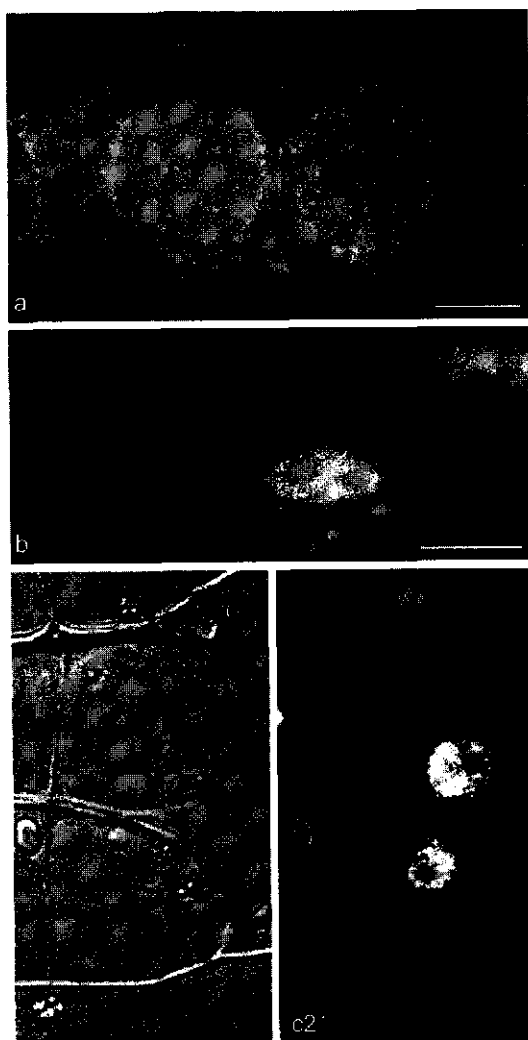
Figure 1 Labeling with anti-spectrin of plant nuclei in tissue sections.

Scale bars represent 5 μm.

(**a**) Image of a cryo-section (15 μm thick) of cortical cells of broad bean (*Vicia faba*) roots, close to the meristematic zone. Labeling with anti-human erythrocyte spectrin (C567622) shows some speckles in the nucleoplasm and staining at the nuclear periphery.

(**b**) Image of a cryo-section (15 μm thick) of cortical cells from the elongation zone of a vetch (*Vicia sativa)* root extracted with 1% Triton X-100. Labeling with anti-chicken erythrocyte spectrin (S1390) shows a speckled pattern in the nucleoplasm. The nucleoli are negative.

(**c**) Image of a LR White section (4 μm) of cells from the shoot apical meristem of an etiolated pea *(Pisum sativum)* plumule treated with a 0.5% Triton X-100, followed by 250 μg/ml DNAse I, then labeled with anti-spectrin S1390. (**c1**) Differential Interference Contrast (DIC) image, and (**c2**) corresponding fluorescence image showing speckled labeling in the nucleoplasm. The nucleoli are negative.

Nuclear isolation

We isolated nuclei from etiolated pea plumules using the isolation procedure described by Datta *et al.*, 1985, and obtained nuclei in high density. Freshly isolated nuclei were translucent, spherical to oval in shape, and had an average diameter of 6 μm (Fig. 2a). Nuclear integrity was checked with differential interference contrast (Fig. 2a) and with a methylgreen / pyronine Y staining to discriminate DNA (green) from RNA (purple) (Fig 2b). Most nuclei appeared intact and contained 2 to 5 nucleoli. Occasionally the nuclear

Figure 2 Isolated pea nuclei. Scale bars represent 5 µm.
(a) DIC image of unfixed isolated purified nuclei showing nuclear integrity and absence of aggregation. (b) Isolated fixed nucleus stained for RNA with pyronine Y (in purple/dark regions) and DNA with methylgreen (in green/light regions). Dark spots show the presence of nucleoli.
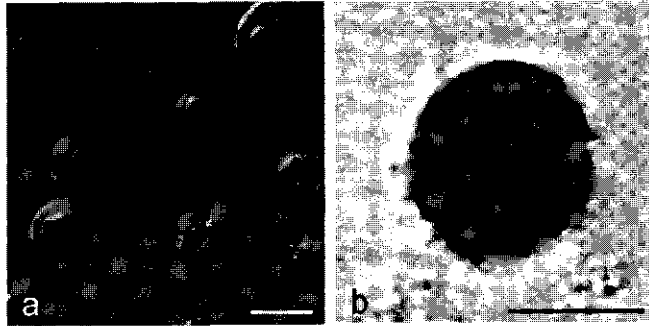
periphery was stained (Fig. 2b). Purified isolated pea nuclei were either extracted for protein assays or mounted on slides for immunolabeling. The number of isolated nuclei was counted in a Bürker-cytometer and estimated to be 1.9×10^7 nuclei /ml.

Spectrin-like epitopes in extracts of isolated nuclei

Total proteins or a fraction of spectrin-like proteins were extracted from isolated purified pea nuclei and total proteins were extracted from nuclear matrices (NMs). The protein extracts were separated in SDS gradient polyacrylamide gels. Pure spectrin was run in parallel and served as a reference for immunolabeling. After protein transfer, the Western blots were probed with two anti-spectrin antibodies.

Immunolabeling of pure human erythrocyte spectrin with anti-spectrin S1515 showed a prominent doublet of bands at 240/220 kDa, typical for α/β-spectrin (Fig. 3, lane 1). In this lane the antibody also recognized some polypeptides with apparent molecular masses of approximately 85/80 kDa, and 60 kDa. Occasionally, smaller bands, i.e. at 30 kDa, occurred (not shown). When samples of pure spectrin were frozen/thawed or boiled in denaturing SDS more often, the presence of these smaller polypeptides at 85/80 kDa, 60 kDa and 30 kDa further increased, while the 240/220 kDa labeling decreased. A similar increase of immunoreactive polypeptides at approximately 85/80 kDa, 60 kDa and 30 kDa, at the expense of a labeling at 240/220 kDa, was obtained when pure erythrocyte spectrin was immunolabeled with anti-spectrin S1390 (not shown). Silver staining of all proteins in the pea nuclear extract showed a similar doublet of bands at a molecular mass of 240/220 kDa (Fig. 3, lane 3). The detection limit of the silver staining is about 10 ng protein (Kovarík *et al.*, 1987).
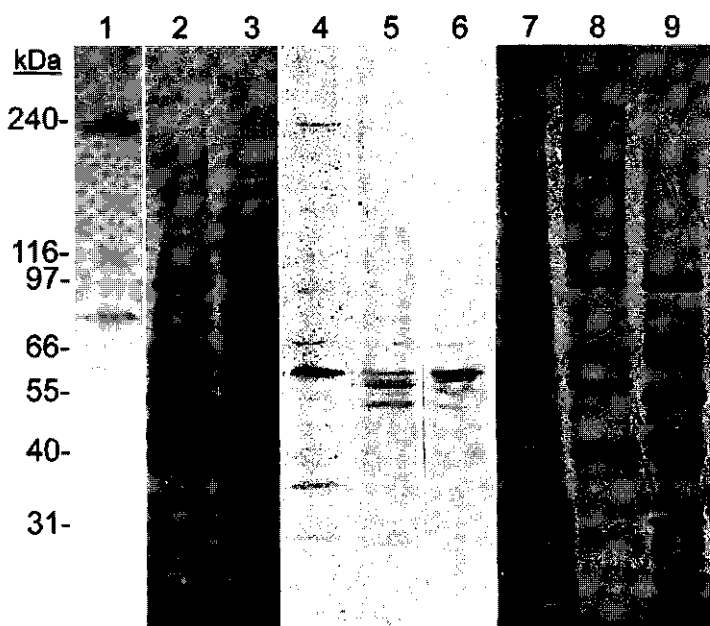
Figure 3. Western blot from a 4-15% polyacrylamide SDS gel, stained with silver (lanes 2, 3, 7, 8, 9) for total protein staining, or labeled with anti-spectrin (lanes 1, 4, 5, 6). The labeling was detected with chromogenic alkaline phosphatase reaction. Per lane 20 μg total protein was loaded (lanes 2-9).

(lane 1:) pure human erythrocyte spectrin (1.3 μg) labeled with anti-spectrin S1515

(lane 2:) protein markers of mid molecular weight (Promega)

(lane 3:) pea nuclear extract

(lane 4:) pea nuclear extract labeled with anti-spectrin S1390

(lane 5:) pea nuclear matrix fraction labeled with anti-spectrin S1390

(lane 6:) pea nuclear matrix fraction labeled with anti-spectrin S1515

(lane 7:) pea nuclear matrix fraction

(lane 8:) protein markers of high molecular weight (Promega)

(lane 9:) protein markers of mid molecular weight (Promega).

The doublet also specifically immunostained with anti-spectrin (S1390) (Fig. 3, lane 4), which shows the presence of 240/220 kDa spectrin-like proteins in pea nuclei. Similar to pure spectrin (lane 1), but much stronger, an immunoresponsive band was present at 60 kDa in the pea nuclear extract. When in control lanes the first antibody was omitted, no labeling was observed (not shown). We obtained nuclear matrix (NM) fractions by subsequently extracting nuclei with DNAse I, RNAse A and high salt. The amount of protein loaded was similar for all lanes. The profile of total proteins of NM extracts (Fig. 3, lane 7), was

different from the profile of complete nuclear extracts (Fig. 3, lane 3). Comparison of the labeling with anti-spectrin S1390 in the NM extract (Fig. 3, lane 5) and the complete nuclear extract (Fig. 3, lane 4), revealed that the 240/220 kDa bands had disappeared, and that the 60 kDa band remained or was increased in the NM extract. The same result was obtained when NM extracts were labeled with anti-spectrin S1515 (Fig. 3, lane 6). With a more sensitive chemiluminescence detection (as opposed to chromogenic alkaline phosphatase detection), high molecular mass spectrin-like proteins were still not observed in NM extracts (data not shown). Nevertheless, it is important to note that a significant immunostaining of spectrin-like epitopes remained present in NM extracts (Fig. 3, lanes 5 and 6), indicating a strong association of spectrin-like molecules with the nuclear matrix. No labeling was observed in the control lanes where the first antibody was omitted.

In a different approach, we used a spectrin extraction buffer based on low salt and high pH (Michaud *et al.*, 1991), to obtain a nuclear extract enriched in spectrin-like proteins. By immunoblot assay, the extracted proteins showed to be approximately 60 kDa or less in molecular mass (not shown; pattern similar to lane 4). No labeling of spectrin-like proteins was detected at high molecular mass.

The immunoreactive polypeptides at approximately 240/220 kDa in pea nuclear extracts are indicative for the presence of a plant spectrin in these nuclei. The 60 kDa band of spectrin-like proteins, also observed when the 240/220 kDa pure erythrocyte spectrin breaks down, was present in both the nuclear extract and the NM fraction, and was observed with two different anti-spectrin antibodies (Fig. 4, lanes 5 and 6), which further substantiates the presence of spectrin-like molecules that possibly originate from a breakdown of a 240/220 kDa nuclear plant spectrin.

Immunolocalization of spectrin-like epitopes in pea nuclei

Isolated fixed nuclei, adhered to slides, were immunolabeled. With anti-spectrin S1390, a strong peripheral staining was observed, and weak spots were present in the nucleoplasm (Figs. 4a2, 4b). When nuclei were partially extracted with 0.5% Triton X-100, the signal was present throughout the nucleoplasm, and localized in bright dots (compare Figs. 4a2, 4b with Figs. 4c2, 4d). The peripheral labeling remained in isolated nuclei, but in sections of vetch root cells, a peripheral labeling of nuclei was not observed with S1390 (Fig. 1b). Nucleoli were negative, even after prolonged extraction. When we used anti-spectrin S1515 with similar labeling conditions, we also obtained a speckled distribution in the nucleoplasm (Figs. 4e2-4h). The speckled pattern was prominent; however, the peripheral staining was less pronounced than was observed with S1390 (i.e. compare Figs. 4c2 with 4e2).
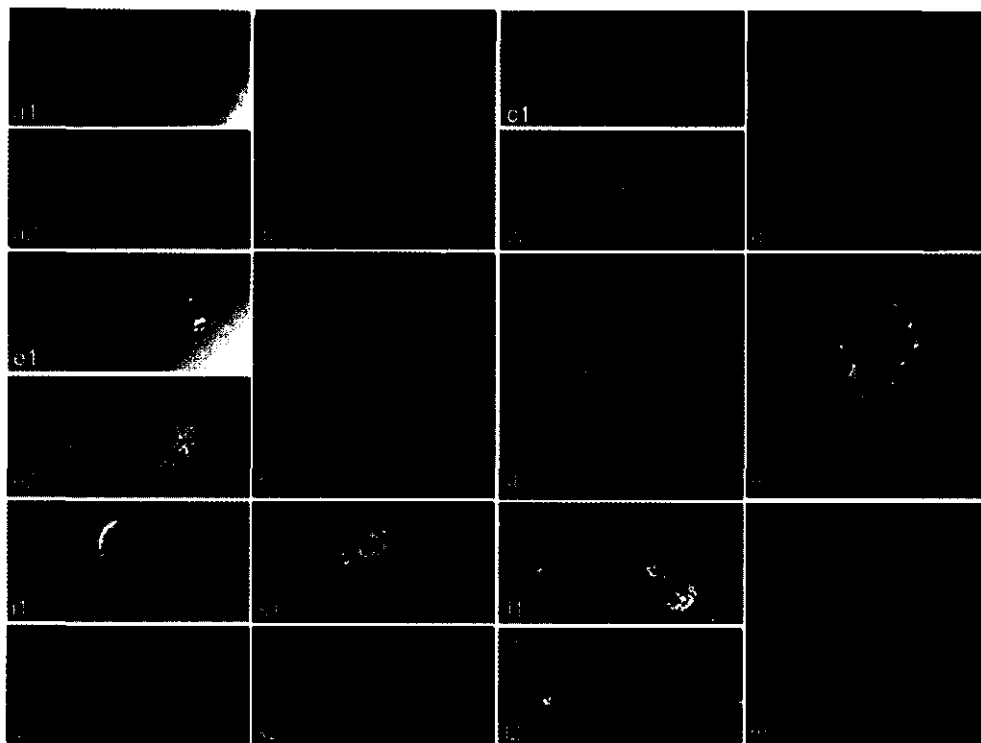
Nuclei were further extracted to obtain NMs and labeled with anti-spectrin S1390. The peripheral staining remained weak, but the speckled pattern was comparable, or even more prominent after incubation with DNAse and RNAse at 250 µg/ml each (Fig. 4f). The same result was obtained when nuclease treatment was followed by extraction with 1.6 M NaCl (Fig. 4h).

Using a confocal microscope, we observed that each optical plane within a nucleus had such a speckled distribution of labeling (as in Figs. 4d, 4f), which indicates that the spectrin-like proteins are evenly distributed in the nucleoplasm. Dual channel confocal microscopy was used to image simultaneously DNA (in red) and spectrin-like proteins (in green). Merged images of identical confocal planes were almost free of yellow dots (Figs. 4d, 4f), which indicates that DNA and spectrin-like epitopes have little or no co-localization. In 5-10% of the nuclei, the labeling appeared to be in paths, mostly radiating from nucleoli to the nuclear periphery (Fig. 4g). In 30-40% of the nuclei, bigger spots of spectrin-like proteins were found accumulated in the vicinity of the large nucleoli (Fig. 4h). All labelings were done on more than 15 slides (> 100 nuclei/slide) in at least 5 different experiments. With both anti-spectrin S1515 and S1390 the typical speckled distribution of label was observed in 90% ± 5% of the sampled nuclei.

Figure 4 (left) Labeled isolated pea nuclei.

(a-b) Labeling of nuclei with anti-spectrin (S1390, 1/300) shows a predominant staining at the nuclear membrane **(a1)** DIC image, **(a2)** corresponding labeled image, **(b)** merged confocal images of one optical section of a nucleus showing spectrin-like epitopes (in green) and DNA (in red).

(c-d) Labeling of nuclei with anti-spectrin S1390 shows a bright signal at the nuclear periphery, and in a speckled pattern throughout the nucleoplasm. Nucleoli are negative **(c1)** DIC image , **(c2)** corresponding labeled image after incubation with 1% BSA-c and anti-spectrin S1390 at 1/600 dilution, **(d)** merged image of spectrin-like epitopes (green), obtained with anti-spectrin (S1390, 1/300) after 0.5% Triton X-100, and the corresponding DNA image (red), shows almost complete absence of overlap (in yellow).

(e-h) Labeling of nuclei with anti-spectrin (S1515, 1/300), after 0.5% Triton X-100 extraction, shows a speckled staining throughout the nucleoplasm and no overlap with DNA. Nucleoli are negative. Nuclei in **(f)** and **(h)** were further extracted with 250 µg/ml DNAse I and 250 µg/ml RNAse A, and **(h)** subsequently with 1.6 M NaCl.

(e1) DIC image **(e2)** corresponding fluorescence image shows discrete foci of spectrin-like epitopes throughout the nucleoplasm, **(f)** merged image of spectrin-like epitopes (green) and DNA (red) shows almost complete absence of overlap (yellow), **(g)** Note nuclear paths of apparently aligned dots of label, **(h)** Note strong accumulation of spectrin-like epitopes at the periphery of the large nucleolus, **(i1)** DIC image, **(i2)** corresponding image shows absence of staining after labeling with FITC conjugated goat anti-mouse (control), **(k1)** Confocal optical plane showing DNA stained with propidium-iodide, **(k2)** the same plane showing absence of staining with pre-immune mouse serum (control),

(l-m) Nuclei labeled with anti-fibrillarin, **(l1)** confocal optical plane showing DNA with propidium-iodide staining, **(l2)** corresponding image showing fibrillarin in nucleoli, **(m)** merged image of strong fibrillarin staining in nucleoli (green) and DNA (red) showing absence of overlap (yellow).

When blocking of nuclei was increased, and antibodies were incubated at lower concentration, bright nuclear labelings were still observed. For instance, when nuclei were blocked with 1% BSA, followed by 1% BSA-c, instead of 0.1% BSA-c, and incubated with anti-spectrin S1390 at 1/600, instead of 1/300 dilution, in the presence of 0.05% Triton X-100 and 0.1% BSA-c, strong nuclear labeling was observed (Fig. 4c2). When, prior to labeling, nuclei were further extracted with nucleases (Fig. 4f) and high salt (Fig. 4h), the labeling remained or enhanced, which excludes aspecific binding to nucleic acids. When anti-spectrin was omitted in the labeling procedure, no signal, or a weak glow was observed (Fig. 4i2). Similar negative control labelings were obtained when pre-immune serum of mice (Fig. 4k2) or rabbits was applied. To check whether nucleoli were accessible at conditions used for anti-spectrin labeling, we applied 72B9, a monoclonal antibody against fibrillarin, a structural protein of nucleoli. In Fig. 4l2 and 4m, labeling was observed throughout nucleoli, providing a positive control for nucleolar accessibility.

DISCUSSION

This paper describes the presence and localization of spectrin–like epitopes in plant nuclei. The data are based on cross-reactivity of polyclonal antibodies, which were raised against α- and β-spectrin from human and chicken red blood cells. Three different polyclonal antibodies detected with high affinity similar bands on Western blots and detected similar patterns in various plant nuclei.

We show that the location and intensity of labeling correlates with the penetration of the antibodies into the nuclei. At increased fixation, increased section thickness, or when extraction with Triton X-100 and DNAse/RNAse was omitted, the labeling was often absent, or mainly at the nuclear periphery (Fig 1a, 4a2, 4b). However, after a partial extraction with 1% Triton X-100, spectrin-like proteins were detected, in addition to the peripheral location. The labeling occurred in distinct bright speckles throughout the nucleoplasm. In almost 10% of the nuclei, also a labeling in tracks was observed. Similar localizations were observed with anti-human erythrocyte spectrin (S1515 and C567622), and anti-chicken erythrocyte spectrin (S1390), in sections of root cortical cells of broad bean and vetch, and in cells of pea seedlings plumules.

When isolated pea nuclei were treated with nucleases and high salt, the signal increased, but the distribution in speckles was not affected. The speckled labeling in the nucleoplasm after extraction with 0.5% Triton X-100, 250 µg/ml DNAse I and 250 µg RNAse A, and 1.6 M NaCl indicates a strong association of the spectrin-like epitopes with the nuclear matrix. Nucleoli were never labeled. Nucleoli were well accessible for antibodies, since labeling with anti-fibrillarin resulted in a bright nucleolar staining.

The bright staining of spectrin-like proteins at the periphery of isolated nuclei might point at the presence of remnants of endoplasmatic reticulum (ER) connected with the nuclear envelope. Spectrin-like proteins have been localized in the ER around nuclei in living onion cells, after microinjection with labeled anti-spectrin (Reuzeau *et al.*, 1997). However, the peripheral staining of nuclei remained as distinct dots after treatment with 0.5% Triton X-100, which dissolves the ER membranes (Fig. 4d). Therefore, it seems more likely that the spectrin-like proteins are an intrinsic part of the nucleus at its periphery. This view is supported by a study of Bachs *et al.* (1990), which showed co-purification of a 240 kDa nuclear α-spectrin with nuclear envelopes from rat liver nuclei.

To identify nuclear spectrin-like epitopes, we extracted purified isolated nuclei of pea. The extract showed the presence of a 240/220 kDa doublet, that co-migrated with α-, β-erythrocyte spectrin, and was detected with anti-chicken erythrocyte spectrin S1390 (Fig.3, lane 4). To elucidate whether the plant spectrin-like protein is, indeed, a part of the nuclear matrix, we repeatedly extracted nuclei with DNAse I and RNAse A, followed by high salt

extractions to obtain nuclear matrices (NMs), referred to as nuclear envelope matrices by Li and Roux (1992). Blots of NM fractions showed a strong signal at 60 kDa, visible both with anti-spectrin antibody S1515 and S1390, which indicates that spectrin-like proteins in pea nuclei are associated with the nuclear matrix. However, the high molecular weight (HMW) polypeptides, typical for spectrin-like proteins were lost. Such loss of immunoreactive HMW polypeptides has been observed earlier in various extraction procedures for spectrin-like proteins (animal cells: Burridge *et al.*, 1982; Bachs *et al.*, 1990; plant cells: De Ruijter and Emons, 1993; Holzinger *et al.*, 1999), and has been explained as (proteolytic) breakdown. We were not able to prevent the loss of the 240/220 kDa polypeptides by the use of a complex protease inhibitor cocktail. Also pure spectrin, which served as the reference protein, showed some loss of the 240/220 kDa doublet, while an immunoreactive 60 kDa polypeptide increased. The breakdown was caused by repeated freezing and heating in SDS-DTT.

Labeling of epitopes based on cross-reactivity of antibodies shows the presence of a similar epitope, but does not proof the presence of a similar protein. At present a plant spectrin gene has not been characterized yet. However, McCurdy and Kim (1998) cloned and sequenced a gene *ATFIM1*, encoding a fimbrin-like polypeptide in *Arabidopsis thaliana*, and also in wheat, a fimbrin-like protein has been found (Cruz-Ortega *et al.*, 1997). Since fimbrin and spectrin are actin cross-linking proteins of the spectrin gene family in animal species, these data show that a spectrin gene family is present in plants. The identity of the plant nuclear spectrin-like protein can be further defined when sequence information and mono-specific antibodies for plant spectrin epitopes become available.

Tracks of anti-spectrin labeling, i.e. from nucleoli to the nuclear periphery, were occasionally observed in pea nuclei, in addition to the speckled distribution (Fig. 4g). Similarly, in chicken osteoclasts, spectrin has been localized by immuno electron microscopy, along filamentous structures within the nucleus (Hunter *et al.*, 1998). In oocyte nuclei distinct intranuclear tracks, composed of bundles of actin, also extend from nucleoli to the nuclear periphery (Parfenov *et al.*, 1995). The presence of actin containing tracks is indicated by the detection of a myosin-like protein, an actin binding motor protein, in intra-nuclear tracks. A nuclear myosin-like protein (Mlp 1p) has been isolated in yeast, with homologues in vertebrate and *Drosophila* nuclei, and these proteins also localize in distinct tracks, connecting the nuclear pore complex with the nuclear interior (Strambio-de-Castillia *et al.*, 1999). Overexpression of Mlp 1p in yeast increased the nuclear protein transport, which points at the presence of actin-Mlp 1p in these tracks. Little is known about nuclear import and export signals, but it is becoming clear that actin binding proteins are involved (plant cells: Smith and Raikhel, 1999). Spectrin may bind to actin and stabilize the structure of the nuclear tracks.

The speckled pattern of anti-spectrin labeling in the nucleoplasm is comparable with the speckled pattern obtained when small nuclear ribo-nucleoproteins (snRNPs) are labeled. The snRNPs play an integral role in the processing of pre-mRNA in eukaryotic nuclei and generally distribute to interchromatin granules, referred to as 'speckles' (reviewed by Lamond and Carmo-Fonseca, 1993 and Spector, 1993). These nuclear domains are part of the nuclear matrix. The speckles of snRNPs represent storage and assembly sites in animal nuclei (reviewed by Van Driel *et al.*, 1995), and this has also been reported for wheat (*Triticum aestivum* L.) and barley (*Hordeum vulgare* L.) (Glyn and Leitch, 1995), pea (*Pisum sativum* L.) (Beven *et al.*, 1995), and rapeseed (*Brassica napus* L.) (Straatman *et al.*, 1996). Actin and spectrin not only show a similar distribution in tracks, but in eukaryotic cells, nuclear actin has also been found in distinct aggregates in the nucleoplasm (Milankov and De Boni, 1993). The actin was distributed in a speckled pattern and correlated with snRNP-activity (Sahlas *et al.*, 1993). However, to be able to correlate the speckled pattern of spectrin-like epitopes with a speckled pattern of snRNPs, or a speckled distribution of actin aggregates, a double labeling should be performed, followed by accurate quantitative evaluation of the degree of overlap between two fluorochromes by nearest neighbor analysis (Manders *et al.*, 1992; Sahlas *et al.*, 1993).

We conclude that plant spectrin-like proteins are part of the nuclear matrix, where they could have a function in stabilizing specific domains in the nucleus.

ACKNOWLEDGEMENTS

REFERENCES

Ankenbauer T, Kleinschmidt JA, Walsh MJ, Weiner OH, Franke WW, 1989. Identification of a widespread nuclear actin binding protein. *Nature* 342: 822-825.

Bachs O, Lanini L, Serratosa J, Coll MJ, Bastos R, Aligué R, Rius E, Carafoli E, 1990. Calmodulin-binding proteins in the nuclei of quiescent and proliferatively activated rat liver cells. *J Biol Chem* 265: 18595-18600.

Beck KA, Nelson WJ, 1996. The spectrin-based membrane skeleton as a membrane protein-sorting machine. *Am J Physiol* 270: 1263-1270.

Bennett V, 1990. Spectrin-based membrane skeleton: a multipotential adaptor between plasma membrane and cytoplasm. *Physiol Rev* 70: 1029-1065.

Bennett V, Gilligan DM, 1993. The spectrin-based membrane skeleton and micron-scale organization of the plasma membrane. *Ann Rev Cell Biol* 9: 27-66.

Beven AF, Simpson GG, Brown JW, Shaw PJ, 1995. The organization of spliceosomal components in the nuclei of higher plants. *J Cell Sci* 108: 509-518.

Blumenthal SSD, 1997. Biological and immunological analyses of pea nuclear lamins. Ph.D. thesis, University of Texas, Austin, USA.

Burridge K, Kelly T, Mangeat P, 1982. Nonerythrocyte spectrins: actin-membrane attachment proteins occurring in many cell types. *J Cell Biol* 95: 478-486.

Carotenuto R, Maturi G, Infante V, Capriglione T, Petrucci TC, Campanella C, 1997. A novel protein cross-reacting with antibodies against spectrin is localised in the nucleoli of amphibian oocytes. *J Cell Sci* 110: 2683-2690.

Carlier MF, 1998. Control of actin dynamics. *Curr Opin Cell Biol* 10:45-51.

Clark GB, Dauwalder M, Roux SJ, 1998. Immunological and biochemical evidence for nuclear localization of annexin in peas. *Plant Phys Biochem* 36: 621-627.

Cruz-Ortega R, Cushman JC, Ownby JD, 1997. cDNA clones encoding 1,3-beta-glucanase and a fimbrin-like cytoskeletal protein are induced by Al toxicity in wheat roots. *Plant Physiol* 114:1453-60.

Datta N, Chen YR, Roux SJ, 1985. Phytochrome and calcium stimulation of protein phosphorylation in isolated pea nuclei. *Biochem Biophys Res Comm* 128: 1403-1408.

De Boni U, 1994. The interphase nucleus as a dynamic structure. *Int Rev Cytol* 150 : 149-171.

De Jong L, van Driel R, Stuurman N, Meijne AM, Van Renswoude J, 1990. Principles of nuclear organization. *Cell Biol Int Rep* 14: 1051-1074.

De Ruijter N, Emons AM, 1993. Immunodetection of spectrin antigens in plant cells. *Cell Biol Int* 17: 169-182.

De Ruijter NCA, Emons AMC, 1999. Actin-binding proteins in plant cells. *Plant Biol* 1: 26-35.

De Ruijter NCA, Rook MB, Bisseling T, Emons AMC, 1998. Lipochito-oligo-saccharides re-initiate root hair tip growth in *Vicia sativa* with high calcium and spectrin-like antigen at the tip. *Plant J* 13: 341-350.

Dubreuil RR, 1991. Structure and evolution of the actin crosslinking proteins. *Bioessays* 13: 219-326.

Faraday CD, Spanswick RM, 1993. Evidence for a membrane skeleton in higher plants. A spectrin-like polypeptide co-isolates with rice root plasma membranes. *FEBS* 318: 313-316.

Glyn MC, Leitch AR, 1995. The distribution of a spliceosome protein in cereal (Triticeae) interphase nuclei from cells with different metabolic activities and through the cell cycle. *Plant J* 8: 531-540.

Hartwig J, 1994. Actin-Binding Proteins 1: spectrin superfamily. Subfamily 1: The spectrin family, *Protein Profile* 1: 715-749.

Holzinger A, De Ruijter NCA, Emons AMC, Lütz-Meindl U, 1999. Spectrin-like proteins in green algae (Desmidiaceae). *Cell Biol Int*, in press.

Hozák P, Sasseville AMJ, Raymond Y, Cook PR, 1995. Lamin proteins form an internal nucleoskeleton as well as a peripheral lamina in human cells. *J Cell Sci* 108: 635-644.

Hunter SJ, Gay CV, Osdoby PA, Peters LL, 1998. Spectrin localization in osteoclasts: immunocytochemistry, cloning, and partial sequencing. *J Cell Biochem* 71: 204-15.

Jiang CJ, Weeds AG, Hussey PJ, 1997. The maize actin-depolymerizing factor, ZmADF3, redistributes to the growing tip of elongating root hairs and can be induced to translocate into the nucleus with actin. *Plant J* 12: 1035-43.

Kovarík A, Hlubinova K, Vrbenska A, Prachar J, 1987. An improved colloidal staining method of protein blots on nitrocellulose membranes. *Folia Biologica* 33: 253-257.

Laemmli UK, 1970. Cleavage of structural proteins during the assembly of the head of bacteriophage T4. *Nature* 227: 680-685.

Lamond AI, Carmo-Fonseca M, 1993. Localisation of splicing snRNPs in mammalian cells. *Mol Biol Rep* 18 : 127-133.

Lamond AI, Earnshaw WC, 1998. Structure and function in the nucleus. *Science* 280: 547-553.

Li H, Roux SJ, 1992. Casein kinase II protein kinase is bound to lamina-matrix and phosphorylates lamin-like protein in isolated pea nuclei. *Proc Natl Acad Sci* USA 89: 8434-8438.

Lippincott-Schwartz J, 1998. Cytoskeletal proteins and Golgi dynamics. *Curr Opin Cell Biol* 10: 52-59.

Manders EM, Stap J, Brakenhoff GJ, Van Driel R, Aten JA, 1992. Dynamics of three-dimensional replication patterns during the S-phase, analysed by double labelling of DNA and confocal microscopy. *J Cell Sci* 103: 857-862.

Marchesi VT, Steer E, 1968. Selective solubilization of a protein of the red cell membrane. *Science* 159: 203-204.

McCurdy DW, Kim M, 1998. Molecular cloning of a novel fimbrin-like cDNA from *Arabidopsis thaliana*. *Plant Mol Biol* 36: 23-31.

Michaud D, Guillet G, Rogers PA, Charest PM, 1991. Identification of a 220 kDa membrane-associated plant cell protein immunologically related to human β-spectrin. *FEBS* 294: 77-80.

Milankov K, De Boni U, 1993. Cytochemical localization of actin and myosin aggregates in interphase nuclei in situ. *Exp Cell Res* 209: 189-199.

Mínguez A, Moreno Díaz de la Espina S, 1993. Immunological characterization of lamins in the nuclear matrix of onion cells. *J Cell Sci* 106: 431-439.

Moir RD, Spann TP, Goldman RD, 1995. The dynamic properties and possible functions of nuclear lamins. *Int Rev Cytol* 162B: 141-82.

Moreno Díaz de la Espina S, 1995. Nuclear matrix isolated from plant cells. *Int Rev Cyt* 162B: 75-139.

Parfenov VN, Davis DS, Pochukalina GN, Sample CE, Bugaeva EA, Murti KG, 1995. Nuclear actin filaments and their topological changes in frog oocytes. *Exp Cell Res* 217: 385-394.

Puius YA, Mahoney NM, Almo SC, 1998. The modular structure of actin-regulatory proteins. *Curr Opin Cell Biol* 10: 23-34.

Reimer G, Pollard KM, Penning CA, Ochs RL, Lischwe MA, Busch H, Tan EM, 1987. Monoclonal autoantibody from a (New Zealand black x New Zealand white) F_1 mouse and some human scleroderma sera target an M 34,000 nucleolar protein of the U3 RNP particle. *Arthritis Rheum* 30: 793-800.

Reuzeau C, Doolittle KW, McNally JG, Pickard BG, 1997. Covisualization in living onion cells of putative integrin, putative spectrin, actin, putative intermediate filaments, and other proteins at the cell membrane and in an endomembrane sheath. *Protoplasma* 199: 173-197.

Ryabova LV, Virtanen I, Wartiovaara J, Vassetzky SG, 1994. Contractile proteins and nonerythroid spectrin in oogenesis of Xenopus laevis. *Mol Reprod Dev* 37: 99-109.

Sahlas DJ, Milankov K, Park PC, De Boni U, 1993. Distribution of snRNPs, splicing factor SC-35 and actin in interphase nuclei: immunocytochemical evidence for differential distribution during changes in functional states. *J Cell Sci* 105: 347-357.

Sauman I, Berry SJ, 1994. An actin infrastructure is associated with eukaryotic chromosomes: structural and functional significance. *Eur J Cell Biol* 64: 348-56.

Scheer U, Hinssen H, Franke WW, Jockusch BM, 1984. Microinjection of actin-binding proteins and actin antibodies demonstrates involvement of nuclear actin in transcription of lampbrush chromosomes. *Cell* 39: 111-22.

Sikorski AF, Swat W, BrzezinskaM, Wroblewski Z, Bisikirska B, 1993. A protein cross-reacting with anti-spectrin antibodies is present in higher plant cells. *Z Naturforsch* 48c: 580-583.

Smith HM, Raikhel NV, 1999. Protein targeting to the nuclear pore. What can we learn from plants? *Plant Physiol* 119: 1157-1164.

Spector DL, 1993. Macromolecular domains within the cell nucleus. *Annu Rev Cell Biol* 9: 265-315.

Straatman KR, Trompetter CM, Schul W, Schel, JHN, 1996. Fluorescent labelling of nascent RNA reveals nuclear transcription domains throughout plant cell nuclei. *Protoplasma* 192: 145-149.

Strambio-de-Castillia C, Blobel G, Rout MP, 1999. Proteins connecting the nuclear pore complex with the nuclear interior. *J Cell Biol* 144: 839-855.

Stuurman N, De Jong L, Van Driel R, 1992. Nuclear frameworks: concepts and operational definitions. *Cell Biol Int Rep* 16: 837-852.

Stuurman N, Heins S, Aebi U, 1998. Nuclear lamins: their structure, assembly, and interactions. *J Struct Biol* 122: 42-66.

Tong CG, Reichler S, Blumenthal S, Balk J, Hsieh HL, Roux SJ, 1997. Light regulation of the abundance of mRNA encoding a nucleolin-like protein localized in the nucleoli of pea nuclei. *Plant Physiol* 114: 643-652.

Van Driel R, Wansink DG, Van Steensel B, Grande MA, Schul W, De Jong L, 1995. Nuclear domains and the nuclear matrix. *Int Rev Cytol* 162A: 151-189.

Vendrell M, Aligue R, Bachs O, Seratosa J, 1991. Presence of calmodulin and calmodulin-binding proteins in the nuclei of brain cells. *J Neurochem* 57: 622-628.

Wan LH, Xing M, 1998. Immunolocalization of actin in intact and DNA- and histone-depleted nuclei and chromosomes of *Allium cepa. Cell Res* 8: 51-62.

Willmitzer I, Wagner KG, 1981. The isolation of nuclei from tissue-cultured plant cells. *Exp Cell Res* 135: 69-77.

- Chapter 5 -

The role of actin in root hair morphogenesis:
studies with
lipochito-oligosaccharide as a growth stimulator
and cytochalasin as an actin perturbing drug

Norbert C.A. de Ruijter[1,*], Deborah D. Miller[1,*],
Ton Bisseling[2] and Anne Mie C. Emons[1]

[1]*Laboratory of Plant Cytology and Morphology, Wageningen Agricultural University,
Arboretumlaan 4, 6703 BD, Wageningen, The Netherlands*
[2]*Laboratory of Molecular Biology, Wageningen Agricultural University,
Dreijenlaan 3, 6703 HA, Wageningen,, The Netherlands*

Short title: Actin filament function in morphogenesis

*The first two authors have contributed equally to the work

SUMMARY

Root hairs develop from bulges on root epidermal cells and elongate by tip growth, in which Golgi vesicles are targeted, released, and inserted into the plasma membrane on one side of the cell. We studied the role of actin in vesicle delivery and retention by comparing the actin filament configuration during bulge formation, root hair initiation, sustained tip growth, growth termination, and in full-grown hairs. Lipochito-oligosaccharides (LCOs) were used to interfere with growth (De Ruijter *et al.,* 1998), and cytochalasin D (CD) was used to interfere with actin function. Actin filament bundles lie net-axially in cytoplasmic strands in the root hair tube. In the subapex of growing hairs, these bundles flare out into fine bundles. The apex is devoid of actin filament bundles. This subapical actin filament configuration is not present in full-grown hairs; instead, actin filament bundles loop through the tip. After LCO application, the tips of hairs that are terminating growth swell and a new outgrowth appears from a site in the swelling. At the start of this outgrowth, net-axial fine bundles of actin filaments reappear, and the tip region of the outgrowth is devoid of actin filament bundles. CD at 1.0 µM, which does not affect cytoplasmic streaming, does not inhibit bulge formation and LCO-induced swelling, but it inhibits initiation of polar growth from bulges, elongation of root hairs, and LCO-induced outgrowth from swellings. We conclude that elongating net-axial fine bundles of actin filaments, which we call FB-actin, function in polar growth by targeting and releasing Golgi vesicles to the vesicle-rich region, while actin filament bundles looping through the tip impede vesicle retention.

Keywords: Actin filament, cytochalasin D, cytoskeleton, lipochito-oligosaccharide, morphogenesis, tip growth

INTRODUCTION

Plant cell morphogenesis is cell growth at defined sites in defined directions and amounts. Plant cell growth involves the insertion of Golgi vesicle membranes into the plasma membrane with the simultaneous delivery of Golgi vesicle content into the extracellular matrix, the cell wall. For this exocytosis process, the vesicles have to be transported to the growth site, released and inserted into the plasma membrane. In this study we ask the questions whether the actin cytoskeleton is involved in targeting and releasing the Golgi vesicles to the site of exocytosis, and how the structure of that cytoskeleton is when it supports these functions. We have chosen the root hair for this research since these fast growing cells grow at their tips only, which makes the exocytosis process in the tip of these cells more prominent than in intercalary growing cells.

Growing root hairs have a characteristic pattern of cytoplasmic streaming, in which the cytoplasm flows towards the tip in strands located near the plasma membrane and returns before reaching the tip, often in strands near the center. This pattern of streaming has been called reverse fountain streaming in pollen tubes (Iwanami, 1956). Cytoplasmic streaming in plant cells requires actin filaments. Microinjection of the actin binding protein profilin in *Tradescantia* stamen hair cells, at concentrations that depolymerized the actin filaments, stopped streaming (mature cells: Staiger *et al.*, 1994; growing cells: Valster *et al.*, 1997). The streaming pattern in root hairs and other tip-growing cells suggests that this process is somehow involved in targeting of Golgi vesicles from their site of production, the Golgi bodies present in the cytoplasm below the vesicle-rich region, to the base of the vesicle-rich region, where they are released and retained.

Our approach is to compare the configuration of the actin cytoskeleton of root hairs during development. We distinguish four different stages: bulge formation (Dolan *et al.*, 1994) from the epidermal cell, tip-growth of the root hair, growth termination, and full-grown hairs. The study of this developmental process is feasible for root hairs, since all developmental stages are present along the root and from individual hairs the growth status can be determined in the light microscope (De Ruijter *et al.*, 1998; Miller *et al.*, 1997). To further probe the relationship between the actin filament configuration and vesicle targeting and release, we applied lipochito-oligosaccharides (LCOs) to reinitiate polar growth (De Ruijter *et al.*, 1998), and used cytochalasin D (CD) to interfere with the actin cytoskeleton.

Because microinjection of fluorescent phalloidin disturbed the polarized cytoarchitecture of vetch root hairs (D.D. Miller, unpublished results), we were not able to study the actin cytoskeleton in living cells. Therefore, we used fixed cells. Many electron microscopic studies have shown that freeze-substitution after freeze-fixation is superior to chemical fixation (root hairs: Emons and Derksen, 1986; Emons, 1987; Ridge, 1988; Galway *et al.*,

1997). It is also the method of choice for light microscopy (Baskin *et al.*, 1996). Therefore, we have chosen this method for the immunolocalization of actin filaments. We used labeling of sections and of whole mounts, of which the sections generally gave the best results. The advantage of sectioning is that no wall degrading enzymes are needed, which may disturb the cortical actin cytoskeleton. This procedure has the disadvantage that only parts of single hairs can be studied. Since we needed to observe large populations of cells for the drug studies, we improved a chemical fixation procedure such that the cytoarchitecture resembled that of living cells and the actin cytoskeleton resembled that of immuno-labeled cells after freeze-substitution. No wall degrading enzymes were used and actin filaments were stained with fluorescein-phalloidin.

We show that growth initiation, termination, re-initiation by LCO, and termination by CD involve a reorganization of the actin cytoskeleton. These reorganizations are all consistent with two related hypotheses. First, vesicle targeting and release require the presence of net-axially elongating fine bundles of actin filaments (in short: FB-actin). Second, the accumulation and retention of vesicles require the absence of actin filament bundles at the extreme hair tip. We conclude that only when the actin configuration meets both requirements are vesicle targeting, release, and retention possible and can tip growth persist.

RESULTS

Root hair growth correlates with elongation of subapical, net-axial fine bundles of actin filaments and absence of actin filament bundles at the tip

Root hairs are appendages of root epidermal cells, trichoblasts. Before root hair emergence, actin filament bundles in the trichoblasts are oriented mostly longitudinally to the root axis; during root hair development they keep this orientation (Figures 1g,h). The first step is the formation of a bulge on a trichoblast (Dolan *et al.*, 1994). In vetch, every epidermal cell forms a bulge and subsequently a root hair (D.D. Miller, unpublished result). The bulge has a fairly triangular shape, and consists of a layer of peripheral cytoplasm with strands (s) around a large vacuole (v) (Figure 1a). Actin filament bundles in the bulges (Figure 1g, arrowhead) are mostly in the same orientation as in the epidermal cell and pass through the cytoplasm at the periphery of the bulge. Bulges develop into growing root hairs which have a smaller diameter, possess polarized cytoplasm (Figures 1c1 chemically fixed cell; 1b,c2,d living cells), and extend in the direction of the tip. The polarized distribution of the cytoplasm is evident in the light microscope by the occurrence of a cytoplasmic dense subapical region (Figures 1c1,c2,d; large bracket) that contains organelles and small vacuoles. An even more smooth-looking region is located at the apex of the hair (Figures 1b,c1,c2,d; small bracket). From electron microscopic studies it is known that this smooth

region, of 1-3 μm from the tip, almost exclusively contains secretory vesicles (*Vicia sativa*, unpublished results; for *Vicia villosa*, Sherrier and VandenBosch, 1994). We will refer to this region as the vesicle-rich region. While the hair grows, the vacuole increases in size, but the cytoplasmic dense region, with the vesicle-rich region closest to the tip, remains at the tip (Figure 1c).

Actin filament bundles in growing hairs (Figures 1g,h,i,j) are present in all the cytoplasmic strands. These bundles lie longitudinally, perpendicular to their net-orientation in the epidermal cell (Figures 1g,h). In the subapical region the filament bundles flare out into thinner and thinner bundles and maybe even into single filaments (see also Figure 4b), but the difference between a single filament of 8 nm and a thin bundle of filaments can not be resolved in the light microscope. We refer to this subapical actin filament configuration as net-axial fine bundles of actin filaments (FB-actin). In the microscope it can be determined that foci of actin seen in the subapex of growing hairs in micrographs, as for instance in Figure 1h,j,l, are not actin patches but sites where actin filaments bend out of the focal plane. A small region devoid of actin filaments is found at the very apex (arrows in Figures 1g,h,i,j) and is not yet present in the bulge (arrowhead Figure 1g). Since actin filaments come nearer to the tip in the cortical than in the central cytoplasm, the region devoid of actin filaments (arrows) is seen as a cleft at the cell apex. This cleft is approximately 5-8 μm wide and 2-6 μm deep (Figures 1g,h,i,j), and approximately coincides with the vesicle-rich region. When antibodies are used for actin visualization, a fuzzy staining is seen in the subapex (Figure 1i,j), which is not present with fluorescein-phalloidin (Figure 1g), indicating the presence of monomeric actin in this region.

The cytoarchitecture of hairs in which growth is terminating, zone II hairs (Heidstra *et al.*, 1994), is different from that of growing, zone I, hairs. In zone II hairs the main vacuole is close to the tip, the subapical region with dense cytoplasm is short and contains small vacuoles and numerous cytoplasmic strands that can extend through the tip (Figure 1e). Actin filament bundles are found within the cytoplasmic strands in the vacuolated region of these root hairs (Figure 1k) and come close to the hair tip, but do not become as thin and densely distributed as in the growing hairs. A region devoid of actin is not present.

Full-grown hairs, zone III hairs, have one large vacuole in the center of the cell and peripherally located cytoplasm (Figure 1f1 chemically fixed cell, 1f2 living cell). The actin filament bundles are found in the layer of cytoplasm at the periphery of the cell, also looping through the tip (Figure 1l). Not all filament bundles pass through the tip; some turn in the cortical cytoplasm before they reach the apex ((s) in Figure 1f and arrowhead in Figure 1m).

In summary (Figure 2a), growing hairs possess thick actin filament bundles in the cytoplasmic strands from base to subapex, net-axially aligned fine bundles of actin filaments, FB-actin, in the subapex, and no actin filament bundles in the extreme tip. In hairs that are
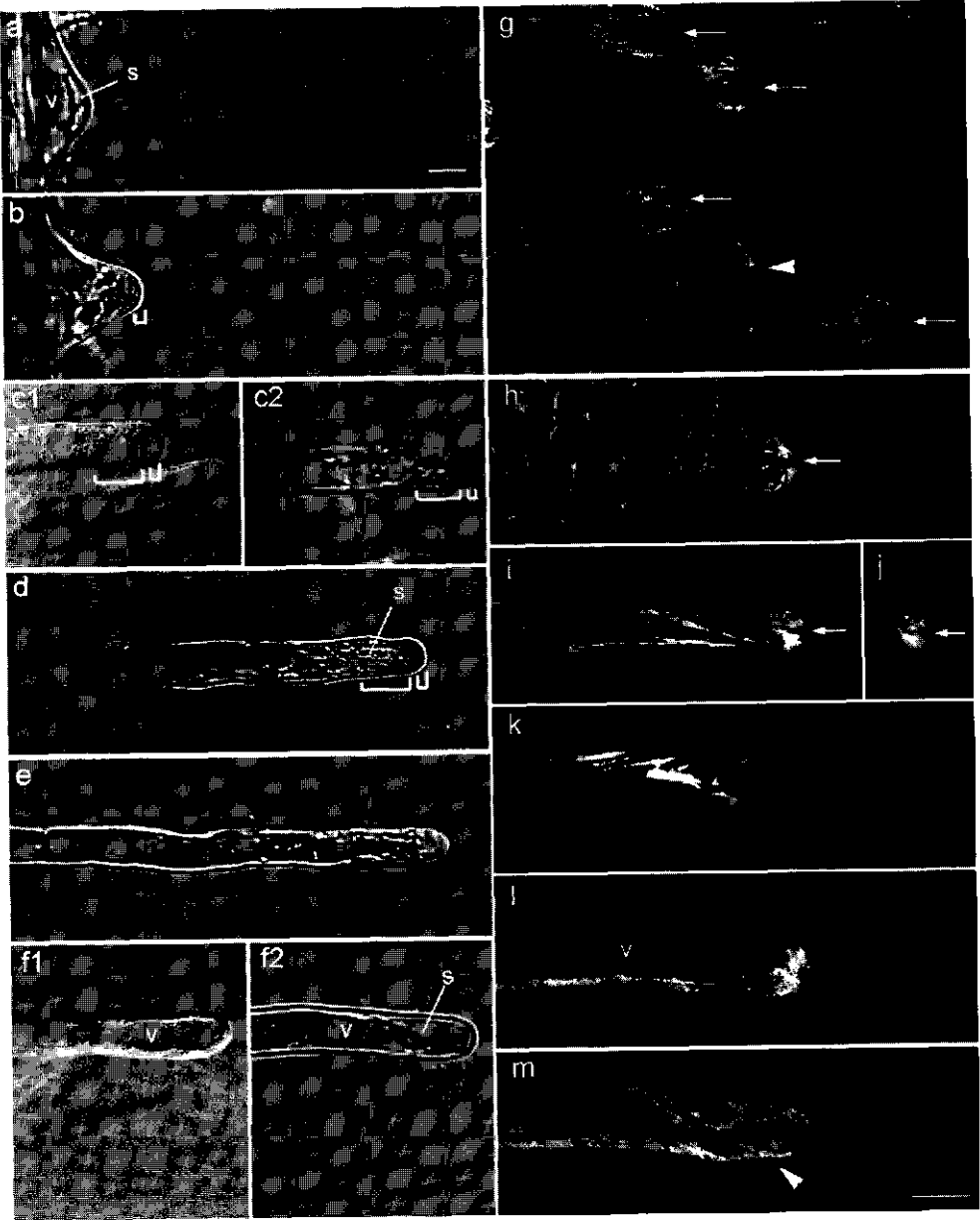
Figure 1

Figure 1 (left): Cytoarchitecture and corresponding actin cytoskeleton of vetch root hairs during development.

(**a-f**) Differential interference contrast (DIC) images of subsequent stages of a living root hair during its development, including two images that show the quality of the optimized chemical fixation (**c1** and **f1**). The magnification is the same in all images. Bar in (**a**) equals 15 µm.

(**a**) Triangular bulge on trichoblast. Cytoplasmic strands (s) are at the periphery and a large vacuole (v) occupies most of the cell.

(**b,c,d**) Growing hairs. A smooth region is present at the tip, which contains Golgi vesicles (small bracket). A subapical region is traversed by cytoplasmic strands (s) with many organelles (large bracket). From b-d the vacuole increases in size.

(**e**) Root hair in which growth is terminating with several small vacuoles up to the tip.

(**f1,f2**) Full-grown hair with one large vacuole (v) and only peripheral cytoplasm (s).

(**g-m**) Projections of z-series of confocal images of the actin filament configuration in subsequent stages of root hair development. The magnification is the same in all images. Bar in (**m**) equals 15 µm.

(**g**) Ester-aldehyde fixed, whole mount fluorescein-phalloidin stained trichoblasts with bulges and short root hairs. The actin filament bundles in the epidermal part of the cell are oriented parallel to the long axis of the root and pass through the peripheral cytoplasm of the bulge (arrowhead), while the tips of growing root hairs are devoid of actin filament bundles (arrows).

(**h-m**) Freeze-substituted root hairs labeled with anti-actin.

(**h**) Young growing root hair after whole mount immunolabeling. The actin filament bundles in the root hair proper are oriented parallel to the long axis of the hair, with FB-actin subapically, and a region devoid of label at the cell apex (arrow).

(**i**) Actin filaments in a median plane of a whole mount preparation. Actin filament bundles are parallel to the long axis of the hair, subapically bundles are finer and denser (FB-actin); The very tip is devoid of actin (arrow).

(**j**) Projection of z-series through a root hair; the arrow indicates the cleft devoid of actin filament bundles.

(**k**) Actin filament distribution in a hair in which growth is terminating. Filamentous actin comes up to the tip; a region devoid of actin filaments is not present.

(**l and m**) Longitudinal optical sections of a full-grown root hair at the median (**l**) and cortical (**m**) plane.

(**l**) The dark region in the center is the vacuole (v).

(**m**) In the peripheral cytoplasm, bundles of actin filament loop through the extreme tip, some actin filament bundles (arrowhead) do not loop through the extreme tip, but all bundles lie in the cortical cytoplasm.

Bars equal 15 µm.
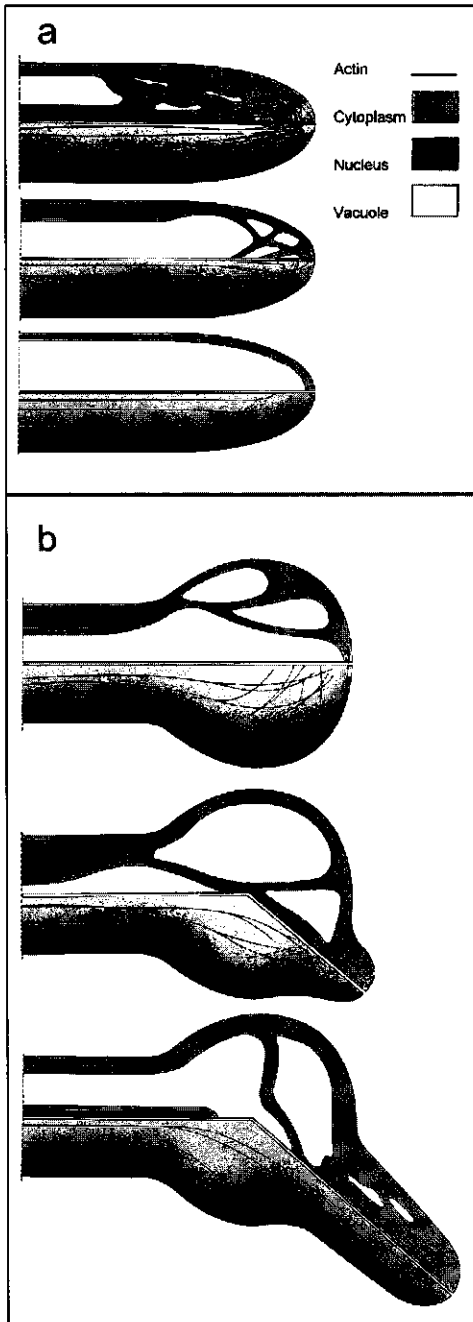
Figure 2: (a) Schematic illustration of the actin configuration during vetch root hair development. The upper half of each image represents a median view of the cell while the lower half represents a cortical view. Description is from upper to lower image.

Growing root hair: actin filaments are found as thick bundles in cytoplasmic strands over the full length of the root hair, and become thinner as they approach the tip. In the subapical region the actin filament bundles are finer (FB-actin) and less axial. In the very apex a region devoid of actin filaments is present. In the median plane the actin filaments are not as close to the apex as in the cortical plane.

Root hair in which growth is terminating: actin filament bundles are present in all cytoplasmic strands; the region with FB-actin is short and comes up to the apex.

Full-grown root hair: actin filament bundles are located in the cortical cytoplasm surrounding the central vacuole and traverse the extreme tip of the hair.

(b) Schematic illustration of the actin configuration during vetch root hair deformation after 10^{-10} M LCO addition. The upper half of each image represents a median view of the cell while the lower half represents a cortical view. Description is from upper to lower image. Swelling: actin filaments are located in the cortical cytoplasm and in cytoplasmic strands crossing the vacuole. Small outgrowth from a swollen root hair tip: the actin filament configuration in the tip of the outgrowth is similar to the configuration in the tip of a growing root hair. Long outgrowth from a swollen root hair tip: the actin filaments in the outgrowth have the same configuration as those in a growing root hair.

terminating growth, actin filament bundles come up to the hair tip. In full-grown hairs, thick bundles of actin filaments loop through the extreme tip. We find a correlation between the presence of FB-actin and delivery of vesicles to the base of the vesicle-rich region, as well as between the presence of transverse bundles of actin filaments and the absence of vesicles at the hair tip. Since LCOs reinitiate growth in zone II hairs of vetch (De Ruijter *et al.*, 1998), it is possible to investigate these correlations by applying LCOs to roots.

Lipochito-oligosaccharides reinitiate the elongation of subapical fine bundles of actin filaments and vesicle delivery to a tip region free of actin filament bundles

Rhizobium bacteria excrete LCOs, Nod factors, when they encounter legume plants. LCOs are sufficient to induce root hair deformation at concentrations as low as 10^{-12} M (Lerouge *et al.*, 1990; Spaink *et al.*, 1991; Price *et al.*, 1992; Sanjuan *et al.*, 1992; Schultze *et al.*, 1992; Firmin *et al.*, 1993; Mergaert *et al.*, 1993; Heidstra *et al.*, 1994). In vetch roots growing between glass slides, only the root hairs that have almost reached their full-grown length, zone II hairs, deform after LCO addition. Deformation is swelling of the hair tip and outgrowth of a hair from the swelling (Heidstra *et al.*, 1994). Analysis of cytoarchitecture, pattern of cytoplasmic streaming, occurrence of a spectrin-like epitope, and presence of a tip-focused $[Ca^{2+}]_c$ gradient has shown that LCOs reinitiate polar growth in zone II root hairs of *Vicia sativa* (vetch) (De Ruijter *et al.*, 1998).

Vetch root hairs were treated with 10^{-10} M LCO (*Rhizobium leguminosarum bv viciae* NodRlv V). After LCO addition the tips of susceptible, zone II, root hairs swell (Figure 3a), and subsequently new outgrowths develop (Figures 3b: arrow, and 3c-e). In swollen tips (Figures 3f2,g3), actin filaments lie close to the plasma membrane (Figures 3f1: arrow, and 3g2) in various orientations (Figure 3g1), indicating an absence of polar cytoarchitecture. At some point, the cell changes its growth direction from expansion over the complete surface of the swelling, i.e. undirected growth, to polar growth from one site in the swelling. The initiation of a new site with polar growth (Figure 3h3) can be seen (arrow) as a slightly more cytoplasmic dense region. In this region actin accumulates (arrows in Figures 3h1,h2). As polar growth continues, the cytoarchitecture (Figure 3d) and the actin filament configuration in the outgrowth (Figure 3i,j) resemble that of growing hairs. Actin filament bundles are again absent from the extreme apex of the new outgrowth, while FB-actin is present subapically (compare Figures 3i,j with Figures 1i,j). The schematic illustration in Figure 2b summarizes the results. In freeze-substituted hairs, foci of actin, as reported by Cárdenas *et al.* (1998) in the outgrowth after LCO-treatment, were not observed. In our study, the actin cytoskeleton in the outgrowth is exactly the same as that in young growing hairs. We have seen such foci in non-optimized chemical fixations and they may be artifacts of the
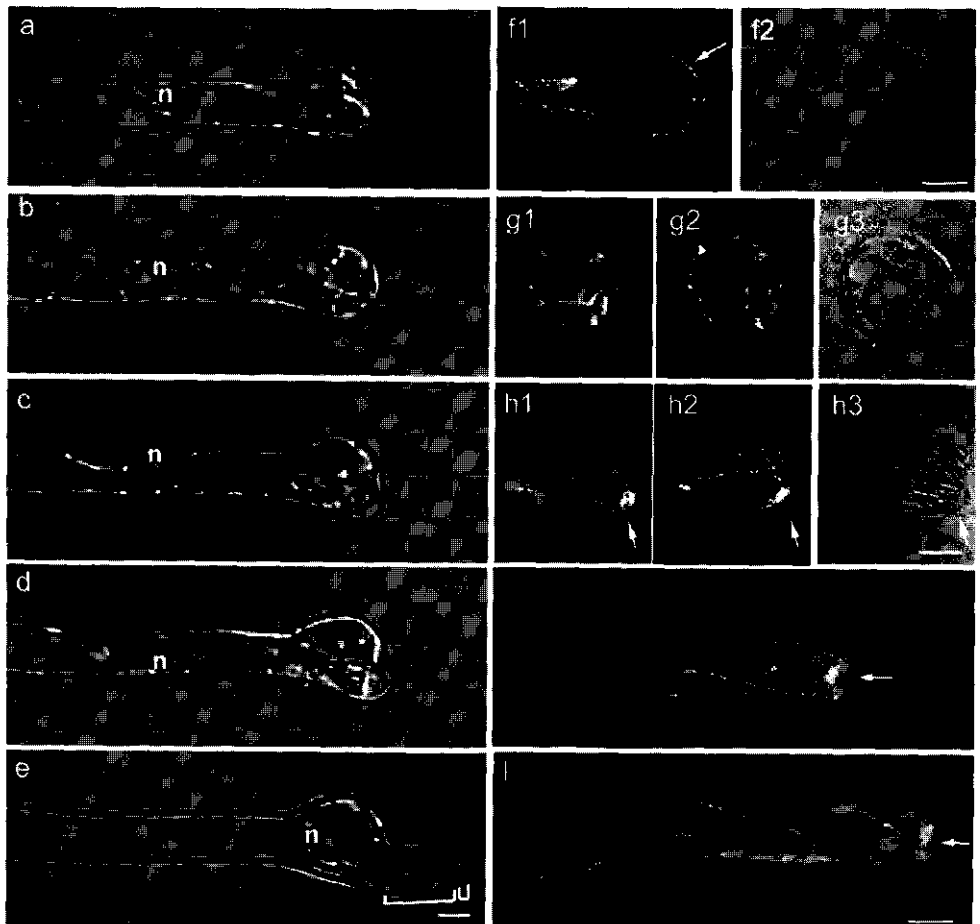
Figure 3

procedure in which high amounts of rhodamine-phalloidin were injected in the *Phaseolus* root hairs (Cárdenas *et al.*, 1998).

Again, we find that subapical FB-actin in a net-axial orientation, together with a zone free of actin filament bundles coincides with tip growth. We test the correlations between the presence of FB-actin and targeting/release of Golgi vesicles, as well as between the presence of transverse bundles of actin filaments in the extreme tip and the absence of Golgi vesicles further, by using cytochalasin D.

Figure 3 (left): Cytoarchitecture and corresponding actin cytoskeleton during root hair deformation after LCO

(a-e) A time-series of DIC images after 10^{-10} M LCO addition, showing the cytoarchitectural changes occurring in one living zone II root hair of vetch. (n) indicates the nucleus. a

Bar in **(e)** equals 10 μm.

(a) t = 2 h 17 min, swelling at the tip .

(b) t = 2 h 28 min, initiation of a new outgrowth starts with the local accumulation of cytoplasm (arrow); numerous cytoplasmic strands are present in the swelling.

(c) t = 2 h 36 min, the cytoplasm at the site of the new outgrowth increases and a new polarized tip is formed.

(d) t = 2 h 43 min, the new tip continues to grow and a new polarized tip is present.

(e) t = 3 h 54 min, the cytoarchitecture of the outgrowth resembles a polarly growing hair, with a vesicle-rich region at the apex (small bracket) and a cytoplasmic dense region with organelles subapically (large bracket); the nucleus (n) has entered the outgrowth.

For **(f-j)**: Actin filaments labeled with anti-actin after freeze-substitution, and corresponding DIC images.**(f2, g3, h3)**. Bars equal 10 μm.

(f1) Swelling of a zone II root hair at ~ 1 h 30 min after 10^{-10} M LCO addition. Thick actin filament bundles in this BMM section are longitudinally oriented along the length of the root hair. Actin filaments are located in the peripheral cytoplasm of the vacuolated swelling (arrow). **(f2)** DIC image of the same hair

(g1, g2, g3) Transversal sections through a swelling. **(g1)** In the peripheral cytoplasm actin filament bundles lie in various orientations. **(g2)** Farther from the periphery, small punctate dots indicate cross-sections through the filament bundles.**(g3)** DIC image of **g2**.

(h1, h2, h3) Longitudinal sections through a swelling during the initial stage of outgrowth. **(h1)** median plane, **(h2)** peripheral plane. The strong labeling indicates the new outgrowth (arrow) **(h3)** DIC image of the same cell

(i,j) Whole mount immunolabeling. **(i)** Short outgrowth with longitudinal actin filaments; FB-actin is present subapically, but absent from the very apex (arrow). **(j)** Long outgrowth with an actin cytoskeleton similar to that of a normal growing hair with bundles in the basal part, FB-actin in the subapical region and a small region devoid of actin at the apex (arrow).

Cytochalasin D stops elongation of subapical net-axial fine bundles of actin filaments and stops tip growth

Cytochalasin D (CD) binds to the growing end of actin filaments and blocks filament elongation (Pollard and Mooseker, 1981). If growth depends on elongation of FB-actin, CD should terminate root hair growth.

We used CD in concentrations that did not affect cytoplasmic streaming. To prevent recovery in low CD concentrations, we kept the [CD] in the growth medium constant by replacing it for new growth medium with CD every 15 min. No effect was observed in control hairs, when PGM without CD was replaced every 15 min.
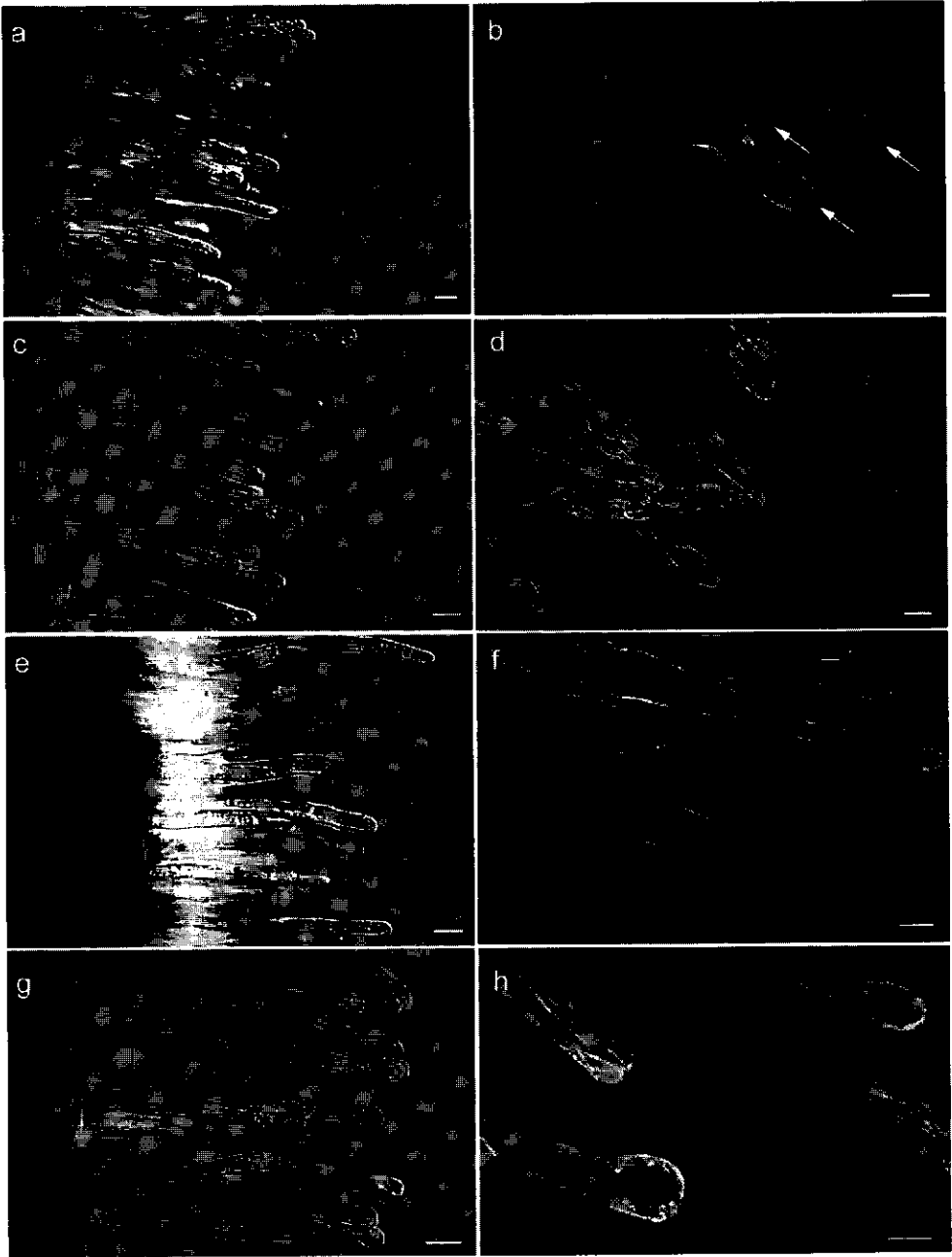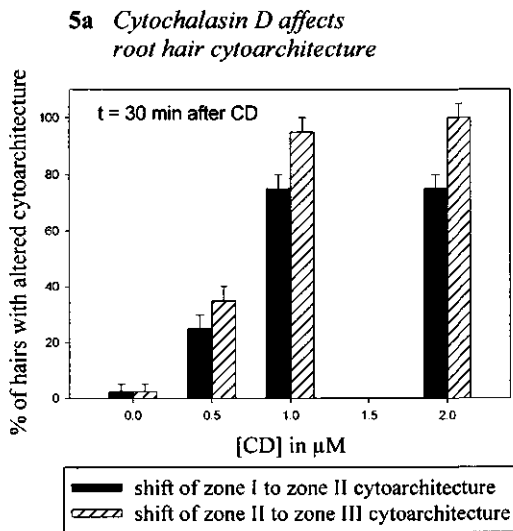
Figure 4

Figure 4 (left): Cytoarchitecture and corresponding actin cytoskeleton of vetch root hairs before and after treatment with CD or CD and LCO. (**a, c, e and g**) DIC images of living vetch root hairs and (**b, d, f and h**) the actin cytoskeleton of hairs at a similar stage, fixed with ester-aldehyde and stained with fluorescein-phalloidin. Bars equal 15 μm. (**a**) Control root hairs of zone I with dense cytoplasm at the tips. (**b**) Actin filaments in control growing root hairs (zone I) with bundles of actin filaments in the hair tube, FB-actin in the subapical region and no actin filaments in the tips (arrows). (**c**) Root hairs of zone I treated with CD have obtained the cytoarchitecture of hairs terminating growth (zone II), (**d**) Root hairs of zone I treated with CD with actin filament bundles up to the hair tip as in hairs terminating growth. Note that the hairs are short. (**e**) Root hairs that were terminating growth (zone II), treated with CD have obtained the cytoarchitecture of full-grown hairs. (**f**) Root hairs that were terminating growth (zone II), treated with CD with actin filament bundles looping through the hair tip, as in full-grown hairs. (**g**) Root hairs first treated with CD and then with LCO do form a swelling but not an outgrowth from the swelling. (t = 2 h 15 min after LCO addition, in 0.5 μM CD in PGM). (**h**) Root hairs first treated with CD and then with LCO, with actin filaments typical for swellings.

At constant [CD] of 0.5-1.0 μM, cytoplasmic streaming in the hair tube was not affected, but the cytoarchitecture of the tip region in zone I and II hairs changed dramatically. In growing hairs (zone I) the prolonged treatment increased the effects of CD. The percentage of hairs that obtained another cytoarchitecture was doubled when roots were treated for 1 h instead of 30 min with 0.5 μM CD (not shown). Zone II hairs were more sensitive to CD than zone I hairs; in the same time or at lower [CD], more hairs of zone II obtained an altered cyto-architecture (Figure 5a).

5a *Cytochalasin D affects root hair cytoarchitecture*

t = 30 min after CD

[CD] in μM

— shift of zone I to zone II cytoarchitecture
⬜ shift of zone II to zone III cytoarchitecture

Figure 5:

(**5a**) *Cytochalasin D affects root hair cytoarchitecture* Histogram showing the percentage of root hairs in zone I and II that had obtained the cytoarchitecture of respectively zone II and III after 30 min (y-axis), related to the concentration of CD in μM (x-axis). The shift to a cytoarchitecture of the next developmental stage increases with the concentration of CD; zone II hairs are more sensitive than zone I hairs.

5b *Cytochalasin D does not inhibit swelling by LCO*

5c *Cytochalasin D inhibits root hair outgrowth from swellings by LCO*

5d *Cytochalasin D does not inhibit initiation of bulges*

5e *Cytochalasin D inhibits root hair tip growth from bulges*
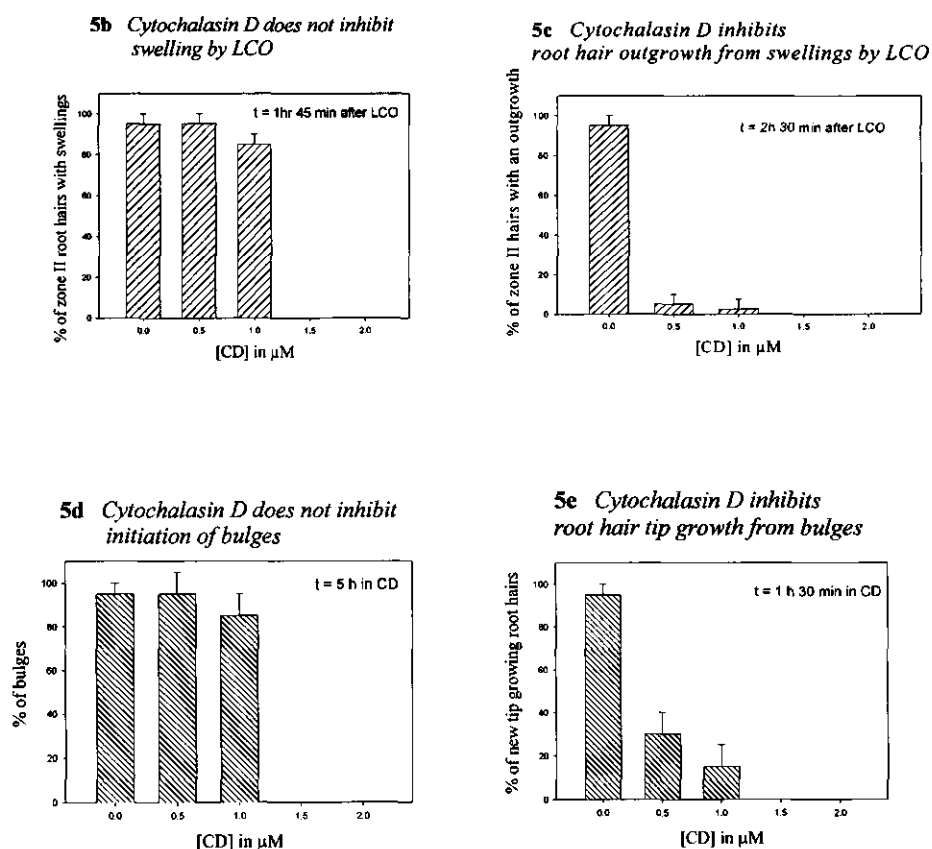
Figure 5 (b-e): Effects of CD on root hair swelling by LCO and outgrowth (b, c) and on formation and polar tip growth from bulges (d, e).

(5b) *Cytochalasin D does not inhibit swelling by LCO.*

Histogram showing the percentage of zone II hairs that develop swellings after application of 10^{-10} M LCO (y-axis) related to the concentration of CD in µM (x-axis). This percentage is similar to the control without CD, which shows that CD up to 1.0 µM does not significantly inhibit swelling. Root hairs were treated with constant (i.e. every 15 min refreshed) [CD], starting at 15 min prior to application of LCO. Swellings were scored at 1 h 45 min after LCO.

(5c) *Cytochalasin D inhibits root hair outgrowth from swellings by LCO.*

Histogram showing the percentage of zone II hairs that develop an outgrowth on a swelling after application of 10^{-10} M LCO (y-axis) related to the concentration of CD in µM (x-axis). CD strongly inhibits the outgrowth. Root hairs were treated with constant (i.e. every 15 min refreshed) CD, starting at 15 min prior to application of LCO. Outgrowths were scored at 2 h 30 min after LCO.

Higher concentrations of CD, between 2 and 5 μM, stopped cytoplasmic streaming, but bundles of actin filaments remained present in the cytoplasmic strands (not shown), 10 μM CD killed most root hairs within 15 min.

Actin staining was performed on hairs that had been treated with 1.0 μM CD for 30 min, at which time 75% of these hairs had stopped growing (Figures 4c and 5a). The subapical region with FB-actin had disappeared in these hairs (compare Figures 4b and 4d), and bundles of actin filaments came up to the tip. Thus, CD blocks the elongation of FB-actin and stops growth. This result suggests that elongation of FB-actin is essential for vesicle delivery and confirms our hypothesis that vesicle delivery to the vesicle-rich region requires the presence of such an actin filament configuration. A further test of this hypothesis is the combined use of CD and LCO. Namely, if tip growth indeed depends on the presence of elongating FB-actin, CD should inhibit LCO-initiated root hair outgrowth from swellings.

Cytochalasin D at 1.0 μM does not inhibit swelling and bulge formation, but inhibits polar outgrowth

We applied 10^{-10} M LCO to roots that were in 0.5 (or 1.0) μM CD (Figures 5b,c). After one hour in LCO, 45% (75%) of zone I hairs had obtained the cytoarchitecture of zone II hairs (Figure 4c). Furthermore, their actin configuration had become similar to that of hairs that are terminating growth (zone II) (Figure 4d). Irrespective of CD, 90-100% of these hairs started to swell by LCO (Figure 4g and 5b), in a time course comparable to normal zone II hairs and with a cytoarchitecture similar to swellings in control hairs (compare Figures 3a with 4g). Furthermore, the actin cytoskeleton in these swellings was similar to that of control swellings which had been incubated in LCO without CD (compare Figures 3f1 with 4h). Thus, 0.5 to 1.0 μM CD had no inhibitory effect on LCO-induced swelling of the root hair tip (Figure 5b).

(5d) (left) *Cytochalasin D does not inhibit initiation of bulges.*
Histogram showing the percentage of normal bulges that develop after application of CD (y-axis) related to the concentration of CD in μM (x-axis). This percentage is similar to the control without CD, which shows that CD up to 1.0 μM does not significantly inhibit bulge formation. New bulges were scored after 5 hrs constant (i.e. every 15 min refreshed) [CD].

(5e) (left) *Cytochalasin D inhibits root hair tip growth from bulges.*
Histogram showing the percentage of bulges that develop a normal, thin, polarly growing root hair with a hair tube diameter smaller than 20 μm (y-axis) related to the concentration of CD in μM (x-axis). CD strongly inhibits polar growth. New hairs with polar growth were scored after 1 h 30 min in constant (i.e. every 15 min refreshed) [CD].
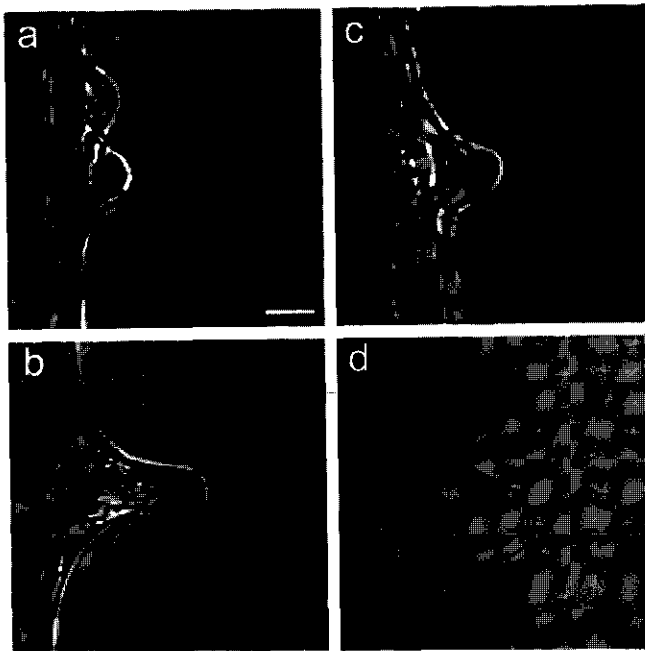
Figure 6:

Influence of CD on bulge formation and on polar tip growth from bulges

(a) DIC image of a control bulge. Bar equals 15 µm.

(b) DIC image of a control root hair at 1 h 30 min after start of polar growth. Note that the root hair diameter is half the width of the bulge.

(c) DIC image of a bulge grown in 1 µM CD.

(d) DIC image of extended bulge grown for 5 hours in CD without polar cyto-architecture. Note that the extension is as wide as the bulge.

However, the outgrowth from the swelling was completely inhibited by 0.5 µM CD (Figure 5c). These experiments, in which CD and LCO were combined, show that LCO can not re-initiate tip growth in the presence of CD. This result confirms the hypothesis, that vesicle targeting and release to the site of growth require the presence of elongating FB-actin.

In a differently designed experiment we applied LCO first and then treated roots with CD at different stages of the root hair deformation process. Again swelling was not blocked by CD. Furthermore, again the initiation of the outgrowth was completely inhibited at concentrations as low as 0.5 µM CD (similar to Figures 5b,c). When CD was applied at the time LCO had already induced an outgrowth from a swelling, the outgrowth obtained the cytoarchitecture of a hair that stops growing. Thus, this outgrowth behaved as growing hairs in CD, in which the cytoarchitecture changes to that of hairs that are terminating growth, and growth stops prematurely. This experiment corroborates the results obtained when CD was used before LCO.

The cytoarchitecture of the cytoplasm in the swelling resembles the cytoarchitecture of the cytoplasm of the bulges that form on trichoblasts prior to polar growth of root hairs. Both swellings (Figure 3a) and bulges (Figure 1a) do not have the polar arrangement of the cytoplasm with a localized vesicle-rich region and dense subapical cytoplasm. Furthermore, both stages lack the subapical FB-actin and possess actin filament bundles at the plasma membrane (bulges: Figures 1g arrowhead, swellings: Figure 3f1,g1,g2). Therefore, we

studied the effect of CD on bulges. Roots growing in 1 µM CD form bulges in high frequencies (85%), while only 15% of these bulges develop into polarly growing root hairs (Figures 5d,e). Bulges grown in 1 µM CD (Figure 6c) look similar to control bulges (Figure 6a). Polarly growing root hairs have a smaller diameter than bulges (Figure 6b), but prolonged treatment with CD gives rise to extended bulges, which are as wide as the initial bulges and have no polarized cytoarchitecture (Figure 6d). We conclude that in cytoarchitecture and actin cytoskeleton, as well as in sensitivity to CD, the bulges resemble the swellings.

DISCUSSION

In this paper we report a specific actin filament configuration in *Vicia sativa* root hairs during initiation of root hairs on bulges, elongation of root hairs, and growth re-initiation by lipochito-oligosaccharide (LCO) nodulation factors. This typical actin cytoskeleton, which is continuous with bundles of actin filaments in cytoplasmic strands in the basal part of the cell, consists of elongating net-axial fine bundles of actin filaments (FB-actin) in the subapical region, while the cytoplasm in the extreme hair tip is devoid of actin filaments.

Comparison of bulges and swellings

Root hairs with polarized cytoarchitecture originate from bulges, which arise on trichoblasts. The actin cytoskeleton in the bulges does not have the FB-actin and the tip region without actin filament bundles, but has actin filament bundles at the plasma membrane. This actin configuration is also observed in LCO-induced swellings. 1 µM CD does not inhibit bulge formation and swelling, whereas it does inhibit polar growth. This suggests that bulge formation and swelling involve a different mechanism than tip growth.

For bulges and root hairs these observations comply well with the distribution of cytoplasmic calcium ions. Wymer *et al.* (1997) followed $[Ca^{2+}]_c$ prior to and during bulging of the trichoblast of *Arabidopsis* and found no sustained $[Ca^{2+}]_c$ increase preceding the bulging. Furthermore, in the *rhd-2* mutant of *Arabidopsis*, which forms bulges, but no root hairs, the elevated $[Ca^{2+}]_c$ at the bulge periphery was absent (Wymer *et al.*, 1997). A tip-directed $[Ca^{2+}]_c$ gradient was set up in a later stage of bulging and was sustained during root hair growth (Wymer *et al.*, 1997). Such a tip-directed $[Ca^{2+}]_c$ gradient at the periphery of the swelling is also set up when an outgrowth forms on the swelling (De Ruijter *et al.*, 1998). Since swelling is an active process, which requires mRNA and protein synthesis (Vijn *et al.*, 1995), we think that swelling is growth, but undirected growth.

Bundles of actin filaments at the plasma membrane inhibit exocytosis

In our confocal images of actin skeletons of vetch root hairs, the extreme tip of the hairs is devoid of bundles of actin filaments. This phenomenon has been observed with fluorescence microscopy in several other tip-growing plant and fungal cells that had been prepared by methods other than chemical fixation (Roberson, 1992; Jackson and Heath, 1993; Meske and Hartmann, 1995; Miller *et al.*, 1996). In growing lily pollen tubes, injected with fluorescein-phalloidin, a region correlating with the vesicle-rich region is devoid of actin filaments (Miller *et al.*, 1996). Jackson and Heath (1993) observed a cleft devoid of filamentous actin at the tips of growing *Saprolegnia* hyphae that had been stained with rhodamine-phalloidin during electroporation. When such cells were fixed in formaldehyde, the apical cleft disappeared, leaving the tip diffusely stained. This work confirms that chemical fixation can induce differential actin staining depending on the fixation method employed (; Doris and Steer, 1996; He and Wetzstein, 1995).

We worked out a chemical fixation procedure that kept the polarized aspect of growing root hairs intact. In this procedure m-maleimidobenzoyl N-hydroxysuccinimide ester was used to stabilize actin filaments prior to fixation by aldehydes (Sonobe and Shibaoka, 1989), and no wall degrading enzymes were used. Furthermore, instead of non-ionic detergents, generally applied to permeabilize and extract cells, we used lysophosphatidyl-choline to facilitate staining by fluorescein-phalloidin, without disturbing the fragile cytoplasmic polarity (Figure 1c1). By this procedure the vesicle-rich region is devoid of filamentous actin. When fixation was performed without maleimide ester, the polar cytoarchitecture of the hair was often destroyed, and cytoplasmic strands, with actin filament bundles in them, were found all the way to the hair tip.

Braun and Wasteneys (1998) report an actin patch in the apical dome of characean rhizoids and protonemata after microinjection with rhodamine-phalloidin. The position of the patch coincided with the position of the aggregate of endoplasmatic reticulum in the center of the 'Spitzenkörper'. They do not report on filamentous actin at the very tip. For root hairs, we can not conclude that there is absolutely no filamentous actin in the tip region. Short actin filaments, linking cytoskeletal components such as spectrin to the plasma membrane, would probably be missed with the light microscope techniques, and have to be studied in glancing sections with immunogold electron microscopy. However, it is clear that bundles of actin filaments are always absent from the vesicle-rich region, from which we hypothesize that the retention of vesicles at the extreme tip, requires an absence of bundles of actin filaments, thus enabling their fusion with the plasma membrane. Also in animal cells during exocytosis, filamentous actin is a barrier to membrane fusion (sperm acrosome reaction: Spungin *et al.*, 1995; pancreatic acinar cells: Muallem *et al.*, 1995; chromaffin cells: Tchakarov *et al.*, 1998).

Elongating fine bundles of actin filaments deliver Golgi vesicles

If one observes the growing root hair from tip to base, actin filaments are seen first in the region where the transition occurs from vesicle-rich region to subapical region, which contains other organelles besides Golgi vesicles. As far as can be resolved in the light microscope, the region free of actin filaments coincides with the vesicle-rich region. The subapical FB-actin may keep vesicles available for release to the vesicle-rich region at the hair tip. A function as a scaffold, to buffer the interchange between a vesicle reserve and an immediate releasable pool of vesicles, has also been reported for actin filaments in animal cell exocytosis (review: Yao and Forte, 1996). The actin patch (Czymmek *et al.* 1996) in the 'Spitzenkörper' could function in a similar way.

Often, tip growth and intercalary growth of plant cells are seen as two different processes, tip growth being governed by the actin cytoskeleton and intercalary growth by microtubules (Kropf *et al.,* 1998). However, both types of growth rely on exocytosis of Golgi vesicles that have to be brought to the right places for growth to proceed in the right amount and direction. The microtubule cytoskeleton seems to determine the growth direction of a cell (Baskin *et al.*, 1994; Wymer *et al.*, 1996), but actin filaments may actually target the vesicles to the plasma membrane. In intercalary growing cells and in swelling root hair tips, the presence of FB-actin or single filaments would be hard to detect with the light microscope, since it can be expected that in these cells the region with Golgi vesicles is not more that one vesicle thick. In this respect, Foissner *et al.* (1996) obtained interesting data with video microscopy during wound wall formation in characean internodal cells. Wounding of these cells induced a transient reorganization of the actin cytoskeleton from parallel bundles to a fine-meshed network of actin filaments. This fine-meshed network was functional in movement of Golgi vesicles to the plasma membrane for wall repair. This event is comparable to what we find for root hair tip growth. A similar function for actin filaments, targeting of Golgi vesicles to and retaining them at the plasma membrane, can be envisaged for intercalary growing cells as well.

Cytochalasin D inhibits elongation of FB-actin

CD at 0.5 μM had different effects on the subapical FB-actin than on the thick bundles of actin filaments in the cytoplasmic strands. Actin filament bundles in the cytoplasmic strands remained intact and must have remained functional, since cytoplasmic streaming continued. However, CD transformed the cytoarchitecture of growing hairs into that of full-grown hairs. FB-actin was transformed to thick bundles of actin filaments. The effect of CD on the root hairs can best be explained as an arrest of elongation of the FB-actin at the front of the subapical region, while bundling of FB-actin at the base of this region continues. The existing vesicles still incorporate into the plasma membrane at the hair tip, while new

vesicles are not delivered to the tip anymore, which eventually stops growth prematurely. This idea also explains the high CD sensitivity of root hairs that terminate growth. Since there are only few vesicles at the tip of such hairs (zone II), CD alters the type of cytoarchitecture more rapidly and/or by lower [CD] than when there are still many vesicles to incorporate into the plasma membrane (zone I).

Since there are these two populations of actin filaments in the growing root hairs, our results shed light on the action of CD in plant cells. It has been reported several times that CD causes bundling of actin filaments in plant cells (pollen tubes: Lancelle and Hepler, 1988; root cells: Palevitz, 1988; characean internodes: Collings *et al.*, 1995). In fact, superficial inspection would have led to the same observation in root hairs. Our results, however, show that CD has the usual depolymerizing effect (Pollard and Mooseker, 1981) on a certain category of actin filaments. The FB-actin at the front of the subapical region of growing hairs disappears. Again, this explanation of the effect of CD clarifies why younger hairs (in zone I) with subapical FB-actin are less sensitive for CD than zone II hairs. Also in the wounded characean internodal cells, CD led to the disappearance of the fine actin filament network, and inhibited transport of vesicles towards the wounded surface (Foissner and Wasteneys, 1997).

Actin filament elongation by LCO occurs after plasma membrane localized [Ca^{2+}]$_c$ increase

The experiments in which LCO was applied to CD-treated roots are informative for understanding the process involved in root hair deformation by LCO. The establishment of polarity, as well as polar growth itself, is inhibited by [CD] as low as 0.5 μM. On the contrary, [CD] even up to 2.0 μM does not block the first morphogenic effect of LCO, i.e. swelling of the root hair tip. This result implicates that, even though swelling is a growth process (Vijn *et al.*, 1995), it does not need new actin polymerization. We know that LCO initiates a membrane localized high [Ca^{2+}]$_c$ gradient at the tip of *Vicia sativa* root hairs (De Ruijter *et al.*, 1998). The [Ca^{2+}]$_c$ gradient is present at the plasma membrane of the whole swelling tip. From the result that swelling is independent of actin filament polymerization, it can be deduced that the high [Ca^{2+}]$_c$ at the plasma membrane functions in a process that temporally comes before the advent of new actin filament assembly. According to Felle *et al.* (1998), working with alfalfa, a Ca^{2+} influx at the plasma membrane is the fastest physiological response to Nod factors reported so far. Soon after this, Ca^{2+} spiking is seen in alfalfa (Ehrhardt *et al.*, 1996). Cárdenas *et al.* (1998) have shown that in *Phaseolus* root hairs the actin cytoskeleton disintegrates within 10 min after LCO application, after which it recuperates. It seems that LCO-induced increase of intracellular Ca^{2+} accompanies actin filament disintegration. We show now that new actin filament elongation is a crucial step for

root hair deformation, and thus for root hair curling in the presence of bacteria, and that it occurs after calcium ion increase and actin disintegration.

MATERIALS AND METHODS

Growth of plant material and root hair deformation

Vicia sativa spp. nigra L. (vetch) seeds were surface sterilized, imbibed in sterile water and placed on 0.8% agarose. Plates were put at 4°C for three days to synchronize germination at 20°C. Seedlings were grown in Fåhraeus slides (Heidstra *et al.*, 1994) containing plant growth medium (PGM) consisting of 1.36 mM $CaCl_2$, 0.97 mM $MgSO_4$, 1.12 mM Na_2PO_4, 1.36 mM KH_2PO_4 and 20 μM Fe-citrate, pH 6.5 (modified from Fåhraeus, 1957). Some seedlings were treated with 10^{-10} M *Rhizobium leguminosarum bv viciae* Nodulation (Nod) factors NodRlv V [Ac, C18:4] (Spaink *et al.*, 1991) diluted in PGM while in controls PGM was replaced by PGM.

Actin visualization

Optimized ester-aldehyde fixation and fluorescein-phalloidin staining:

Root hairs were prefixed for 5 min in freshly prepared 200 μM m-maleimido benzoyl N-hydroxysuccinimide ester (MBS, Sigma M2786) in PGM to stabilize actin filaments, fixed with 2% paraformaldehyde and 0.05% glutaraldehyde for 20 min, followed by 4% paraformaldehyde and 0.1% glutaraldehyde for 20 min. Aldehydes were freshly prepared and in Actin Stabilizing Buffer (ASB: 100 mM PIPES pH 6.8, 1 mM $MgCl_2$, 1 mM $CaCl_2$, 75 mM KCl) with 1 mM 4-2-aminoethylbenzene sulfonyl fluoride (AEBSF; Sigma, A8456). Roots were washed three times in ASB buffer prior to permeabilization with 100 μg/ml L-α-lysophosphatidylcholine (Sigma, L4129) in ASB. Actin filaments were stained within 10 min with 0.33 μM fluorescein-phalloidin (F-432, Molecular Probes) in ASB with 0.05% acetylated BSA (BSA_{ac}) (Aurion, Wageningen, NL) to lower aspecific binding, then mounted in anti-fading agent CITIFLUOR AF3 (Citifluor, Canterbury, UK).

Freeze-substitution and labeling with anti-actin:

Roots were removed from the slide; the root tip was excised, placed on a formvar-coated loop, plunge-frozen in liquid propane, and substituted for 36-40 h in 3.7% formaldehyde in pure methanol, or in pure acetone. The sample was brought to room temperature and then rehydrated in series.

For whole mount labeling the cell wall was partially digested with 0.3% cellulase Onozuka R10 (Serva, Heidelberg, Germany), 0.3% cellulysin (Calbiochem, La Jolla, CA)

and 0.3% pectinase (Sigma) for 15 min at room temperature. The roots were washed and treated with 1% Triton X-100, 0.05% Nonidet P40, and 2 mM PMSF for 2 min, then washed and blocked with 1% BSA$_{ac}$ and 0.05% Tween-20 in PBS for 15 min. Roots were incubated with monoclonal pea anti-actin antibody (Andersland *et al.*, 1994), diluted 1:100, overnight at 4°C. After washing, the secondary antibody, Cy3 conjugated goat anti-mouse F$_{ab}$ fragments (Jackson ImmunoResearch Laboratories Inc.) diluted 1:200, was applied for 2 h followed by washing. Labeled roots were mounted in antifading agent and root hairs were imaged with a confocal microscope. Most roots were embedded in butyl methyl methacrylate (BMM) similar to Baskin *et al.* (1992; 1996). After substitution the roots were brought to room temperature and washed in acetone or methanol. Infiltration of the resin took place at 2 h intervals with increasing amounts of 80% butyl methacrylate, 20% methyl methacrylate (E. Merck, Darmstadt, Germany), and 0.5% benzoinethylether (Merck) in methanol or acetone; 1:5; 1:2; 1:1; 2:1; 5:1; pure; pure (modified from Baskin *et al.*, 1996). The samples were polymerized under long-wavelength UV light at 0°C for 24 h. After embedment, 3 μm sections were prepared. Once sectioned, the BMM was removed by acetone for 25 min followed by 3 washes in PBS with 0.05% Tween-20. The tissue was blocked with 1% BSA$_{ac}$ and 0.05% Tween-20 in PBS for 15 min. Subsequently, the root tissue was incubated in pea anti-actin antibody 1:10, for 2 h at 37°C. Three 10 min washes in PBS with 0.05% Tween-20 followed. Secondary antibody, Cy3 goat anti-mouse antibody, was diluted 1:200 and applied for 2 h at 37°C. Another three 10 min washes in PBS plus 0.05% Tween-20 followed. Labeled sections were mounted in anti-fading agent.

Microscopy and image analysis

Root hairs were observed in the Fåhraeus slides during growth and Nod factor-induced deformation using a Nikon 20x DIC 0.5 NA or 40x Plan DIC 0.7 NA objective on a Nikon Optiphot microscope. Images were recorded on a Panasonic wv-E550 3-CCD camera using a Prysm framegrabber with AcQuis 2.0 software (Synoptics Ltd., Cambridge, UK).

Actin filaments were recorded on a Bio Rad MRC 600 confocal laser scanning microscope (CLSM) equipped with an Argon Krypton laser with a 60x 1.4 NA objective. Neutral density filters were set to obtain 10% transmission intensity from the laser beam, using the 488 nm line for fluorescein-phalloidin with DM 488 BA 522 DF 35, and the 568 nm line for Cy3 conjugated goat anti-mouse antibodies with DM 560 long pass BA 585. Optical sections were obtained at 1.0 μm steps with a moderately closed pinhole (setting 3 or 4), using high gain settings and 3 -5 Kalman averages. z-Series were projected using Confocal Assistant 2.04. Images were contrast enhanced in Adobe Photoshop (Adobe Systems Inc., Mountain View, CA, USA) and printed with a Kodak XLS 8600 dye sublimation printer.

Cytochalasin treatment of root hairs

The boundaries of the original developmental stages of zone I, II, and III of four days old roots were marked on the Fåhraeus slides. Cytochalasin D (CD) (Sigma, C8273) was freshly diluted in PGM from a 20 mM stock in 100% DMSO, to a final concentration of 0.5, 1.0 or 2.0 and applied to the roots, which were incubated in the dark. To prevent recovery of the hairs, [CD] was kept constant by applying fresh CD every 15 min. The percentage of hairs with altered cytoarchitecture was determined every 30 min during 5 h, for each [CD]. Each experiment was done on 12 roots or more, and changes in the cytoarchitecture were imaged at the DIC microscope.

To determine the effect of CD on LCO-induced root hair deformation, we first treated roots with 0.5 or 1.0 µM CD for 15 min, then applied 10^{-10} M LCO NodRlv V [Ac, C18:4] and maintained a constant [CD] for 4 h. The effect of CD on root hair deformation was expressed as percentage of swellings, and percentage of (swellings with) outgrowths. We also first applied 10^{-10} M LCO (t = 0 h) for 15 min, then treated with CD either prior to swellings (t = 1 h), prior to the initiation of an outgrowth from a swelling (t = 1 h 30 min) or during growth of the outgrowth (t = 2 h). The appropriate timing for CD application was determined by a control slide that was incubated with LCO, 15 min prior to the experiment.

ACKNOWLEDGEMENTS

REFERENCES

Andersland, J.M., Fisher, D.D., Wymer, C.L., Cyr, R.J. and Parthasarathy, M.V. (1994) Characterization of a monoclonal antibody prepared against plant actin. *Cell Motil. Cytoskel.*, **29**, 339-344.

Baskin, T.I., Busby, C.H., Fowke, L.C., Sammut. M. and Gubler, F. (1992) Improvements in immunostaining samples embedded in methacrylate: localization of microtubules and other antigens throughout developing organs in plants of diverse taxa. *Planta*, **187**, 405-413.

Baskin, T.I., Wilson, J.E., Cork, A. And Williamson, R.E. (1994) Morphology and microtubule organization in *Arabidopsis* roots exposed to oryzalin or taxol. *Plant Cell Physiol.*, **35**, 935-942.

Baskin, T.I., Miller, D.D., Vos, J.W., Wilson, J.E. and Hepler, P.K. (1996) Cryofixing single cells and multicellular specimens enhances structure and immunocytochemistry for light microscopy. *J. Microsc.* **182**, 149-161.

Braun, M. and Wasteneys, O. (1998) Distribution and dynamics of the cytoskeleton in graviresponding protonemata and rhizoids of characean algae: exclusion of microtubules and a convergence of actin filaments in the apex suggest an actin-mediated gravitropism. *Planta* **205**, 39-50.

Cárdenas, L., Vidali, L., Domínguez, J., Pérez, H., Sánchez, F., Hepler, P.K. and Quinto, C. (1998) Rearrangement of actin microfilaments in plant root hairs responding to *Rhizobium etli* nodulation signals. *Plant Physiol*, **116**, 871-877.

Collings, D.A., Wasteneys, G.O. and Williamson, R.E. (1995) Cytochalasin rearranges cortical actin of the alga *Nitella* into short, stable rods. *Plant Cell Physiol.*, **36**, 765-772.

Czymmek, K.J., Bourett, T.M. and Howard, R.J. (1996) Immunolocalization of tubulin and actin in thick-sectioned fungal hyphae after freeze-substitution fixation and methacrylate de-embedment. *J. Microsc.*, **181**, 153-161.

De Ruijter, N.C.A., Rook, M.B., Bisseling, T. and Emons, A.M.C. (1998) Lipochito-oligosaccharides reinitiate root hair tip growth in *Vicia sativa* with high calcium and spectrin-like antigen at the tip. *Plant J.*, **13**, 341-350.

Dolan, L., Duckett, C.M., Grierson, C., Linstead, P., Schneider, K., Lawson, E., Dean, C., Poethig, S. and Roberts, K. (1994) Clonal relationships and cell patterning in the root epidermis of *Arabidopsis. Development*, **120**, 2465-2474.

Doris, F.P. and Steer, M.W. (1996) Effects of fixatives and permeabilisation buffers on pollen tubes: implications for localisation of actin microfilaments using phalloidin staining. *Protoplasma*, **195**, 25-36.

Ehrhardt, D.W., Wais, R. and Long, S.R. (1996) Calcium spiking in plant root hairs responding to *Rhizobium* nodulation signals. *Cell*, **85**, 1-20.

Emons, A.M.C. (1987) The cytoskeleton and secretory vesicles in root hairs of *Equisetum* and *Limnobium* and cytoplasmic streaming in root hairs of *Equisetum. Annals of Bot.*, **60**, 625-632.

Emons, A.M.C. and Derksen, J.W.M. (1986) Microfibrils, microtubules and microfilaments of the trichoblast of *Equisetum hyemale. Acta Bot. Neerl.*, **35**, 311-320.

Fåhraeus, G. (1957) The infection of clover root hairs by nodule bacteria studied by a simple glass slide technique. *J. Gen.Microbiol.*, **16**, 374-81.

Felle, H.H., Kondorosi, E., Kondorosi, A. and Schultze, M. (1998) The role of ion fluxes in Nod factor signalling in *Medicago sativa. Plant J.*, **13**, 455-463.

Firmin, J.L., Wilson, K.E., Carlson, R.W., Davies, A.E. and Downie, J.A. (1993) Resistance to nodulation of cv. Afghanistan peas is overcome by *nodX*, which mediates an O-acetylation of the *Rhizobium leguminosarum* lipo-oligosaccharide nodulation factor. *Mol. Microbiol.*, **10**, 351-360.

Foissner, I., Lichtscheidl, I.K. and Wasteneys, G.O. (1996) Actin-based vesicle dynamics and exocytosis during wound wall formation in characean internodal cells. *Cell Motil. Cytoskel.*, **35**, 35-48.

Foissner, I. and Wasteneys, G.O. (1997) A cytochalasin-sensitive actin filament meshwork is a prerequisite for local wound wall deposition in *Nitella* internodal cells. *Protoplasma*, **200**, 17-30.

Galway, M.E., Heckman, Jr., J.W. and Schiefelbein, J.W. (1997) Growth and ultrastructure of *Arabidopsis* root hairs: the *rhd3* mutation alters vacuole enlargement and tip growth. *Planta*, **201**, 209-218.

He, Y. and Wetzstein, H.Y. (1995) Fixation induces differential tip morphology and immunolocalization of the cytoskeleton in pollen tubes. *Physiol. Plant.*, **93**, 757-763.

Heidstra, R., Geurts, R., Franssen, H., Spaink, H.P., van Kammen, A. and Bisseling, T. (1994) Root hair deformation activity of nodulation factors and their fate on *Vicia sativa*. *Plant Physiol.*, **105**, 787-797.

Iwanami, Y. (1956) Protoplasmic movement in pollen grains and pollen tubes. *Phytomorphology*, **6**, 288-295.

Jackson, S.L. and Heath, I.B. (1993) The dynamic behavior of cytoplasmic F-actin in growing hyphae. *Protoplasma*, **173**, 23-34.

Kropf, D.L., Bisgrove, S.R. and Hable, W.E. (1998) Cytoskeletal control of polar growth in plant cells. *Curr. Opin. Cell Biol.*, **10**, 117-122.

Lancelle, S.A. and Hepler, P.K. (1988) Cytochalasin-induced ultrastructural alterations in *Nicotiana* pollen tubes. *Protoplasma Suppl*, **2**, 65-75.

Lerouge, P., Roche, P., Faucher, C., Maillet, F., Truchet, G., Promé, J-C. and Dénarié J. (1990) Symbiotic host-specificity of *Rhizobium meliloti* is determined by a sulphated and acylated glucosamine oligosaccharide signal. *Nature*, **344**, 781-784.

Mergaert, P., van Montagu, M., Promé, J-C. and Holsters, M. (1993) Three unusual modifications, a D-arabinosyl, an N-methyl, and a carbomoyl group are present on Nod factors of *Azorhizobium caulinodans* strain ORS571. *Proc. Natl. Acad. Sci.*, **90**, 1551-1555.

Meske, V. and Hartmann, E. (1995) Reorganization of microfilaments in protonemal tip cells of the moss *Ceratodon purpureus* during the phototropic response. *Protoplasma*, **188**, 59-60.

Miller, D.D., de Ruijter, N.C.A. and Emons, A.M.C. (1997) From signal to form: aspects of the cytoskeleton-plasma membrane-cell wall continuum in root hair tips. *J. Exp. Bot.*, **48**, 1881-1896.

Miller, D.D., Lancelle, S.A. and Hepler, P.K. (1996) Actin microfilaments do not form a dense meshwork in *Lilium longiflorum* pollen tube tips. *Protoplasma*, **195**, 123-132.

Muallem, S., Kwiatkowska, K., Xu, X. and Yin, H.L. (1995) Actin filament disassembly is a sufficient final trigger for exocytosis in nonexitable cells. *J. Cell Biol.*, **128**, 589-598.

Palevitz, B.A. (1988) Cytochalasin-induced reorganization of actin in Allium root cells. *Cell Motil. Cytoskel.*, **9**, 283-298.

Pollard, T.D. and Mooseker, M.S. (1981) Direct measurement of actin polymerization rate constants by electron microscopy of actin filaments nucleated by isolated microvillus cores. *J. Cell Biol.*, **88**, 654-659.

Price, N.P.J., Relic', B., Talmont, F., Lewin, A., Promé, D., Pueppke, S.G., Maillet, F., Dénarié, J., Promé, J-C. and Broughten, W.J. (1992) Broad-host-range *Rhizobium* species strain NGR234 secretes a family of carbamoylated, and fucosylated, nodulation signals that are O-acetylated or sulphated. *Mol. Microbiol.*, **6**, 3573-3584.

Ridge, R.W. (1988) Freeze-substitution improves the ultrastructural preservation of legume root hairs. *Bot. Mag. Tokyo*, **101**, 427-441.

Roberson, R.W. (1992) The actin cytoskeleton in hyphal cells of *Sclerotium rolfsii*. *Mycologia*, **84**, 41-51.

Sanjuan, J., Carlson, R.W., Spaink, H.P., Bhat, U.R., Barbour, W.M., Glushka, J. and Stacey, G. (1992) A 2-O-methylfucose moiety is present in the lipo-polysaccharide nodulation signal of *Bradyrhizobium japonicum*. *Proc. Natl. Acad. Sci.*, **89**, 8789-8793.

Schultze, M., Quiclet-Sire, B., Kondorosi, E., Virelizier, H., Glushka, J.N., Endre, G., Géro, S.D. and Kondorosi, A. (1992) *Rhizobium meliloti* produces a family of sulfated lipo-oligo-saccharides exhibiting different degrees of plant host specificity. *Proc. Natl. Acad. Sci.*, **89**, 192-196.

Sherrier, D.J. and VandenBosch, K.A. (1994) Secretion of cell wall polysaccharides in Vicia root hairs. *Plant J.*, **5**, 185-95.

Sonobe, S. and Shibaoka, H. (1989) Cortical fine actin filaments in higher plant cells visualized by rhodamine-phalloidin after pretreatment with m-maleimidobenzoyl N-hydroxysuccinimide ester. *Protoplasma*, **148**, 80-86.

Spaink, H.P., Sheely, D.M., van Brussel, A.A.N., Glushka, J., York, W.S., Tak, T., Geiger, O., Kennedy, E.P., Reinhold, V.N. and Lugtenberg, B.J.J. (1991) A novel highly unsaturated fatty acid moiety of lipo-oligosaccharide signals determines host specificity of *Rhizobium*. *Nature*, **354**, 125-130.

Spungin, B., Margalit, I. and Breitbart, H. (1995) Sperm exocytosis reconstructed in a cell-free system: evidence for the involvement of phospholipase C and actin filaments in membrane fusion. *J. Cell Sci.*, **108**, 2525-2535.

Staiger, C.J., Yuan, M., Valenta, R., Shaw, P.J., Warn, R.M. and Lloyd, C.W. (1994) Microinjected profilin affects cytoplasmic streaming in plant cells by rapidly depolymerizing actin microfilaments. *Curr. Biol.*, **4**, 215-219.

Tchakarov, L.E., Zhang, L., Rosé, S.D., Tang, R.N. and Trifaró, J.M. (1998) Light and electron microscopic study of changes in the organization of the cortical actin cytoskeleton during chromaffin cell secretion. *J. Histochem. Cytochem.*, **46**, 193-203.

Valster, A.H., Pierson, E.S., Valenta, R., Hepler, P.K. and Emons, A.M.C. (1997) Probing the plant actin cytoskeleton during cytokinesis and interphase by profilin microinjection. *The Plant Cell*, **9**, 1815-1824.

Vijn, I., Martinez-Abarca, F., Yang, W.C., Das Neves, L., Van Brussel, A., Van Kammen, A. and Bisseling, T. (1995) Early nodulin gene expression during Nod factor-induced processes in *Vicia sativa*. *Plant J.*, **8**, 111-119.

Wymer, C.L., Wymer, S.A., Cosgrove, D.J. and Cyr, R.J. (1996) Plant cell growth responds to external forces and the response requires intact microtubules. *Plant Physiol.*, **110**, 425-430.

Wymer, C.L., Bibikova, T.N. and Gilroy, S. (1997) Cytoplasmic free calcium distributions during the development of root hairs of *Arabidopsis thaliana*. *Plant J.*, **12**, 427-439.

Yao, X. and Forte, J.G. (1996) Membrane-cytoskeleton interaction in regulated exocytosis and apical insertion of vesicles in epithelial cells. In *Current topics in Membranes* Volume 43 (Nelson, A. and James, W., eds). New York, San Diego: Academic Press, pp. 73-96.

- Chapter 6 -

Rhizobium Nod factors induce an increase in sub-apical fine bundles of actin filaments in *Vicia sativa* root hairs within minutes

A Research Note

Norbert C.A. de Ruijter[1], Ton Bisseling[2], Anne Mie C. Emons[1]

[1]*Laboratory of Plant Cytology and Morphology, Wageningen University Arboretumlaan 4, 6703 BD, Wageningen, The Netherlands and*
[2]*Laboratory of Molecular Biology, Wageningen University, Dreijenlaan 3, 6703 HA, Wageningen, The Netherlands.*

Short title: Nod factors induce an increase in FB-actin

We studied the response of the actin cytoskeleton in vetch root hairs after application of host specific Nod factor. Within 3 to 15 min the number of sub-apical fine bundles of actin filaments (FB-actin) increased in all developmental stages. Tip-growth resumed only in hairs in which the FB-actin density and the length of the region with FB-actin exceeded a minimal value.

Lipochito-oligosaccharides (LCOs, Nod factor) purified from *Rhizobium* spp. induce root hair deformation (Mylona et al. 1995), which is swelling of the tip followed by an outgrowth from that swelling within three hours (Heidstra et al. 1994). In an assay, in which LCOs are applied to vetch roots growing between coverslip and slide, the root hair response is restricted to those hairs that are terminating growth (Heidstra et al. 1994). A certain cyto-architecture of the hairs is mandatory for the ability to deform in response to LCOs (Heidstra et al. 1997, Miller et al. 1997) and the response is a re-initiation of tip growth (de Ruijter et al. 1998).

In root hairs, the presence of dense sub-apical, net-axial fine bundles of actin filaments, which we have called FB-actin, correlates with tip growth (Miller et al. 1999). However, the actin cytoskeleton in root hairs that deform by LCOs contains bundled filaments up into, and transversely looping through the hair tip (Miller et al. 1999). Thus, in order to obtain the FB-actin, the cytoskeleton must change. Breakdown and rearrangements of actin filaments have been reported for root hairs of alfalfa after the incubation with appropriate Nod factors (Allen et al. 1996). Cárdenas et al. (1998) have reported a diffuse fluorescence of injected fluorescent phalloidin in root hair tips within minutes after exposure of LCOs from *Rhizobium etli* to roots of *Phaseolus vulgaris*, which they interpreted as fragmented filaments. Paradoxically, when we observe vetch root hairs after LCO application in the differential interference contrast (DIC) microscope, cytoplasmic strands remain present at any time (Miller et al. 1999). Cytoplasmic strands disappear when actin filaments are depolymerized, which was shown by microinjection of the monomeric actin binding protein profilin into *Tradescantia* sp. stamen hair cells (full-grown cells: Staiger et al. 1994; growing cells: Valster et al. 1997). From these experiments it was concluded that bundles of filamentous actin are required for the presence of cytoplasmic strands. Thus, there is an apparent contradiction between our observation of intact cytoplasmic strands in living root hairs shortly after exposure to LCOs, and the observations of Cárdenas et al. (1998) of a fragmented actin cytoskeleton.

We optimized a chemical fixation and staining method to visualize the actin cytoskeleton in intact vetch root hairs and obtained results similar to the results obtained after freeze fixation and freeze substitution (Miller et al. 1999), the most reliable method. The actin
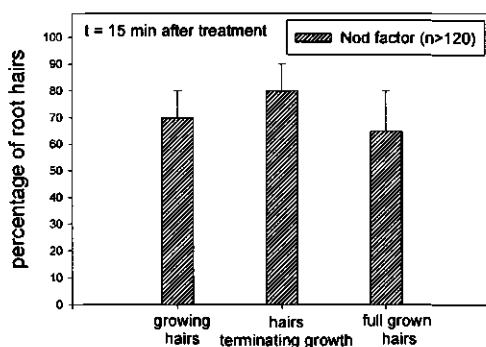
cytoskeleton of 80-90% of all root hairs stained with fluorescein-phalloidin. This procedure thus allowed the study of a population of hairs in each developmental stage at various times after LCO application, instead of a few injected hairs. For all times after LCO application (3, 6, 9, 12, 15 and 30 min) at least 12 different roots were examined in at least 6 different experiments, and the same number of roots was used for controls. To exclude recording any effects on the actin cytoskeleton of a change of medium itself, in controls new growth medium was applied instead of LCOs. In all roots, 70-80% of the root hairs of all developmental stages responded to LCO application within 3 to 15 min. This response was an increase of the number of sub-apical bundles of actin filaments (Fig. 1A). The hairs that were terminating growth obtained a density of bundles of actin filaments that is similar to the density seen in growing control hairs (Fig. 1B).

For a detailed analysis, we compared densities of actin filament bundles in control and LCO treated root hairs over 50 µm distance from the tip. Fluorescent bundles of actin filaments were imaged in a confocal laser-scanning microscope at 1 µm z-steps. Z-Series were flat projected and all actin bundles were counted at distinct distances from the tip, on a grid with lines placed perpendicular to the root hair. During imaging and processing similar settings were used for all treatments and developmental stages. Numbers of actin filament bundles were corrected for width, and their mean values were plot versus distance from the tip for each developmental stage (Figs. 2A, 3A, 4A). These profiles of mean actin filament bundle density reflect relative values, since the procedure does not record the thinnest bundles of actin filaments or actin filament bundles present in between the optical sections of a z-series. However, similar settings during imaging and processing provided reproducibility and allowed data comparison.

In growing hairs, which keep on growing after application of LCOs, an increase in FB-actin occurred over 5-40 µm from the hair tip (Fig. 2A). Mean actin filament bundle densities were determined from randomly chosen growing root hairs that had been imaged at 3 to 15 min after application of LCOs (Fig. 2A). Figure 2B and 2C are representative for the actin cytoskeleton of a control and a LCO treated hair. The number of actin filament bundles increased significantly, while their orientation remained net-axial and the root hair tip remained free of filamentous actin.

In root hairs that respond to LCOs with root hair deformation, i.e. those that are terminating growth, the mean number of actin filament bundles almost doubled over a distance of at least 50 µm from the root hair tip, within 3 to 15 min (Figs. 1A, 3A). The mean filament bundle density became almost similar to the density in a growing hair (compare Figures 2A and 3A). Figure 3B and 3C are examples of hairs that are terminating growth. The control hair (Fig. 3B) has actin filament bundles up to the tip, and only few FB-actin. After LCO application dense sub-apical FB-actin appeared up to the hair tip (Fig. 3C).

A *Percentage of root hairs with an increase in the number of actin filaments in the subapex*

Figure 1:

Effect of LCOs on sub-apical actin filaments in root hairs.

(A) Percentage of vetch root hairs with an increase in the number of sub-apical actin filaments at 15 min after application of 10^{-10} M *Rhizobium leguminosarum* bv *viciae* Nod Rlv V [Ac, $C_{18:4}$] (LCO's) (y axis) is displayed for each developmental stage (x axis). Root hairs in each developmental stage respond to LCOs. Increase is relative to bundle densities in control root hairs, to which fresh growth medium without LCOs was applied. A random population of root hairs from at least 12 different roots was examined in at least six different experiments, and the same number was used for the controls. Error bars indicate standard error (SE).

B *Percentage of root hairs with a subapical actin filament bundle density similar to or above the density in growing hairs*

(B) Percentage of vetch root hairs with a density of sub-apical actin filament bundles similar to or above the density in growing hairs (y axis) is displayed for each developmental stage (x axis) at 15 min after application of fresh medium with or without Nod factor. Hairs terminating growth obtain a new actin filament bundle density that correlates with growth. A and B, Error bars indicate SE.

A: *Growing root hairs*
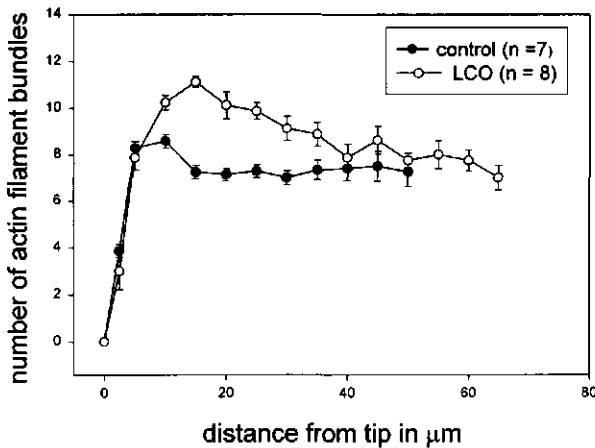
Figure 2:
Growing root hairs.**(A)** Mean densities of actin filament bundles (y axis) are displayed vs distance from the tip (x axis). For each developmental stage of vetch root hairs, density profiles show an increase in actin filament bundles after application of lipochito-oligo-sacharides (LCOs). Position on the root and differential interference contrast (DIC) image prevent sampling errors. Random sampling was done within each zone at 3 to 15 min after treatment, z-series were processed, and means of numbers of actin filaments displayed. Error bars indicate SE. **(B-C)** Staining of actin filaments in root hairs. Root hairs were prefixed for 3 min in 200 µM m-maleimido benzoyl N-hydroxy succinimide ester in medium. Cytoplasmic streaming stopped within 1 min. Roots were fixed for 20 min in a final concentration of 4% p-formaldehyde and 0.1% glutaraldehyde in actin stabilizing buffer (ASB: 100 mM PIPES pH 6.8, 1 mM $MgCl_2$, 1 mM $CaCl_2$, 75 mM KCl) with 1 mM 4-2-aminoethylbenzene sulfonyl fluoride. Root hairs were permeabilized for 12 min with 100 µg of L-α-lyso-phosphatidylcholine per ml in ASB. Actin filaments were stained with 0.33 µM fluorescein-phalloidin in ASB supplemented with 0.05% acetylated bovine serum albumin (BSA). Roots were mounted in CITIFLUOR-glycerol.
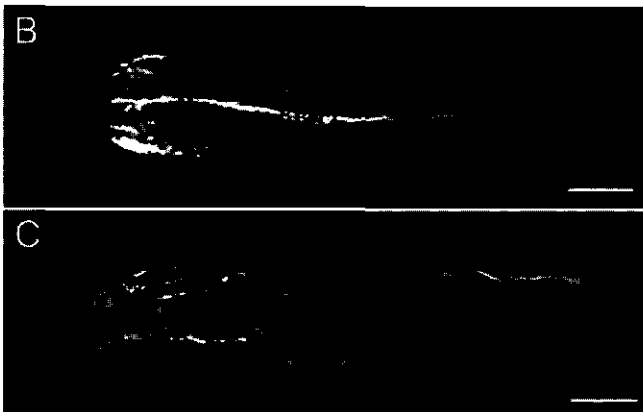
A: *Hairs terminating growth*
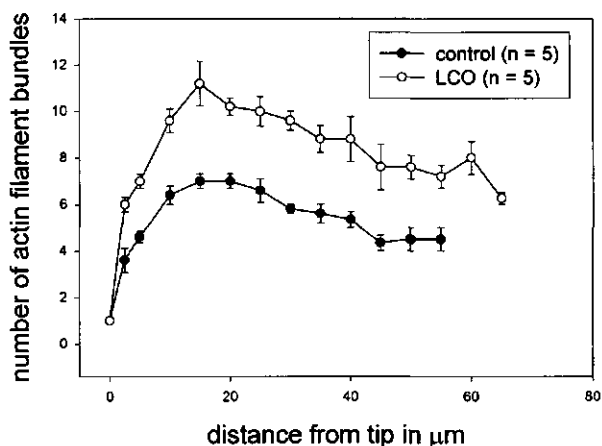
Figure 3:
(A-C): Root hairs that are
terminating growth.
See Figure 2 caption.
(B) Typical distribution and
density of actin filament
bundles after replacing growth
medium ($t = 6$ min) and
(C) after application of
lipochito-oligosaccharides
(LCOs; $t = 3$ min).
Bar = 10 μm.
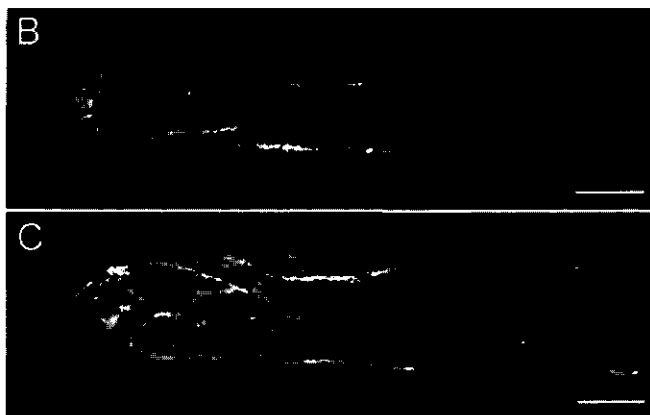
These fine bundles of actin filaments often had a wider range of orientations in relation to the long axis of the hair, than growing hairs after LCO application (compare Figures 3C and 2C). This difference is reflected in the number and orientation of cytoplasmic strands (not shown).

A: *Full-grown root hairs*
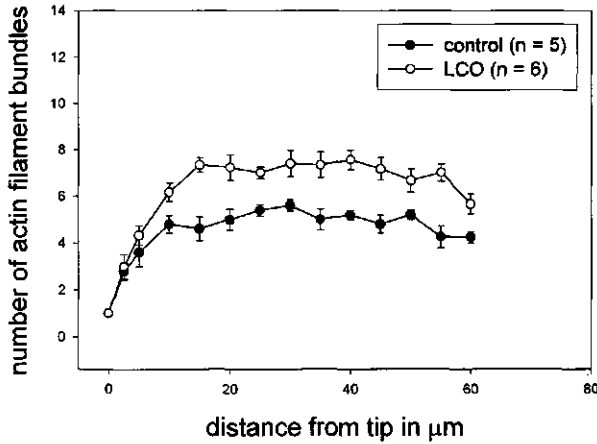
Figure 4:
(A-C) Full-grown root hairs.
See Figure 2 caption.
(B) Typical distribution and
density of actin filament
bundles after replacing growth
medium (*t* = 15 min) and
(C) after application of
lipochito-oligosaccharides
(LCOs *t* = 15 min).
Bar = 10 μm.
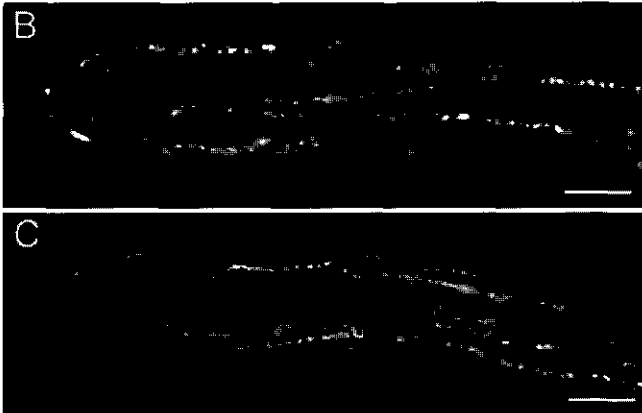
Also full-grown root hairs responded to the application of LCOs with an increase of actin filament bundles. However, most full-grown hairs responded after a longer time span of 9-15 min after LCO application, compared to a 3-9 min interval wherein most other hairs responded. In Figure 4A the comparison of control and LCO treated full-grown hairs shows a 30-40% increase in density of actin filament bundles over 10-50 μm from the tip. The final densities attained, never reached those of control growing hairs (compare density profile of control in Figure 2A with LCO profile in Figure 4A). Figures 4B and 4C are micrographs of
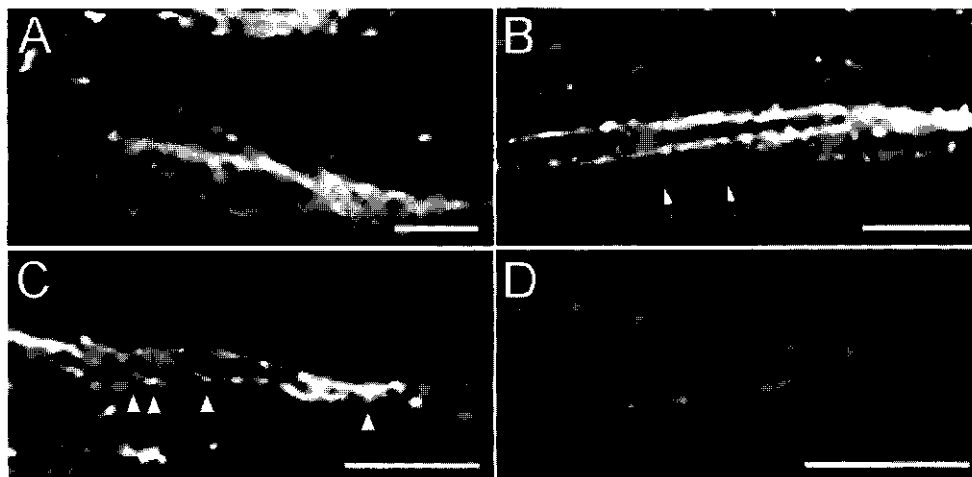
Figure 5:

Details showing examples of diverging fine bundles of actin filaments continuous with thicker bundles, in lipochito-oligosaccharide (LCO)-treated vetch root hairs. In all images the tip of the root hair is at left. Bar = 5 μm. (A) Projected z-series of sub-apex of a growing root hair after LCO application (t =12 min). Shown is an increase in number of actin filament bundles closer to the tip. (B) Projected z-series of a root hair terminating growth after LCO application (t = 5 min) at 30-40 μm from the tip. Shown are fine filaments deviating from a thick bundle of actin filaments (arrows). (C) Partial z-projection over 5 μm depth within a growing root hair after LCO application (t = 3 min) at 50-60 μm from the tip. Arrowheads indicate sites of apparent local unbundling in a thick bundle of actin filaments. (D) One single optical section showing a site at 25 μm from the tip where a bundle of actin filaments splits into two thinner bundles in a hair that was terminating growth when LCOs were applied (t = 30 min).

a control and a LCO-treated full-grown hair, showing an increase of FB-actin after the application of the signal.

In an earlier report, we have defined FB-actin as dense actin filaments in the sub-apical area of a growing root hair (Miller et al. 1999). Our quantitative approach allows us now to define FB-actin more precise. By the method used, FB-actin is characterized by a minimal density of 7-8 actin filament bundles present over a minimal length of 10 μm behind the tip-region devoid of actin filaments. These minimal values in the sub-apical area are typical for hairs terminating growth (control in Figure 3A). In these cells, LCO application leads to a rise above the minimal values for FB-actin and indeed to a re-initiation of tip growth. Tip growth is exocytosis at the tip, which implies a localized insertion of Golgi vesicles into the plasma membrane, and the delivery of their content into the expanding cell wall. Therefore, the functional significance of the LCO-induced increase of actin filament bundles seems to

be the preparation for the delivery of new Golgi vesicles. The density of actin filament bundles in full-grown hairs that had responded to LCOs, never exceeded the minimal values for FB-actin, which may be the reason why these hairs do not respond with root hair deformation.

Figure 5 shows details of actin filament bundles after LCO application. Mechanisms that may explain the increase are *(i)* unbundling of thick actin filament bundles into finer bundles, *(ii)* increased polymerization in new directions, or *(iii)* new nucleation and polymerization of fine bundles of actin filaments. From the present experiments, one is not able to choose between these possibilities.

Our observations show, in a quantitative manner, how LCOs change the configuration of the actin cytoskeleton. The changes are too fast to be caused by new gene transcription and *de novo* protein synthesis. This implies that LCOs trigger a signal transduction cascade that leads to molecules that influence the actin cytoskeleton. After perception of the LCO signal molecule, an influx of calcium ions into the root hairs takes place in *Medicago sativa* (Felle et al. 1998). Gehring et al. (1997) have measured an increase of the cytoplasmic calcium concentration ($[Ca^{2+}]_c$) in root hairs of *Vigna unguiculata* within seconds after application of LCOs, and the elevated $[Ca^{2+}]_c$ lasted for at least 10 min. This high $[Ca^{2+}]_c$ in the root hair tip may modify the equilibrium between monomeric actin, actin binding proteins and actin filaments. Acting in synergy, actin binding proteins such as profilin (Staiger et al. 1997) and Actin Depolymerizing Factor (ADF) (Rozycka et al. 1995), present in tips of growing hairs (Jiang et al. 1997), may cause the formation of FB-actin.

The determination of the changes in the actin cytoskeleton provides a new assay for deciphering the signaling cascade after LCO application to roots.

ACKNOWLEDGEMENTS

REFERENCES

Allen, N. S., and Bennett, M. N. 1996. Electro-optical imaging of F-actin and endoplasmic reticulum in living and fixed plant cells. Scann. Micr. Suppl. 10: 177-187.

Cárdenas, L., Vidali, L., Domínguez, J., Pérez, H., Sánchez, F., Hepler, P., and Quinto, C. 1998. Rearrangement of actin microfilaments in plant root hairs responding to *Rhizobium etli* nodulation signals. Plant Physiol. 116: 871-877.

De Ruijter, N. C. A., Rook, M. B., Bisseling, T., and Emons, A. M. C. 1998. Lipochito-oligosaccharides reinitiate root hair tip growth in *Vicia sativa* with high calcium and spectrin-like antigen at the tip. Plant J. 13: 341-350.

Felle, H. H., Kondorosi, E., Kondorosi, A., and Schultze, M. 1998. The role of ion fluxes in Nod factor signalling in *Medicago sativa*. Plant J. 13: 455-463.

Gehring, C. A., Irving, H.R., Kabbara, A. A., Parish, R.W., Boukli, N. M., and Broughton, W. J. 1997. Rapid, plateau-like increases in intracellular free calcium are associated with Nod-factor-induced root-hair deformation. Mol. Plant-Microbe Interact. 10: 791-802.

Heidstra, R., Geurts, R., Franssen, H., Spaink, H. P., Van Kammen, A. and Bisseling, T. 1994. Root hair deformation activity of nodulation factors and their fate on *Vicia sativa*. Plant Physiol. 105: 787-797.

Heidstra, R., Yang, W.C., Yalcin, Y., Peck, S., Emons, A. M. C., Van Kammen, A. and Bisseling, T. 1997. Ethylene provides positional information on cortical cell division but is not involved in Nod factor-induced tip growth in *Rhizobium* induced nodulation. Development 24: 1781-1787.

Jiang, C-J., Weeds, A. G., and Hussey, P. J. 1997. The maize actin-depolymerizing factor, ZmADF3, redistributes to the growing tip of elongating root hairs and can be induced to translocate into the nucleus with actin. Plant J. 12: 1035-1043.

Miller, D. D., de Ruijter, N. C. A., and Emons, A. M. C. 1997. From signal to form: aspects of the cytoskeleton-plasma membrane-cell wall continuum in root hair tips. J. Exp. Bot. 48: 1881-1896.

Miller, D. D., de Ruijter, N. C. A., Bisseling, T., and Emons, A. M. C. 1999. The role of actin in root hair morphogenesis: studies with lipochito-oligosaccharides as a growth stimulator and cytochalasin as an actin perturbing drug. Plant J. 17: 141-154.

Mylona, P., Pawlowski, K., and Bisseling, T. 1995. Symbiotic nitrogen fixation. Plant Cell 7: 869-885.

Rozycka, M. D., Khan, S., Lopex, I., Greenland, A. J., and Hussey, P. J. 1995. A *Zea mays* pollen cDNA encoding a putative actin-depolymerizing factor. Plant Physiol. 107: 1011-1012.

Staiger, C. J., Gibbon, B. C., Kovar, D. R., and Zonia, L. E. 1997. Profilin and actin-depolymerizing factor: modulators of actin organization in plants. Trends Plant Sci. 2: 275-281.

Staiger, C. J., Yuan, M., Valenta, R., Shaw, P. J., Warn, R. M., and Lloyd, C. W. 1994. Microinjected profilin affects cytoplasmic streaming in plant cells by rapidly depolymerizing actin microfilaments. Curr. Biol. 4: 215-219.

Valster, A. H., Pierson, E. S., Valenta, R., Hepler, P. K., and Emons, A. M. C. 1997. Probing the plant actin cytoskeleton during cytokinesis and interphase by profilin microinjection. Plant Cell 9: 1815-1824.

- Chapter 7 -

Actin-binding proteins in plant cells

Norbert C.A. de Ruijter and Anne Mie C. Emons

*Department of Plant Sciences, Laboratory of Plant Cytology and Morphology,
Wageningen Agricultural University, The Netherlands*

SUMMARY

Actin occurs in all plant cells, as monomers, filaments and filament assemblies. In interphase, actin filaments form a cortical network, co-align with cortical microtubules, and extend throughout the cytoplasm functioning in cytoplasmic streaming. During mitosis, they co-align with microtubules in the preprophase band and phragmoplast, and are indispensable for cell division. Actin filaments continually polymerize and depolymerize from a pool of monomers, and signal transduction pathways affecting cell morphogenesis modify the actin cytoskeleton. The interactions of actin monomers and filaments with actin-binding proteins (ABPs) control actin dynamics. By binding to actin monomers, ABPs, such as profilin, regulate the pool of monomers available for polymerization. By breaking filaments or capping filament ends, ABPs, such as Actin Depolymerizing Factor (ADF), prevent actin filament elongation or loss of monomers from filament ends. By bivalent cross-linking to actin filaments, ABPs , such as fimbrin and other members of the spectrin family, produce a variety of higher order assemblies, from bundles to networks. The motor protein ABPs, which are not covered in this review, move organelles along actin filaments. The large variety of ABPs shares a number of functional modules. A plant representative of ABPs with particular modules, and therefore particular functions, is treated in this review.

Keywords: Actin-binding proteins, ADF/cofilin, cytoskeleton, fimbrin, plant cells, profilin, spectrin.

INTRODUCTION

The cytoskeleton is an integrated lattice that connects cytosolic components with the plasma membrane. This filamentous assembly models cytoplasmic architecture and components move along it and are targeted to specific sites in the cell. The cytoskeleton connects to receptors, transduces signals, and effects cell responses. The cytoskeleton indeed is the scaffold, highway, and signaling device of all eukaryotic cells. This dynamic structure is made of three classes of filamentous assemblies: microtubules, actin filaments, which are often called microfilaments in electron microscopy studies, and intermediate filaments.

Microtubules have a diameter of approximately 25 nm and are made of tubulin; actin filaments are approximately 8 nm; intermediate filaments measure approximately 10 nm and are made of a variety of proteins. From the plant cytoskeleton, most is known about microtubules, reviewed by Cyr (1994), Cyr and Palevitz (1995), Wymer and Lloyd (1996), and Marc (1997). The microtubule assemblies in plant cells are the preprophase band, the spindle, the phragmoplast, the cortical interphase microtubules and the microtubules around the interphase nucleus (Hepler et al., 1993; Cyr, 1994). Whether filamentous actin colocalises with microtubules in the spindle is not clear. However, in all other assemblies actin filaments colocalise with the microtubules (for living cells see Cleary et al., 1992; Hepler et al., 1993). Reviews on the function of the plant actin cytoskeleton include: Staiger and Schliwa (1987), Emons et al. (1991), Williamson (1993) and Asada and Collings (1997). From the three classes of cytoskeletal structures in plant cells, least is known about the intermediate filaments. In animal cells intermediate filaments can form very stable structures of for instance keratin. An antibody against animal intermediate filaments co-distributed with all microtubular arrays in onion root tip cells (Dawson et al., 1985), and cytochalasin B, a drug that disturbs the actin cytoskeleton, did not affect their distribution in carrot and maize suspension cells (Goodbody et al., 1989).

Function and organization of microtubules and actin filaments is largely determined by their regulatory proteins, the so-called microtubule associated proteins (MAPs) and actin-binding proteins (ABPs). Three important distinct regulatory mechanisms of ABPs are (1) the assembly/disassembly of filaments from monomers, which regulates site-specific polymerization/depolymerization, (2) the severing/(un)capping of filaments, which regulates filament elongation or loss of monomers from filament ends, and (3) the cross-linking of filaments, which regulates the formation of higher order assemblies of the actin filaments. This review will address a plant example of each of these three categories. We will not discuss another important category of actin-binding proteins, the myosins, motor proteins of

which several genes are present in plants (Kinkema et al., 1994). For a review on myosins and other motor proteins see Asada and Collings (1997).

Actin

Actin is a ubiquitous component of plant cells (Staiger and Schliwa, 1987; McDowell et al., 1996). It occurs in cells as actin monomers with a molecular mass of 42-45 kDa and an isoelectric point of 5.4 (Bershadsky and Vasiliev, 1988) and as filaments composed of these actin monomers. Actin monomers may be bound to actin monomer binding proteins, such as profilin, or to phospho-inositides of membranes. In the filament, actin molecules have a polar alignment, forming a double-stranded twisted rope with a major repeat distance of 38 nm, involving 13 molecules. Actin filaments are transient structures that continually polymerize and depolymerize. Since within a filament the actin monomers assemble in the same polar fashion, actin filaments have a distinct polarity with a fast-growing plus end, also called the barbed end, and a slow or non-growing minus end, the so-called pointed end. Polymerization and depolymerization occur by the stepwise addition and detachment of actin monomers at both exposed ends, but polymerization is more efficient at the plus end than at the minus end. Unpolymerized actin is present in cells bound to ADP or to ATP. ATP-actin polymerizes more easily than ADP-actin. For a recent review on actin dynamics, and its control, see Carlier (1998).

Plant actin has been isolated from maize pollen (Ren et al., 1997). It polymerized with the same kinetics as vertebrate α-actin. The critical concentration for assembly was 0.6 μM. The pollen actin interacted specifically and in a characteristic fashion with several ABPs (Ren et al., 1997).

In comparison to other eukaryotes, higher plant actin gene families are much more diverse and contain 10-100 times more functional actin genes (McDowell et al., 1996). In *Arabidopsis* actin is encoded by 10 genes, which fall into six subclasses, five of which are expressed in a tissue-specific fashion. These authors hypothesize that these actin isoforms are expressed to perform distinct functions within different cells and tissues in *Arabidopsis*. A number of examples supports this idea, since non-conservative amino acid substitutions map the surface of the *Arabidopsis* actin proteins, thus providing a potential structural basis for specialized functions via distinct actin-actin or actin-ABP interactions (Sheterline and Sparrow, 1994; McDowell et al., 1996).

Actin filament assemblies in plant cells

Actin filaments can be visualized with fluorescently tagged phalloidin. This toxic bicyclic heptapeptide from poisonous *Amanita* mushrooms (Wieland and Faulstich, 1978) binds to actin monomers in actin filaments and, when present in high enough concentrations, prevents the depolymerization of actin filaments. Conjugated fluorochromes permit the *in situ* localization of actin filaments. Actin can also be detected in cells with anti-actin antibodies, and anti-actin antibodies directed against plant actin are available (Andersland et al., 1994). At the ultrastructural level, the localization of actin in plant cells has been determined with gold-labeled anti-actin antibodies in, for instance, pollen tubes (Lancelle and Hepler, 1991) and by decoration with heavy meromyosin fragments in, for instance, root hairs (Seagull and Heath, 1979). The latter probe also allows the determination of the polarity of the actin filaments. In fact, the terminology barbed and pointed ends for plus and minus ends respectively, comes from the arrow-like pattern of heavy meromyosin on individual actin filaments in electron micrographs.

In plant interphase cells, actin filaments extend throughout the cytoplasm of the cell. The filaments form a net around the nucleus, from which they radiate in bundles to the cell periphery, in vacuolated cells in cytoplasmic strands (Sonobe and Shibaoka, 1989). The actin filaments occur in thick subcortical bundles (Parthasarathy et al., 1985; McCurdy and Gunning, 1990) and as single filaments along microtubules (Lancelle and Hepler, 1991). When actin filaments are depolymerised by the injection of the actin monomer binding protein profilin all cytoplasmic strands in *Tradescantia* stamen hair cells disappear (Staiger et al., 1994; Valster et al., 1997). This experiment shows that actin filaments are the backbone of the cytoplasmic strands, which cannot exist without them. The assemblies of the plant cytoskeleton during mitosis and cytokinesis are subsequently the preprophase band, the metaphase/anaphase spindle, and the telophase phragmoplast (Hepler et al., 1993; Cleary et al., 1992). Except in the spindle, actin filaments co-align with microtubules, and we do not know their separate functions in most cases. However, the main cytoskeletal element in interphase cytoplasmic strands, in which cytoplasmic streaming occurs, is filamentous actin.

Processes in plant cells in which the actin cytoskeleton is involved

Actin filaments possess biophysical and biochemical properties required for cell locomotion, division, compartmentalization and modeling of cytoarchitecture. Though most plant cells do not move and their final form is maintained by the commonly stiff secondary cell wall, intracellular movement may be vigorous and the distinctive shape of cells during growth is

regulated by the internal cytoskeleton together with the expanding primary cell wall. The plant actin cytoskeleton responds to internal and external stimuli (Staiger et al., 1997) and therefore is involved in the processes induced by these stimuli.

Actin filament assemblies dramatically change under the influence of as yet unknown internal stimuli during the cell cycle. Actin filaments function in mitosis (Cleary et al., 1992; Zhang et al., 1993; Cleary, 1995) and are indispensable in cell division (Staehelin and Hepler, 1996; Valster et al., 1997). At the onset of prophase the cortical filaments become co-aligned with microtubules, generally transverse to the long axis of the cell and form the preprophase band (Cleary et al., 1992; Hepler et al., 1993). These actin filaments disassemble at nuclear envelope breakdown. At cytokinesis actin filaments lie within the phragmoplast parallel to the microtubules, but not in the zone where cell plate vesicles aggregate (Cleary, 1995). Similarly to the microtubules, the two rings of short actin filaments perpendicular to the growing cell plate expand in girth and disassemble when the cell plate fuses with the mother cell plasma membrane (Cleary et al., 1992). At that stage, actin filament bundles are present in the cortical cytoplasm except in the area where the preprophase band was and where the Golgi vesicles derived cell plate fuses with the mother plasma membrane. This fusion process seems to require a plasma membrane area devoid of filamentous actin. Also at growing pollen tube tips, where Golgi vesicles fuse with the existing plasma membrane, the area bordering the plasma membrane is devoid of actin filaments (Miller et al., 1996). We find a similar phenomenon in root hairs. The extreme root hair tip is devoid of actin filaments, whereas fine bundles of actin needed to deliver the vesicles, are present just below this actin filament-free area (Miller et al., 1999).

Reactions of plant cells to external stimuli that evoke a response in cell morphogenesis depend on reorganization of the actin cytoskeleton. Examples are phytochrome-controlled growth (Waller and Nick, 1997), light-induced plastid migration (Dong et al., 1996), wound repair in *Chara* (Foissner et al., 1996), response to pathogen attack (Takemoto et al., 1997), gravistimulation (Volkmann et al.,1991) and response of susceptible legume root hairs to nitrogen-fixing bacteria (Cárdenas et al., 1998; Miller et al, 1999).

Regulation of the actin cytoskeleton by actin-binding proteins

The actin cytoskeleton exerts a diversity of functions in many cell processes. This is possible because actin filaments form distinct assemblies with unique and functionally significant biophysical and biochemical properties in distinct situations. The diversity of actin filament assemblies is possible by the association and interaction of actin monomers and filaments

with actin-binding proteins (ABPs). In fact, the site-specific formation and type of assembly of actin filaments is directed by ABPs. Studies on the structure of these regulatory proteins have been very helpful in deciphering their function. Such studies have revealed that nature uses a limited number of fundamental modules in ABPs, which perform specific catalytic and recognition functions (Puius et al., 1998). Modification, shuffling, and combination of these modules gives a large spectrum of proteins that mediate many different biological functions. Research on the modular structure of ABPs has revealed that specific modules that bind to actin in specific ways control the formation of specific actin filament assemblies by their own properties. For polymerization to take place, a critical concentration of actin monomers is needed. Therefore, ABPs that bind to monomeric actin are the first ABP category that can control site-specific filament elongation. A second category regulates the actin cytoskeleton by cross-linking actin filaments in a number of physically different and specific ways, depending on their own spatial configuration. The third category exerts its influence by severing, and capping/uncapping actin filaments. By breaking filaments or capping filament ends, these ABPs prevent actin filament elongation or loss of monomers from filament ends. Changes in the activity of actin-regulatory proteins themselves are induced by changes in pH and intermediates of signaling pathways including phospho-inositides and calcium ions (Janmey et al., 1994).

The actin monomer-binding protein profilin

Actin filament assemblies change during the progression of the plant cell cycle, from the interphase cytoskeleton to the preprophase band, to the phragmoplast and back to the interphase cytoskeleton. During the cell's growth phase the actin cytoskeleton itself has to elongate, which is evident in tip-growing cells such as root hairs. Meanwhile, the actin cytoskeleton responds to external stimuli such as light, wounding, gravistimulation, pathogens, and symbionts. Therefore, an essential component of actin filament regulation must be the site-specific assembly/disassembly of actin filaments. The profilins are ABPs that regulate the dynamics of actin polymerization *in vivo* and stimulate the formation of specific actin filament assembly's *in vitro* (Finkel et al., 1994).

Profilin is a 12-15 kDa protein that binds to monomeric actin to form profilactin and thus sequesters actin monomers (review: Carlier and Pantaloni, 1997). If monomeric actin in cells is continuously bound, the equilibrium between monomeric and polymeric actin is shifted to the monomeric side. Therefore, existing actin filaments are broken down. This breakdown of actin filaments occurs, for instance, when profilin is microinjected into cells (full-grown *Tradescantia blossfeldiana* stamen hair cells: Staiger et al. (1994), growing and dividing

Tradescantia virginiana stamen hair cells: Valster et al. (1997)). However, a different, but just as important role of profilin at physiological concentration is the positive effect on filament assembly through several mechanisms. This effect on filament assembly seems to be related to profilin's capacity to control the ratio of ATP-actin to ADP-actin. Because ATP-actin subunits polymerize more readily than ADP-actin subunits, the ratio between the two, and therefore the availability of profilin, plays a key regulatory role in actin filament assembly and turnover (Goldschmidt-Clermont et al., 1992). Thus, profilin may promote actin depolymerization by sequestering actin monomers, or may promote actin polymerization, by stimulating addition of monomeric actin to the plus end of actin filaments. This dual function of profilin, probably dependent on the cell's physiology and the availability of other ABPs, makes this ABP a complex regulator of actin organization.

Profilin is the best-characterized ABP of plants (review: Staiger et al., 1997). It was identified in plants as a pollen allergen by Valenta et al. (1991). Profilin has now been isolated from a wide range of plant species (Staiger et al., 1993; Mittermann et al., 1995; Huang et al., 1996) and occurs probably in all plant tissues (Darnowski et al., 1996). Angiosperm profilins are encoded by multigene families of profilin. For instance, maize is predicted to have at least five profilin genes (Staiger et al., 1993; Gibbon et al., 1998) and in *Arabidopsis thaliana* as many as 10 gene members have been isolated (Huang et al., 1996), but the implications of this diversity have not been addressed. Although the amino acid sequence similarity of plant profilins with yeast and vertebrate profilins is as low as 30%, the three-dimensional conformation is well-conserved (Thorn et al., 1997) and the function of profilin in cells is similar (Rothkegel et al., 1996; Staiger et al., 1997). Purified higher plant profilins bind to actin from a green alga, but also from cardiac muscle (Ruhlandt et al., 1994). Birch pollen profilin delays the rate as well as the extent of actin polymerization *in vitro* of rabbit skeletal muscle actin (Giehl et al., 1994). *Arabidopsis* profilins promote assembly of actin filaments *in vitro* at the barbed ends, comparable to vertebrate profilins (Perelroizen et al., 1996). When injected in *Tradescantia* stamen hair cells, profilin causes the depolymerization of actin filaments in a dose-dependent manner (Staiger et al., 1994; Valster et al., 1997), which is consistent with an actin monomer binding function of profilin. Plant profilin exerts the same actin monomer sequestering function, when it is over-expressed in *Schizosaccharomyces pombe* (Xia et al., 1996). On the other hand, overexpression of plant profilin in mammalian cells gives the opposite effect, namely a stabilization of the actin filament network, however, without increase in the amount of filamentous actin (Rothkegel et al., 1996). *Arabidopsis* profilin complements a null allele of *Schizosaccharomyces cerevisiae* and a temperature sensitive profilin mutant of

Saccharomyces pombe (Christensen et al., 1996). Furthermore, a maize profilin can rescue an aberrant phenotype in profilin-deficient *Dictyostelium* cells (Karakesisoglou et al., 1996).

Like many ABPs, profilin is a multi-functional protein. It also reversibly binds to poly-L-proline and to the membrane phospholipid phosphatidyl-inositol 4,5-biphosphate (PIP_2) (review: Sohn and Goldschmidt-Clermont, 1994). The binding to PIP_2 results in a dissociation of the profilactin complex, and provides a link between a major signal transduction pathway, the phosphatidyl-inositol cycle, and the actin cytoskeleton (Aderem, 1992). When profilactin is dissociated, monomeric actin becomes available for polymerization. In animal cells, profilin is targeted to specific positions in cells, for instance to the leading edge of locomoting animal cells (Buß et al., 1992; Machesky and Pollard, 1993; Finkel et al., 1994; Giuliano and Taylor, 1994). A role of profilin in controlling phospho-inositide turnover in plants has been demonstrated (Drøbak et al., 1994), but there is no evidence yet that profilin is targeted to cell membranes in plant cells (Vidali et al., 1995; Vidali and Hepler, 1997). A possible role for profilin in signaling is indicated by experiments in pollen of *Papaver rhoeas,* where profilin regulates actin based cytoskeletal protein assembly and protein kinase or phosphatase activity. Since profilins can alter the phosphorylation state of cytosolic proteins in pollen, they may regulate pollen tube growth (Clarke et al., 1998). Functional differences of maize profilin isoforms were detected in *Tradescantia virginiana* living stamen hair cells. However, these differences may be caused by differences in binding to proline-rich sequences, rather than to differences in binding to monomeric actin (Gibbon et al., 1998).

The actin severing/capping proteins ADF and cofilin

Actin Depolymerizing Factor (ADF) is the second rather well-characterized ABP of plant cells (review: Staiger et al. 1997). The non-plant ADF family members of ABPs, also called cofilin, bind to actin monomers as well as to actin filaments *in vitro*, and stimulate the depolymerization of actin filaments in a pH dependent manner (Theriot, 1997). They have a molecular mass of 15-22 kDa, and inhibit nucleotide exchange on actin, bind actin and rapidly depolymerize actin filaments and probably sever actin filaments (Moon and Drubin, 1995). By increasing the rate of pointed-end disassembly, ADF increases the rate of actin filament turnover, since the disassembly increases the availability of monomeric actin which in turn increases the rate of barbed end growth (Carlier, 1997). Genetic and localization studies have shown that ADFs *in vivo* are distributed throughout the cytoplasm, especially in regions where actin filaments accumulate and their turnover is high (Sun et al., 1995; Moon and Drubin, 1995). Capping proteins, an ABP family with similar actin-binding modules as

ADF/cofilin, have the same severing function but, in addition, cap actin filament barbed ends (Puius et al., 1998). By thus decreasing the number of growing, barbed ends, capping proteins increase the growth rate of the non-capped filaments (Carlier and Pantaloni, 1997). Capping proteins have not been found in plant cells yet.

However, a number of actin depolymerizing factors (ADFs) have been found in plants. Kim et al. (1993) identified an ADF in pollen of *Lilium longiflorum* and Rozycka et al. (1995) and Lopez et al. (1996) found ADF in pollen of *Zea mays*. Plant ADF appears to promote actin dynamics *in vitro* (Jiang et al., 1997b) and to be modulated by pH (Lopez et al., 1996). As with profilin, the deduced amino acid sequences of plant ADFs share only approximately 30% homology with vertebrate sequences. However, regions containing the putative actin-binding sites and the presumed phosphorylation site share the greatest similarity with mammalian sequences (Staiger et al. 1997). *In vitro* experiments have been performed with maize ADF. As with all non-plant ADFs (Theriot, 1997), maize ADF binds to monomeric actin in a 1:1 complex (Staiger et al., 1997). In *Dictyostelium,* cofilin (ADF) plays a role in rapid remodeling of the cortical actin meshwork into actin filament bundles (Aizawa et al., 1997). Rearrangement of fine actin filament bundles into thicker bundles occurs at the base of the subapical region of growing vetch root hairs (Miller et al., 1999). Interestingly, in maize root hairs, ADF has been localized to this region (Jiang et al., 1997a). Danyluk and coworkers (1996) have isolated a cDNA corresponding to a putative ADF in cold-acclimated wheat, which is strongly upregulated by low temperature. It has two conserved domains identified as actin- and PIP_2-binding domains. Whether the product of this gene is involved in reorganization of the actin cytoskeleton during low temperature acclimation is not known.

The actin cross-linking proteins fimbrin and spectrin

In living cells, actin filaments are organized into highly-ordered assemblies. In plant cells, these assemblies are the cortical cytoskeleton, the preprophase band, the phragmoplast, and the bundles in cytoplasmic strands. This organization is controlled by bivalent actin cross-linking proteins, which utilize two discrete binding sites on actin filaments (Puius et al., 1998). The type of higher order assemblies of actin filaments which are formed *in vitro,* depend on the ratio of actin-binding protein to actin, on their binding affinity, and on the nature of the actin-binding protein itself (Ayscough, 1998). Interestingly, the different ABPs of the actin filament cross-linking protein family are of different size, and the size of these proteins determines the distance of the actin filaments bound by them, and, consequently, the type of actin filament assembly made (Puius et al., 1998). Cross-linkers that bring the two actin-binding sites close together direct the formation of tightly packed actin filament

bundles, whereas cross-linkers that form large bridges between actin filaments direct the formation of loose assemblies (Puius et al., 1998).

The actin cross-linking ABP category includes the spectrin family, that is spectrin, fimbrin, α-actinin, dystrophin, and ABP120. These proteins are characterized by a conserved 27 kDa actin filament binding domain (Matsudaira, 1991), of which the structure has recently been determined in fimbrin (Goldsmith et al., 1997). Fimbrin is a 68-70 kDa actin-bundling protein, which has two actin-binding domains of 250 amino acids, tandemly arranged on the same polypeptide chain and composed of a tandem repeat of two calponin homology (CH) domains (Puius et al., 1998). The binding of actin filaments by fimbrin results in tight bundles of actin filaments (Matsudaira et al., 1983). Work on yeast (Adams et al., 1991) and *Dictyostelium* (Rivero et al., 1996) indicates that fimbrin-associated actin may strengthen actively-growing regions of the cell, that otherwise might be weakened during growth.

A gene encoding a 76 kDa fimbrin-like polypeptide, *ATFIM1*, has been cloned and sequenced from *Arabidopsis thaliana* (McCurdy and Kim, 1998). It shares 40% identity with non-plant fimbrins and contains two tandem repeats. Each of these repeats has a region consisting of 27 amino acids, which are up to 74% identical to the actin-binding domain of non-plant fimbrins.

The gene product of *ATFIM1* most likely bundles actin filaments in plant cells. The hybridization and RT-PCR analyses revealed that this AtFim1 is encoded by a single gene which is expressed in all major organs that were examined: leaves, roots, stems, flowers and siliques (McCurdy and Kim, 1998). These authors identified a second fimbrin-like cDNA, *ATFIM2*, from an expressed sequence tag (EST) collection. This indicates that fimbrin-like proteins are encoded by a small multigene family in *Arabidopsis*. Sequence comparison of the yeast fimbrin homologue, Sacóp, with AtFim1 shows that all nine residues of yeast fimbrin involved in the actin/fimbrin interaction are identical or conserved in *Arabidopsis* fimbrin, and all cluster in a putative actin-binding domain (Brower et al., 1995; McCurdy and Kim, 1998). A similar genetic analysis was done to compare the fimbrin-binding site on actin of yeast, of rabbit skeletal muscle, and of *Arabidopsis*. Interestingly, eight residues in yeast actin involved in the actin/fimbrin interaction, all cluster in one region, close to absolutely conserved regions in all actin's. Therefore, McCurdy and Kim (1998) hypothesize that AtFim1 may interact with all eight functional actin isoforms present in *Arabidopsis* (McDowell et al., 1996). Another fimbrin-like protein has been reported to occur in wheat (Cruz-Ortega et al., 1997).

In vitro experiments with plant fimbrin and actin should reveal its actin-binding properties. The localization of plant fimbrin *in vivo*, its overexpression, and the reaction of cells when

plant fimbrin is injected should reveal its significance as a regulatory ABP in plant cells. From structural information, fimbrin is expected to keep actin filaments 10 nm apart (McCurdy and Kim, 1998).

The CH-actin-binding domain is present in fimbrins and in all other ABPs of the spectrin family, the ABPs with actin cross-linking properties. Spectrin and fodrin (non-erythrocyte spectrin) are thought to be ubiquitous in animal cells (Hartwig, 1994). In red blood cells spectrin is the main protein of the so-called membrane skeleton. This meshwork of filaments in the cortical cytoplasm is held together by short actin peptides and anchored to integral membrane proteins of the plasma membrane (Bennett and Gilligan, 1993). Spectrins are multifunctional ABPs that can form extensive flexible structures (Pumplin and Bloch, 1993). These structures function in maintaining shape and mechanical properties of cells, in regulating vesicle membrane interactions (Bennett, 1990), specifically in maintaining Golgi structure, and regulating vesicular transport to and from the Golgi (Holleran and Holzbauer, 1998), in Ca^{2+}/calmodulin-regulated coupling of plasma membrane proteins to actin (Tanaka et al., 1991), and in mediating signal transduction through interactions with extracellular proteins via integrins (Burridge et al.,1988).

In plant cells, spectrin has been reported to be present along the plasma membrane of *Vicia faba* leaf cells (Wang and Yan, 1991; Michaud et al., 1991). The same procedure, cross-reaction of a plant epitope with an antibody against animal spectrins, shows the presence of a spectrin-like epitope in a variety of plant cells and tissues. Two different antibodies, raised against human and chicken erythrocyte spectrin, gave positive results on Western blots of these plants as well as on their cells. Native plant extracts on blots from IEF gels contained a band at pI 4.8, where the purified animal spectrin is also found (De Ruijter and Emons, 1993). The spectrin-like epitope was found in protoplasts from potato leaves, suspension cultures and developmental stages of somatic embryos of carrot, immature zygotic maize embryos, embryogenic calli of maize, primary root tips of germinating seeds of maize and secondary root tips of bean (De Ruijter and Emons, 1993). The spectrin-like protein was localized predominantly at the plasma membrane, especially of growing cells (De Ruijter and Emons, 1993). Faraday and Spanswick (1993) analyzed a microsome fraction from rice roots which was enriched in plasma membranes, and found a 230 kDa protein that was specifically recognized by polyclonal antibodies to human erythrocyte spectrin. Reuzeau et al. (1997) injected fluorescently-tagged anti-human erythrocyte spectrin in living epidermal cells of onion. This protein labeled a mesh covering the endoplasmatic reticulum and localized tiny spots at the periphery of the cell. Since all studies of spectrin-like antigens in plant cells were done with antibodies raised against heterologous, animal spectrin, we can

not exclude that the proteins that were recognized are different from animal spectrin. Therefore, cloning and sequencing of the plant spectrin gene is a necessity for further research.

Labeling of root hairs with anti-spectrin has identified this epitope as a powerful marker of tip growth. The spectrin-like epitope localizes in the tip of growing hairs, is absent from full-grown hairs and reappears when tip growth is reinitiated by Nod factor in the hairs that are terminating growth (De Ruijter et al., 1998). In the root hairs, the spectrin-like protein co-localizes with a tip-focused gradient of cytoplasmic calcium ions, and is expected to be involved in the exocytosis process, which takes place abundantly at tips of tip-growing cells. Spectrin has also been localized at tips of growing pollen tubes (Derksen et al., 1995) and hyphae (Kaminskyj and Heath, 1995). The cell wall at the tip of growing root hairs is very thin, not more than 30 nm in *Vicia sativa* (Emons unpublished, measured in transmission electron micrographs) and should be flexible, since during active growth the wall at the tip is continuously remodeled. One of the possible functions of an actin-spectrin cytoskeleton in tips of tip-growing plant cells may, therefore, be the strengthening of this actively growing region of the cell.

Methods to study the effect of actin-binding proteins on actin filaments in living cells

Ideally, function of cellular components should be determined in the living cell, in this case either by following the cellular organization and actin filament distribution after microinjection of the ABP in question, or after genetic modification in expression or characteristic of the ABP in question. To decipher the interaction between ABPs and actin filaments, microinjection has been used in a few cases in flowering plants. Staiger et al. (1994) used the actin monomer-binding protein profilin to probe the function of actin filaments in full-grown cells and used *Tradescantia blossfeldiana* stamen hair cells. The cells reacted in a dose-dependent manner. Cytoplasmic streaming came to a standstill and cytoplasmic strands became thinner and eventually snapped back in the cortical cytoplasm. The same events were observed in growing *Tradescantia virginiana* stamen hair cells, showing that in order to exist, cytoplasmic strands require actin filaments (Valster et al., 1997). When plant profilin was co-injected with monomeric plant actin, the destructive effects of profilin could be titrated (Ren et al., 1997). Pollen actin prevented profilin effects in a dose-dependent fashion. Gibbon et al. (1998) tested the activity of profilin isoforms by scoring nuclear displacement in *Tradescantia* stamen hair cells. This assay shows the power of microinjection for the study of protein function in living cells (Gibbon et al., 1998).

Valster et al. (1997) also used the injection of profilin to probe the function of actin during cytokinesis. Double injections of profilin and rhodamine phalloidin, the latter to stain the actin filaments, revealed that profilin indeed depolymerized the phragmoplast actin filaments in a dose-dependent fashion, and that the cell plate was not formed anymore. These experiments show that phragmoplast actin filaments are involved in the formation of the cell plate during cytokinesis, most probably by transporting Golgi vesicles to the growing cell plate. An important follow-up of this research would be the double injection of first profilin and then labeled tubulin, to better understand the combined action of the two cytoskeletal structures, microtubules and actin filaments, in this process. Profilins from different sources were injected into the green alga *Micrasterias* (Holzinger et al., 1997). All profilins disturbed the actin cytoskeleton and strongly affected the development of *Micrasterias.*

Though they are not as specific as actin-binding proteins themselves, actin-perturbing drugs can be used as probes to gain insight in the dynamics of the actin cytoskeleton. Especially cytochalasins have been used in plant cells. *In vitro*, cytochalasins inhibit elongation of animal actin filaments by capping the plus ends (Pollard and Mooseker, 1981). Cytochalasins A and B also inhibit monosaccharide transport across the plasma membrane, but cytochalasins C,D,E,H and 21,22-dihydrocytochalasin B do not (Cooper, 1987). However, for plant cells it has been reported several times that cytochalasins cause bundling of actin filaments (pollen tubes: Lancelle and Hepler, 1988; root cells: Palevitz, 1988; characean internodes: Collings et al., 1995). A study in which cytochalasins were used to interfere with the actin cytoskeleton in root hairs possibly provides a better understanding of the reaction of the actin cytoskeleton to this drug (Miller et al., 1999). In vetch root hairs, cytochalasin D, which is about 10 times more effective then cytochalasin B (Cooper et al., 1987), had no effect on cytoplasmic streaming at 0.5 μM. This cytochalasin D concentration had different effects on actin filament bundles in cytoplasmic strands than on the less-bundled actin filaments in the subapical region. Actin filament bundles in the cytoplasmic strands remained intact and functional, while indeed cytoplasmic streaming continued. However, cytochalasin D arrested the elongation of actin filaments at the front of this subapical zone, in which the actin filaments were less bundled before application of the drug. Thus, cytochalasin D did have the usual depolymerizing effect (Pollard and Mooseker, 1981), but only on a certain category of actin filaments. It stopped the elongation of the fine bundles of actin filaments at the front of the subapical region of growing hairs. A similar phenomenon has been observed when characean internodal cells were wounded. Cytochalasin D led to the disappearance of fine filaments of the actin network, which normally transport vesicles towards the wound surface (Foissner and Wasteneys, 1997).

Concluding remarks

The interaction between ABPs and actin monomers and filaments is necessary for modulating the organization and behavior of the actin cytoskeleton. In all morphogenetic and many other reactions of cells to internal and external signals, ABPs are the intermediaries between a signal transduction cascade and the cell's behavior. The continuous (de)polymerization of actin filaments and their variable interactions with different associating proteins allow the cell to respond with great flexibility and sensitivity to signals from the cell and its surroundings. The study of ABPs in plant cells has only just started. More research on subcellular localization, developmental expression, *in vitro* actin-binding properties, and *in vivo* reaction of the actin cytoskeleton after microinjection of ABPs, and in loss- and gain- of function mutants is imperative to understand the functioning of the plant cell cytoskeleton. Ideally, *in vitro* experiments, microinjection and genetic approaches should be combined, since the complexity of any *in vivo* system makes interpretation of results difficult. In microinjection studies it is difficult to control the level of the protein injected, and at the moment it is hardly possible to effect transient and localized increases of protein levels. On the other hand, genetic redundancy or partial redundancy of function complicate studies in which genes are deleted or mutated.

A research topic that needs to be addressed is the nucleation of actin filaments. Also in animal cells, actin filament nucleation promoting proteins have yet to be identified (Welch et al., 1997), but the actin-related proteins Arp2 and Arp3 may serve as a template for actin nucleation (Kelleher et al., 1995) comparable to γ-tubulin in microtubule nucleation. The Arp2/3 protein complex promotes actin polymerization at the surface of *Listeria monocytogenes* (Welch et al., 1997).

New plant ABPs and isoforms as well as other proteins that regulate actin filament function are expected to be identified. Of course the question arises of what regulates the ABPs. Phosphorylation/dephosphorylation may be one of the mechanisms (reviewed by Moon and Drubin, 1995). Other regulatory mechanisms involve pH (Theriot, 1997), Ca^{2+} and GTP-binding proteins (Davidson and Haslam, 1994). Fine-tuning of a great number of networks of molecular interactions appears to control cellular homeostasis. A multi-disciplinary approach, with a focus on the new advanced microscopy techniques, is expected to give insight in the functioning of the cytoskeleton in the next decade.

ACKNOWLEDGEMENTS

REFERENCES

Adams, A.E.M., Botstein, D. and Drubin, D.G. (1991) Requirement of yeast fimbrin for actin organisation and morphogenesis *in vivo*. *Nature*, **354**, 404-408.

Aderem, A. (1992) Signal transduction and the actin cytoskeleton: the roles of MARCKS and profilin. *Trends Biol. Sci.*, **17**, 438-443.

Aizawa, H., Fukui, Y. and Yahara, I. (1997). Live dynamics of *Dictyostelium* cofilin suggests a role in remodelling actin latticework into bundles. *J. Cell Sci.*, **110**, 2333-2344.

Andersland, J.M., Fisher, D.D., Wymer, C.L., Cyr, R.J. and Parthasarathy, M.V. (1994). Characterization of a monoclonal antibody prepared against plant actin. *Cell Motil. Cytoskel.*, **29**, 339-344.

Asada, T. and Collings, D. (1997) Molecular motors in higher plants. *Trends Plant Sci.* 2, 29-37.

Ayscough, K.R. (1998) *In vivo* functions of actin-binding proteins. *Curr. Opin. Cell Biol.*, **10**, 102-111.

Bennett, V. (1990) Spectrin-based membrane skeleton: a multipotential adaptor between plasma membrane and cytoplasm. *Physiol. Rev.*, **70**, 1029-1065.

Bennett, V. and Gilligan, D.M. (1993) The spectrin-based membrane skeleton and micron-scale organization of the plasma membrane. *Ann. Rev. Cell Biol.*, **9**, 27-66.

Bershadsky, A.D. and Vasiliev, J.M. (1988) In *Cytoskeleto*n (Siekevitz, P., ed). New York, London: Plenum Press, 25.

Brower, S.M., Honts, J.E. and Adams, A.E.M. (1995) Genetic analysis of the fimbrin-actin binding interaction in *Saccharomyces cerevisiae*. *Genetics*, **140**, 91-101.

Burridge, K., Fath, K., Kelly, T., Nuckolls, G. and Turner, C. (1988) Focal adhesions: Transmembrane junctions between the extracellular matrix and the cytoskeleton. *Ann. Rev. Cell Biol.*, **4**, 487-525.

Buß, F., Temm-Grove, C., Henning, S. and Jockusch, B.M. (1992) Distribution of profilin in fibroblasts correlates with the presence of highly dynamic actin filaments. *Cell Motil. Cytoskel.*, **22**, 51-61.

Cárdenas, L., Vidali, L., Domínguez, J., Pérez, H., Sánchez, F. , Hepler, P.K. and Quinto, C. (1998) Rearrangement of actin microfilaments in plant root hairs responding to *Rhizobium etli* nodulation signals. *Plant Physiol.*, **116**, 871-877.

Carlier, M.-F. (1998) Control of actin dynamics. *Curr. Opin. Cell Biol.*, **10**, 45-51.

Carlier, M-F., Laurent, V., Santolini, J., Melki, R., Didry, D., Xia, G-X., Hong, Y., Chua, N-H. and Pantaloni, D. (1997) Actin depolymerizing factor (ADF/cofilin) enhances the rate of filament turnover: implication in actin-based motility. *J. Cell Biol.*, **136**, 1307-1323.

Carlier, M.-F. and Pantaloni, D. (1997) Control of actin dynamics in cell motility. *J. Mol. Biol.*, **269**, 459-467.

Christensen, H.E.M., Ramachandran, S., Tan, C.-T., Surana, U., Dong, C.-H. and Chua, N.H. (1996) *Arabidopsis* profilins are functionally similar to yeast profilins: identification of a vascular bundle-specific profilin and a pollen-specific profilin. *Plant J.*, **10**, 269-279.

Clarke, S.R., Staiger C.J., Gibbon, B.C. and Franklin-Tong, V.E. (1998) A potential signalling role for profilin in pollen of *Papaver rhoeas*. *Plant Cell*, **10**, 967-979.

Cleary, A.L., Gunning, B.E.S., Wasteneys, G.O. and Hepler, P.K. (1992) Microtubule and F-actin dynamics at the division site in living *Tradescantia* stamen hair cells. *J. Cell Sci.*, **103**, 977-988.

Cleary, A.L. (1995) F-actin redistributions at the division site in living *Tradescantia* stomatal complexes as revealed by microinjection of rhodamine-phalloidin. *Protoplasma*, **185**, 152-165.

Collings, D.A., Wasteneys, G.O. and Williamson, R.E. (1995) Cytochalasin rearranges cortical actin of the alga *Nitella* into short, stable rods. *Plant Cell Physiol.*, **36**, 765-772.

Cooper, J.A. (1987) Effects of cytochalasin and phalloidin on actin. *J. Cell Biol.*, **105**, 1473-1478.

Cruz-Ortega, R., Cushman, J-C. and Ownby, J-D. (1997) cDNA clones encoding 1,3-beta-glucanase and a fimbrin-like cytoskeletal protein are induced by Al toxicity in wheat roots. *Plant Physiol.*, **114**, 1453-1460.

Cyr, R.J., (1994) Microtubules in plant morphogenesis: Role of the cortical array. *Ann. Rev. Cell Biol.*, **10**, 153-158.

Cyr, R.J. and Palevitz, B.A. (1995) Organization of cortical microtubules in plant cells. *Curr. Opin. Cell Biol.*, **7**, 65-71.

Danyluk, J., Carpentier, E. and Sarhan, F. (1996) Identification and characterization of a low temperature regulated gene encoding an actin-binding protein from wheat. *FEBS Lett.*, *389*, 324-327.

Darnowski, D.W., Valenta, R. and Parthasarathy, M.V. (1996) Identification and distribution of profilin in tomato (*Lycopersicon esculentum* Mill.) *Planta*, **198**, 158-161.

Davidson, M.M.L. and Haslam, R.J. (1994) Dephosphorylation of cofilin in stimulated platelets-roles for a GTP-binding protein and Ca^{2+}. *Biochem. J.*, **301**, 41-47.

Dawson, P.J., Hulme S.J. and Lloyd, C.W. (1985) Monoclonal antibody to intermediate filament antigen cross-reacts with higher plant cells. *J. Cell Biol.*, *100*, *1793-1798*.

Derksen, J., Rutten, T., van Amstel, T., De Win, A., Doris, F. and Steer, M. (1995) Regulation of pollen tube growth. *Acta Bot. Neerl.*, **44**, 93-119.

De Ruijter, N. and Emons, A. (1993) Immunodetection of spectrin antigens in plant cells. *Cell Biol. Int.*, **17**, 169-182.

De Ruijter, N.C.A., Rook, M.B., Bisseling, T. and Emons, A.M.C. (1998) Lipochito-oligosaccharides reinitiate root hair tip growth in *Vicia sativa* with high calcium and spectrin-like antigen at the tip. *Plant J.*, **13**, 341-350.

Dong, X.-J., Ryu, J.-H., Takagi, S. and Nagai, R. (1996) Dynamic changes in the organization of microfilaments with the photocontrolled motility of chloroplasts in epidermal cells in *Vallisneria. Protoplasma*, **195**, 18-24.

Drøbak, B.K., Watkins, P.A.C., Valenta, R., Dove, S.K., Lloyd, C.W. and Staiger, C.J. (1994) Inhibition of plant plasma membrane phosphoinositide phospholipase C by the actin-binding protein, profilin. *Plant J.*, **6**, 389-400.

Emons, A.M.C., Pierson, E. and Derksen, J. (1991) Cytoskeleton and intracellular movement in plant cells. In *Biotechnology Current Progress*. (Cheremisinoff, P.N. and Ferrante, L.M., eds). Lancaster, PA, U.S.A: Technomic Publishing Company, Inc., 311-335.

Faraday, C.D. and Spanswick, R.M. (1993) Evidence for a membrane skeleton in higher plants. A spectrin-like polypeptide co-isolates with rice root plasma membranes. *FEBS Lett.*, **318**, 313-316.

Finkel, T., Theriot, J.A., Dise, K.R., Tomaselli, G.F. and Goldschmidt-Clermont, P.J. (1994) Dynamic actin structures stabilized by profilin. *Proc. Natl. Acad. Sci.*, **91**, 1510-1514.

Foissner, I., Lichtscheidl, I.K. and Wasteneys, G.O. (1996) Actin-based vesicle dynamics and exocytosis during wound wall formation in characean internodal cells. *Cell Motil. Cytoskel.*, **35**, 35-48.

Foissner, I. and Wasteneys, G.O. (1997) A cytochalasin-sensitive actin filament meshwork is a prerequisite for local wound wall deposition in *Nitella* internodal cells. *Protoplasma*, **200**, 17-30.

Gibbon, B.C. Zonia, L.E., Kovar, D.R., Hussey, P.J. and Staiger, C.J. (1998) Pollen profilin function depends on interaction with proline-rich motifs. *Plant Cell*, **10**, 981-993.

Giehl, K., Valenta, R., Rothkegel, M., Ronsiek, M., Mannherz, H.G. and Jockusch, B.M. (1994) Interaction of plant profilin with mammalian actin. *Eur. J. Biochem.*, **226**, 681-689.

Giuliano, K.A. and Taylor, D.L. (1994) Fluorescent actin analogs with a high affinity for profilin *in vitro* exhibit an enhanced gradient of assembly in living cells. *J. Cell Biol.*, **124**, 971-983.

Goldschmidt-Clermont, P.J., Furman, M.I., Wachsstock, D., Safer, D., Nachmias, V.T. and Pollard, T.D. (1992) The control of actin nucleotide exchange by thymosin β_4 and profilin. A potential regulatory mechanism for actin polymerisation in cells. *Mol. Biol. Cell*, **3**, 1015-1024.

Goldschmidt-Clermont, P.J. and Janmey, P.A. (1991) Profilin, a weak CAP for actin and RAS. *Cell*, **66**, 419-421.

Goldsmith, S.C., Pokala, N., Shen, W., Fedorov, A.A., Matsudaira, P. and Almo S.C. (1997) The structure of an actin-crosslinking domain from human fimbrin. *Nat. Struct. Biol.*, **4**, 708-712.

Goodbody, K.C. Hargreaves, A.J. and Lloyd, C.W. (1989) On the distribution of microtubule-associated intermediate filament antigens in plant suspension cells. *J. Cell Sci.*, **93**, 427-438.

Hartwig, J. (1994) In *Protein Profile, Actin binding proteins 1: spectrin superfamily.* In Volume **1**, issue 7 (Sheterline, ed.) London, UK: Academic Press Lim., 715-740.

Hepler, P.K., Cleary, A.L., Gunning, B.E.S., Wadsworth, P., Wasteneys, G.O. and Zhang, D. H. (1993) Cytoskeletal dynamics in living plant cells. *Cell Biol. Int.*, **17**, 96-83.

Holleran, E.A. and Holzbauer, E.L.F. (1998) Speculating about spectrin: new insights into the Golgi-associated cytoskeleton. *Trends Cell Biol.*, **8**, 26-29.

Huang, S., McDowell, J.M., Weise, M.J. and Meagher, R.B. (1996) The *Arabidopsis* profilin gene family. Evidence for an ancient split between constitutive and pollen-specific profilin genes. *Plant Physiol.*, **111**, 115-126.

Holzinger, A., Mittermann, I., Laffer, S., Valenta, R. and Meindl, U. (1997) Microinjection of profilins from different sources into the green alga *Micrasterias* causes transient inhibition of cell growth. *Protoplasma*, **199**, 124-134.

Hussey, P.J., Yuan, M., Calder, G., Kahn, S. and Lloyd C.W. (1998) Microinjection of pollen-specific actin-depolymerizing factor ZmADF1, reorientates F-actin strands in *Tradescantia* stamen hair cells. *Plant J.*, **14**, 353-357.

Janmey, P.A. (1994) Phosphoinositides and calcium as regulators of cellular actin assembly and disassembly. *Ann. Rev. Physiol.* 56, 169-91.

Jiang, C-J., Weeds, A.G. and Hussey, P.J. (1997a) The maize actin-depolymerizing factor, ZmADF3, redistributes to the growing tip of elongating root hairs and can be induced to translocate into the nucleus with actin. *Plant J.*, **12**, 1035-1043.

Jiang, C-J., Weeds, A.G., Kahn, S. and Hussey, P.J. (1997b) F-actin and G-actin binding are uncoupled by mutation of conserved tyrosine residues in maize actin depolymerizing factor (ZmADF). *Proc. Natl. Acad. Sci. USA*, **94**, 9973-9978.

Kaminskyj, S.G.W. and Heath, I.B. (1995) Integrin and spectrin homologues and cytoplasm-wall adhesion in tip growth. *J. Cell Sci.*, **108**, 849-856.

Karakesisoglou, I., Schleicher, M., Gibbon, B.C. and Staiger, C.J. (1996) Plant profilins rescue the aberrant phenotype of profilin-deficient *Dictyostelium* cells. *Cell Motil. Cytoskel.*, **34**, 36-47.

Kelleher, J.F., Atkinson, S.J. and Pollard, T.D. (1995) Sequences, structural models, and cellular localization of the actin-related proteins Arp2 and Arp3 from *Acanthamoebae. J. Cell Biol.*, **131**, 385-397.

Kim, S.R., Kim, Y. and An, G. (1993) Molecular cloning and characterization of anther-preferential cDNA encoding a putative actin-depolymerizing factor. *Plant Mol. Biol.*, **21**, 39-45.

Kinkema, M., Wang, H. and Schiefelbein J. (1994) Molecular analysis of the myosin gene family in *Arabidopsis thaliana. Plant Mol. Biol.*, **26**, 1139-1153.

Lancelle, S.A. and Hepler, P.K. (1988) Cytochalasin-induced ultrastructural alterations in *Nicotiana* pollen tubes. *Protoplasma Suppl.*, **2**, 65-75.

Lancelle, S.A. and Hepler, P.K. (1991) Association of actin with cortical microtubules revealed by immunogold localization in *Nicotiana* pollen tubes. *Protoplasma*, **165**, 167-172.

Lopez, I., Anthony, R.G., Maciver, S.K., Jiang, C-J., Khan, S., Weeds, A.G. and Hussey, P.J. (1996) Pollen specific expression of maize genes encoding actin depolymerizing factor-like proteins. *Proc. Natl. Acad. Sci.*, **93**, 7415-7420.

Machesky, L.M. and Pollard, T.D. (1993) Profilin as a potential mediator of membrane-cytoskeleton communication. *Trends Cell Biol.*, **3**, 381-385.

Magdolen, V., Drubin, D.G., Mages, G. and Bandlow, W . (1993) High levels of profilin suppress the lethality caused by overproduction of actin in yeast cells. *FEBS Lett.*, **316**, 41-47.

Marc, J. (1997) Microtubule-organizing centres in plants. *Trends Plant Sci.*, **2**, 223-230.

Matsudaira, P. (1991) Modular organization of actin cross-linking proteins. *Trends Biol. Sci.*, **16**, 87-92.

McCurdy, D.W. and Gunning, B.E.S. (1990) Reorganization of actin filaments and microtubules at preprophase and mitosis in wheat root tip cells: a double label immunofluorescence study. *Cell Motil Cytoskel.*, **15**, 76-87.

McCurdy, D.W. and Kim, M. (1998) Molecular cloning of a novel fimbrin-like cDNA from *Arabidopsis thaliana. Plant Mol. Biol.*, **36**, 23-31.

McDowell, J.M., Huang, S., McKinney, E.C., An, Y.-Q. and Meagher, R.B. (1996) Structure and evolution of the actin gene family in *Arabidopsis thaliana. Genetics*, **142**, 587-602.

Meagher, R.B., Williamson, R.E. (1994) The plant cytoskeleton. In *Arabidopsis* (Meyerowitz, E. and Somerville, C., eds). Cold Spring Harbor, NY: Cold Spring Harbor Lab. Press, 1049-1084.

Michaud, D., Guillet, G., Rogers, P.A. and Charest, P.M. (1991) Identification of a 220 kDa membrane-associated plant cell protein immunologically related to human ß-spectrin. *FEBS Lett.*, **294**, 77-80.

Miller, D.D., de Ruijter, N.C.A. and Emons, A.M.C. (1997) From signal to form: aspects of the cytoskeleton-plasma membrane-cell wall continuum in root hair tips: A review article. *J. Exp. Bot.*, **48**, 1881-1896.

Miller, D.D., Lancelle, S.A. and Hepler, P.K. (1996) Actin microfilaments do not form a dense meshwork in *Lilium longiflorum* pollen tube tips. *Protoplasma*, **195**, 123-132.

Miller, D.D., De Ruijter, N.C.A., Bisseling, T. and Emons, A.M.C. (1999) The role of actin in root hair morphogenesis: studies with lipochito-oligosaccharides as a growth stimulator and cytochalasin as an actin perturbing drug. *Plant J.*, **17**, 141-154.

Mittermann, I., Swoboda, I., Pierson, E., Eller, N., Kraft, D., Valenta, R. and Heberle-Bors, E. (1995) Molecular cloning and characterization of profilin from tobacco (*Nicotiana tabacum*): increased expression during pollen maturation. *Plant Mol. Biol.*, **27**, 137-146.

Moon, A. and Drubin, D.G. (1995) The ADF/cofilin proteins: stimulus-responsive modulators of actin dynamics. *Mol. Biol. Cell*, **6**, 1423-1431.

Palevitz, B.A. (1988) Cytochalasin-induced reorganization of actin in *Allium* root cells. *Cell Motil. Cytoskel.*, **9**, 283-298.

Parthasarathy, M.V., Perdue, T.D., Wittzmun, A. and Alvernaz, J. (1985) Actin network as a normal component of cytoskeleton in many vascular plant cells. *Am. J. Bot.*, **72**, 1318-1323.

Perelroizen, I., Didry, D., Christensen, H., Chua, N.-H. and Carlier, M.-F. (1996) Role of nucleotide exchange and hydrolysis in the function of profilin in actin assembly. *J. Biol. Chem.*, **271**, 12302-12309.

Pollard, T.D. and Mooseker, M.S. (1981) Direct measurement of actin polymerization rate constants by electron microscopy of actin filaments nucleated by isolated microvillus cores. *J. Cell Biol.*, **88**, 654-659.

Puius, Y.A., Mahoney, N.M. and Almo, S.C. (1998) The modular structure of actin-regulatory proteins. *Curr. Opin. Cell Biol.*, **10**, 23-34.

Pumplin, D.W. and Bloch, R.J. (1993) The membrane skeleton. *Trends Cell Biol.*, **3**, 113-117.

Ren, H., Gibbon, B.C., Ashworth, S.L., Sherman, D.M., Yuan, M. and Staiger, C.J. (1997) Actin purified from maize pollen functions in living plant cells. *Plant Cell*, 9, 1445-1457.

Reuzeau, C., Doolittle K.W., McNally, J.G. and Pickard B.G. (1997) Covisualization in living onion cells of putative integrin, putative spectrin, actin, putative intermediate filaments, and other proteins at the cell membrane and in an endomembrane sheath. *Protoplasma*, 199, 173-197.

Rivero, F., Koppel, B., Peracino, B., Bozzaro, S., Siegert, F., Weijer, C.J., Schleicher, M., Albrecht, R. and Noegel, A.A. (1996) The role of the cortical cytoskeleton-F-actin cross-linking proteins protect against osmotic-stress, ensure cell-size, cell-shape and motility, and contribute to phagocytosis and development. *J. Cell Sci.*, 109, 2679-2691.

Rothkegel, M., Mayboroda, O., Rohde, M., Wucherpfennig, C., Valenta, R. and Jockusch, B.M. (1996) Plant and animal profilins are functionally equivalent and stabilize microfilaments in living animal cells. *J. Cell Sci.*, 109, 83-90.

Rozycka, M.D., Khan, S., Lopex, I., Greenland, A.J. and Hussey, P.J. (1995) A *Zea mays* pollen cDNA encoding a putative actin-depolymerizing factor. *Plant Physiol.*, 107, 1011-1012.

Ruhlandt, G., Lange, U. and Grolig, F. (1994) Profilins purified from higher plants bind to actin from cardiac muscle and to actin from a green alga. *Plant Cell Physiol.*, 35, 849-854.

Seagull, R.W. and Heath, I.B. (1979) The effects of tannic acid on the *in vivo* preservation of microfilaments. *Eur. J. Cell Biol.*, 20, 184-188.

Sheterline, P. and Sparrow, J.C. (1994) Actin. Protein Profile, 1, 1-62

Sohn, R.H. and Goldschmidt-Clermont, P.J. (1994) Profilin: at the crossroads of signal transduction and the actin cytoskeleton. *BioEssays*, 16, 465-472.

Sonobe, S. and Shibaoka, H. (1989) Cortical fine actin filaments in higher plant cells visualized by rhodamine-phalloidin after pretreatment with m-maleimidobenzoyl N-hydroxysuccinimide ester. *Protoplasma*, 148, 80-86.

Staehelin, L.A. and Hepler, P.K. (1996) Cytokinesis in higher plants. *Cell*, 84, 821-824.

Staiger, C.J., Gibbon, B.C., Kovar, D.R. and Zonia, L.E. (1997) Profilin and actin-depolymerizing factor: modulators of actin organization in plants. *Trends Plant Sci.*, 2, 275-281.

Staiger, C.J., Goodbody, K.C., Hussey, P.J., Valenta, R., Drøbak, B.K. and Lloyd, C.W. (1993) The profilin multigene family of maize: differential expression of three isoforms. *Plant J.*, 4, 631-641.

Staiger, C.J. and Schliwa, M. (1987) Actin localization and function in higher plants. *Protoplasma*, 141, 1-12.

Staiger, C.J., Yuan, M., Valenta, R., Shaw, P.J., Warn, R.M. and Lloyd, C.W. (1994) Microinjected profilin affects cytoplasmic streaming in plant cells by rapidly depolymerizing actin microfilaments. *Curr. Biol.*, 4, 215-219.

Sun, H.Q., Kwiatkowska, K. and Yin, H.L. (1995) Actin monomer binding proteins. *Curr. Opin. Cell Biol.*, 7, 102-110.

Takemoto, D., Furuse, K., Doke, N. and Kawakita, K. (1997) Identification of chitinase and osmotin-like protein as actin-binding proteins in suspension-cultured potato cells. *Plant Cell Physiol.*, 38, 441-448.

Tanaka .T., Kadowaki, K., Lazarides, E., Sobue, K (1991) Calcium ion-dependent regulation of the spectrin-actin interaction by calmodulin and protein 4.1. *J. Biol. Chem.*, **266**, 1134-1140.

Theriot, J.A. (1997) Accelerating on a treadmill: ADF/cofilin promotes rapid filament turnover in the dynamic cytoskeleton. *J. Cell Biol.*, **136**, 1165-1168.

Thorn, K.S., Christensen, H.E.M., Shigeta, R.Jr., Huddler, D.Jr., Shalaby, L. Lindberg,U., Chua, N.H. and Schutt, C.E. (1997). The crystal structure of a major allergen from plants. *Structure*, **5**, 19-32.

Valenta, R., Duchêne, M., Pettenburger, K., Sillaber, C., Valent, P., Bettelheim, P., Breitenbach, M., Rumpold, H., Kraft, D. and Scheiner, O. (1991) Identification of profilin as a novel pollen allergen; IgE autoreactivity in sensitized individuals. *Science*, **253**, 557-560.

Valenta, R., Ferreira, F., Grote, M., Swoboda, I., Vrtala, S., Duchêne, M., Devillier, P., Meagher, R.B., McKinney, E., Heberle-Bors, E., Kraft, D. and Scheiner, O. (1993). Identification of profilin as an actin-binding protein in higher plants. *J. Biol. Chem.*, **268**, 22777-22781.

Valster, A.H., Pierson, E.S., Valenta, R., Hepler, P.K. and Emons, A.M.C. (1997) Probing the plant actin cytoskeleton during cytokinesis and interphase by profilin microinjection. *Plant Cell*, **9**, 1815-1824.

Vidali, L. and Hepler, P.K. (1997) Characterization and localization of profilin in pollen grains and tubes of *Lilium longiflorum*. *Cell Motil. Cytoskel.*, **36**, 323-338.

Vidali, L., Pérez, H.E., López, V.V., Noguez, R., Zamudio, F. and Sánchez, F. (1995) Purification, characterization, and cDNA cloning of profilin from *Phaseolus vulgaris*. *Plant Physiol.*, **108**, 115-123.

Volkmann, D., Buchen, B., Hejnowicz, Z., Tewinkel, M. and Sievers, A. (1991) Oriented movement of statoliths studied in a reduced gravitational field during parabolic flights of rockets. *Planta*, **185**, 153-161.

Waller, F. and Nick, P. (1997) Response of actin microfilaments during phytochrome-controlled growth of maize seedlings. *Protoplasma*, **200**, 154-162.

Wang, Y. and Yan, L. (1991). Immunochemical identification of spectrins on the plasma membrane of leaf cells of *Vicia faba*. *Chin. Sci. Bull.*, **36**, 862-866.

Welch, M.D., Iwamatsu, A. and Mitchison, T.J. (1997) Actin polymerization is induced by Arp2/3 protein complex at the surface of *Listeria monocytogenes*. *Nature*, **385**, 265-269.

Welch, M. D. Mallavarapu, A., Rosenblatt, J. and Mitchison, T.J. (1997) Actin dynamics *in vivo*. *Curr. Opin. Cell Biol.*, **9**, 54-61.

Wieland, T. and Faulstich, H. (1978) Amatoxins, phallotoxins, phallolysin, and antamanide: the biologically active components of poisonous *Amanita* mushrooms. *CRC Crit. Rev. Biochem.*, **5**, 185-260.

Williamson, R.E. (1993) Organelle movements. *Ann. Rev. Plant Physiol. Plant Mol. Biol.*, **44**, 181-202.

Wymer, C. and Lloyd, C. (1996) Dynamic microtubules: implications for cell wall patterns. *Trends in Plant Sci.*, **7**, 222-228.

Xia, G., Ramachandran, S., Hong, Y., Chan, Y-S., Simanis, V. and Chua, N-H. (1996) Identification of plant cytoskeletal, cell-cycle related and polarity-related proteins using *Schizosaccharomyces pombe*. *Plant J.*, **10**, 761-769.

Zhang, D.H., Wadsworth, P. and Hepler, P.K. (1993) Dynamics of microfilaments are similar but distinct from microtubules during cytokinesis in living, dividing plant cells . *Cell Motil. Cytoskel.*, **24**, 205-213.

- Chapter 8 -

Plant cell growth: lessons from root hairs

General discussion

Norbert de Ruijter

Two important factors in plant morphogenesis are cell division and cell expansion. The cytoskeleton is involved in cell division, for instance in the determination of the orientation of the plane of cell division (Chapter 1). Cell division is commonly followed by cell expansion. Cell expansion implies an increase in cell volume, which involves a concerted action of many cell organelles. An important organelle is the Golgi apparatus, which consists of Golgi bodies, from which Golgi vesicles bud, that can contain cell wall precursors (Driouich *et al.*, 1993). The conditions required for cell expansion are turgor pressure, a flexible, pliable cell wall, and exocytosis of Golgi vesicles. Thus, only in turgid cells, where the cell wall is not rigid yet, cell expansion can take place, if Golgi vesicle membranes are inserted into the plasma membrane, and the content of the vesicles is delivered to the existing wall (Roberts, 1994). Consequently, the Golgi vesicle is the unit of plant cell expansion (see also: Miller *et al.*, 1997).

Depending on the cell facets that expand, we discern isodiametric cell growth, diffuse (or intercalary) cell growth, and cell tip growth. In *isodiametric cell growth*, all wall facets expand more or less evenly; thus the final cell shape is proportional to the original cell shape. In *diffuse cell growth* (Kropf *et al.*, 1998), also called intercalary growth (Miller *et al.*, 1997), cell expansion occurs in mainly one direction, often the direction perpendicular to the previous division plane, but a lateral expansion can also take place to a lesser extent. Diffuse expansion takes for instance place in root cells present in cell files. They expand in the direction of the long axis of the root, and cause root elongation. In *cell tip growth*, also called polar cell growth, the cell expands at one side. Best known examples of higher plant cells with tip growth are root hairs and pollen tubes. In lower plants and fungi the phenomenon occurs for instance at spore or zygote germination (Kropf, 1992), in rhizoids (Brownlee and Pulsford, 1988), fungal hyphae (Howard, 1997) and in yeast bud formation (Pringle, 1995; Drubin and Nelson, 1996).

In tip growing cells, the cell expands at one site. Therefore, these cells are most suited to study the plant growth process at the cellular level (Chapters 2 and 5). During cell tip growth, Golgi vesicles fuse with the plasma membrane at one side of the cell; the tip. Prior to this fusion, the following cascade of events has to take place: vesicle production by budding from Golgi bodies, translocation of the vesicles by a transport system, local release of vesicles from the transport system close to or at the plasma membrane, retention of vesicles at that site, docking and attachment of vesicles at the plasma membrane, priming of vesicles (i.e. waiting for Ca^{2+}), fusion of vesicles with the plasma membrane (triggered by Ca^{2+}), while discharging the vesicle content (reviewed by Battey and Blackbourn, 1993).

In this concluding chapter we summarize the cell biological characteristics of cell tip growth, that have been addressed in this thesis. For each characteristic, we compare our results with data that have been obtained in other tip growing cells. Further, we discuss how these phenomena of cell tip growth could function. Then we discuss whether these characteristics are pertinent to cell expansion in general.

The following cell biological phenomena, that occur simultaneously, are characteristic for cell tip growth:

- Accumulation of Golgi vesicles at the site of cell growth
- Increased intracellular cytoplasmic calcium concentration at the plasma membrane at the site of cell growth (Chapter 2)
- Accumulation of a spectrin-like protein at the site of cell growth (Chapters 2 and 3)
- Absence of actin filaments bundles in the vesicle rich region (Chapter 5)
- Presence of a dense network of bundles of actin filaments (FB-actin) adjacent to the Golgi vesicle rich region (Chapters 5 and 6)

Accumulation of Golgi vesicles at the site of cell growth

The tip growing root hairs have a characteristic cyto-architecture. When studied by differential interference contrast (DIC) microscopy, the very tip of a root hair appears smooth. A sub-apical region of dense cytoplasm follows this smooth area. In the smooth area, large organelles are never observed (Chapter 2).

The smooth area also occurs in growing pollen tubes, and has been called there the clear zone (Pierson *et al.*, 1994). Electron micrographs of freeze substituted growing pollen tubes (i.e. *Lilium longiflorum*, Lancelle *et al.*, 1992), or root hairs (i.e. *Equisetum hyemale* and *Limnobium stoloniferum*: Emons, 1987; *Arabidopsis thaliana*: Galway *et al.*, 1997; *Vicia villosa*: Sherrier and Vandenbosch, 1994) show an accumulation of Golgi vesicles in the apical domain of these tip growing cells, as was also observed in *Vicia sativa* (Fig. 1, courtesy: H. Leferink-ten-Klooster).

The area that appears smooth in the DIC microscope is, therefore, called the vesicle rich region. When vesicles fuse, new membrane is brought into the existing plasma membrane, and cell wall matrix is delivered to the existing cell wall. Golgi vesicles are also present at the plasma membrane in cells with isodiametric and diffuse cell expansion (Emons *et al.*, 1992), but commonly the abundance of vesicles is less, when growth is more diffuse.

Figure 1: An electron micrograph of a longitudinal section through the tip of a growing *Vicia sativa* root hair shows an abundance of Golgi vesicles in the growing tip (courtesy: H. Leferink-ten-Klooster).

Increased intracellular cytoplasmic calcium concentration at the plasma membrane at the site of cell growth

In growing tips of root hairs of *Vicia sativa*, a tip-focused gradient of cytoplasmic calcium concentration ($[Ca^{2+}]_c$) was found, while the distribution of the $[Ca^{2+}]_c$ of full-grown hairs was similar from tip to base. The $[Ca^{2+}]_c$ of at least 75% of the tips of growing hairs was 1.25 ± 0.75 µM, while at least 75% of the tips of full-grown hairs had a $[Ca^{2+}]_c$ of 150 ± 150 nM (De Ruijter *et al.*, 1998; Chapter 2).

The same correlation of growth and high calcium at the tip was observed in root hairs of *Arabidopsis thaliana* (Wymer *et al.*, 1997), and *Sinapis alba* (Herrmann and Felle, 1995; Felle and Hepler, 1997). A tip-focused calcium gradient has also been observed in pollen tubes (Pierson *et al.*, 1994), fungal hyphae (Jackson and Heath, 1993a), and in tip-growing rhizoids of brown algae (*Fucus serrata*: Brownlee and Pulsford, 1988; *Pelvetia compressa*, Pu and Robinson, 1998). Studies, in which calcium selective vibrating probes were used, have shown an influx of extracellular calcium at tips, which correlate with expansion (Schiefelbein *et al.*, 1992; Herrmann and Felle, 1995). Inhibition of Ca^{2+} channels has provided circumstantial evidence for the local presence of activated Ca^{2+} channels (Reiss and Herth, 1985; Schiefelbein *et al.*, 1992; Felle and Hepler, 1997). In plant cells, as in animal cells (Clapham, 1995), exocytosis appears to be dependent on, and triggered by, a rise in the $[Ca^{2+}]_c$ at the plasma membrane.

Since exocytosis correlates with locally elevated $[Ca^{2+}]_c$, it can be postulated that in diffuse growing cells, the $[Ca^{2+}]_c$ proximal to the wall facets that expand, is elevated. This can be tested when living root cortical cells are loaded with a ratiometric calcium dye and imaged at a high resolution. The peripheral cytoplasm against the radial and tangential walls of for instance elongating root cells is expected to have a higher $[Ca^{2+}]_c$ than the peripheral cytoplasm alongside the transversal walls. However, in diffuse cell expansion, it can be expected that the elevation of the $[Ca^{2+}]_c$ at the plasma membrane will be much lower.

Technical limitations often hamper the measurement of $[Ca^{2+}]_c$ close to wall facets in diffuse growing cells. All currently available calcium dyes have to bind calcium first, to be able to report its concentration by a spectral shift in the absorption or emission of the fluorescent dye. Their affinity for calcium ions implies that the $[Ca^{2+}]_c$ reporters all have a buffering capacity, and can therefore only be used in a limited concentration range. To be able to record enough emitted light, the biologically acceptable concentrations would have to be exceeded. By molecular engineering, better probes like Cameleon (Miyawaki *et al.*, 1997, 1999) are available now, which make use of genetically engineered endogenous calcium binding proteins. In combination with new microspectroscopic techniques, like fluorescent lifetime imaging, such new probes allow more sensitive recordings of $[Ca^{2+}]_c$ in cells.

Indications for growth-correlated elevated calcium in cells with isodiametric and diffuse cell expansion, have been obtained in carrot (*Daucus carota* L.) during somatic embryogenesis with chlorotetracycline (CTC) for membrane-bound calcium (Timmers, 1989), and have been further substantiated with fluo-3 for cytoplasmic calcium (Timmers *et al.*, 1991). All cells in proembryogenic masses and in young globular stage somatic embryos increase in volume, and all cells show a homogeneous high cytosolic calcium level. These cells expand in all directions, which points to a correlation of isodiametric growth and elevated calcium. In more developed globular stage embryos and heart-shaped embryos the expanding cells are more abundant in the protoderm, and this tissue has a homogeneous high $[Ca^{2+}]_c$. Torpedo-shaped embryos showed a $[Ca^{2+}]_c$ gradient from the tips of the cotyledons to the base, which also reflects a gradient of growing cells. However, within the cells with elevated $[Ca^{2+}]_c$, a gradient towards the cell periphery has not been reported.

Accumulation of a spectrin-like protein at the site of cell growth

The plant spectrin-like protein localizes specifically in growing tips of root hairs of vetch (*Vicia sativa*) (De Ruijter *et al.,* 1998; Chapter 2). This localization is comparable with labeling of spectrin-like proteins in the tips of growing tobacco pollen tubes (Derksen,

1996), and in tips of growing hyphae of the oomycete *Saprolegnia ferax* (Kaminskyj and Heath, 1995).

Confocal laser scanning microscopy showed not only a peripheral labeling of the growing root hair tips, but also a speckled labeling in the area that overlaps the vesicle rich-region (Chapter 2). The dotted labeling could represent Golgi vesicles coated with spectrin-like proteins, and would explain how these proteins are transported to the plasma membrane. With immuno-electron microscopy spectrin-like epitopes have also been detected on exocytotic vesicles in young developing cells of the green algae *Micrasterias denticulata* (Holzinger *et al.*, 1999).

In red blood cells, spectrin is a prominent part of the membrane-associated cytoskeleton (Goodman *et al.*, 1988). A sub-membranous actin-spectrin network, widespread in all kingdoms (Hartwig, 1994), gives often structural support to the plasma membrane (Bennett, 1990; Bennett and Gilligan, 1993; Devarajan and Morrow, 1996). Also in higher plants, spectrin-like proteins localize at membranes (Chapter 2; De Ruijter and Emons, 1993 (Chapter 3); Reuzeau *et al.*, 1998), and accumulate in a purified plasma membrane fraction of rice roots (Faraday and Spanswick, 1993).

A spectrin-based sub-membranous cytoskeleton at the site of growth where the wall is still flexible and lacks rigidity could provide mechanical membrane stability at this site. Especially at the tip of tip growing cells, where the primary cell wall is thin (Emons and Wolters-Arts, 1983), and might not be able yet to withstand turgor pressure, increased structural support for the plasma membrane is a feasible function for spectrin.

The presence of spectrin-like epitopes in isodiametric and diffuse growth has already been shown in elongating plant cells (Chapter 3). For instance, in suspension cells of carrot (*Daucus carota*), in meristematic cells of maize (*Zea mays)* (Chapter 3), and in cells of the apical meristem of cauliflower (*Brassica oleracea*) inflorescence (unpublished results), strong labeling was found at the cell borders with different anti-erythrocyte spectrin antibodies. Also isodiametric growth is accompanied by spectrin-like proteins. For example, the spectrin-like epitope is present at the plasma membrane during swelling of root hair tips, after application of lipochito-oligosaccharides (Chapter 2).

Spectrin-like proteins also occur in plant nuclei. Their speckled localization, as well as their localization in the nuclear matrix suggests that the spectrin-like protein has a function in structural stability (Chapter 4).

The nature of the plant epitope that is recognized by anti-spectrin antibodies is not yet known. However, evidence for the presence of a spectrin gene family in higher plants exists, since sequences of plant fimbrin have been found (Cruz-Ortega *et al.*, 1997; McCurdy and Kim, 1998).

Absence of actin filaments bundles in the vesicle rich region

Growing root hair tips of vetch are characterized by the absence of actin filament bundles in the vesicle rich region (Chapters 5 and 6). A region free of actin filament bundles is only present when the cytoarchitecture of the hair is well preserved, for instance after a freeze fixation or an optimized ester-aldehyde fixation. This absence of actin filaments in the extreme tip is in agreement with the fact that cytoplasmic streaming is not observed in this vesicle rich region.

An absence of actin filaments in the apical dome of tip growing cells has been observed more often. Jackson and Heath (1993b) found a region lacking actin filaments at the very apex of growing *Saprolegnia* hyphae. Also in growing *Lilium* pollen tubes, micro-injected with fluorescent phalloidin, the growing tip was devoid of actin filaments (Miller *et al.*, 1996). In rat pancreatic acinar cells, a direct correlation exists between exocytosis and local depolymerization of cortical filamentous actin (Muallem *et al.*, 1995).

It has been shown that the binding of phalloidin to actin competes with the binding of ADF/cofilin to actin (Ressad *et al.*, 1998). In root cells of maize, Jiang *et al.* (1997) showed that a high density of ADF hampers staining of actin filaments with labeled phalloidin. Although ADF accumulates in growing tips of maize root hairs (Jiang *et al.*, 1997), the absence of phalloidin stained bundles of actin filaments in vetch root hair tips is not caused by ADF-shielded actin filaments, since their absence was confirmed with immunolabeling with anti-actin antibodies (Miller *et al.*, 1999). However, the region devoid of filamentous actin is smaller after freeze-fixation and immunolabeling, than after chemical fixation and fluorescent phalloidin staining.

During cytokinesis in plant cells, filamentous actin is absent from the site where the expanding cell plate will fuse with the maternal plasma membrane (Cleary *et al.*, 1995). Possibly, the local absence of actin is necessary for insertion of vesicles into the plasma membrane. An area devoid of actin filament bundles could, thus, be an example of positive regulation of exocytosis. Whether actin filament bundles are absent from the site of exocytosis in diffuse growing cells is not known, but we hypothesize that in an extremely thin layer along the plasma membrane, at the site of vesicle fusion, actin filaments are absent.

Presence of a dense network of bundles of actin filaments (FB-actin) adjacent to the Golgi vesicle rich region

Growing root hair tips show a reverse-fountain cytoplasmic streaming pattern; in the sub-apical region cytoplasmic streaming slows down, and reverses its direction, before it reaches the tip (Chapter 2). The sub-apical cytoplasm of growing hairs is very dynamical. An actin configuration with dense net-axial fine bundles of actin filaments is characteristic for this sub-apical region of growing vetch root hairs (Miller *et al.*, 1999; Chapter 5). We have called such an actin configuration FB-actin (Chapters 5 and 6). FB-actin was quantified for root hairs in each developmental stage. This revealed a correlation of growth with a minimal density of 7-8 actin filament bundles, over a minimal length of 10 µm, adjacent to the vesicle rich region (De Ruijter *et al.*, 1999; Chapter 6).

In other tip growing cells, the presence of dense and fine actin filaments behind the vesicle rich region has also been reported. Kost *et al.* (1998) visualized a sub-apical band of actin filaments with a GFP-talin fusion protein expressed in living tobacco pollen tubes. Miller *et al.* (1996) also observed dense actin filaments in the sub-apical region of *Lilium* pollen tubes.

Since in the sub-apical region the direction of cytoplasmic streaming turns, and all large organelles follow the flow, while vesicles accumulate at the tip, Golgi vesicles must be released here. It is not known whether vesicles are released directly from the Golgi bodies or are first released from the Golgi bodies, transported by actin filaments and then released. The dense FB-actin may be a transport system or may provide a web that allows only vesicles to pass, while it excludes larger organelles. The continuous release and retention of vesicles builds and refills the reservoir of vesicles, the vesicle rich region. In this vesicle rich region, the vesicles may be pushed towards the tip by the ongoing delivery of vesicles while they are being swallowed into the plasma membrane during exocytosis. Therefore, a transport system is not needed within the vesicle rich region.

FB-actin is considered a prerequisite for vesicle delivery to the site of cell expansion in tip growing cells. By extrapolating this to diffuse growth, we postulate that wall facets that expand should have a thin cortical actin web able to deliver and hold vesicles. With the light microscope such a thin actin web is difficult to image. Interesting data were obtained by studying the wound response in characean internodal cells (Foissner *et al.*, 1996). These cells are able to rapidly deposit wall material at the site of membrane damage. The sudden local vesicle delivery in these cells correlates with a transient, local reorganization of actin filaments from parallel bundles to a fine-meshed network (Foissner *et al.*, 1996).

Fig. 2 An immunofluorescence micrograph of the actin cytoskeleton, 75 min after LCO application, shows a short area with FB-actin pointing to a new outgrowth (arrows). Note that these bundles enclose an area at the plasma membrane devoid of actin filament bundles (arrowhead). The image is a z-projection of a series of confocal images over 10 μm depth at 0.5 μm intervals. Bar = 15 μm.

Lipochito-oligosaccharides induced root hair deformation: an assay to study signal transduction leading to growth

In Chapter 2 (De Ruijter *et al.*, 1998) we show that host specific Nod factors, lipochito-oligosaccharides (LCOs), signal molecules from *Rhizobium* bacteria, are able to reinitiate growth in *Vicia sativa* root hairs. Growth was reinitiated in root hairs that were in the developmental stage of growth termination. These hairs responded to the signal by root hair deformation, which is swelling of the root hair tip, followed by an outgrowth from that swelling (Heidstra *et al.*, 1994). The swelling of the most distal part of the hair can be considered as isodiametric growth, and the outgrowth is a re-initiation of tip cell growth. Swelling is an active process, requiring protein synthesis (Vijn *et al.*, 1995).

Within minutes after application of LCOs, we observed a significant increase in the density of actin filament bundles in the root hair (De Ruijter *et al.*, 1999a; Chapter 6). The actin cytoskeleton in root hair tips appears to be a target of LCOs. The increase in sub-apical actin filament bundles is such that FB-actin reappears in root hairs that were terminating growth. The actin filament bundles not only increased in density, but were also less net-axially oriented. The reappearance of FB-actin in a less focussed fashion allows vesicle delivery in a less focussed way, which leads to swelling. During swelling, $[Ca^{2+}]_c$ was

elevated and spectrin-like proteins accumulated at the plasma membrane (De Ruijter *et al.*, 1998).

When tip growth reinitiates from the swelling all the characteristics for tip growth are re-established. Fine and dense actin filament bundles focus at the site of the outgrowth (Fig. 2). During the onset of an outgrowth, a local "hot spot" of elevated $[Ca^{2+}]_c$ (see Chapter 2, Fig. 6e), and a local accumulation of spectrin-like proteins were observed (see Miller *et al.*, 1997). In DIC images the reappearance of a vesicle rich area was observed (Chapter 2) as well as the typical reverse fountain cytoplasmic streaming pattern.

Exocytosis and the cascades of reactions in the cell that lead to exocytosis can only be understood by using a multidisciplinary approach. Concepts must ultimately be tested in growing living cells. The study of plant growth regulation will remain an active field in the future. Root hairs possess the characteristics necessary to serve as an experimental system for studying interactions at the plant cell surface, triggered by internal or external signals and leading to cell morphogenesis. The use of genetic analysis and well-characterized signal molecules such as LCOs will give insight into the signal transduction pathways involved in root hair growth and plant cell morphogenesis.

REFERENCES

Battey NH, Blackbourn HD, 1993. The control of exocytosis in plant cells. *New Phytologist* **125,** 307-38.

Bennett V, 1990. Spectrin-based membrane skeleton: a multipotential adaptor between plasma membrane and cytoplasm. *Physiol Rev* **70**: 1029-1065.

Bennett V, Gilligan DM, 1993. The spectrin-based membrane skeleton and micron-scale organization of the plasma membrane. *Ann Rev of Cell Biol* **9,** 27-66.

Brownlee C, Pulsford A 1988. Visualization of the cytoplasmic Ca^{2+} gradient in *Fucus serratus* rhizoids: correlation with cell ultrastructure and polarity. *J Cell Sci* **91,** 249-256.

Clapham DE, 1995. Calcium signaling. *Cell* **80:** 259-268.

Cleary AL, 1995 F-actin redistributions at the division site in living *Tradescantia* stomatal complexes as revealed by microinjection of rhodamine-phalloidin Protoplasma 185: 152-165

Cruz-Ortega, R., Cushman, J-C. Ownby, J-D, 1997. cDNA clones encoding 1,3-beta-glucanase and a fimbrin-like cytoskeletal protein are induced by Al toxicity in wheat roots. *Plant Physiol.* **114**: 1453-1460.

Derksen J, 1996. Pollen tubes: a model system for plant cell growth. *Bot Acta* **109**: 341-345.

De Ruijter N, Emons AM, 1993. Immunodetection of spectrin antigens in plant cells. *Cell Biol Int* 17:169-182.

De Ruijter NCA, Rook MB, Bisseling T, Emons AMC, 1998. Lipochito-oligosaccharides reinitiate root hair tip growth in *Vicia sativa* with high calcium and spectrin-like antigen at the tip. *Plant J.* **13**: 341-350.

De Ruijter NCA , Bisseling T, Emons AMC, 1999. *Rhizobium* Nod factors induce an increase in sub-apical fine bundles of actin filaments in *Vicia sativa* root hairs within minutes. *Mol. Plant-Microbe. Interact.* **12**: 829-832.

Devarajan P, Morrow JS, 1996. The spectrin cytoskeleton and organization of polarized epithelial cell membranes. *Current Topics in Membranes* **43**: 97-128.

Driouich A, Faye L, Staehelin LA, 1993. The plant Golgi apparatus: a factory for complex polysaccharides and glycoproteins. *Trends Biochem Sci* 18: 210-214.

Drubin DG, Nelson WJ, 1996. Origins of cell polarity. *Cell* 9: 335-344.

Emons AMC, 1987. The cytoskeleton and secretory vesicles in root hairs of *Equisetum* and *Limnobium*, and cytoplasmic streaming in root hairs of *Equisetum*. *Ann of Bot* **60**: 625-632.

Emons AMC, Vos JW, Kieft H, 1992. A freeze fracture analysis of the surface of embryogenic and noon-embryogenic suspension cells of *Daucus carota*. *Plant Sci* **87**: 85-97.

Emons AMC, Wolters-Arts AMC, 1983. Cortical microtubules and microfibril deposition in the cell wall of root hairs of *Equisetum hyemale*. *Protoplasma* **117**, 68-81.

Faraday CD, Spanswick RM, 1993. Evidence for a membrane skeleton in higher plants. A spectrin-like polypeptide co-isolates with rice root plasma membrane. *FEBS* **318**, 313-316.

Felle HH, Hepler PK, 1997. The cytosolic Ca^{2+} concentration gradient of *Sinapis alba* root hairs as revealed by Ca^{2+}-selective microelectrode tests and Fura-dextran ratio imaging. *Plant Physiol* **114**: 39-45.

Foissner I, Lichtscheidl IK, Wasteneys, GO, 1996. Actin-based vesicle dynamics and exocytosis during wound wall formation in characean internodal cells. *Cell Motil Cytoskeleton* **35**: 35-48.

Galway ME, Heckman Jr. JW, Schiefelbein JW, 1997. Growth and ultrastructure of *Arabidopsis* root hairs: the *rhd3* mutation alters vacuole enlargement and tip growth. *Planta* **201**, 209-18.

Goodman SR, Krebs KE, Whitfield CF, Riederer BM, Zagon IS, 1988. Spectrin and related molecules. *CRC Crit. Rev. Biochem.* **23**, 171-234.

Hartwig JH, 1994. Subfamily 1: The Spectrin Family. In: Sheterline P. ed. Protein Profile. *Actin-Binding Proteins 1: spectrin superfamily.* Volume **1**, London UK: Academic Press, 715-40.

Heidstra R, Geurts R, Franssen H, Spaink HP, van Kammen A, Bisseling T, 1994. Root hair deformation activity of Nodulation factors and their fate on *Vicia sativa*. *Plant Physiol* **105**, 787-97.

Herrmann A, Felle H, 1995. Tip growth in root hair cells of *Sinapis alba* L.: significance of internal and external Ca^{2+} and pH. *New Phytologist* **129**, 523-33.

Holzinger A, de Ruijter NCA, Emons AMC, Lütz-Meindl U, 1999. Spectrin-like proteins in green algae (Desmidiaceae). *Cell Biol Int,* in press.

Howard FM, 1997. How hyphae grow: morphogenesis explained? *Protoplasma* **197**, 137-147.

Jackson SL, Heath IB, 1993a. Roles of calcium ions in hyphal tip growth. *Microbiol Rev* **57**: 367-382.

Jackson SL, Heath IB, 1993b. The dynamic behavior of cytoplasmic F-actin in growing hyphae. *Protoplasma* 173: 23-34.

Jiang CJ, Weeds AG, Hussey PJ, 1997. The maize actin-depolymerizing factor, ZmADF3, redistributes to the growing tip of elongating root hairs and can be induced to translocate into the nucleus with actin. *Plant J* 12: 1035-1043.

Kaminskyj SGW, Heath IB, 1995. Integrin and spectrin homologues, and cytoplasm-wall adhesion in tip growth. *J of Cell Sci* 108, 849-856.

Kost B, Spielhofer P, Chua NH, 1998. A GFP-mouse talin fusion protein labels plant actin filaments in vivo and visualizes the actin cytoskeleton in growing pollen tubes. *Plant J* 16: 393-401.

Kropf DL, 1992. Establishment and expression of cellular polarity in fucoid zygotes. *Microbiol Rev* 56: 316-339.

Kropf DL, Bisgrove SR, Hable WE, 1998. Cytoskeletal control of polar growth in plant cells. *Curr Opin Cell Biol* 10: 117-122.

Lancelle SA, Hepler PK, 1992. Ultrastructure of freeze-substituted pollen tubes of *Lilium longiflorum*. *Protoplasma* 167, 215-230.

McCurdy DW, Kim M, 1998. Molecular cloning of a novel fimbrin-like cDNA from *Arabidopsis thaliana*. *Plant Mol Biol*. 36, 23-31.

Miller DD, Lancelle SA, Hepler PK, 1996. Actin microfilaments do not form a dense meshwork in *Lilium longiflorum* pollen tube tips. *Protoplasma* 195, 123-132.

Miller DD, De Ruijter NCA, Emons AMC, 1997. From signal to form: aspects of the cytoskeleton-plasma membrane-cell wall continuum in root hair tips. *J Exp Bot* 48: 1881-1896.

Miller DD, Leferink-ten Klooster HB, Emons AMC, 1997. Ultrastructural analysis of root hairs during development and after treatment with rhizobial signal molecules. Proc. Meeting Dutch Soc. for Microsc., Papendal, 52-53.

Miller DD, De Ruijter NCA, Bisseling T, Emons AMC, 1999. The role of actin in root hair morphogenesis: studies with lipochito-oligosaccharide as a growth stimulator and cytochalasin as an actin perturbing drug. *Plant J* 17: 141-154.

Miyawaki A, Llopis J, Heim R, McCaffery JM, Adams JA, Ikura M, Tsien RY, 1997. Fluorescent indicators for Ca^{2+} based on green fluorescent proteins and calmodulin. *Nature* 388: 882-887.

Miyawaki A, Griesbeck O, Heim R, Tsien RY, 1999. Dynamic and quantitative Ca^{2+} measurements using improved Cameleons. *Proc Natl Acad Sci USA* 96:2135-2140.

Muallem S, Kwiatkowska K, Xu X, Yin HL, 1995. Actin filament disassembly is a sufficient final trigger for exocytosis in nonexcitable cells. *J Cell Biol* 128: 589-598.

Pierson ES, Lichtscheidl IK, Derksen J, 1990. Structure and behavior of organelles in living pollen tubes of *Lilium longiflorum*. *J of Exp. Bot.* 41, 1461-1468.

Pierson ES, Miller DD, Callaham DA, Shipley AM, Rivers BA, Cresti M, Hepler PK, 1994. Pollen tube growth is coupled to the extracellular calcium ion flux and the intracellular calcium gradient: effect of BAPTA-type buffers and hypertonic media. *Plant Cell* 6: 1815-1828.

Pringle JR, Bi E, Harkins HA, Zahner JE, De Virgilio C, Chant J, Corrado K, Fares H, 1995. Establishment of cell polarity in yeast. *Cold Spring Harb Symp Quant Biol* **60**: 729-744.

Pu R, Robinson KR , 1998. Cytoplasmic calcium gradients and calmodulin in the early development of the fucoid alga *Pelvetia compressa. J Cell Sci* **111**:3197-3207.

Reiss H-D, Herth W, 1985. Nifedipine-sensitive calcium channels are involved in polar growth of lily pollen tubes. *J of Cell Sci* **76,** 247-54.

Ressad F, Didry D, Xia GX, Hong Y, Chua NH, Pantaloni D, Carlier MF, 1998. Kinetic analysis of the interaction of actin-depolymerizing factor (ADF)/cofilin with G- and F-actins. Comparison of plant and human ADFs and effect of phosphorylation. *J Biol Chem* **273**: 20894-20902.

Roberts K, 1994. The plant extracellular matrix: in a new expansive mood.*Curr Opin Cell Biol.* **6**:688-694

Schiefelbein JW, Shipley A, Rowse P, 1992. Calcium influx at the tip of growing root-hair cells of *Arabidopsis thaliana. Planta* **187,** 455-459.**Sherrier DJ, VandenBosch KA,** 1994. Secretion of cell wall polysaccharides in *Vicia* root hairs. *Plant J* **5,** 185-195.

Timmers ACJ, De Vries SC, Schel JHN, 1989. Distribution of membrane boudn calcium and activate calmodulin during somatic embryogenesis of *Daucus carota* L. *Protoplasma* **153**: 24-29.

Timmers AC, Reiss HD, Schel JH, 1991. Digitonin-aided loading of Fluo-3 into embryogenic plant cells. *Cell Calcium* **12**: 515-521.

Vijn I, Martinez-Abarca F, Yang WC, das Neves L, van Brussel A, van Kammen A, Bisseling T, 1995. Early nodulin gene expression during Nod factor induced processes in *Vicia sativa. Plant J* **8**: 111-119.

Wymer CL, Bibikova TN, Gilroy S, 1997. Cytoplasmic free calcium distributions during the development of root hairs of *Arabidopsis thaliana. Plant J* **12**: 427-439.

Samenvatting

Dit proefschrift behandelt de rol die het actine-cytoskelet heeft bij top-groei van plantencellen. Groei van plantencellen is mogelijk door een combinatie van celdeling en celexpansie. Het celskelet, dat bestaat uit microtubuli en actine filamenten, speelt een belangrijke rol bij beide processen. Bij de celdeling worden twee dochtercellen gevormd uit een oudercel. De oriëntatie van het delingsvlak bepaalt vrijwel altijd de richting van celexpansie. Het is dan ook belangrijk voor de vormontwikkeling, de morfogenese van de plant, dat dit delingsvlak op de juiste plaats wordt aangelegd. Tijdens de meeste stadia van celdeling hebben microtubuli en actine filamenten dezelfde ligging.

In hoofdstuk 1 is het celskelet van microtubuli zichtbaar gemaakt tijdens alle stadia van de celdeling in lange en korte cellen van de primaire wortel van de tuinboon (*Vicia faba* L.). In alle cellen bleek een preprofase-band van microtubuli in het middenvlak van de cel te worden aangelegd, loodrecht op de lengte-as van de wortel. We constateerden dat de as van de spoelfiguur in de korte cellen van meta- tot anafase in toenemende mate kantelde, waardoor scheve celplaten werden gevormd. Waarschijnlijk wordt de kanteling tijdens de kerndeling in kleine cellen veroorzaakt door ruimtegebrek. De celplaat draaide echter eerst in het transversale vlak terug voordat de celplaat vergroeide met de plasmamembraan en celwand van de oudercel, exact op die plaats waar eerder de preprofase-band had gelegen. Wanneer de celdeling voltooid is, kunnen cellen groeien.

Groei van plantencellen is het gevolg van exocytose, de versmelting van Golgi-blaasjes met de plasmamembraan waarbij hun inhoud afgegeven wordt aan de bestaande wand. Wanneer deze wand flexibel is en onder turgordruk staat, wordt de membraan vergroot en de wand expandeert. De basis- principes van plantencelgroei kunnen het beste bestudeerd worden in cellen waarin dit groeiproces sterk gelokaliseerd voorkomt, zoals in de uiterste top van top-groeiende cellen van hogere planten, zoals wortelharen en pollenbuizen.

In Hoofdstuk 2 worden een aantal karakteristieken van top-groeiende cellen genoemd, die bestudeerd zijn in ontwikkelingsstadia van wortelharen van wikke (*Vicia sativa* L.). Er kon worden aangetoond dat lipochito-oligosacchariden (LCO's), goed gekarakteriseerde signaalmoleculen, die door bacteriën worden uitgescheiden, in staat zijn om top-groei te re-initiëren in wortelharen die vrijwel volgroeid waren. Top-groei en de richting van groei reinitiatie blijken te correleren met de aanwezigheid van een steile cytoplasmatische gradiënt van calcium ionen aan de plasmamembraan. Verder werd gevonden dat een spectrine-achtig eiwit ook karakteristiek is voor top-groei.

Immunolokalisatie van dit spectrine-achtige eiwit in planten werd daarnaast uitgevoerd in niet top-groeiende cellen, hetgeen aantoonde dat dit eiwit met name jonge groeiende cellen labelt (Hoofdstuk 3). Dit plant spectrine-achtige eiwit werd verder geïdentificeerd via de bepaling van het molecuulgewicht en het iso-electrische punt, middels elektroforese gevolgd door immunoblotting. Het anti-spectrine antilichaam labelt ook plantenkernen, hetgeen verder werd bestudeerd in Hoofdstuk 4.

Om de aanwezigheid en lokalisatie spectrine-achtige eiwitten van de kern te analyseren, werden verscheidene plantenweefsels en geisoleerde kernen gelabeld. De resultaten, gepresenteerd in Hoofdstuk 4, tonen aan dat deze spectrine-achtige eiwitten in de kern voorkomen in een gespikkeld patroon en af en toe als lijntjes. De gebruikte extractie-procedures laten zien dat het eiwit sterk gebonden is aan de kernmatrix. Het spectrine-achtige eiwit verleent mogelijk stabiliteit aan de structuur van de kern.

In Hoofdstuk 5 wordt het actine-cytoskelet van wortelharen van wikke beschreven, vanaf het ontstaan van de wortelharen tot aan het moment dat ze volgroeid zijn. Actine filamenten zijn sterk dynamisch, maar tevens het skelet van cytoplasmadraden. Groeiende haren vertonen in een hoge dichtheid dunne bundels van actine filamenten in het sub-apicaal gelegen gebied (FB-actine). In de uiterste top zijn geen actine bundels aanwezig, terwijl in volgroeide haren actine bundels door de top heen lopen. Vergelijkbare actine-configuraties werden verkregen door een vriessubstitutie methode gevolgd door immunolabeling en een voor deze cellen verbeterde chemische fixatie gevolgd door actine-kleuring met fluorescent gelabeld phalloidine. Aangezien LCO's geschikt waren gebleken om wortelhaargroei te reinitiëren (Hoofdstuk 2), werd dit signaal molecuul gebruikt om het actine-cytoskelet te bestuderen tijdens dit proces. Manipulatie van het actine-cytoskelet met cytochalasine D, een drug die het groeiende uiteinde van actine filamenten bezet, waardoor deze niet meer kunnen groeien, veroorzaakte het stoppen van de top-groei, maar wortelhaar initiatie en zwelling na LCO applicatie bleken niet aangetast. Klaarblijkelijk is een verlenging van de actine filamenten van het FB-actine een vereiste voor top-groei.

Inderdaad bleken LCO's in staat om het actine-cytoskelet te veranderen, hetgeen wordt beschreven in Hoofdstuk 6. De dichtheid van de sub-apicaal gelegen bundels actine filamenten nam sterk toe binnen 3-15 min na de toediening van LCO's. Door een kwantitatieve aanpak waren we in staat om de minimale dichtheid van FB-actine en de lengte van de zone met FB-actine die nodig is voor groei, te definiëren. Alleen in haren waarin FB-actine die waarden overschreed, ging de top-groei door of werd gereinitieerd. De snelle reactie van actine filamenten geeft aan dat actine een doelwit is van signaal transductie routes die een verandering van de celgroei tot gevolg hebben. Zulk dynamisch actine-cytoskelet moet worden gereguleerd. Die regulatie zal mede worden uitgevoerd door actine-

bindende eiwitten. Over de rol van actine-bindende eiwitten in planten is nog vrij weinig bekend. Een overzicht van de huidige kennis over actine-bindende eiwitten in plantencellen staat in Hoofdstuk 7 van deze dissertatie.

In Hoofdstuk 8 zijn de gevonden karakteristieken van groei in top-groeiende cellen bijeen gezet en geëxtrapoleerd naar cellen die isodiametrisch of voornamelijk langs één lengteas expanderen. We concluderen dat top-groeiende cellen, zoals wortelharen, inzicht geven in basisprincipes van plantencelgroei en een systeem zijn om het effect van signaal moleculen op plantencelgroei te volgen.

Dankwoord

Voor u ligt het proefschrift waarin een aantal resultaten zijn beschreven van het onderzoek dat door mij is uitgevoerd in de laatste 7 jaar. In die periode heb ik in aan het laboratorium voor Plantencytologie en -morfologie in verschillende projecten onder leiding van *André van Lammeren, Jan Schel* en *Anne Mie Emons* celbiologisch onderzoek gedaan. Het was in meerdere opzichten een leerzame periode, waarin promotie werk en andere onderzoek- en onderwijs-activiteiten regelmatig wel, maar soms ook niet hand-in-hand gingen. Beste André, Jan en Anne Mie, hartelijk dank voor de begeleiding en de ruimte die jullie me hebben geboden om binnen mijn functie als analist tot deze promotie te komen. De tijd die ik moest steken in het leren schrijven van wetenschappelijke artikelen kon tenslotte niet besteed worden aan het verkrijgen van nog meer resultaten.

Professor *Willemse*, mijn promotor, u wil ik vooral bedanken voor de kritische commentaren en getoonde interesse voor de resultaten van het onderzoek. Bovendien heeft u mede gestimuleerd dat deze ongebruikelijke promotie mogelijk werd.

Dit proefschrift is tot stand gekomen door hard werken en doorzetten, maar de inhoud was niet tot die kwaliteit gegroeid zonder de inhoudelijke begeleiding van mijn copromotor *Anne Mie Emons*. Beste Anne Mie, mede door je gevoel voor laboratorium praktijk, en aanstekelijk enthousiasme was je een belangrijke motor van dit proefschrift. In de eindfase waren je correcties om te komen tot een exacter formuleren een grote hulp. Bedankt.

De snelle technische ontwikkelingen, toenemende onderzoeksfaciliteiten en het grote aantal gastmedewerkers, postdocs en studenten op ons laboratorium hebben ertoe bijgedragen dat het werk steeds inspirerend bleef. Al was de druk soms hoog, ik heb aan alle onderzoek-, onderwijs- en beheerstaken met veel plezier gewerkt.

Dankzij goede microscopische faciliteiten en aanwezige kennis bij collega's voor wat betreft structurele analyse, kon het grootste deel van het werk binnen de vakgroep worden uitgevoerd. Enkele hoofdstukken konden echter alleen ontstaan dankzij de samenwerking met derden. Mijn speciale dank gaat uit naar *Martin Rook* (Universiteit Utrecht). Martin, dankzij jouw vaardigheden met de Unix besturing van de Nikon RMC 8000 konden calcium ionen concentraties in levende wortelharen worden bepaald. From *Sonal Blumenthal* I learned the nuclear isolation technique. Dear Sonal, thanks to your experience in isolating and extracting pea nuclei, and a great cooperation, the presence of spectrin-like proteins in pea nuclei could be shown.

Via de onderzoeksgroep van prof. dr. *Ton Bisseling* van het laboratorium voor Moleculaire Biologie aan de Wageningen Universiteit kregen we de beschikking over Nod factoren, signaalmoleculen van *Rhizobium* bacteriën, waarmee wortelhaargroei werd gestimuleerd. Vooral *Ton Bisseling, Paco Martínez-Abarca Pastor, Renze Heidstra en*

Dorus Gadella wil ik noemen, maar daarnaast was ook de belangstelling en kritische analyse van de resultaten van veel anderen op "molbi" een grote hulp.

Ook de volgende mensen kunnen hier niet onvermeld blijven:

Henk Kieft, voor alle assistentie bij problemen met computers. Truus van de Hoef-van Espelo voor alle secretariële aangelegenheden. *Allex Haasdijk, Paul van Snippenburg en Sijbout Massalt* voor jullie kundige hulp bij tekenwerk en (digitale) fotografie. *Tanja Vrenssen-Borst*, voor de vele blots die je maakte tijdens je stage. *Henk Franssen en Jan Brady*, voor advies bij het moleculair-biologisch werk. *Anja Geitmann, Daphne Foreman* and *David Collings* for all the fun and support. 'Buuf *Ageeth Versteegh*, voor het invoeren van een groot deel van mijn literatuur bestand. Mijn schoonouders *Dick en Jannie van der Kamp* voor de vele keren van april tot en met juni 1999 dat jullie hebben opgepast op Ivanka en Marco, wanneer ik weer eens te druk was om vrij te nemen. Paranimf *Tijs Ketelaar*, bedankt voor je gezelligheid als student in 1995 en als kamergenoot vanaf 1997. Je grote enthousiasme en je sterke verhalen die allemaal echt gebeurd zijn, zijn een verademing als we even te serieus worden en verhogen de goede sfeer binnen onze onderzoeksgroep.

Mijn ouders en vrienden, en alle collega's die ik hier nog niet bij naam heb kunnen noemen, allen bedankt voor jullie hulp en belangstelling, ze heeft zeker bijgedragen tot de voltooiing van deze dissertatie.

Lieve *Ivanka* en *Marco*, papa is klaar en dat gaan we vieren. Door jullie gezelligheid en drukte was het gemakkelijk het onderzoek af en toe te vergeten en was het tegelijkertijd onmogelijk om te vergeten wat ècht belangrijk is.

Tenslotte *Agnes*, jouw hulp was veel groter dan je zelf zult toegeven. Enorm bedankt voor je grote vertrouwen en steun, ook wanneer de planning weer eens niet werd gehaald.

Norbert, 1-augustus-1999.

Curriculum Vitae

Norbertus Cornelis Aloysius de Ruijter werd op 21 april 1962 geboren te Amsterdam. In 1981 behaalde hij het diploma Atheneum B aan het Mencia de Mendoza Lyceum te Breda en hij begon in datzelfde jaar de 4-jarige hogere laboratorium opleiding Hoger Natuurwetenschappelijk Onderwijs (HNWO) aan het toenmalige Dr. Struycken Instituut te Etten-Leur. Hij rondde deze opleiding in 1985 af met een stage aan de vakgroep Moleculaire Genetica van de Landbouwuniversiteit Wageningen, onder de begeleiding van dr. J. Visser. In die periode werd onderzoek verricht aan 'De inductie en sub-cellulaire lokalisatie van extracellulaire enzymen bij *Aspergillus niger'*. Aansluitend werd hij bij dezelfde vakgroep aangesteld in een gelijknamig project gefinancierd door de Nederlandse Organisatie voor Wetenschappelijk Onderzoek (NWO). Na 5 maanden werd dit dienstverband verbroken in verband met het vervullen van de dienstplicht. De dienstplicht werd vervuld bij de Medische troepen van de Koninklijke Landmacht. Na de kaderopleiding werkte hij gedurende 1 jaar in de klinisch chemische routine van het Militair hospitaal Dr. A. Matthijssen te Utrecht, waar hij tevens enkele analytische bepalingen optimaliseerde, waaronder de kwantificering van hemoglobine in hersenvocht met behulp van HPLC. Vanaf 1987 werkte Norbert als biochemisch-celbiologisch analist bij de vakgroep Plantencytologie en morfologie van de Landbouwuniversiteit te Wageningen. Het uitvoeren van onderzoek, begeleiden van doctoraalstudenten en het beheren van onderzoeksapparatuur, waaronder geavanceerde microscopen, behoort daar tot zijn taken. Daarnaast is hij actief betrokken bij het organiseren en geven van diverse onderwijselementen en cursussen. Zijn affiniteit met onderzoek was groot zodat hij op eigen verzoek de gelegenheid kreeg een proefschrift te bewerken, met prof. dr. M.T.M. Willemse als promotor. In de periode 1990-1994 werd in verschillende projecten gewerkt onder leiding van dr. J.H.N. Schel, dr. A.A.M. van Lammeren en dr. A.M.C. Emons. Vanaf 1995 werd het onderzoek voornamelijk verricht binnen projecten van dr. A.M.C. Emons, hetgeen resulteerde in de totstandkoming van dit proefschrift.

List of publications

Fransz P.F., de Ruijter N.C.A. and Schel J.H.N. (1989) Isozymes as biochemical markers in embryogenic callus cultures of maize (*Zea mays* L.). *Plant Cell Reports* 8: 67-70.

Pretova A., de Ruijter N.C.A., van Lammeren A.A.M. and Schel J.H.N. (1993) Structural observations during androgenic microspore culture of the 4C1 genotype of *Zea mays* L. *Euphytica* 65: 61-69.

De Ruijter N.C.A. and Emons A.M.C. (1993) Immunodetection of spectrin antigens in plant cells. *Cell Biol. Int.* 17: 169-182.

Schel J.H.N., de Ruijter N.C.A. and Fransz P.F (1994). Isozymes as markers for embryogenic maize callus In: Biotechnology in Agriculture and Forestry, (ed. Bajaj Y.P.S). Springer-Verlag, Heidelberg-Berlin, Vol.25 Maize Chapter VI.6.

De Ruijter N.C.A., Pietrusiewicz J, Montijn M.B., Schel J.H.N., van Lammeren A.A.M. (1997) Spatial limitations induce spindle tilting and result in oblique phragmoplasts in *Vicia faba* L. root tip cells, but do not result in oblique cell walls. *Acta Bot. Neerl.* 46: 279-290.

Miller D.D., de Ruijter N.C.A. and Emons A.M.C. (1997) From signal to form: aspects of the cytoskeleton-plasma membrane-cell wall continuum in root hair tips. *J. Exp. Bot.* 48: 1881-1896.

De Ruijter N.C.A., Rook M.B., Bisseling T. and Emons A.M.C. (1998) Lipochito-oligosaccharides re-initiate root hair tip growth in *Vicia sativa* with high calcium and spectrin-like antigen at the tip. *Plant J.* 13: 341-350.

De Ruijter N.C.A. and Emons A.M.C. (1999) Actin binding proteins in plant cells. *Plant Biology* 1: 26-35.

Miller D.D., de Ruijter N.C.A., Bisseling T. and Emons A.M.C. (1999) The role of actin in root hair morphogenesis: studies with lipochito-oligosaccharides as a growth stimulator and cytochalasin as an actin perturbing drug. *Plant J.* 17: 141-154.

Esseling J., de Ruijter N.C.A. and Emons, A.M.C. (1999). The root hair actin cytoskeleton as backbone, highway, morphogenetic instrument and target for signalling In: Cell and molecular biology of plant root hairs (eds. Ridge R.W., Emons A.M.), Springer-Verlag, Heidelberg.

Holzinger A., de Ruijter N.C.A., Emons A.M.C and Lütz-Meindl U. (1999) Spectrin-like proteins in green algae (Desmidiaceae). *Cell Biol Int,* in press.

De Ruijter N.C.A., Bisseling T. and Emons A.M.C. (1999) *Rhizobium* Nod factors induce an increase in subapical fine bundles of actin filaments in *Vicia sativa* root hairs within minutes. *MPMI,* 12: 829-832.

De Ruijter N.C.A., Ketelaar T., Blumenthal S.S.D., Emons A.M.C. and Schel J.H.N. Spectrin-like proteins in plant nuclei. *Cell Biol.Int.,* submitted.